Optimisation of Hood Panels of a Passenger Car for Pedestrian Protection

A thesis submitted in fulfilment of the requirements for the degree of Master of Engineering

Revathi Krishnamoorthy

School of Aerospace, Mechanical and Manufacturing Engineering
Science, Engineering, and Technology Portfolio
RMIT University
March 2012

Declaration

I, Revathi Krishnamoorthy, declare that this thesis does not incorporate any material published or written by any person where due reference is not mentioned in the text. The research has been carried out since my commencement of Master of Engineering program and I have not submitted the research for any other academic award. Any editorial work carried out by a third party is duly acknowledged.

Revathi Krishnamoorthy

March 2012

Acknowledgements

I would like to thank all those who rendered their support and assistance to this research work.

I would like to convey my sincere gratitude to Dr Monir Takla, thesis senior supervisor, for his guidance and support to the completion of this thesis.

I would like to express a very special and sincere gratitude to Derek Scott, Specialist Engineer, GM Holden Ltd, for his guidance during the progress of this research and the review of the thesis. I would like to thank the generous support provided by Stewart Sheffield, Safety Integration Engineer, GM Holden Ltd. I would also like to thank Dara Chan, Crashworthiness Engineer, GM Holden Ltd, for his help in understanding the effective usage of CAE tools for crash simulations.

The ideas and results in this thesis have benefited from the discussions I have had with experts in various working groups at GM Holden Ltd. I would like to extend my thanks to all those who generously gave up time for discussions. I would like to thank Paul Tran, James Soo, David Libeaut, Girish Basappa, and Sean Choong for their assistance and constructive comments.

I am thankful to Simon Mclean and Jonathan Ridgway for giving me the opportunities to enhance CAE knowledge and being flexible with my working hours to meet the requirements of this study.

I would also like to thank Mary–Jo O'Rourke for proofreading my thesis.

Finally, but no means the least, I want to thank my loving and caring sons, Arvind and Ashwin, whose responsible behaviour enabled me to focus in my work and studies. I cannot thank my lovely husband Ramaswamy Krishnamoorthy enough for everything he has done and put up with, over the last four years of my study.

Nomenclature

A	Acceleration (g)
T	Duration of acceleration (s)
a(t)	Resultant acceleration (g)
t_1	Time at the beginning of the impact (s)
t_2	Time at the end of the impact (s)
η	Efficiency
A_1	Area enclosed by acceleration–displacement curve
A_2	Area of the shape that encloses acceleration–displacement curve
d	Maximum intrusion (m)
v_0	Initial impact velocity (m/s)
μ_η	Mean value of efficiency
μ_{HIC}	Mean value of HIC
σ_{HIC}	Standard deviation of HIC
U_e	Strain energy (J)
M	Bending moment (Nm)
E	Young's modulus (MPa)
I	Sectional modulus (mm^3)
t	Thickness of the beam (mm)
b	Width of the beam (mm)
l	Length of the beam (mm)

σ_y	Stress at yield point (MPa)
t_{al}	Thickness value assigned for aluminium (mm)
t_{st}	Thickness value assigned for steel (mm)
E_{al}	Young's modulus value for aluminium (MPa)
E_{st}	Young's modulus value for steel (MPa)
$\sigma_{y(al)}$	Stress at yield point for aluminium (MPa)
$\sigma_{y(st)}$	Stress at yield point for steel (MPa)
m	Mass of the head impactor (kg)
v	Velocity of the head impactor (m/s)

Acronyms

ABS	Anti–lock Brake System
ACEA	European Automobile Manufacturers Association
AIS	Abbreviated Injury Scale
ANCAP	Australasian New Car Assessment Program
ANOVA	Analysis of variance
CAE	Computer Aided Engineering
DOE	Design of Experiments
DRL	Daytime Running Lights
EEVC WG7	EEVC Working Group 7
EEVC WG10	EEVC Working Group 10
EEVC WG17	EEVC Working Group 17
EU	European Union
Euro NCAP	European New Car Assessment Program
FES	Front–End Subsystem
GIDAS	German In–Depth Accident Study
GSI	Gadd Severity Index
GTR-9	Global Technical Regulation–9
HA	Hood Angle
HIC	Head Injury Criterion
HIRC	Head Injury Risk Curve

HLE	Hood Leading Edge
HLEH	Hood Leading Edge Height
HRRL	Hood Rear Reference Line
IC	Industry Commitment
IRTAD	International Road Traffic and Accident Database
ISO	International Standards Organisation
JAMA	Japanese Automobile Manufacturers Association
JARI	Japan Automobile Research Institute
J-NCAP	Japanese New Car Assessment Program
KAMA	Korean Automobile Manufacturers Association
K-NCAP	Korean New Car Assessment Program
NHTSA	National Highway Traffic Safety Administration
PMHS	Post Mortem Human Surrogate
PPA	Pedestrian Protection Airbag
PPCFC	Pedestrian-Passenger Car Front–end Collision
SAE	Society of Automotive Engineers
SRL	Side Reference Line
TAC	Traffic Accident Commission
UNECE WP29	United Nations Economic Commission of Europe Working Party 29
WAD	Wrap Around Distance
WSTC	Wayne State University cerebral concussion Tolerance Curve

Contents

Figures

Tables

Abstract

This thesis presents a pro–active research work motivated by the prospect of the imminent implementation of the regulatory requirement for pedestrian protection, Global Technical Regulation-9 (GTR-9) (United Nations Economic Commission for Europe 1998) in the near future. To meet the performance criteria for pedestrian protection head impact, it is vital to incorporate the required design parameters into the hood design process at an early stage. These main design parameters are architectural and changing them late in the vehicle design process is very expensive and difficult to implement. The main design parameters are the inner and outer hood thickness, inner and outer hood material, inner hood structure and the available deformation space to hard components such as the engine.

The main objective of this work is to develop a methodology for optimising hood panels of passenger cars to ensure that the pedestrian Head Injury Criterion (HIC) falls below the threshold values specified by both the GTR–9 and the consumer metric, the Australasian New Car Assessment Program (ANCAP). This study investigated the development of a hood configuration that provides robust and homogeneous HIC for different impact positions in the central area of the hood of a large sedan, taking into consideration of the limited space available for deformation.

An extensive series of Computer Aided Engineering (CAE) simulations has been carried out to collect the acceleration data and vertical intrusion data required to validate the proposed methodology and the optimal hood configuration. These impact simulations include a

stationary vehicle set up and a moving head impactor as per GTR-9. The Design of Experiments (DOE) has been set up with the control factors as inputs to the Kriging response surface and Monte Carlo methods to output the responses. The variables considered for the control factors are the inner hood structure, inner hood thickness and material, outer hood thickness and material, and the impact positions. The results from the numerical tests have been utilised to map the response surfaces in order to identify the important variables and to visualise the relationships between the inputs and the outputs.

The optimisation of the hood has been carried out in two main steps. The first step is the selection of the type of the inner hood structure and inner and outer hood material. The second step is the selection of the thickness of the outer hood panel, thickness of the inner hood panel and inner hood structure. The two–stage optimisation approach has been utilised in this research to reduce the number of simulations and modelling complexity.

The proposed optimisation methodology is described in detail and the outcomes provide clear recommendation of the optimal configuration of passenger car hood panels. The steel hood configuration with multi–cone inner hood structure made of 0.5mm for inner hood panel thickness and 1.1mm for outer hood panel thickness is found to give optimal head impact performance with 70mm of deformation space.

A given HIC can be obtained with minimal head displacement if the waveform shape (Shape of resultant acceleration) matches the realistic optimal waveform. Findings show that optimal configuration of hood panels made of steel exhibit high initial peak acceleration and lower rebound velocities, which matches the realistic optimal waveform.

In conclusion, if the vehicle design team's main objective were to reduce the deformation space, the preferred choice for hood material would be steel rather than aluminium. The benefits of minimising the deformation space are significant. They include the freedom of styling, improved aerodynamics, and hence improvements in vehicle stability and fuel economy. The trade–off will be a higher mass than the equivalent aluminium system. On the other hand, if the vehicle design and program team's main objective was to reduce the system mass, then the preferred choice for hood material would be aluminium. The trade–off would be a higher deformation space than that is required for the steel system.

Chapter 1

Introduction

1.1 Pedestrian safety

The term, pedestrian generally refers to a person walking, running, skating, skateboarding and commuting using similar devices.

There is a recent trend for urban design to provide for more walkable communities. Present–day awareness of health, fitness and greenhouse gas emissions has increased the popularity of cycling and walking in urban areas. Therefore, the probability of pedestrian accidents has also increased.

Automobiles have evolved to be a successful medium for transportation due to substantial inventions and developments in various countries. The concept of large–scale production–line manufacturing enabled the affordable pricing of automobiles, which has increased the demand for them globally.

In 1900, the United States of America was the only country manufacturing cars and built only 4,192 passenger cars (Elert 2001). There were no buses or trucks at that time. As of 2010, there are more than 600 million passenger cars worldwide (Worldometers 2010). These

numbers are increasing rapidly. It is estimated that, if the present trends continue, the number of cars in the world will double by 2030.

As the demand for automobiles has increased, automotive design is improving every day in many aspects of comfort, technology, efficiency, performance and safety. However, as many countries and manufacturers have been participating in the manufacture of cars, there are significant differences in the quality and safety performances offered by the vehicles.

The World Health Organization photograph (Figure 1.1) portrays the unsafe conditions for pedestrians, who risk their lives in order to fulfil their day–to–day responsibilities.

Figure 1.1: Unsafe conditions for pedestrians (World Health Organization 2011)

1.2 Kinematics of a pedestrian in an impact

In 1965, Ryan and Mclean (Ryan & McLean 1965) described the sequence of events when a passenger car collides with an adult pedestrian standing erect.

Those sequences are as follows:

- contact between the bumper and the lower legs of the pedestrian
- contact between the leading edge of the hood and upper legs/pelvis of the pedestrian
- contact between the pedestrian's head/upper torso and the top surface of the hood/windscreen/windscreen frame (Figure 1.2)
- Contact between the pedestrian and the ground.

Figure 1.2: Kinematics of a pedestrian in PPCFC (Synaptic analysis consulting group inc)

They also speculated that it would be possible to minimise injuries in Pedestrian–Passenger Car Front–end Collision (PPCFC) by changing the frontal shape of a car. Their study however, did not suggest any design solutions, as they did not have enough data.

In those days, the belief was that the only way to reduce pedestrian fatalities and injuries was to prevent pedestrian–vehicle collisions. Consideration of modification of vehicle design for pedestrian protection was not an option at that time. From this sequence of events, it can be stated that typically the colliding vehicle runs under the pedestrian and the severity of injuries vastly depend on the vehicle shape and certain characteristics such as energy absorption.

1.3 Thesis overview

The Head Injury Criterion (HIC) is used to determine the head injury tolerance in all the tests conducted to evaluate the pedestrian safety performance offered by the vehicles. The research presented in this thesis involves developing a methodology for optimising hood panels of passenger cars to ensure that the HIC value falls below the limits specified by both the Global Technical Regulation–9 (GTR–9) and Australasian New Car Assessment Program (ANCAP) while considering other vehicle design requirements including minimal deformation. The thesis provides a detailed review of research done to optimise the hood panels of a car to improve the protection offered by the vehicle to pedestrians.

The objective is to develop a hood configuration that provides a robust and homogeneous HIC value for different impact positions in the central area of the hood of a large sedan with minimal deformation space. The term "robust" means high test–to–test repeatability and low sensitivity to noise.

Previous sections of this chapter introduced the motivation for the research. Statistical data cited in chapter 2 explain the magnitude of pedestrian mortality rates and the severity of head injuries caused by the PPCFC.

Chapter 3 presents the background work and benchmarking of previous research in improving the protection offered by a vehicle to the pedestrian head in an impact.

Chapter 4 discusses and outlines the requirements of all current and upcoming regulatory and consumer metric protocols for pedestrian protection.

Chapter 5 describes the technical challenges associated with the investigation of optimal hood configuration to meet the requirements of GTR–9 and ANCAP while retaining or maximising styling flexibility and minimal modifications to architecture.

Chapters 2 to 5 discuss the literature review conducted in various aspects of pedestrian protection.

The optimisation methodology, finite element analysis, results and recommendations from the work conducted by the author of this thesis are discussed and presented in chapters 6 to 14.

Chapter 6 presents the methods used in evaluating the protection offered by a vehicle to occupants and pedestrians.

Chapter 7 describes the methodology used to create the models and the set up procedures.

Chapter 8 explains the methodology used to select the design parameters.

Chapter 9 presents the method for developing and refining the concepts for improving pedestrian protection performance.

Chapter 10 discusses the results of the numerical tests and the performance of the developed optimisation methodology.

Chapter 11 presents the design parameters for optimal hood configuration.

Chapter 12 discusses the optimal configuration and results.

Chapter 13 concludes the research findings.

Finally, chapter 14 outlines the recommendations for further research studies to improve the protection of pedestrians in a collision with a passenger car.

Chapter 2

Automotive safety

2.1 Mortality rates

As the number of cars on the roads has increased worldwide, the risk of traffic accidents has also increased and road traffic accidents are a leading cause of deaths due to injuries. The rate of road traffic fatalities increased rapidly after 1998 and the trend is continuing. In many countries, not enough resources are dedicated to recording and analysing reliable data on road traffic fatalities, non–fatal injuries and economic costs.

The World Health Organization's publications reported approximately 1.27 million fatalities in one year in road traffic accidents. It has been estimated that this will rise to 2.4 million fatalities per year by 2030. It is predicted that by 2030, injuries due to road traffic accidents will become the fifth leading cause of death. In addition, approximately 50 million people suffer non–fatal injuries caused by road traffic accidents around the world every year, causing huge devastation and suffering to individuals, families and communities (World Health Organization 2011).

Thus, safety considerations in vehicle design have become a key factor in car production. The statistical data shows that there is a large difference between injury rates in developing and developed countries. Fatalities due to road traffic accidents in low–income and middle–income countries contribute over 90% to global road traffic fatalities.

2.1.1 Mortality rates and vehicle design in developed nations

Over the last 20 years, the number of road traffic fatalities in the European Union (EU) has decreased significantly.

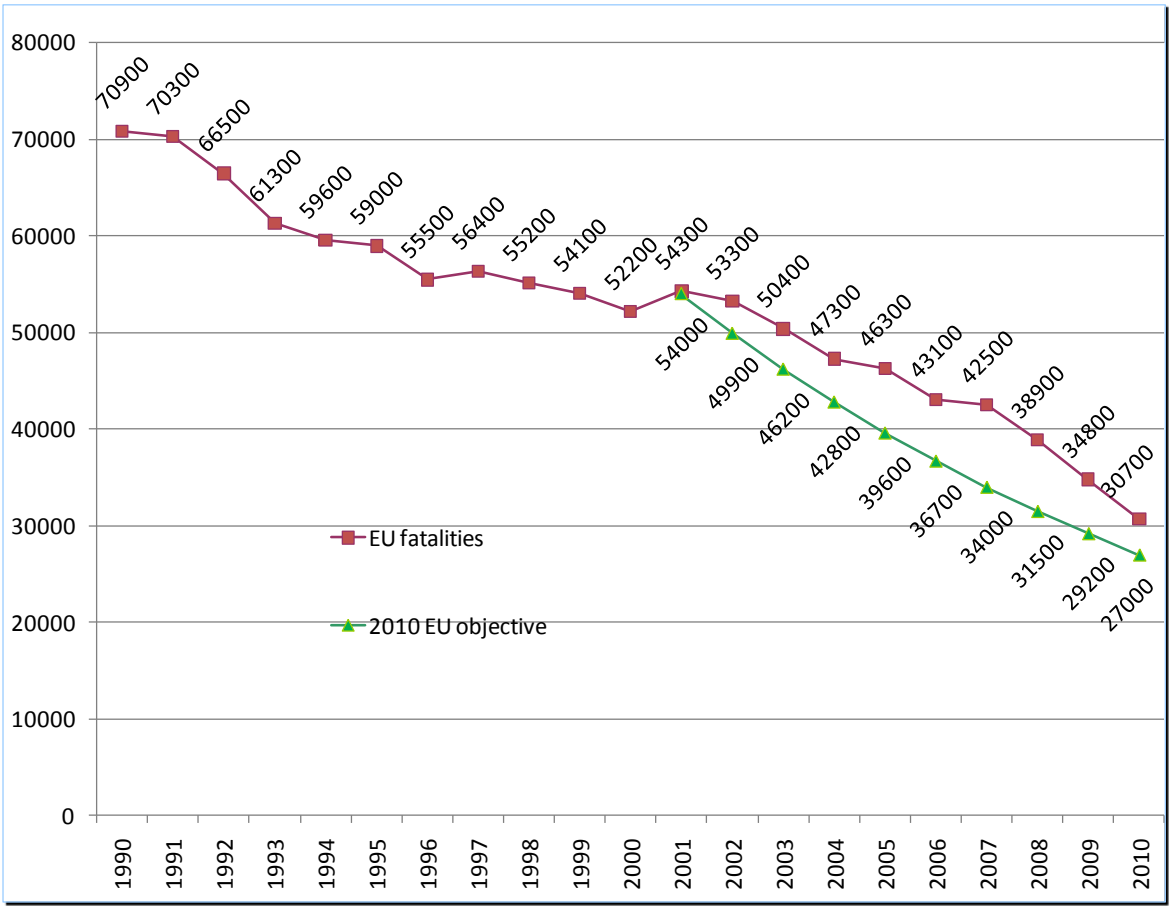

Figure 2.1: Road traffic fatalities by year in EU, 1990–2010 (European Commission 2010)

In 2001, the European Commission set itself a challenging goal of reducing the number of fatalities to 50% by the year 2010 (European Commission 2010) as shown in Figure 2.1.

Initiatives included improvements in vehicle design for both active and passive safety, accident avoidance countermeasures, improvements in infrastructure, improvements in driver and pedestrian behaviour, better and faster emergency medical services, and strict enforcement of traffic regulations.

Against the background of these initiatives, there has been a significant reduction in road traffic fatalities (Figure 2.1 – Red line). Even though it is generally recognised, that significant progress has been made in reducing road traffic fatalities; Figure 2.1 shows that it is not enough to meet the objectives set in 2001 by the EU. To achieve these goals, consideration of all the possible measures to reduce fatality or severe injury is essential.

2.1.2 Mortality rates and vehicle design in developing nations

Due to the rapid increase in economic development in developing countries, the numbers of cars have been increasing substantially, especially in China and India. Therefore, the risk of traffic accidents has also increased. Although continuous developments in motor vehicle safety measures have reduced occupant and pedestrian injuries and fatalities in developed countries, every year occupant and pedestrian fatalities and injuries are increasing significantly in developing countries.

The fourth leading cause of death for 15–59 year olds in the low and middle–income countries is road traffic accidents. Africa has the highest rate of road toll per population due to poor infrastructure (Figure 2.2), weak preventative measures and inadequate post–crash

care. The estimated economic cost of road traffic injuries for all age groups is approximately US $518 billion per year (The World Bank 2001).

Figure 2.2: Unsafe traffic conditions in Africa (World Health Organization 2011)

The rate of road traffic fatalities increased rapidly after 1998 and the trend is continuing. In many developing countries, not enough resources are dedicated to recording and analysing reliable data on road traffic fatalities, non–fatal injuries and economic costs.

2.2 Pedestrian accidents

The World Health Organization's publications highlight that approximately half the road traffic fatalities are vulnerable road users such as pedestrians, cyclists and motorbike riders.

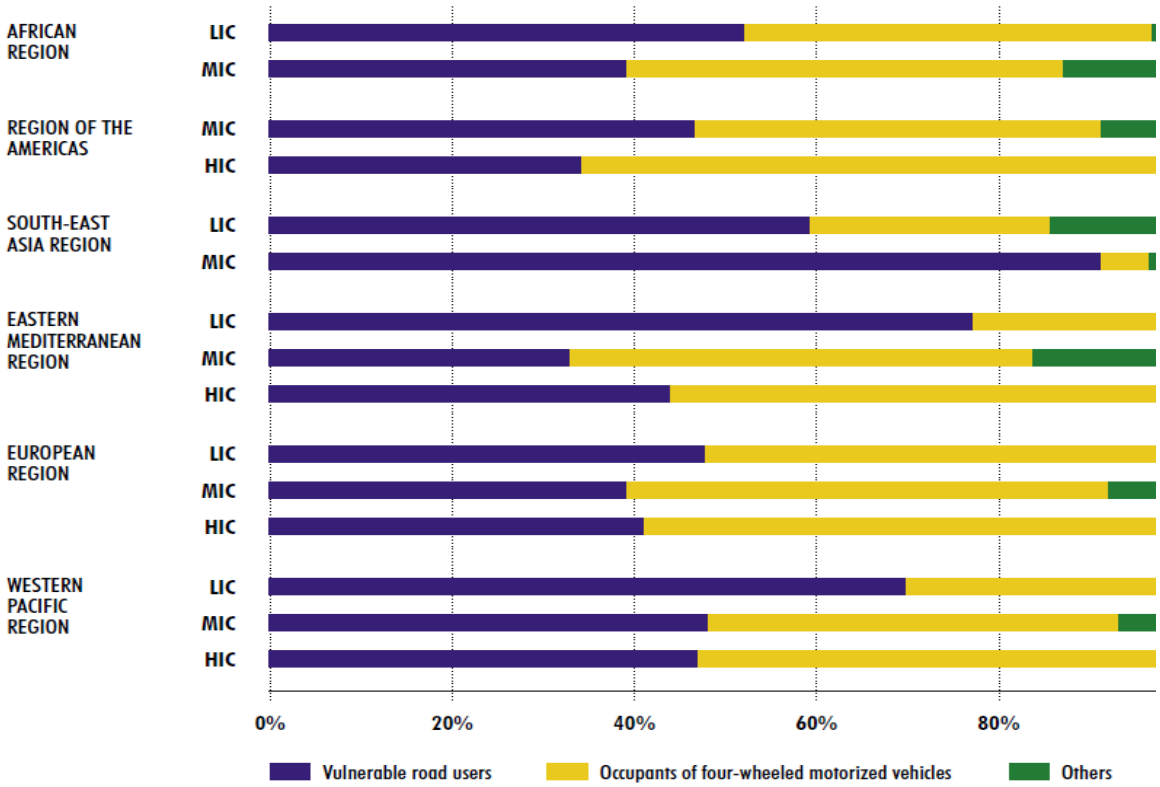

Figure 2.3: Road toll by type of road users (World Health Organization 2011)

Figure 2.3 shows that vulnerable road users contribute significantly to the fatality and injury toll in road traffic accidents, especially in Africa, Asia and the Middle East. This shows the need to protect occupants as well as other vulnerable road users such as pedestrians, to reduce road traffic fatalities.

In Figure 2.3, LIC refers to low–income country, MIC to middle–income country, and HIC to high–income country. It shows that, in general, mortality rates of vulnerable road users are higher in low–income countries in comparison to medium–income and high–income countries.

In the US, National Highway Traffic Safety Administration (NHTSA) in 2008 announced that 49,128 pedestrians (about 12% of road traffic fatalities) died from 1997 to 2006. Even

with the number of pedestrian crashes declining during this period, 4,654 pedestrians died and 70,000 pedestrians were injured in 2007.

In 2001, the World Bank (The World Bank 2001) reported that approximately 760,000 pedestrians die around the world in a year. The EU road accidents database (CARE) reported that pedestrians account for about 20% of road traffic fatalities in 14 European countries in 2011 (Figure 2.4).

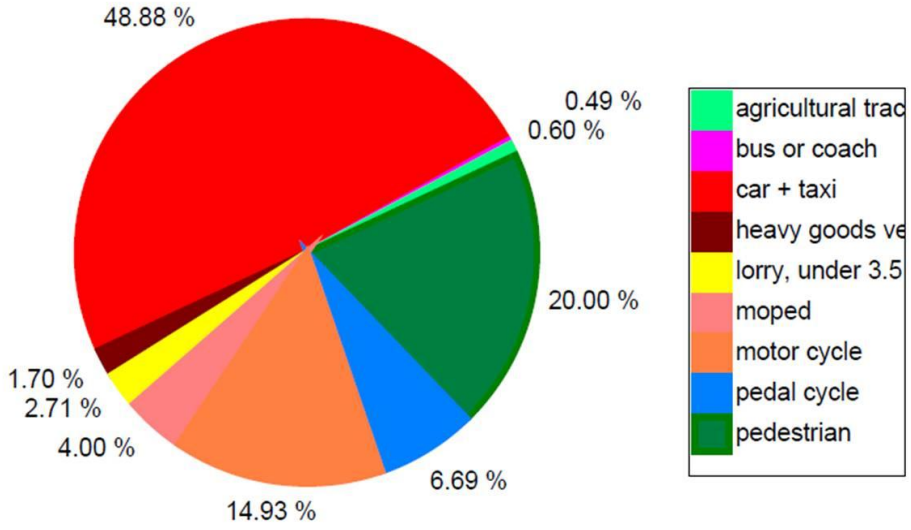

Figure 2.4: Pedestrian fatalities in EU, 2011 (CARE (EU road accidents database) 2011)

In Australia, the Traffic Accident Commission's (TAC) report for 2012 (Transport Accident Commision 2012) shows that 17% of road traffic fatalities were pedestrian fatalities. In Korea, 40% of road traffic fatalities are pedestrian fatalities and in Japan, 32% of the road toll accounts for pedestrians (Oh et al. 2008).

Implementation of various safety initiatives could reduce pedestrian injuries. For example, defining and using pedestrian zones; educating pedestrians to walk safely; enforcing speed limits in pedestrian zones; improving road conditions to reduce blind spots etc. However,

occupant fatality and injury data shows that vehicle design could also play an important role in minimising pedestrian injury in an accident.

2.3 Severity of injuries

The Abbreviated Injury Scale (AIS), which is the standard for classifying the severity of injuries, was introduced in 1969.

AIS score	Injury
1	Minor
2	Moderate
3	Serious
4	Severe
5	Critical
6	Fatal

Table 2.1: Abbreviated injury scale

It ranks the severity of injuries in a sliding scale that increase from one to six; one is minor injury and six is fatal, as shown in Table 2.1. The latest incarnation of the AIS score is the 1990 revision. The AIS is monitored by a scaling committee of the Association for the Advancement of Automotive Medicine (Trauma.org).

Chapter 3

Background research and benchmarking

3.1 Pedestrian protection offered by a vehicle

At present, there are no regulatory vehicle design requirements for pedestrian protection in Australia. ANCAP (Figure 3.1) tests the new cars sold in Australia for pedestrian safety in a pedestrian impact with a passenger car. This represents a subset of a broader program of safety assessments (Australasian New Car Assessment Program 2011).

Figure 3.1: ANCAP – consumer metric in Australia (Australasian New Car Assessment Program 2010)

The number of points awarded to a vehicle indicates the level of pedestrian protection offered by the vehicle. A maximum of 36 points can be scored: 12 points for child head impact; 12 points for adult head impact; 6 points for upper leg impact; and 6 points for lower leg impact. The sum of all points scored determines the number of stars or the descriptive rating awarded for pedestrian safety rating (Table 3.1). In 2011, ANCAP has changed its pedestrian protection star rating to a descriptive rating.

Score	Old star rating	New descriptive rating
27.5 or more	4 stars	Good
18.5 to 27.49	3 stars	Acceptable
9.5 to 18.49	2 stars	Marginal
0.5 to 9.49	1 star	Poor
Less than 0.5	Zero stars	Poor

Table 3.1: ANCAP pedestrian safety rating

Similarly, the European New Car Assessment Program (Euro NCAP) stopped publishing star ratings in 2009 and now publishes the score as a percentage.

The importance of vehicle design for occupant safety was widely accepted around 1960. The continuous improvements in vehicle design for safety driven by the regulations have played a vital role in occupant protection. In recent times, government organisations and auto industries have recognized the need to ensure occupant safety as well as the safety of other road users.

Figure 3.2 shows a summary of pedestrian protection results for all cars sold in Australia as published by ANCAP in June 2010.

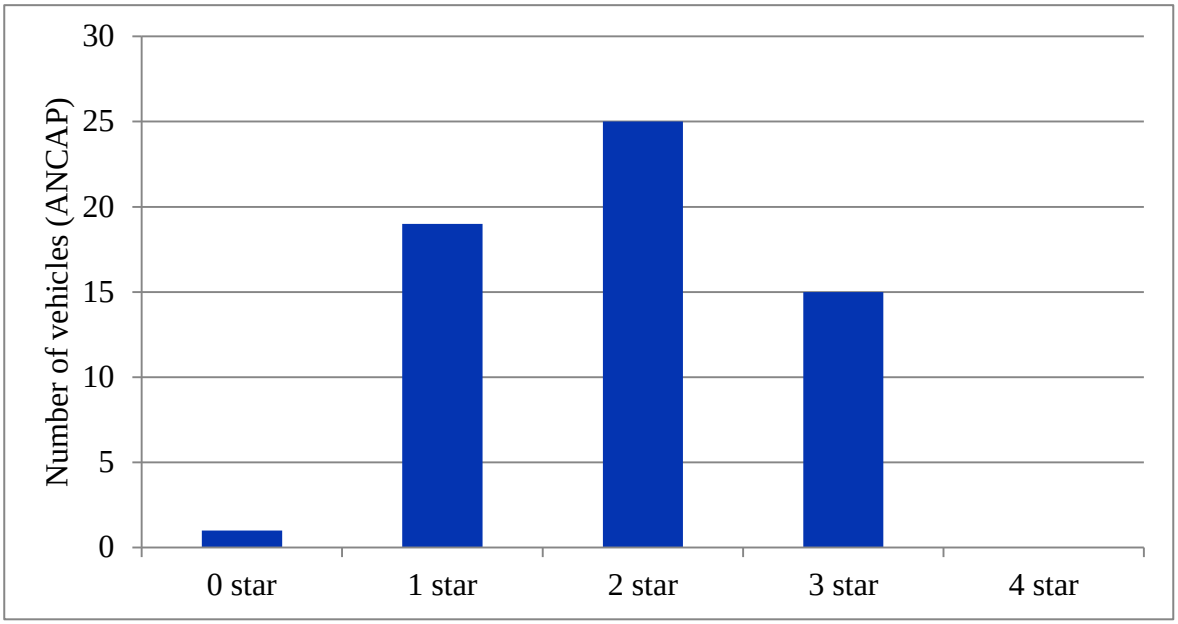

Figure 3.2: ANCAP pedestrian protection results for all cars (Australasian New Car Assessment Program 2010)

The assessment procedures in automobile design fall in these categories: legal regulations, consumer metrics and automakers' internal requirements. These criteria vary between countries. The vehicle design has to meet the assessment criteria specified by the legal regulations in a country to sell the vehicle in that country. Organisations assess the vehicles for various performances and publish the ratings based on the protection offered to occupants and vulnerable road users. In general, safety ratings published by the consumer metrics influence the purchasing decision of the consumer. Automaker's internal requirements specify the assessment criteria to maintain the quality of the vehicle consistently.

At present, due to the legal regulations for pedestrian protection in Europe and Japan, cars produced or manufactured in these countries score better in pedestrian protection consumer metric safety ratings when compared to cars manufactured in other countries. Even though

pedestrian protection in vehicle design is optional in many countries, it is expected to become mandatory in the future. Many countries are in the process of adopting the Global Technical Regulation–9 as a regulatory requirement for vehicle design to meet pedestrian protection.

There are two separate safety ratings currently published by ANCAP, occupant protection rating and pedestrian protection rating. However, the safety rating for occupant protection is the most relevant to customers in choosing a vehicle to purchase, as it is the most prominent safety metric and because it relates to the safety of the purchaser and their family. In contrast, the level of protection provided to pedestrians is generally a lower priority. In addition, the majority of media attention focuses on the adult occupant protection rating, leaving the public largely unaware of pedestrian protection ratings.

To overcome this situation, Euro NCAP has combined occupant safety and pedestrian safety into one overall performance safety rating and other countries such as Australia have announced that they will adopt this approach.

The declining fatality and injury numbers in Europe (Figure 2.1) show that legislation will most likely drive innovative motor vehicle designs for safety.

3.2 Pedestrian injuries

A collision between a pedestrian and a passenger car causes injuries to the whole body. Recovery from head injuries however, takes substantial time and these injuries are more likely to be fatal. In 2003, Iskander Farooq and his team compiled the data from the International Road Traffic and Accident Database (IRTAD) and the German In–Depth Accident Study (GIDAS). They found that 62% of pedestrian fatalities occur due to head injuries.

The statistics show that about 92% of pedestrian fatalities in the US are due to PPCFC (National highway traffic safety administration 2009) as presented in Figure 3.3. The pedestrian's head contact with the vehicle front–end or the ground could cause significant head injuries. However, studies show that head impact with the vehicle front–end is likely to cause more damage than head impact with the ground.

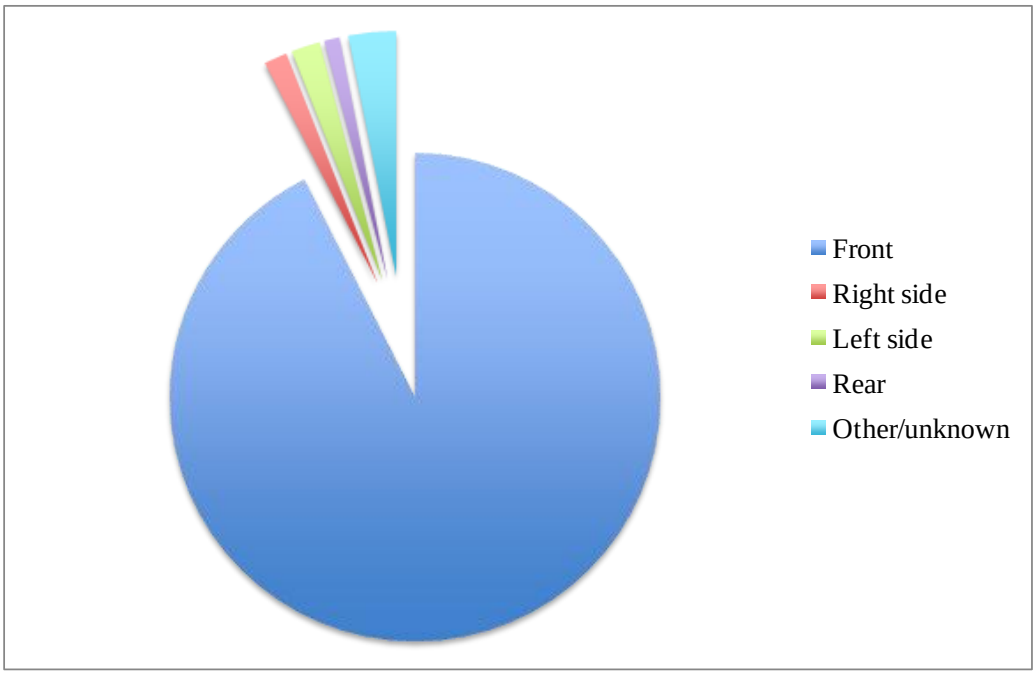

Figure 3.3: Pedestrian fatalities due to collision with a passenger car in the US (National highway traffic safety administration 2009)

Other studies on injuries in children pedestrians show that the injuries to different regions of the body vary based on a child's age. Head and chest impacts are the sources of fatal injuries for younger children. Contact between the pelvis and the abdomen with the leading edge of the hood can cause fatal injuries for an older age group.

According to the International Harm Reduction Association (IHRA) accident data, head and leg injuries account for two thirds of pedestrian injuries. Approximately 84% of AIS 2–6 injuries are caused by pedestrian contact with the vehicle front–end. In Australia (Table 3.2), 39.3% of AIS 2–6, injuries occur due to head impact.

Body region	USA	Germany	Japan	Australia	Total
Head	32.7%	29.9%	28.9%	39.3%	31.4%
Face	3.7%	5.2%	2.2%	3.7%	4.2%
Neck	0.0%	1.7%	4.7%	3.1%	1.4%
Chest	9.4%	11.7%	8.6%	10.4%	10.3%
Abdomen	7.7%	3.4%	4.7%	4.9%	5.4%
Pelvis	5.3%	7.9%	4.4%	4.9%	6.3%
Arms	7.9%	8.2%	9.2%	8.0%	8.2%
Legs	33.3%	31.6%	37.2%	25.8%	32.6%
Unknown	0.0%	0.4%	0.0%	0.0%	0.2%
Total	100%	100%	100%	100%	100%

Table 3.2: Distribution of pedestrian injury AIS 2-6 (Mizuno 2003)

Head impact is the most prominent factor in pedestrian fatalities and injuries. Thus, it represents a key hurdle in the pedestrian protection assessment criteria. Due to these two critical features, it was decided to focus on improving vehicle design to reduce head injuries.

3.3 Head injury evaluation

The three main categories of head injuries are skull fractures, focal brain injuries and diffuse brain injuries. Skull fracture may occur with or without brain damage. Focal brain injuries represent the most serious form of head injury, usually fatal. Diffuse brain injuries disrupt the global neurologic functions of the body (Hutchinson, Kaiser & Lankarani 1998).

Various mechanisms can cause these head injuries. However, the prime mechanism is dynamic loading, where direct contact of the head with a hard object causes the skull to deform, which may result in either direct or indirect fractures. Inertial loading due to severe acceleration also causes brain injuries. Translational acceleration usually results in focal brain injury, whereas rotational acceleration causes diffuse brain injury (Schmitt et al. 2007).

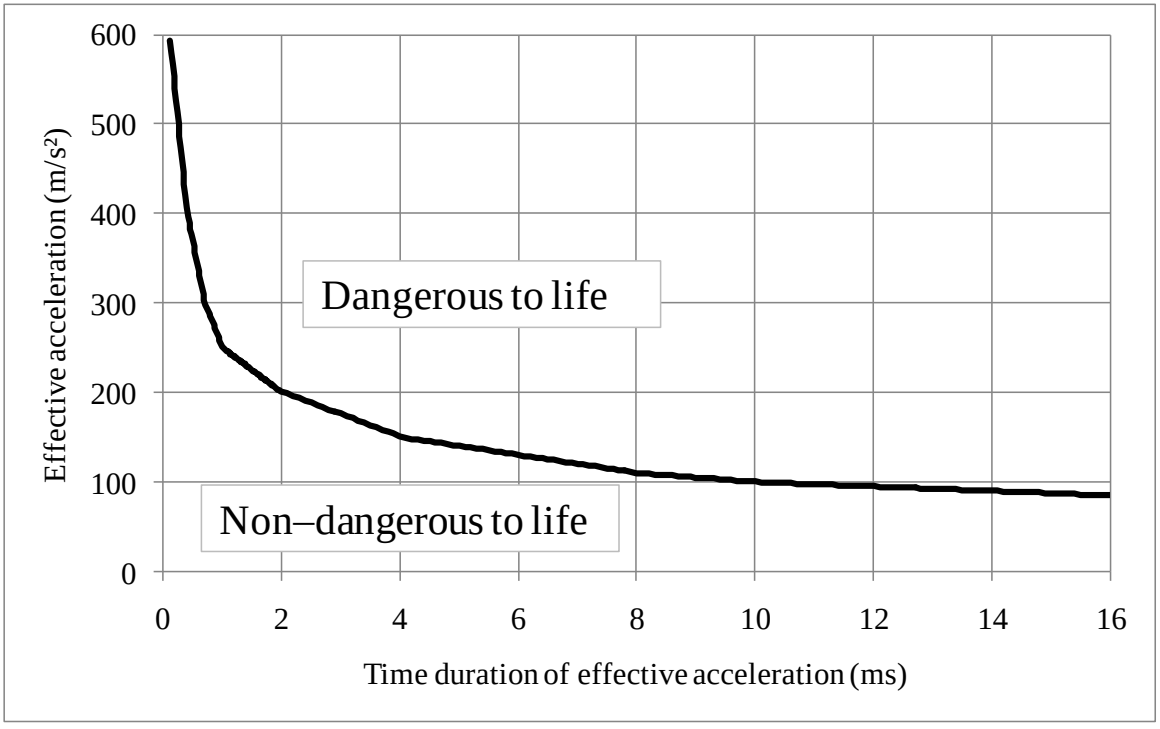

Figure 3.4: Wayne State University cerebral concussion tolerance curve

The Wayne State University cerebral concussion Tolerance Curve (WSTC) shown in Figure 3.4 presents the relationship between the effective acceleration of the head, impact duration and injury risk, assuming that the severity of injury of the human brain is the same at any point on the curve. This curve suggests that high levels of head acceleration may be tolerated for short durations, while lower levels can be tolerated for longer durations. It shows that the zone below the curve is the non–dangerous to life zone and the zone above the curve is the danger to life zone.

Based on the WSTC, the Gadd Severity Index (GSI) was developed in 1966 (Gadd 1966) according to the concept of weighted impulse averaging for estimating the head injury hazard. The GSI is represented by a straight line suggesting that a magnitude of 1000 is the acceptable human head injury tolerance limit and this magnitude equates to:

$$1000 = TA^{2.5} \qquad \textbf{Equation 3.1}$$

Where, A is the constant acceleration and T is the duration of constant acceleration A.

The GSI evolved from Equation 3.1 and it is shown in Equation 3.2:

$$GSI = \int_{t1}^{t2} [a\,(t)]^{2.5} dt \qquad \textbf{Equation 3.2}$$

Where, a(t) is head acceleration as a function of time.

Versace proposed Equation 3.3 to calculate HIC in 1971 (Versace 1971), derived from the GSI and used by NHTSA in the Federal Motor Vehicle Safety Standard No. 208 (FMVSS 208) to evaluate occupant head impact protection. In this definition, a 36ms window was used to scan the acceleration pulse to find the maximum HIC value in occupant protection.

In 1974, Adwani and Owings (Advani & Owings 1974) identified that the GSI measures different acceleration levels for various pulse shapes for constant injury magnitude and impact duration. As a result, calculation of the Head injury criteria in all current pedestrian head impact tests use the formula mentioned in Equation 3.3.

In the pedestrian head impact test, the accelerometer time histories are used to calculate the HIC value using the following formula in Equation 3.3:

$$HIC = Max\left\{\left[\frac{1}{t_2 - t_1}\int_{t_1}^{t_2} a(t)dt\right]^{2.5}(t_2 - t_1)\right\} \qquad \textbf{Equation 3.3}$$

In this equation, a(t) is the resultant acceleration in units of gravity g (1g=9.81 m/s2), t_1 is the beginning and t_2 is the end of the impact, expressed in seconds, for which the value of HIC is the maximum (t_2–t_1 is less than or equal to 15ms).

Therefore, it can be stated that HIC value increases with resultant acceleration and the recording period in head impact.

In 1972, Hodgson (Hodgson, Thomas & Brinn 1973) hypothesised that if the maximum HIC value does not exceed the tolerance limit within a 15ms window, it is safe for cerebral concussion. In 1985, Prasad and Mertz (Prasad & Mertz 1985) analysed forehead impact data from cadavers and suggested to the International Standards Organisation (ISO) working group 6 that a 15ms window should be used to calculate the HIC value.

At present, the standard practice is that the 15ms window is used in pedestrian protection, whereas a 36ms window is used to calculate the HIC value in occupant protection.

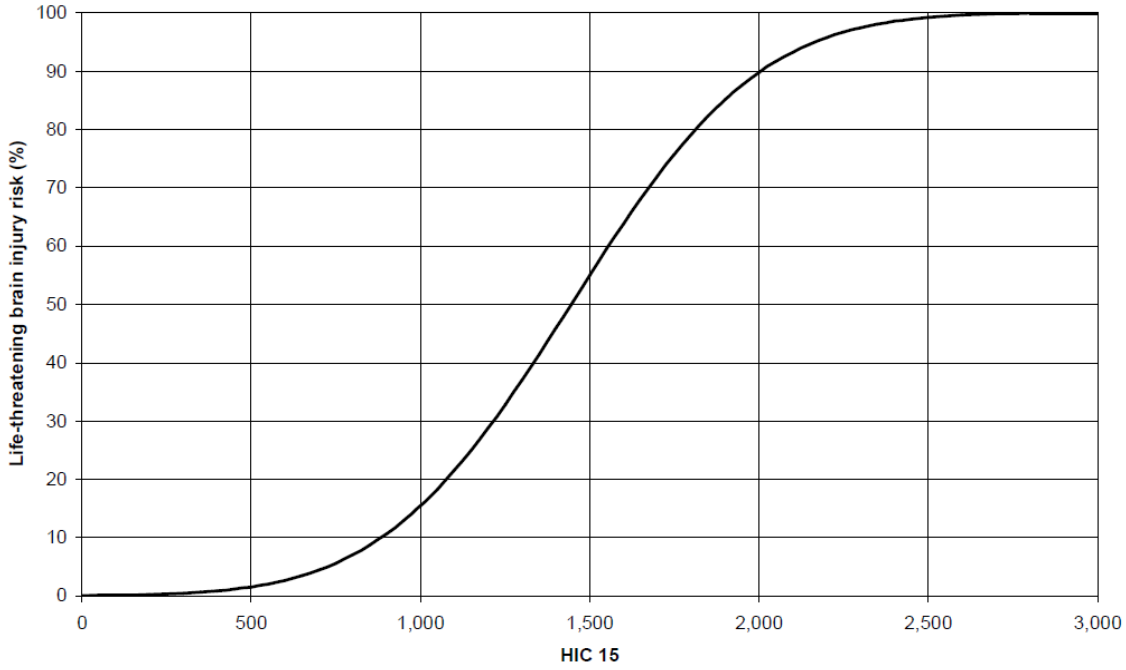

Figure 3.5: Head injury risk curve (Lawrence)

Prasad and Mertz also developed a Head Injury Risk Curve (HIRC) as shown in Figure 3.5, which implies that a HIC value of 1400 results in a 50% probability of life threatening brain injuries and a HIC value of 1000 results in 16% probability of life threatening brain injuries. At present, a HIC value of 1000 is used as the compliance threshold and in consumer metric assessments for pedestrian protection.

3.3.1 Accuracy

In the head impact test, other variables such as impact velocity, head form displacement, peak acceleration, impact duration, time at peak acceleration, and time at rebound also influence the severity of injuries. Zhou (Zhou 1997) derived analytical equations to describe the relationships among these variables using single peak pulses recorded from Federal Motor Vehicle Safety Standard No.201 head protection tests.

The current formula used to calculate the HIC value in pedestrian protection comprehends neither the effects nor measures the thresholds of the upper torso contact with hood before head contact, neck elongation, effects of rotational acceleration or angular acceleration. However, the study conducted to analyse the probability of mild traumatic brain injury in living human beings shows good correlation with the injury probability for any given value for the HIC, as shown in Figure 3.6. This study was based on a large set of head impact data taken from American football players (Funk et al. 2007).

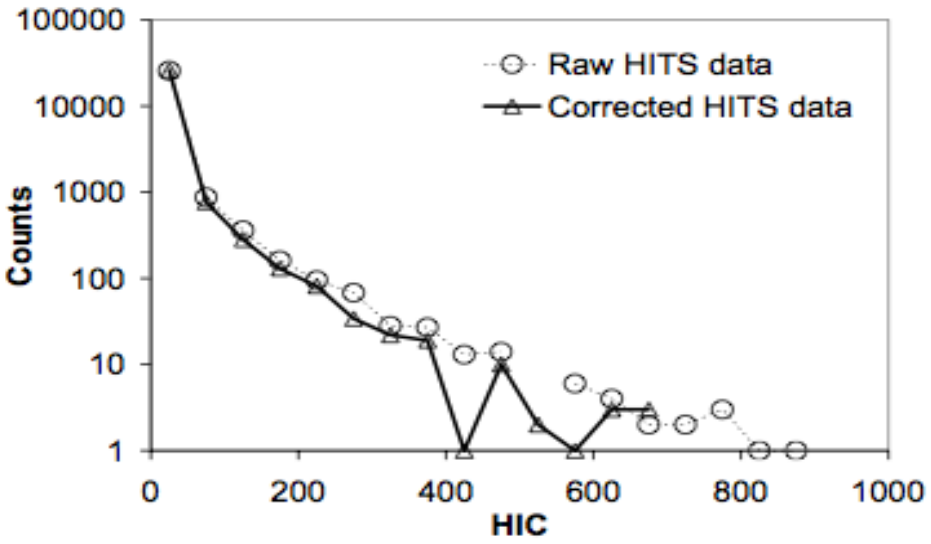

Figure 3.6: Head impacts at various severity levels grouped in HIC value increments of 50 (Funk et al. 2007)

3.4 Optimal waveform

A waveform is the plot of resultant acceleration against time and the shape of the curve describing the relationship between the resultant acceleration and time. Meeting the requirements of the HIC value with the lowest deformation space requires balancing hood stiffness and deformation space, as discussed in chapter 1. The parameters that affect the HIC value are impact velocity, available deformation space, magnitude of peak acceleration and pulse duration. From the Equation 3.3, the resultant acceleration and pulse duration are key factors that affect the HIC value. The impact velocity and the available deformation space affect these key factors. The impact velocity is constant in regulatory and consumer metrics tests. Therefore, the main factors that affect the HIC value are the structural stiffness and the deformation space, which depend on the shape of the waveform.

In 1995, Lim et al. explored options to develop a methodology for estimating the minimum deformation space required in an impact to a pedestrian head. They used generic waveforms and idealised waveforms of square waves, sine waves, and half–sine waves in formulating equations for deformation space requirements.

They used area ratio method to determine the waveform efficiency. In the area ratio method, they used ratios of areas under the acceleration–intrusion curves to determine the efficiency of the waveform, as shown in Figure 3.7 and Equation 3.4:

$$\eta = \frac{A_1}{A_2} \qquad \textbf{Equation 3.4}$$

In which η = efficiency, A_1 = area enclosed by the acceleration–displacement curve of the given waveform and the horizontal plane, A_2 = area of the shape that encloses the geometrical shape of the acceleration–displacement curve of the given waveform.

With this method, the square waveform was determined as the most efficient waveform, with 100% efficiency (Figure 3.7). Lim and his team calculated the efficiency of the other waveforms by benchmarking against the square waveform. Thus, the waveform efficiency of a sine waveform was determined as 63.66% and of a half–sine waveform as 50%.

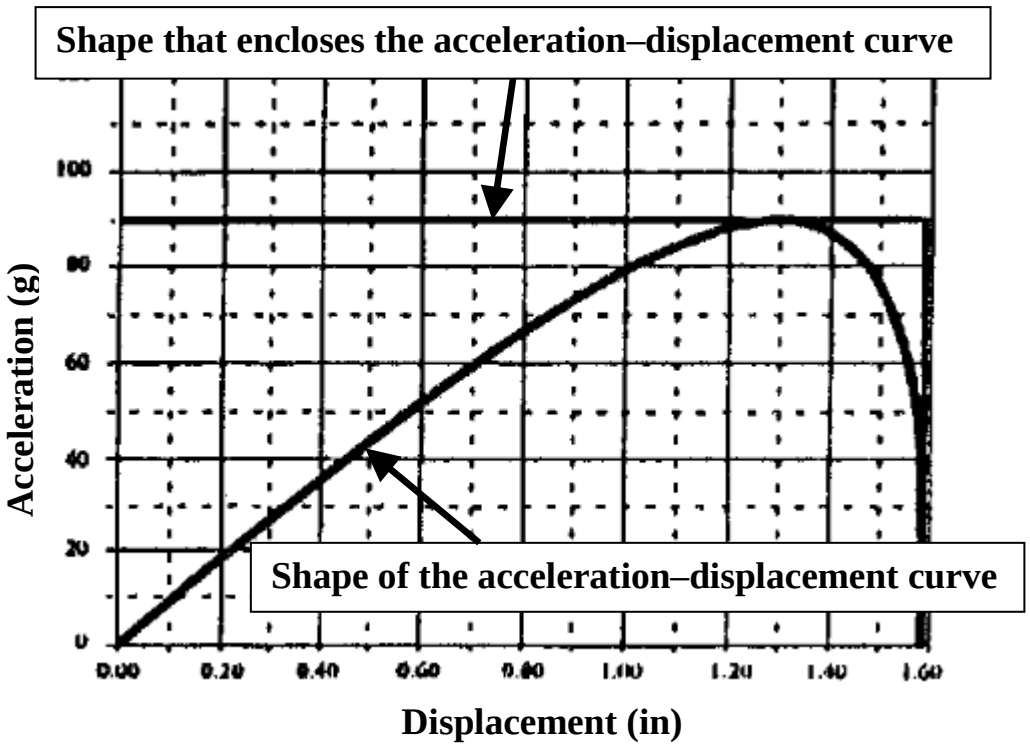

Figure 3.7: Waveform efficiency (η) of a half–sine waveform (Lim et al. 1995)

In 2007, Wu and Beaudet (Wu & Beaudet 2007) challenged the optimality of aiming at the square waveform to achieve the minimal deformation space required to obtain a given HIC value. They derived a realistic optimal waveform that is more practical based on the theoretical optimal waveform, which is WSTC.

As discussed in previous chapters and shown in Equation 3.5 below, HIC value calculation is the average of head acceleration a(t) over an interval t_1 to t_2, followed by a(t) is raised to the 2.5th power and multiplied by the interval. The condition for selection of the interval is that it should provide the maximum result within the 15ms window:

$$HIC = max\left\{\left[\frac{1}{t_2 - t_1}\int_{t_1}^{t_2} a(t)dt\right]^{2.5}(t_2 - t_1)\right\} \qquad \textbf{Equation 3.5}$$

To achieve the maximum result for HIC value for a given magnitude of peak acceleration, the acceleration between t_1 and t_2 should be equal, which produces a square waveform. Therefore, assuming $a(t_1) = a(t_2)$, Wu and Beaudet derived the formula to calculate the maximum intrusion of the hood, which produces a square waveform in a pedestrian head impact as shown in Equation 3.6:

$$d = 11.12 \times 10^{-3}\frac{v_0^{\frac{8}{3}}}{HIC^{\frac{2}{3}}} \qquad \textbf{Equation 3.6}$$

Where d = maximum intrusion in metres, v_0 = impact velocity in m/sec.

Wu and Beaudet stated that numerous other waveforms show same HIC value with smaller deformation space requirements. They concluded that the square waveform is ideal when the criterion is either maximum head acceleration or force. Since HIC is the criterion for head impact, the function derived is directly related to WSTC, which proposes that the head can tolerate large head acceleration for a very short duration and smaller head acceleration for a longer duration.

Therefore, they considered WSTC as the optimal waveform and derived the equation for calculating the head travel or deformation space as stated in Equation 3.7:

$$d = \int v \times dt = 8.342 \times 10^{-3} \times \frac{v_0^{\frac{8}{3}}}{HIC^{\frac{2}{3}}}$$ **Equation 3.7**

Waveform	Deformation space in impact direction (mm)
Optimal	50.50
Square	67.32
Sine	79.49
Half–sine	96.38
Isosceles triangle	83.97
Ramp–up triangle	111.94
Ramp–down triangle	55.98

Table 3.3: Comparison of deformation space requirements for various waveforms

Comparison of the deformation space requirement for a HIC value of 1000 at 40km/h impact velocity of the optimal waveform and other waveforms reveals that the optimal waveform requires the least amount of deformation space and the second best is the ramp–down triangle waveform. Ramp–up triangle waveform in Table 3.3 refers to a triangular waveform with late peak in which the resultant acceleration gradually increases over time and drops down over a short period. Ramp–down triangle waveform is the triangular waveform with early peak in which the resultant acceleration increases from zero to peak within a short period and

decreases gradually. Wu and Beaudet did not consider rebound in these calculations for simplicity.

The optimal waveform (WSTC) suggests that head acceleration could be infinite at time zero, but in reality, this is impossible. Therefore, Wu and Beaudet considered the optimal waveform as the theoretically optimal waveform. When t_p equal a 2ms, delay is applied to obtain peak acceleration, the theoretically optimal waveform becomes realistic and efficient, thus realistic optimal waveform as shown in Figure 3.8.

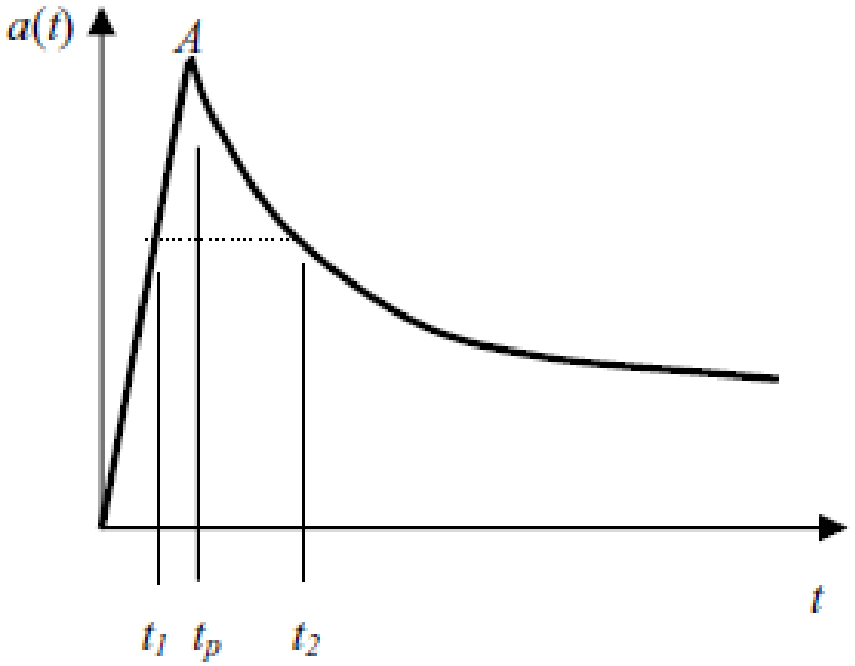

Figure 3.8: Realistic optimal waveform for pedestrian head impact (Wu & Beaudet 2007)

With the realistic optimal waveform, they stated that as design guidance, the deformation space required to obtain a HIC value less than or equal to 1000 is 60mm for a child head at 40km/h impact velocity. For adult head impact, they suggested that the deformation space required is 12% more than the child head impact, due to the steeper impact angle.

In the research presented in this thesis, the impact performance offered by a vehicle to the child head has been tested with 60mm of deformation space as a starting point. Wu and Beaudet derived the value of the required deformation space using theoretical calculations ignoring rebound and other parameters that could influence the head impact performance. In practice, the value of the deformation space required to meet the compliance threshold homogeneously will be higher than 60mm.

3.5 Vehicle design for pedestrian protection head impact

It has been proven (Cavallero & ONSER 1983) that the design of the frontal structure of cars has a substantial effect on the severity of pedestrian injuries in a pedestrian collision with a passenger car.

Currently, the auto industry is evaluating both the passive hood and the active hood for head impact. The main design objective for both is to cushion pedestrian head impact.

The passive hood is where the hood assembly is designed with the required deformation space between the hood assembly and the rigid under hood components.

The active hood pops up in a collision with a pedestrian to provide the required deformation space between the hard components within the engine bay and the hood assembly. The advantage of using this type of hood is that the hood assembly does not need the required deformation space for pedestrian protection when the hood assembly is in closed condition.

Figure 3.9 illustrates the hood pop in a pedestrian collision to the front–end of a car and Figure 3.10 shows one of the mechanisms used to pop the hood up in a pedestrian collision to the front–end of a car.

Figure 3.9: Active hood in a pedestrian impact scenario (Autoblog 2005)

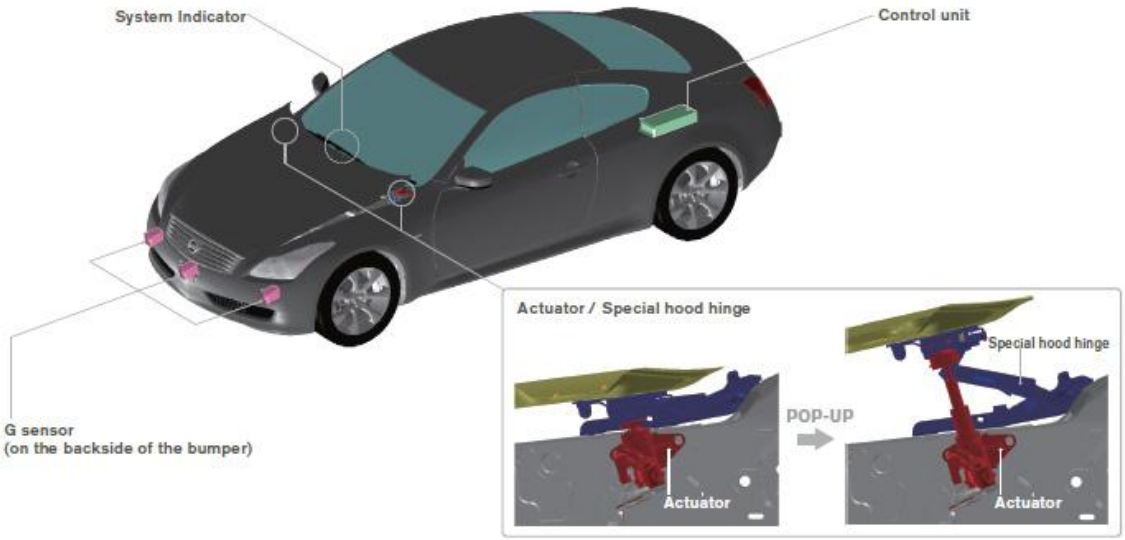

Figure 3.10: Pop-up hood hinge (Nissan)

Designing a car to reduce the HIC value for head impact on a windscreen frame has been a challenge for decades. It is still a challenge for a passive hood solution. In 2009, Autoliv published its innovation (Autoliv 2009), the Pedestrian Protection Airbag (PPA) with an active hood that has a pair of airbags, one at each A–pillar. Activation of the hood and deployment of these airbags in a pedestrian collision to the front–end of a passenger car (Figure 3.11) uses a sensor system.

Figure 3.11: Airbag to cushion pedestrian impact on the A-pillar (Autoliv 2009)

However, there are many disadvantages and uncertainties in using this type of hood. In 2003, Krenn et al. (Krenn et al. 2003) evaluated the active hood and listed some questions that need to be discussed in developing the active hood. They are:

- stiffness of the hood
- generation of free edges on the sides of the hood

- penetration of the hood through the windscreen into the interior of the car in case of a frontal crash
- sensor detection of a pedestrian
- behaviour of drivers, in case of hood activation.

In 2004, Bernd et al. (Bernd et al. 2004) identified that recognition of a pedestrian collision with a passenger car is the critical problem in using the active hood. At present, not all vehicle manufacturers consider the active hood because it also increases mass and cost of the vehicle.

In 1979, a team of doctors and engineers (Cavallero et al. 1983) conducted a study using cadavers and suggested that the vehicle front–end of passenger cars requires specific alterations to reduce pedestrian injuries. They concluded that the vehicles used in their research had great similarity and did not clearly outline the alterations required in vehicle design.

In 1980, Ashton assessed a sample of real accidents and weighed the benefits obtained by two different strategies in vehicle design (Ashton 1980). One strategy was to use vehicle design to reduce the frequency of serious head injuries, while the other was to reduce the frequency of leg and pelvic injuries by vehicle design. He concluded that adopting both strategies in vehicle design offers more reduction in seriously injured and killed pedestrians than adopting either strategy in isolation.

In 1969, Segal (Cornell Aeronautical Laboratory Inc. 1971) concluded that the height of the hood leading edge might influence pedestrian head impact location and severity. Nowadays, the height of the hood leading edge is low in passenger cars, primarily to improve aerodynamic drag, thus improving fuel economy.

In 1982, Fowler and Harris (Fowler 1982) conducted a study to determine the level of pedestrian protection that can be provided by practical car design measures such as hood leading edge height. They suggested that it is possible to reduce the severity of upper leg impact with medium and high hood leading edge heights. The change in hood leading edge height influences head impact velocities. They concluded that detailed study should be conducted on stiffness and geometric variations.

In 2003, Ikeda and Ishitobi (Ikeda et al. 2003) compared steel and aluminium inner hoods with the same beam type with consideration of the Euro NCAP child pedestrian impact protocol. The stiffness of both outer hoods was fabricated the same, by increasing the thickness of the aluminium hood. They increased the thickness of the aluminium inner hood to meet the bending and torsional rigidity of the steel hood. They revealed that the initial energy absorption of the aluminium hood is less than that of the steel hood.

They also compared wave type and beamless hood inners with reduced thickness in comparison with beam type aluminium inner hoods. They reported that the first impact acceleration for the wave type hood is larger than the other two types. They also stated that the displacement contour for the wave type is wider than the other two types. Thus, they concluded that the waveform of the inner hood structure would improve energy absorption in the first impact, therefore decreasing the HIC value for pedestrian protection. They however, did not consider other geometries such as the skeleton structure and multi–cone for the inner hood.

Figure 3.12: Multi–cone structure for inner hood (A2Mac1 2010)

Figure 3.13: Skeleton structure for inner hood (A2Mac1 2010)

Figure 3.14: Cut–out structure for inner hood (A2Mac1 2010)

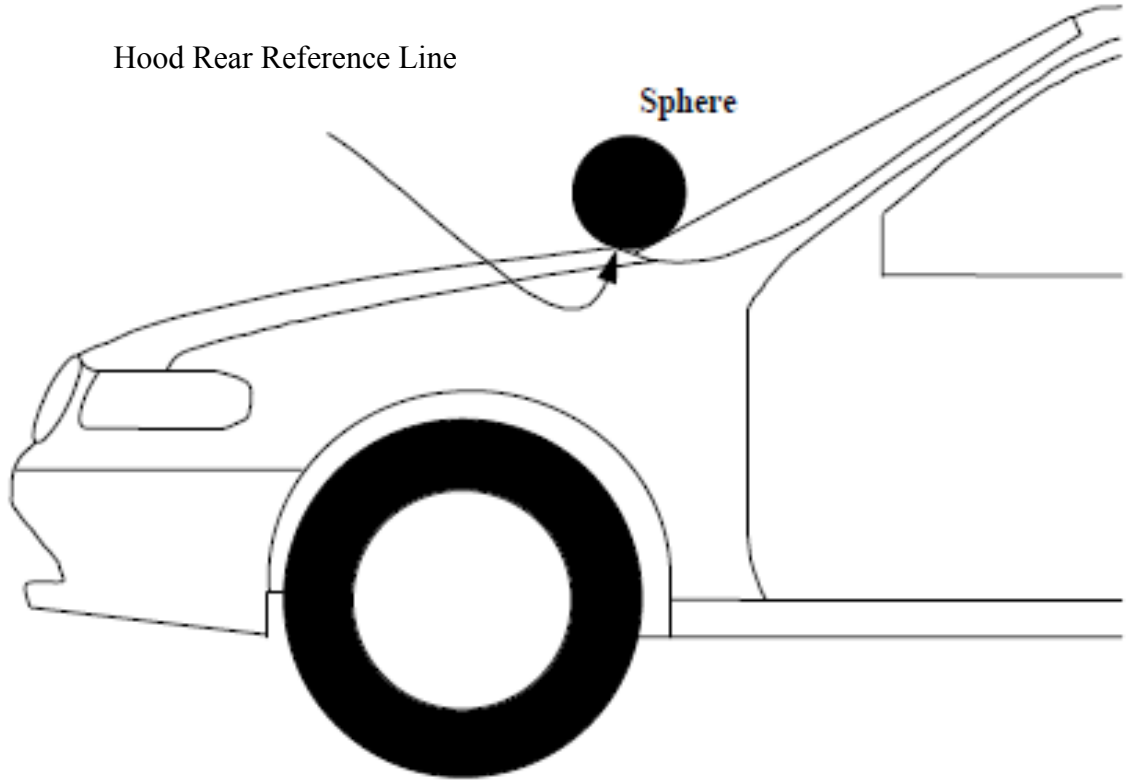

Figure 3.15: Hood rear reference line (United Nations Economic Commission for Europe 1998)

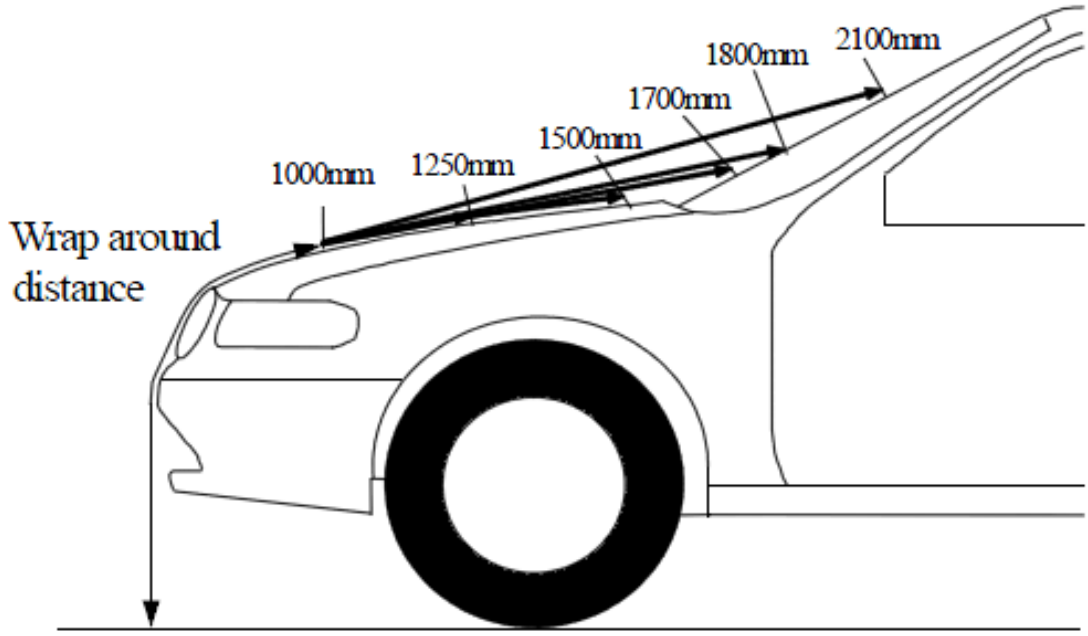

Figure 3.16: Wrap Around Distance (United Nations Economic Commission for Europe 1998)

In 2008, a study was conducted (Baleki & Ferreira 2008) comparing three different inner hood geometries in steel for HIC value and head form intrusion. They compared multi–cone (Figure 3.12), skeleton (Figure 3.13) and cut–out (Figure 3.14) geometries for the inner hood. They concluded that cut–out structure is good for mass reduction but more deformation space is necessary to meet HIC value requirements. The skeleton structure design was recommended for larger hoods where the 1500 Wrap Around Distance (WAD) is forward of the Hood Rear Reference Line (HRRL) as presented in Figure 3.15. The Multi–cone design is the heaviest option of the three and it was recommended for smaller hoods where the 1500 WAD as shown in Figure 3.16 is rearward of the HRRL. Nevertheless, they did not state the performance of other materials such as aluminium for these inner hood geometries.

Due to the lack of this information, the research in this thesis studies the performance of various inner hood structures and materials for hood panels.

Chapter 4

Vehicle design requirements

4.1 Evolution of vehicle design requirements for pedestrian protection

Four regulatory groups; the NHTSA, European Enhanced Vehicle–safety Committee (EEVC), ISO and IHRA, have been working on developing test procedures to evaluate the level of pedestrian protection offered by new vehicles. Working groups of the EEVC were the first to perform several research activities to develop a test procedure for evaluating the pedestrian protection offered by any passenger vehicle's front–end.

The records show that research and development related to vehicle design for pedestrian protection started in 1969 (Cornell Aeronautical Laboratory Inc. 1971). In 1982, EEVC Working Group 7 (EEVC WG7) analysed injury patterns and sources of injury in a pedestrian collision with a passenger car. As discussed earlier, the data showed that head and lower extremities incurred severe injuries most frequently. As a result, EEVC WG7 proposed test methods and regulations to assess head and leg injuries for pedestrian protection. The EEC ad

hoc working group known as ERGA Safety, which concluded that additional research is required to improve these regulations, discussed these test methods.

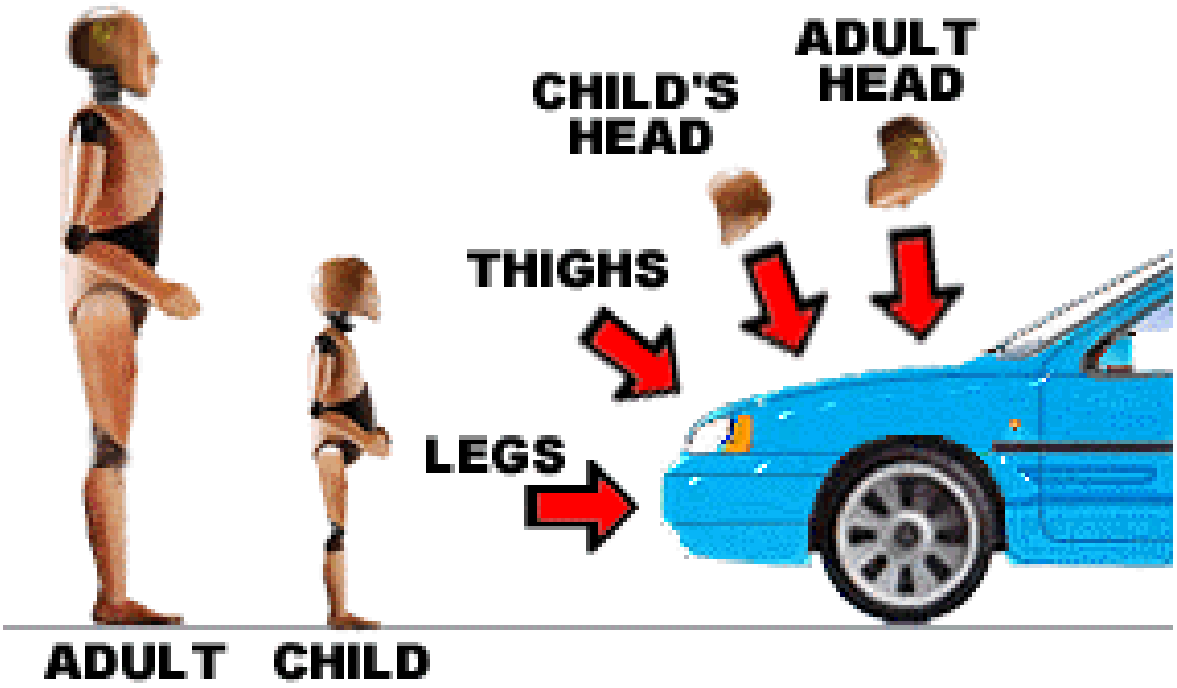

Figure 4.1: Pedestrian protection testing (Safe car guide 2009)

In 1987, EEVC Working Group 10 (EEVC WG10) was set up with a mandate to improve these regulations. In 1996, they proposed a test protocol for pedestrian protection in a PPCFC (Figure 4.1). EEVC Working Group 17 (EEVC WG17) revised these procedures to improve test methods evaluating pedestrian protection in 1998 and updated them in 2002.

In July 2001, the European Automobile Manufacturers Association (ACEA) passed on a commitment relating to the protection of pedestrians and cyclists to the European Commission. This agreement followed months of negotiations between the Commission and ACEA and is part of a total Industry Commitment (IC) including the Japanese (JAMA) and Korean (KAMA) Automobile Manufacturers Associations.

The IC proposed a phased–in approach, combining passive and active safety requirements (head and leg impacts), to improve pedestrian protection in collisions with motor vehicles. The active safety measures were the banning of bull–bars, mandatory equipment with Anti–lock Brake Systems (ABS) and Daytime Running Lights (DRL), to help prevent accidents from occurring. The passive safety measure included a series of subsystem tests to evaluate the vehicle design where the resulting injury levels must be below the prescribed limits.

These procedures involved testing with subsystems for the head, pelvis and leg areas for a number of reasons. Firstly, it may be very difficult to achieve repeatability with full–body dummy testing. Secondly, full body testing can be time consuming and expensive, as it requires a number of dummies to represent various age groups, sizes and shapes. However, the Society of Automotive Engineers (SAE) is developing a criterion for a full–scale pedestrian crash dummy. Honda developed POLAR III, a full–scale pedestrian crash dummy. Nevertheless, none of the assessments for pedestrian protection considers full–scale pedestrian dummies in their testing. The subsystem tests proved to replicate the real world scenario within acceptable limits at low cost.

The ISO and the IHRA pedestrian safety working groups also developed pedestrian protection test procedures. The head impactor mass, impact speed and impact angle were the main differences between these procedures and EEVC test procedures. The world forum for the harmonisation of vehicle regulations, named the “United Nations Economic Commission of Europe Working Party 29 – UNECE WP 29” has been developing the GTR–9 on pedestrian protection. The procedures developed by the IHRA served as a basis for the GTR–9. In addition, the NHTSA terminated development of a pedestrian head impact requirement in the 1990s and supported the IHRA. Therefore, the focus has shifted from the ISO working

group to the IHRA to develop an international procedure to evaluate the pedestrian protection offered by a passenger vehicle.

Japan has developed pedestrian protection regulations based on the EEVC test procedure. At present, these regulations only test head impact performance and do not include leg and pelvis impact performances.

4.2 Regulatory vehicle design requirement for pedestrian protection

At present, only Europe and Japan have enforced regulatory requirements to assess pedestrian protection offered by a vehicle as vehicle design rules.

4.2.1 European commission directive 2003/102/EC: EURO Phase I

EURO Phase I has been implemented as part of the vehicle design regulatory requirements which apply to all motor vehicles of category M1, of a total permissible mass not exceeding 2500kg, and to N1 vehicles derived from M1, of a total permissible mass not exceeding 2500kg, in the EU. Implementation was required between 2005 and 2012, so all vehicles sold in this category in EU have to meet European commission directive 2003/102/EC: EURO Phase I until 2012.

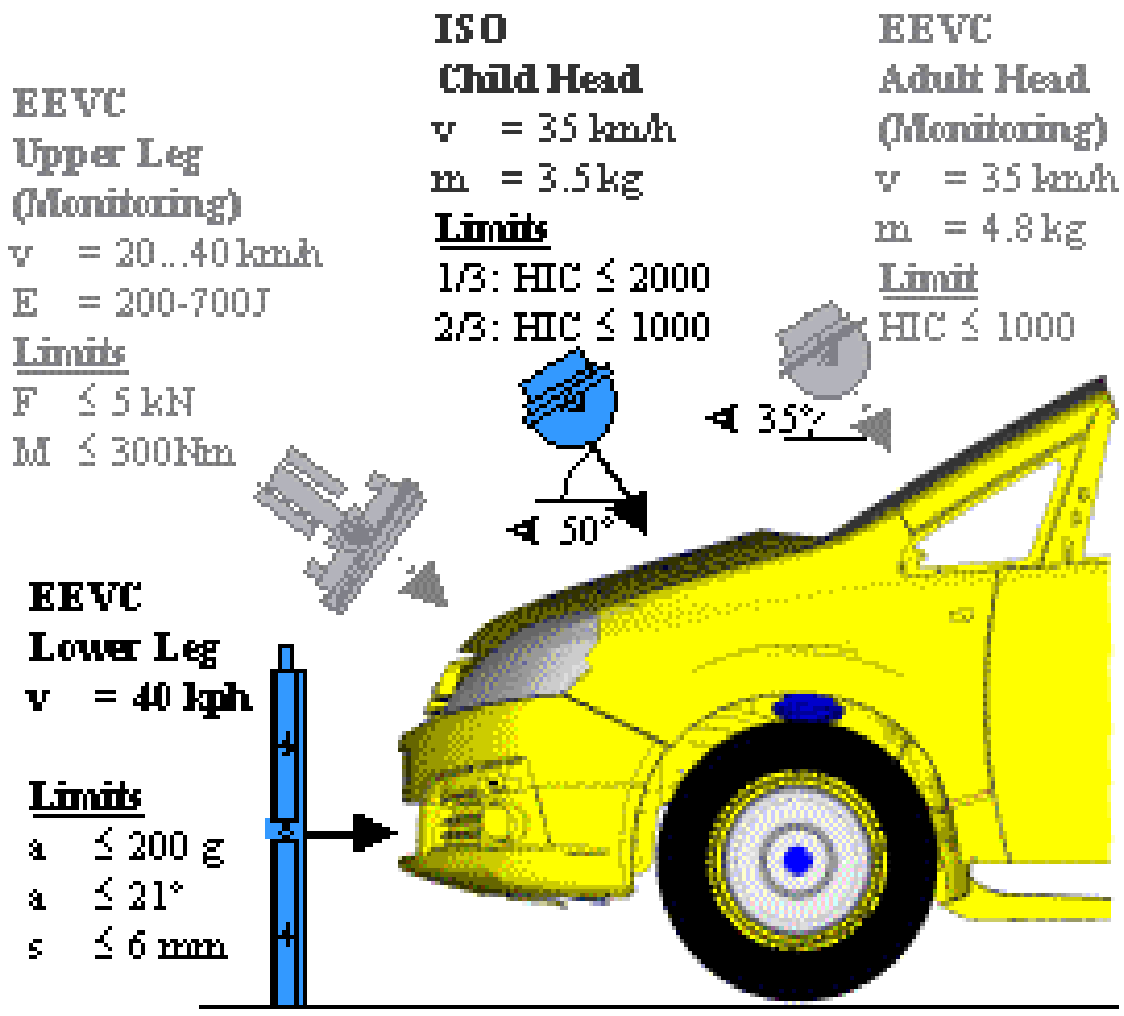

Figure 4.2: Pedestrian protection technical requirements phase I (Wanke, Thompson & Christoph 2005)

EURO Phase I test protocol (The European Parliament and of the council 2003) included four subsystem tests to evaluate the protection offered to the pedestrian in a collision with a passenger car (Figure 4.2). They are:

- lower leg form fired at 40kmh to bumper system
- upper leg form fired at 20 to 40kmh (depending on vehicle shape) to the hood leading edge
- child head form fired onto the hood top at 50° to the horizontal plane, at 35kmh
- adult head form fired onto the windscreen at 35° to the horizontal plane, at 35kmh.

4.2.1.1 Head impact

The head impact area is divided into three equal parts.

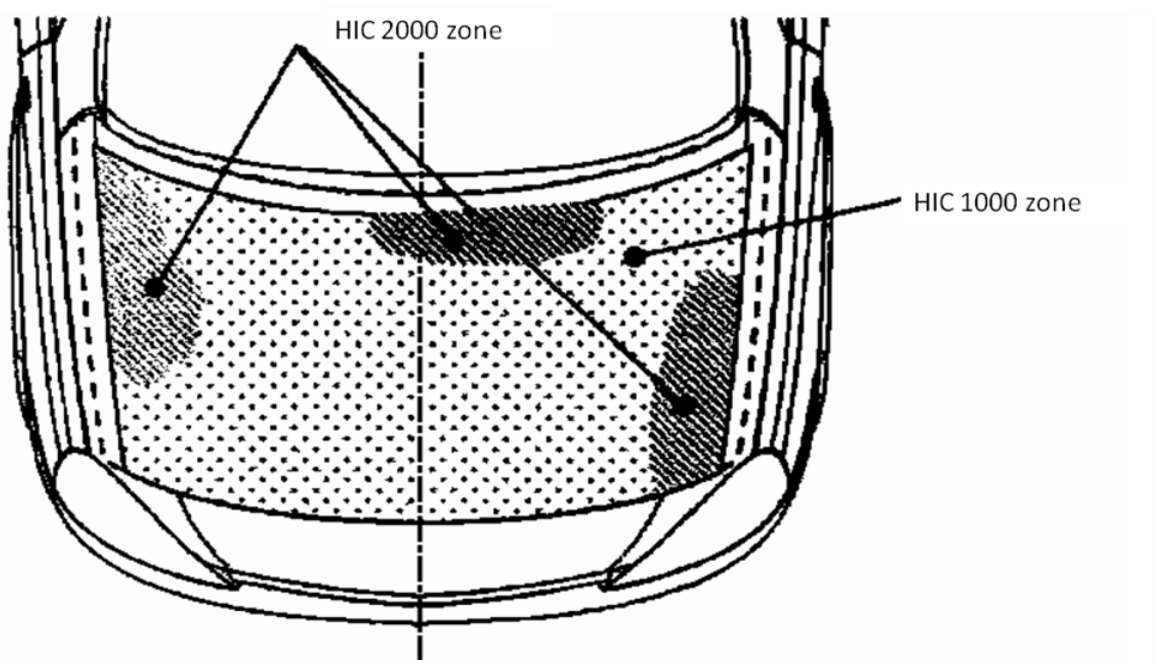

Figure 4.3: Head impact area defined by Euro Phase I

Vehicle manufacturers identify two thirds of the impact area (Figure 4.3) zoned as 'HIC1000' and one–third zoned as 'HIC2000'. The assessment requirements are that the HIC value should not exceed 1000 for two–thirds of the test area and 2000 for one–third of the test area. A minimum of eighteen tests need to be conducted, twelve in the HIC1000 zone and six in the HIC2000 zone. This protocol tests only the protection offered to the child head in this head impact area.

4.2.1.2 Lower leg impact

This protocol tests the protection offered to the lower leg by positioning the bottom face of the impactor at ground level.

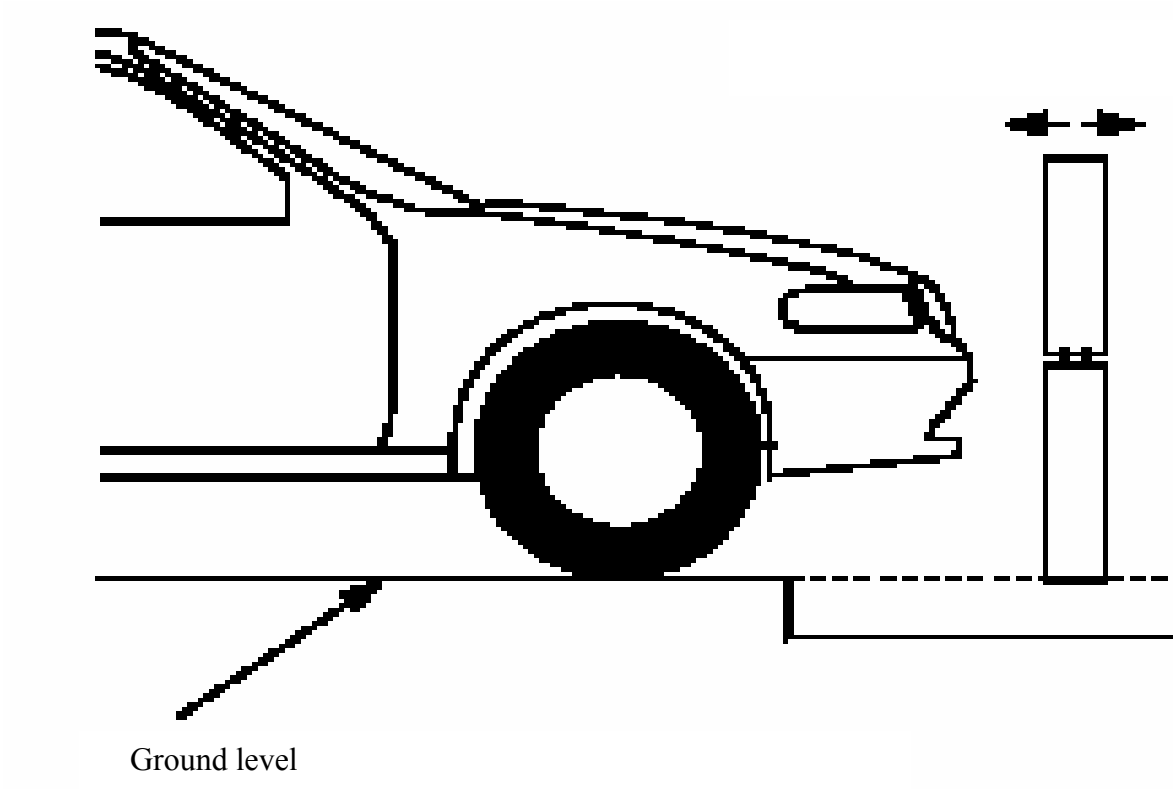

Figure 4.4: Lower leg impactor position defined by Euro Phase I

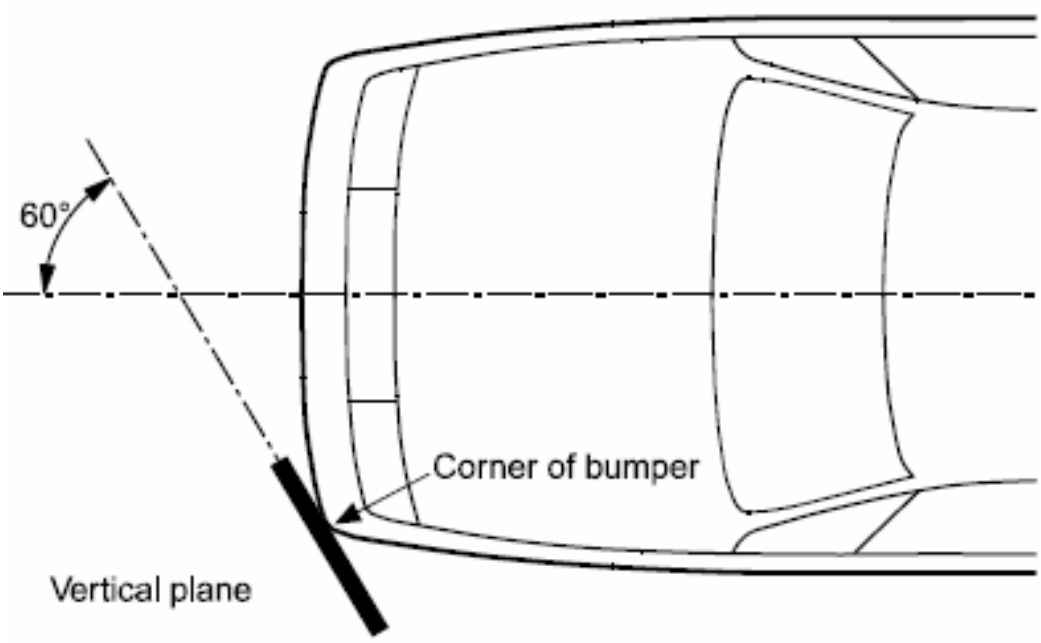

Figure 4.5: Bumper corner defined by Euro Phase I

Figure 4.4 shows the impactor and ground level position. The area between the two bumper corners defines the lower leg impact area (Figure 4.5). The resulting injury values of the lower leg within the lower leg impact area in the evaluation of vehicle design must be below a set of prescribed bounds.

4.2.1.3 Upper leg impact

The upper leg impact test is for monitoring purposes only which means that the injury data is not published but collected to get a better understanding about the injury patterns and vehicle designs.

4.2.2 European Commission Directive 2003/102/EC: EURO Phase II

Phase II regulations would have taken effect from 2010 and phase in until 2015. The European Commission has published a summary of the results of its consultation on the Phase II Directive (2003/102/EC) (The European Parliament and of the council 2003) with the auto industry.

The main technical requirements are shown in Figure 4.6. The respondents pointed out inherent difficulties in implementing phase II. This review on the feasibility of 2003/102/EC–Phase II concluded in 2007 and proposed many changes to the testing protocol. These proposed changes served as a base for the GTR–9 that was published in February 2009.

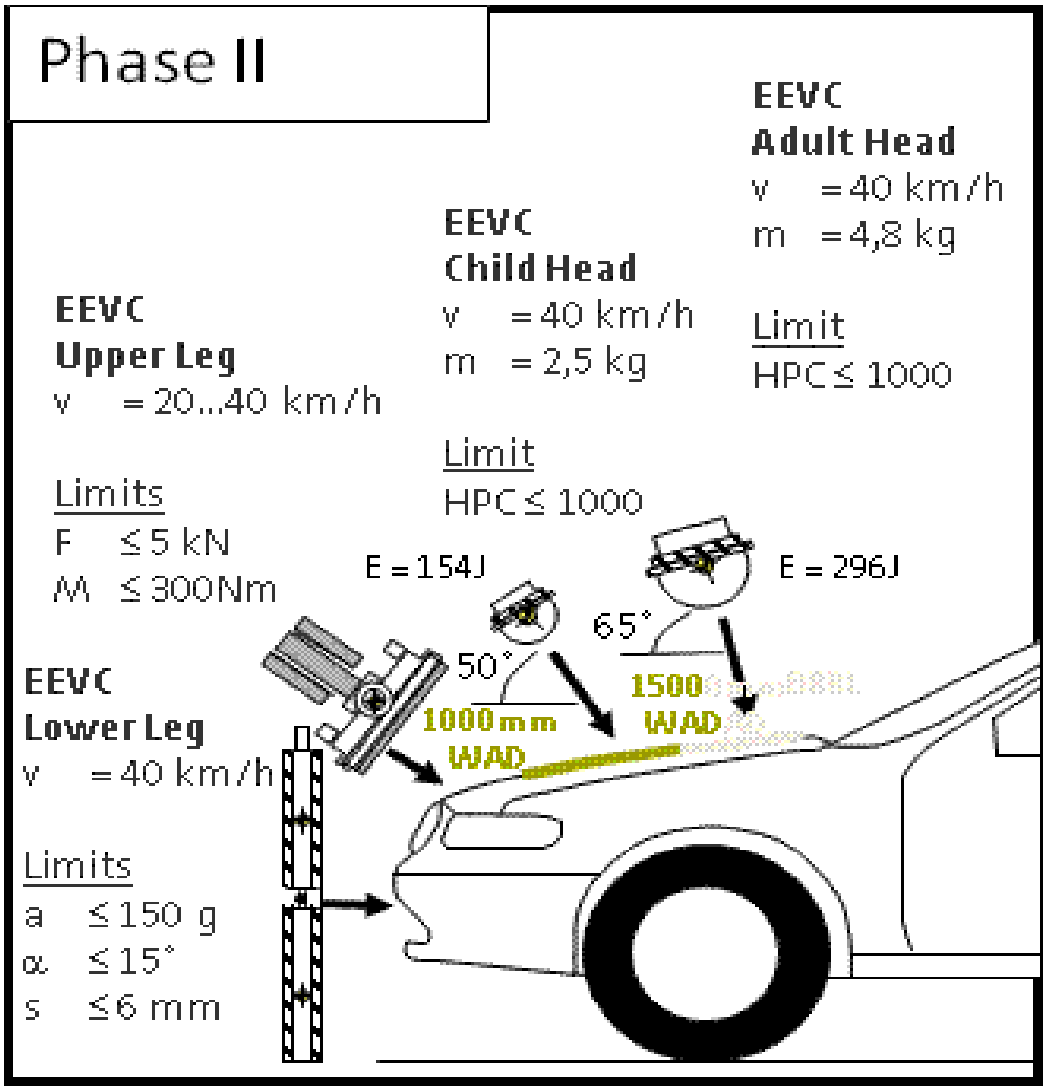

Figure 4.6: Pedestrian protection technical requirements of phase II (Kerkeling, Schafer & Thompson 2005)

4.2.3 Regulatory requirement for pedestrian protection in Japan

All new types of passenger cars and their derivatives from September 2005 were required to meet vehicle design regulations for pedestrian protection in Japan.

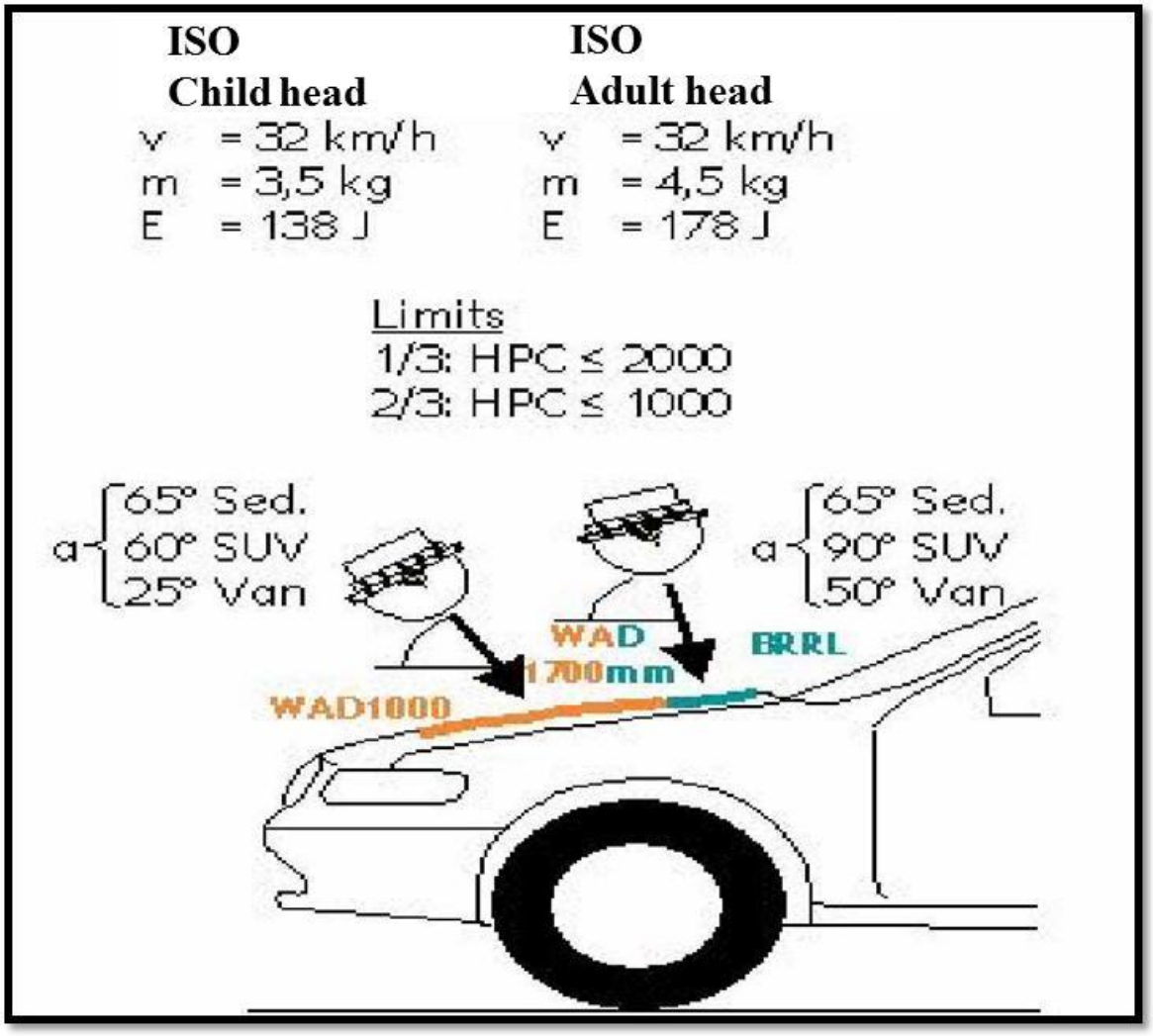

Figure 4.7: Legal requirements for pedestrian protection in Japan (Kerkeling, Schafer & Thompson 2005)

The main assessment criteria are shown in Figure 4.7. All new registrations for passenger vehicles and their derivatives after September 2010 must comply with these regulations. Currently, only pedestrian head protection is assessed by this vehicle design rule in Japan, and protection to the lower or upper leg is not assessed.

4.2.4 Global technical regulations for pedestrian protection (GTR-9)

As mentioned earlier, the GTR–9 has adopted the test procedures developed by the IHRA. Active and passive components are included so as to ensure the same level of pedestrian protection as 2003/102/EC–Phase II. The active component mandates fitting of Brake Assist, a system designed to sense an emergency braking situation and assist the driver in achieving the maximum possible deceleration in the prevailing conditions, thus reducing the braking distance. The passive Component includes a series of subsystem tests where the resulting injury levels must be below the prescribed limits. This component of GTR–9 requires a careful vehicle design that reduces the probability of severe head and lower leg injury to pedestrians in a collision with the car.

Europe, Japan, China, United States of America, India, Korea and Australia are the few among the many countries plan to adopt these regulations as vehicle design regulatory requirements for pedestrian protection. Negotiations are in progress with automakers and governments globally regarding the timing for enforcing GTR–9.

Regulation	EURO Phase-I	EURO Phase-II	JAPAN	GTR-9
Child head impact	Mass=3.5kg Diameter=165mm Velocity=35km/h Angle=50° Impact zone on the hood	Mass=2.5kg Diameter=130mm Velocity=40km/h Angle=50° Impact zone up to WAD1500	Mass=3.5kg Diameter=165mm Velocity=32km/h Angle=Varies with body style Impact zone up to WAD1700	Mass=3.5kg Diameter=165mm Velocity=35km/h Angle=50° Impact zone up to WAD1700
Adult head impact	Monitoring only	Mass=4.8kg Diameter=165mm Velocity=40km/h Angle=65° Impact zone from WAD1500 to HRRL	Mass=4.5kg Diameter=165mm Velocity=32km/h Angle=Varies with body style Impact zone from WAD1700 to HRRL	Mass=4.5kg Diameter=165mm Velocity=35km/h Angle=65° Impact zone from WAD1700 to HRRL
Lower leg Impact	Mass=13.4kg Diameter=132mm Velocity=40km/h Height from ground=0mm	Mass=13.4kg Diameter=132mm Velocity=40km/h Height from ground=0mm	Not Tested	Mass=13.4kg Diameter=132mm Velocity=40km/h Height from ground=25mm
Upper leg impact	Monitoring only	Velocity=20 to 40km/h	Not Tested	Monitoring only

Table 4.1: Comparison of pedestrian protection regulations

The GTR–9 test protocol required four subsystem tests to evaluate the vehicle design for protection of pedestrians in a collision with a passenger car (Table 4.1). They are:

- lower leg form fired at 40kmh to bumper system
- upper leg form fired at 20 to 40kmh (Depending on vehicle shape) to the hood leading edge
- child head form fired at 35kmh to the hood top, at an angle of 50° to the horizontal plane
- adult head form fired onto the hood top at an angle of 65° to the horizontal plane, at 35kmh.

4.2.4.1 Head impact

The total head impact area is determined in a similar manner to the European Commission Directive. Two thirds of the total impact area (Figure 4.3) zoned as ‘HIC1000 and one–third zoned as ‘HIC1700’. The HIC1000 zone must contain at least half of the child impact area. This regulation tests the protection offered to both the child and adult head in this impact area. The impact area for the child head is between 1000 WAD and 1700 WAD. The adult head impact area is between 1700 WAD and 2100 WAD. The impact area does not include the windscreen.

4.2.4.2 Lower leg impact

The bottom face of the lower leg impactor is positioned 25mm above the ground level. The area between the two bumper corners is the lower leg impact area (Figure 4.5). The resulting injury values for the lower leg within the lower leg impact area must be below a set of prescribed limits in the evaluation of vehicle design. The bounds for the injury values are:

- tibia acceleration is less than or equal to 170g
- knee–bending angle is less than or equal to 19°
- knee shear displacement is less than or equal to 6mm.

4.2.4.3 Upper leg impact

The upper leg impact test is for monitoring purposes only.

4.3 Consumer metric vehicle design requirement for pedestrian protection

The various new car assessment programs, usually made up of a consortium of government and non–government safety organisations, have established testing programs in many countries to evaluate new passenger vehicles for safety performance, including pedestrian protection performance, and published the results for consumers.

4.3.1 European New Car Assessment Program (Euro NCAP)

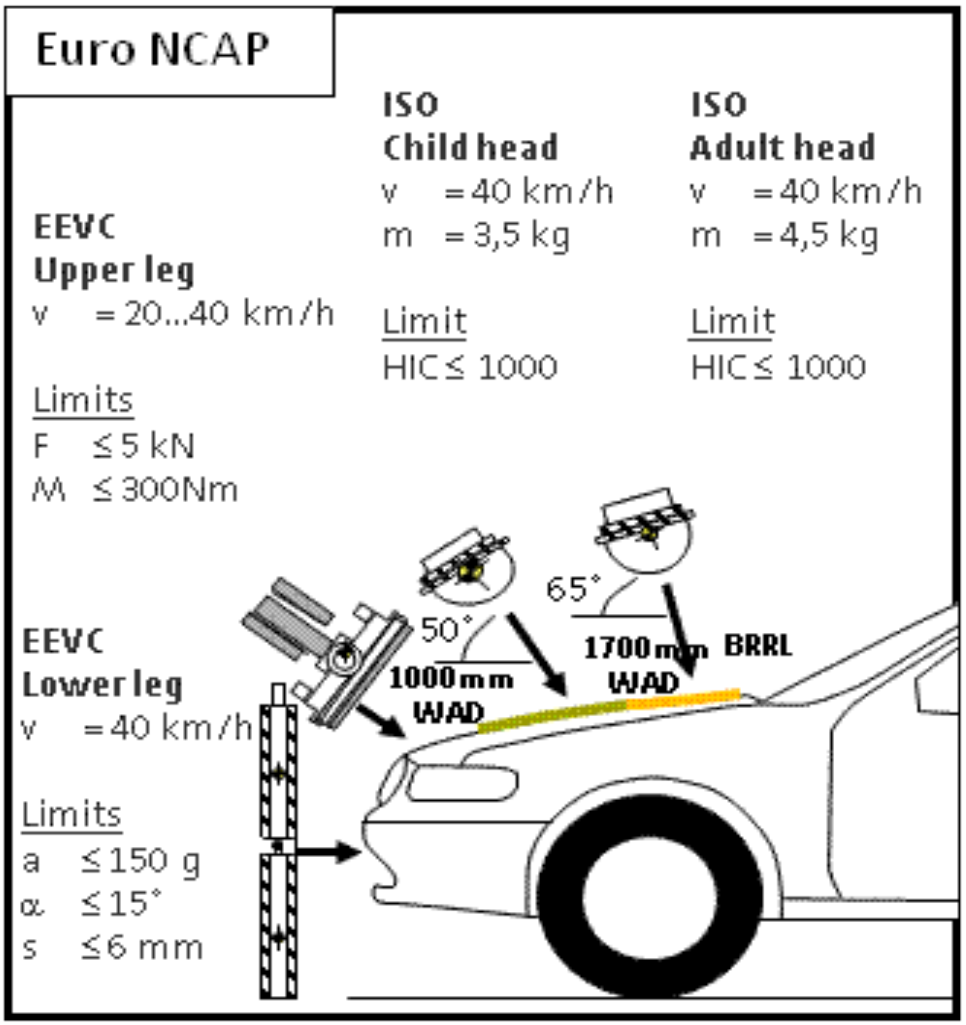

Figure 4.8: Pedestrian protection technical requirements (Euro NCAP 2010)

The pedestrian protection performance rating reported by Euro NCAP is one of the most influential consumer metrics in the European market. The EEVC WG17 pedestrian protection test procedures serve as a base for these test and assessment procedures. The Euro NCAP protocol version 5.3.1, adopted from February 2010, has harmonised the test procedures with the GTR–9. Euro NCAP also proposes four tests through vehicle subsystems (Figure 4.8) similar to those of the GTR–9.

4.3.1.1 Lower leg impact

In this protocol, the lower leg impact area is the area between the bumper corners (Figure 4.5); however, the tests can be conducted outside the impact area if it is deemed injurious. The lower leg impact area is divided into six zones. One point for each subdivision is awarded if the:

- acceleration is less than or equal to150g
- bending angle is less than or equal to 15deg
- displacement is less than or equal to 6mm.

Partial points are awarded if the:

- acceleration is between 150g and 200g,
- bending angle is between 15deg and 20deg
- displacement is between 6mm and 7mm.

Zero points are awarded if the:

- acceleration is more than or equal to200g
- bending angle is more than or equal to20deg
- displacement is more than or equal to7mm.

As mentioned earlier, if the car structure outside the impact area is deemed injurious to the lower leg, the score for the outer most zones will be determined by the results of the test conducted on the most injurious impact point within those zones and outside the lower leg impact area.

4.3.1.2 Head impact

The main difference between GTR–9 and Euro NCAP is the head impact speed. These procedures test the protection to the child head at the front of the hood, whereas the protection to the adult head is at the rear of the hood and occasionally on the front windscreen glass.

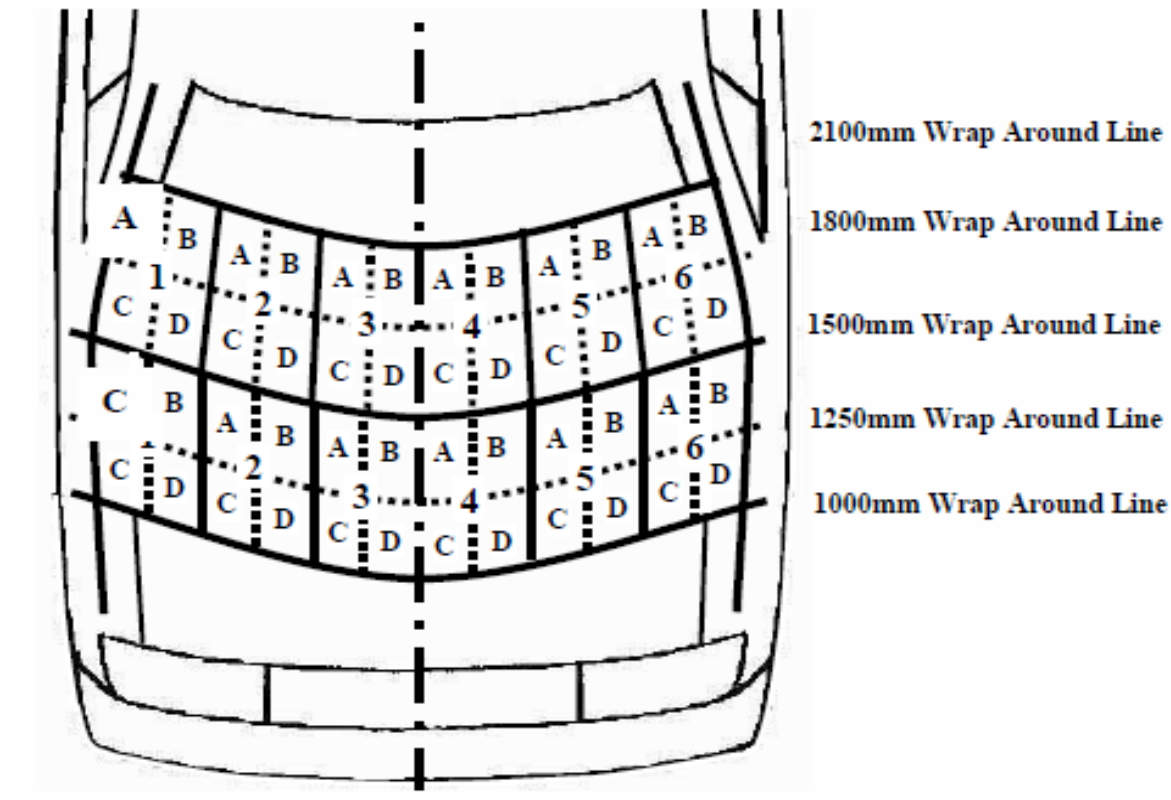

Figure 4.9: Naming head impact zones (Cavallero & ONSER 1983)

This protocol requires a minimum of six tests with each head impactor. There are two impacts carried out in each zone: one impact location with maximum injury potential and the other with minimum injury potential. It prescribes the subdivision of each zone into four quarters and each quarter (Figure 4.9) receives 0.5 points if the HIC value is less than 1000. A linear sliding scale operates between HIC1000 and HIC1350. There are zero points for a HIC value more than 1350.

4.3.1.3 Upper leg impact

The upper leg impact area is divided into six zones. One point is awarded for each subdivision if the:

- force is less than or equal to 5kN
- bending moment is less than or equal to 300Nm.

Partial points are awarded if force is between 5kN and 6kN and bending moment is between 300Nm and 380Nm. Zero points are awarded if the:

- force is more than or equal to6kN
- bending moment is more than or equal to380Nm.

4.3.1.4 Pedestrian protection rating

There is a maximum possible score awarded by Euro NCAP depending on the level of protection offered by a vehicle are:

- 12 points for child head impacts
- 12 points for adult head impacts
- 6 points for lower leg impacts
- 6 points for upper leg impacts.

Therefore, the maximum possible overall score is 36 points. The pedestrian protection rating is awarded as a percentage score. The sum of all the points from these tests determines the overall vehicle star rating as shown in Table 4.2 (European New Car

Assessment Programme 2011). The overall vehicle star rating includes adult protection; child protection; pedestrian protection: and safety assists.

Balance limits for years 2010 and 2011

2010-2011	Box 1: Adult Occupant	Box 2: Child Occupant	Box 3: Pedestrian	Box 4: Safety Assist
5 stars	80%	75%	40%	60%
4 stars	65%	60%	25%	40%
3 stars	35%	30%	15%	25%
2 stars	30%	25%	10%	15%
1 star	20%	15%	5%	5%

Table 3.3c
Balance limits for years 2012

2012	Box 1: Adult Occupant	Box 2: Child Occupant	Box 3: Pedestrian	Box 4: Safety Assist
5 stars	80%	75%	60%	60%
4 stars	70%	60%	50%	40%
3 stars	40%	30%	25%	25%
2 stars	30%	25%	15%	15%
1 star	20%	15%	10%	5%

Table 4.2: Pedestrian protection points required for Euro NCAP overall star rating (Harzheim & Warnecke 2011)

Before 2009, Euro NCAP released three ratings: adult occupant protection, child occupant protection and pedestrian protection. As of 2009, it only releases one overall star rating that combines scores in four areas as mentioned above. Calculation of the overall score involves weighing the points scored in each area based on accident relevance. The pedestrian protection score required to obtain a particular overall star rating increases from 2010 to 2012, as shown in Table 4.2.

Many countries including Australia are following an overall star rating system similar to this.

4.3.1.5 Pedestrian protection protocol changes

In February 2012, Euro NCAP published new test and assessment protocol for pedestrian protection (version 6) that will be implemented from February 2013. The main difference between the current (version 5.3.1) and the new version of the protocol are the head impact test and assessment procedures.

4.3.2 Japanese New Car Assessment Program (J-NCAP)

Japanese New Car Assessment Program (J–NCAP) uses the same head impactors as used in Euro NCAP pedestrian testing protocol. However, the impact angle varies according to the shape of the front–end of the vehicle such as sedan, SUV etc.

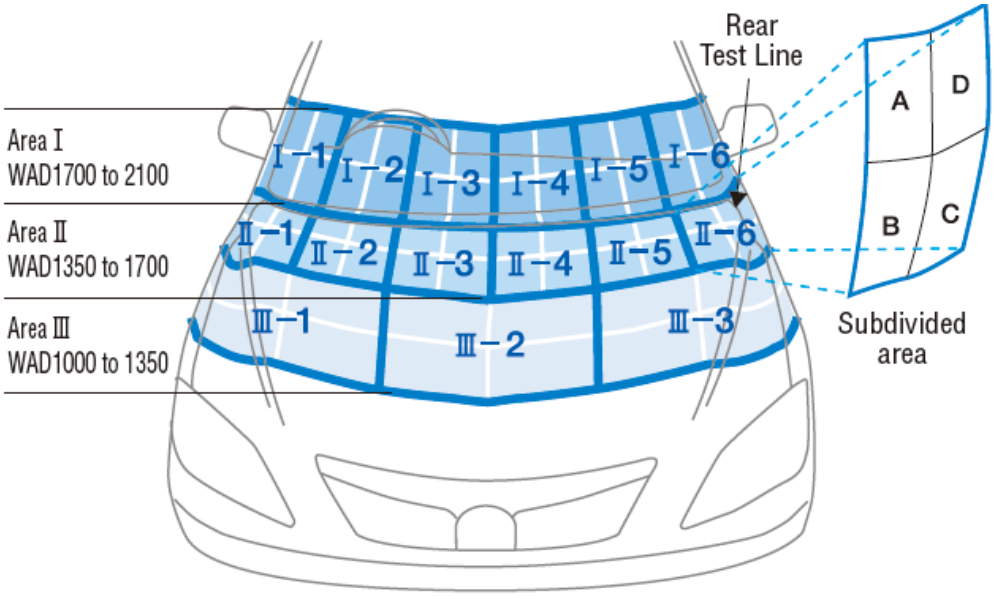

Figure 4.10: Defining head impact area (Schoenmarkers 2011)

These test procedures divide the head impact area as shown in Figure 4.10. The evaluation of impact severity is based on the HIC value in each subdivision. The HIC value is converted into a score using the sliding scale shown in Figure 4.11.

Figure 4.12 shows the procedure to calculate the total score. Five levels ranging from one to five can be achieved depending on the probability of serious injury (AIS4 and above). J–NCAP requires child and adult head impact tests through vehicle subsystems.

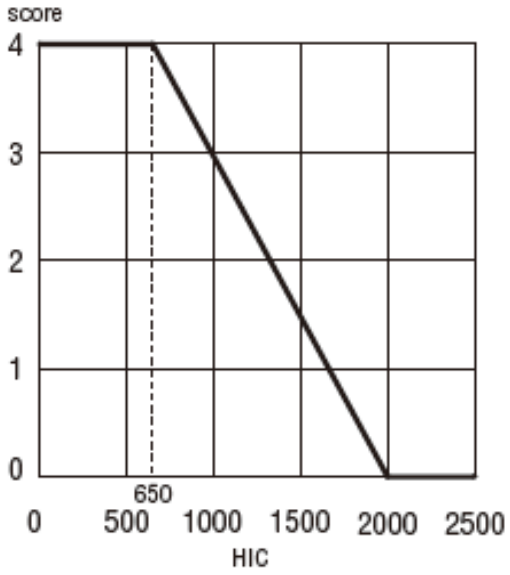

Figure 4.11: Sliding scale of pedestrian head impact performance ((Bovenkerk et al. 2009)

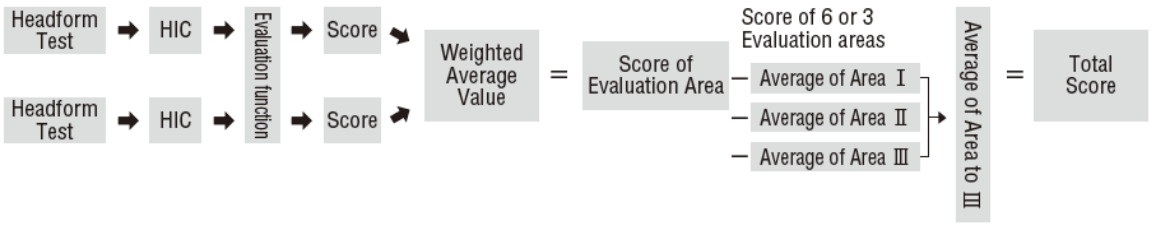

Figure 4.12: Total score evaluation method (Schoenmarkers 2011)

4.3.2.1 Child head impact

Hood angle (HA) is measured at the middle longitudinal plane of the vehicle (Y=0). It is the angle between the horizontal plane and the line drawn between the intersection point of middle longitudinal plane and BLE, and the intersection point of rear edge of the hood and the middle longitudinal plane (Bovenkerk et al. 2009).

The child head impact area is the area between 1000 WAD and 1700 WAD. Child head form fired at 35kmh to hood top – this test uses the ISO child head form with 3.5kg mass. Impact angles to the horizontal plane are:

- 65° if the Hood Leading Edge Height (HLEH) is less than or equal to 835mm
- 60° if HLEH is more than or equal to835mm
- 25° if HA is more than or equal to30°.

4.3.2.2 Adult head impact

The adult head impact area is defined by 1700 WAD and 2100 WAD. Adult head form fired at 35kmh to windscreen or to hood top – this test uses the ISO adult head form with 4.5kg mass. Impact angles to the horizontal plane onto the hood top are:

- 65° if HLEH is less than or equal to 835mm
- 60° if HLEH is more than or equal to 835mm
- 25° if HA is more than or equal to 30°.

Impact angles of the adult head form to the horizontal plane onto the windshield are:

- 40° if HA is less than or equal to 30°
- 45° if HA is more than or equal to 30°.

4.3.3 Korean New Car Assessment Program (K-NCAP)

Korean New Car Assessment Program (K–NCAP) includes three tests through vehicle subsystems.

These procedures are the same as Euro NCAP except that either a lower leg or upper leg form is fired at 40kmh at the bumper system depending on the height of the lower bumper reference line (Figure 4.13).

The maximum possible score is 30 points and the total number of points scored in these tests determines the pedestrian protection star rating awarded to a vehicle (Figure 4.14).

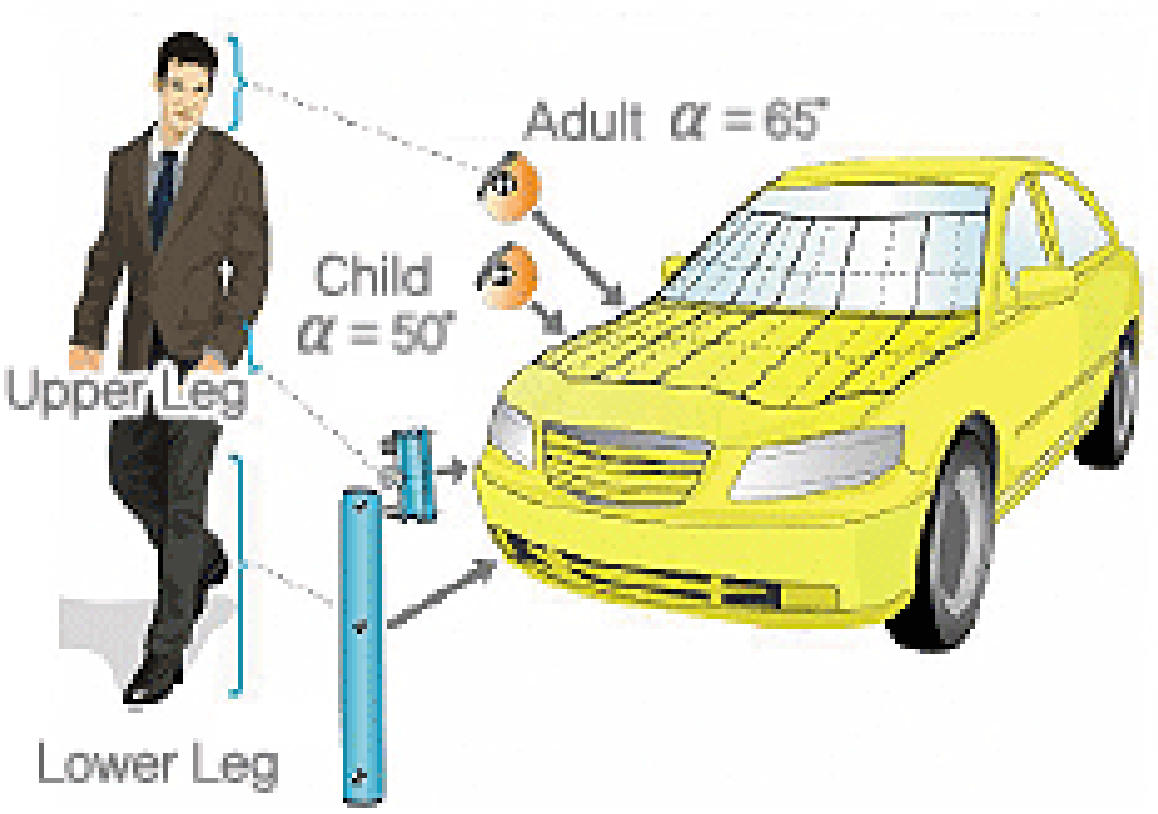

Figure 4.13: Pedestrian protection technical requirements (The World Bank 2006)

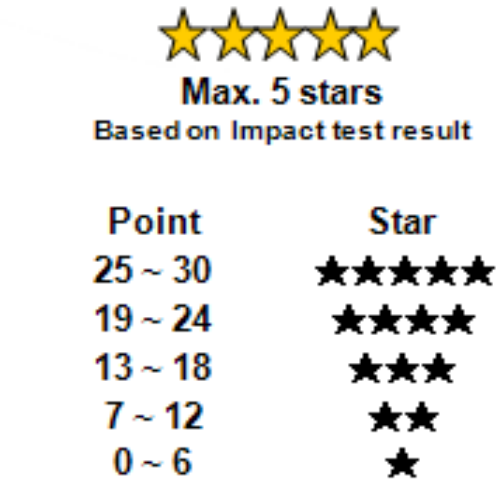

Figure 4.14: Pedestrian protection rating for K–NCAP (The World Bank 2006)

4.3.4 Australasian New Car Assessment Program (ANCAP)

ANCAP has adopted the procedures of the Euro NCAP for pedestrian testing and as such, follows Euro NCAP pedestrian testing protocol version 5.3.

Since ANCAP assessments use the same protocol as Euro NCAP, ANCAP also republishes Euro NCAP results for pedestrian protection. However, the level of pedestrian protection required for overall vehicle performance rating differs from Euro NCAP (Table 4.3).

5 star overall rating	
Year	**Minimum pedestrian rating**
2011	None
2012	Marginal
2013	Marginal
2014	Acceptable
2015	Acceptable
4 star overall rating	
2011	None
2012	None
2013	None
2014	Marginal
2015	Acceptable

Table 4.3: Pedestrian protection points required for overall star rating (Australasian New Car Assessment Program 2011)

ANCAP also differs in windscreen assessment as illustrated in Figure 4.15 where picture on the left shows Euro NCAP assessment method and picture on the right shows the ANCAP assessment method. Impact zones on the windscreen are split into two equal sections if a WAD line falls on the base of the windscreen such that test locations can be selected in both the zones above and below the WAD line. Each split section on the windscreen is awarded up to 0.25 points.

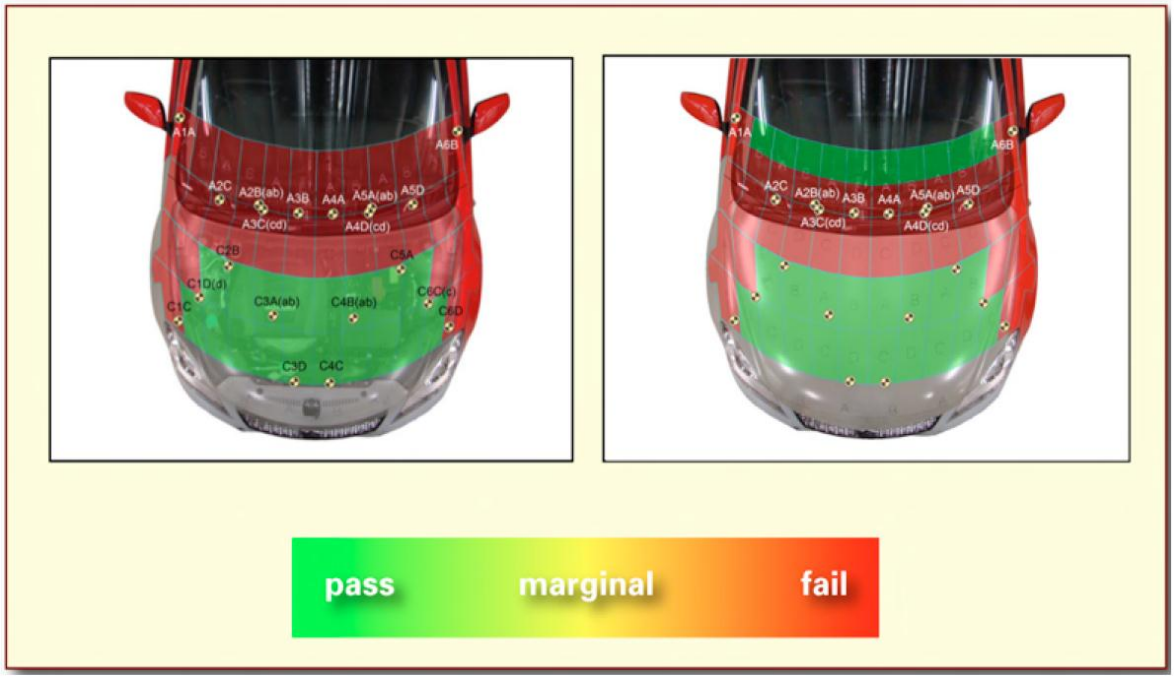

Figure 4.15: Euro NCAP and ANCAP windscreen assessment comparison

4.4 Durability and serviceability requirements

There are numerous requirements other than pedestrian protection for the Front–End Subsystem (FES) to ensure performance, robustness, serviceability and functions of FES.

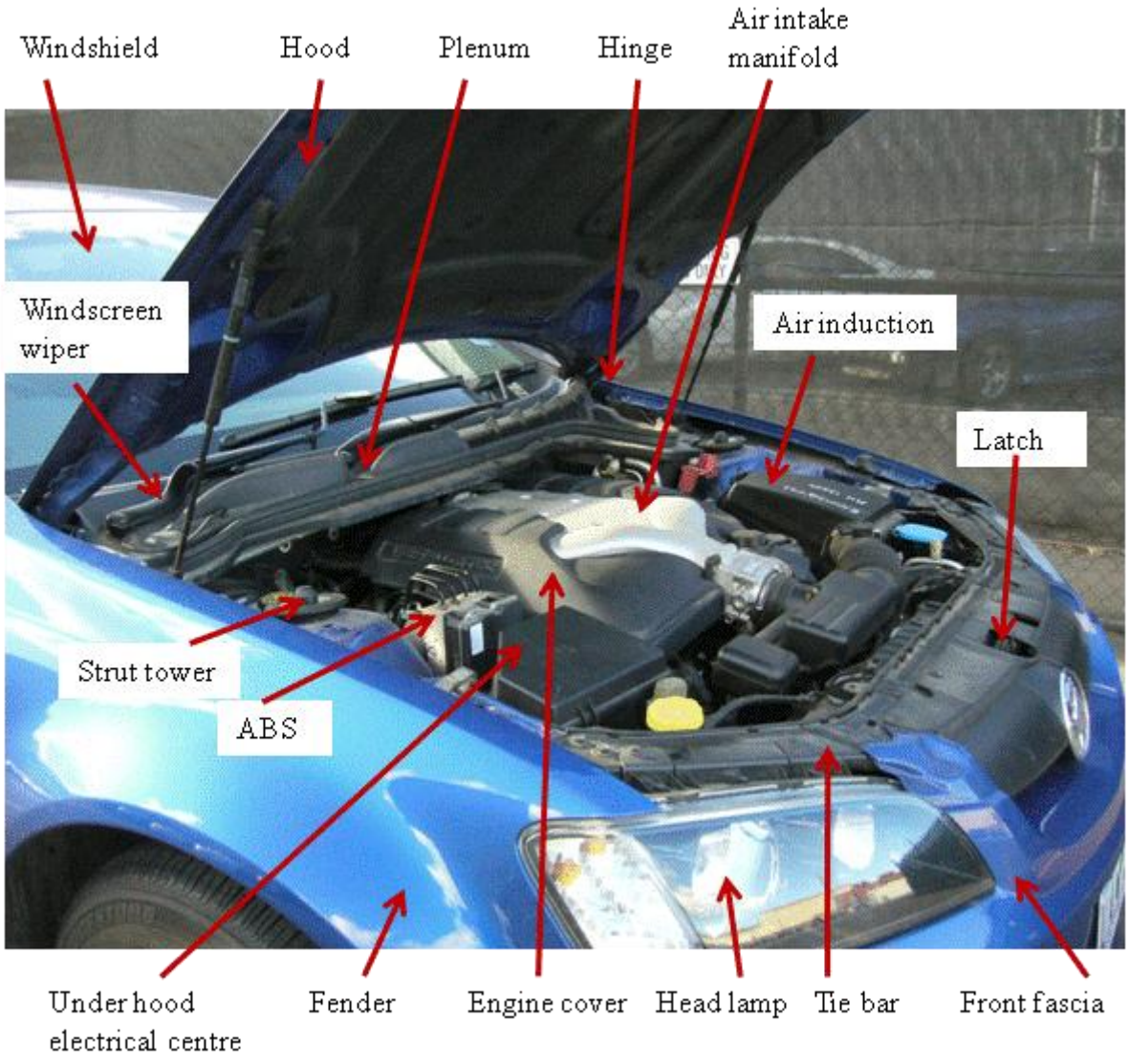

Figure 4.16: Main parts in the front-end of a car

Usually the FES is composed of assemblies that secure, but when required provide access to the engine and front wheel compartments i.e. hood, fenders and fender structures (Figure 4.16).

Like any other design regulations, these regulations vary between countries and revisions take place regularly. The list below shows some of the regulations that will typically shape the FES design process. Apart from these regulations, there are automakers' internal guidelines to maintain quality, appearance, robustness etc.

Australia	
ADR 42/04	General safety requirements
Brazil	
461/72	General safety requirements
Canada	
Bill 101	Charter of the French language
CMVSS113	Hood latch systems
CMVSS219	Windshield zone intrusion
China	
GB 11568–1999	Hood latch system
GB11566–1995	External projections
Europe	
Economic Commission Europe	
ECE R 26.02	External projections
ECE R 61.00	External projections
European Union	
2005/66/EC 2006/368/EC	Frontal protection systems
74/483/EEC 79/488/EEC 87/354/EEC	External projections
Korea	

Article 21	Hood latch system
Article 19	Frame and body
Article 105	Windshield zone intrusion
United States of America	
FMVSS 113	Hood latch system
FMVSS 219	Windshield zone intrusion
FMVSS 541	US theft prevention regulation
FMVSS 542	US theft prevention regulation

The vehicle design requirements to meet these regulations mentioned above generally conflict with pedestrian protection requirements, which adds to the pre–existing design challenges to meet pedestrian protection assessment requirements.

Chapter 5

Evaluating protection offered by a vehicle

5.1 Crash tests

The automotive industry is allocating large amounts of capital, cash and human resources to put safer cars on the roads. Automotive crash testing that replicates real–world crash requirements to meet regulations, robustness and consumer metrics requires well-planned preparation and integration into the vehicle development process.

A vehicle manufacturer may crash as many as 100 vehicles to check various crash configurations throughout the vehicle development cycle. The evaluation of real–world injury risks in various vehicle collision scenarios uses physical models for dummies and impactors. For example, Figure 5.1 shows the physical testing of a vehicle front–end collision with a rigid barrier.

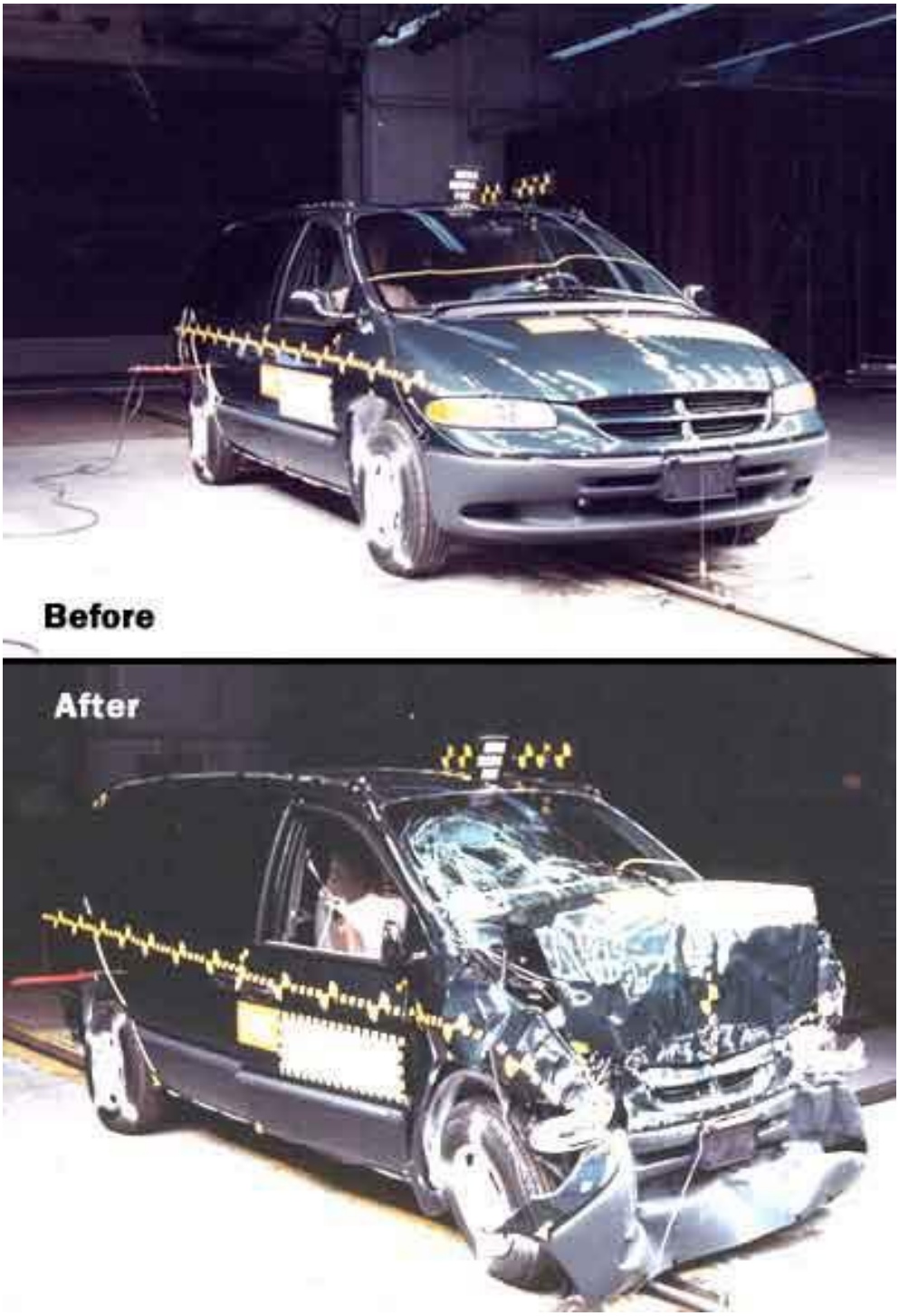

Figure 5.1: Frontal rigid barrier physical test (Nice 2001)

5.2 Occupant protection

Dummies that represent occupants of different ages, sizes and sexes are used in frontal, side, rear and pole crash testing.

The automakers and test facilities use dummies ranging from 6–month–old infant to a 95th percentile male in their anthropometry, to study the injury risks in various accident scenarios (Figure 5.2). The instrumentations located inside the dummies collect relevant information in a crash test e.g. accelerometers measure acceleration in a given direction; load cells measure the force on different body parts; and motion sensors measure deflection.

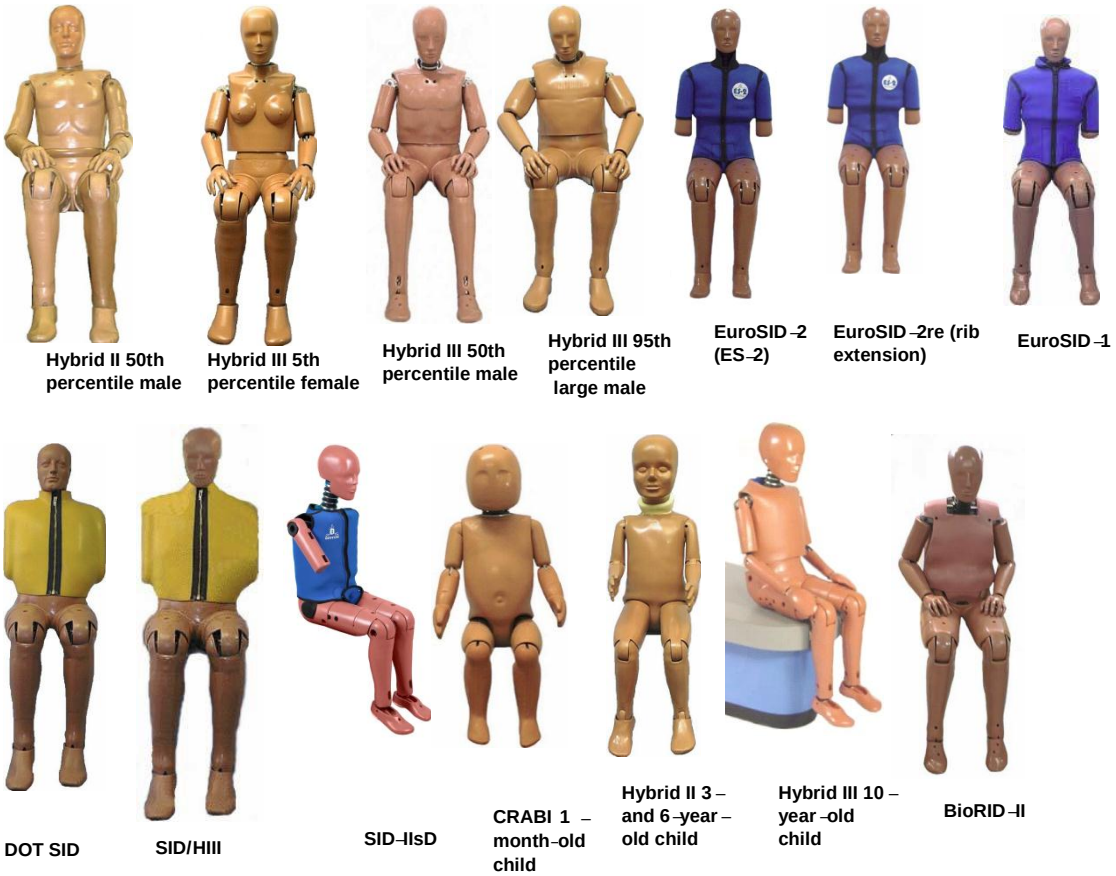

Figure 5.2: Dummies used in crash testing (Transport Research Laboratory 2012)

5.3 Pedestrian protection

In 1989, EEVC WG10 (Hardy et al. 2007) proposed the impactor test method for vehicle pedestrian impacts. They developed four different types of subsystem test.

As discussed earlier, so far all the regulatory requirements and consumer metrics tests that evaluate pedestrian protection use these subsystem tests only (Figure 5.3).

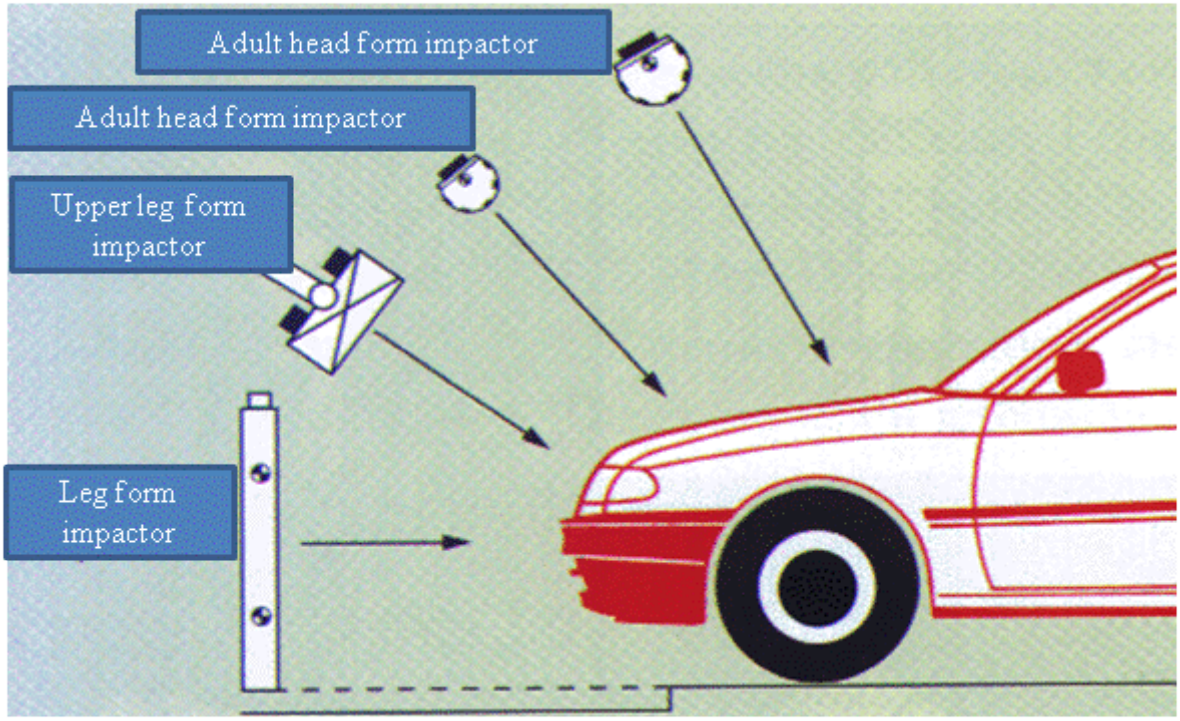

Figure 5.3: Subsystem test method (Hardy et al. 2007)

Institut National de Recherche sur les Transports et leur Sécurité (INRETS) created the original leg form impactor (Hardy et al. 2007). However, EEVC WG 10 and EEVC WG 17 accepted the lower leg impactor developed by Transport Research Laboratory (TRL) (Transport Research Laboratory 2012) to be used in EEVC pedestrian protection testing, due to its high level of performance and repeatability. These TRL–PLI impactors represent the 50th percentile male leg designed for right side impact testing. Accelerometers and

potentiometer in the leg form impactor collect the acceleration and the relative rotation to assess the severity of injuries. The TRL–PLI has a rigid femur and tibia covered with foam to represent soft tissues and skin (Figure 5.5).

In 2000, to improve the accuracy of the leg form, JAMA and the Japan Automobile Research Institute (JARI) initiated the development of a Biofidelic Flexible Pedestrian Leg form Impactor, Flex–PLI (Figure 5.4). This impactor uses four femur joints and five tibia joints to improve the dynamic response.

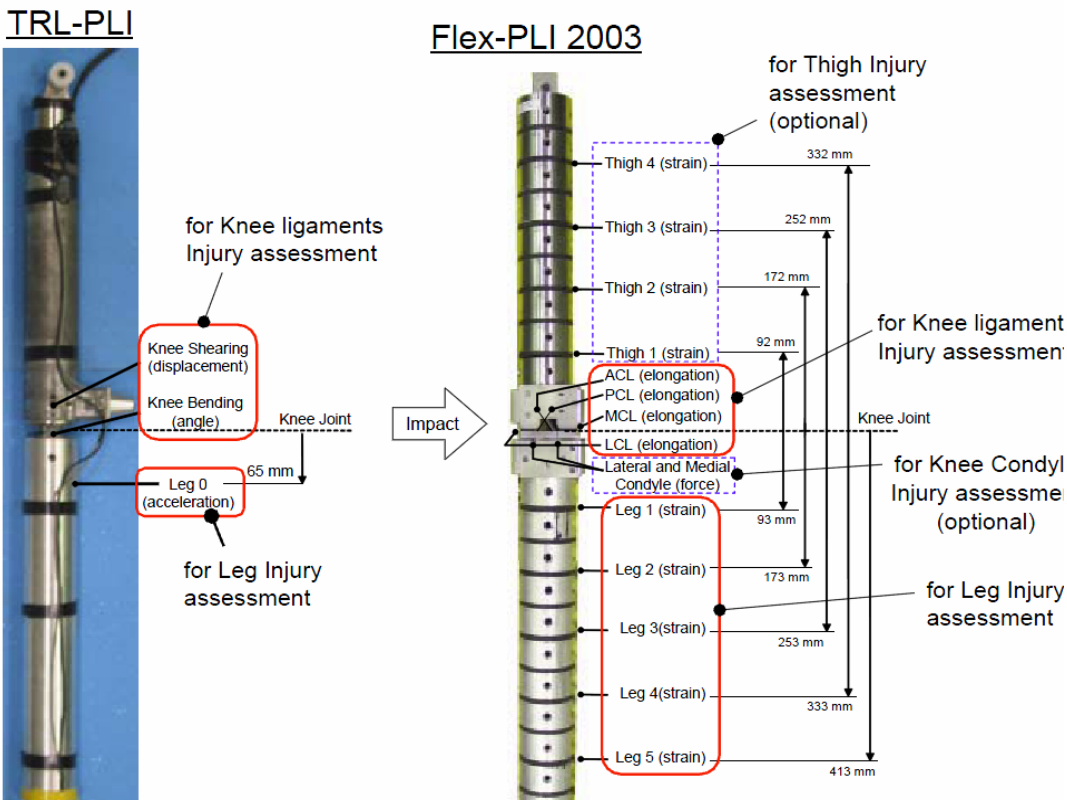

Figure 5.4: Comparison between TRL–PLI and Flex–PLI (World Health Organization 2010)

Figure 5.5: TRL-PLI lower leg impactor

Flex–TEG, a technical evaluation group consisting of government and industry members, is evaluating the possibility of using the Flex–PLI impactor for the GTR–9. The linear guidance propulsion system launches the lower leg impactor in a free flight mode when it has attained steady desirable velocity. This test simulates the human lower leg (tibia, knee joint and femur) in a passenger car front–end impact with a pedestrian.

Figure 5.6: Leg impact and head impact test machines (Centre of automotive safety research 2007)

In 1995, Germany's federal highway research institute (BASt) conducted upper leg form tests. Later TRL improved this upper leg form impactor. The EEVC accepted this upper leg form impactor in its tests, even though JARI reported that the measured forces are still lower than the inertia forces. During the test, a linear guided launcher fires the upper leg impactor onto a static vehicle (Figure 5.6). This test simulates the upper leg covered with foam to replicate flesh and skin and rotates around a friction–loaded pivot to mimic femur and pelvis fractures.

Originally, production of the head form impactors used a plastic sphere covered by a rubber skin. EEVC WG17 updated the head form specifications to an aluminium sphere covered with a 12mm PVC skin without changing the outer diameter and mass for continuity of measurement. The head impactor is launched in the same manner as the lower leg impactor. The head form contains a tri–axial accelerometer that is used to measure the resultant acceleration throughout the impact. The HIC value is calculated using the measured resultant acceleration.

In 2005, a team from the University of Virginia and General Motors Corporation (Kam et al. 2005) conducted a study to develop full–scale pedestrian impact tests using Post Mortem Human Surrogates (PMHS). This study was conducted utilising existing test procedures, real–world data and MADYMO simulations to create an experimental test system with full–scale pedestrians. In this study, the PMHS was positioned laterally in mid–gait stance with the struck leg extended to the rear and both hands extended to the front. The PMHS was attached to an electromagnetic release mechanism, which was triggered to release the PMHS just before impact. After the impact, a catcher mechanism would absorb the kinetic energy from the PMHS to avoid any secondary injuries because of contact with the ground. This study did not lead to the development of a full–scale pedestrian dummy.

In contrast, Honda developed a crash test dummy to understand the kinematics of vehicle pedestrian impacts in 1998 with a second–generation released in 2000, the POLAR II. This dummy gathers measurements from the head, cervical spine, thorax, abdomen, pelvis, femur, knee and tibia. In 2008, Honda introduced the third–generation pedestrian dummy, POLAR III (Figure 5.7). This dummy has an improved ability to evaluate bone fractures in

the lower back and upper leg compared to the POLAR II. Lower back and upper leg injuries are common in pedestrian impact with higher vehicles like SUVs.

At present, both NCAP and regulatory tests use subsystem testing due to their simplicity, repeatability and the ability to predict injury values accurate enough for pedestrian protection. Since the number of tests required to assess pedestrian protection is large, testing with full–scale pedestrian dummies would be expensive and time consuming. The author is not aware of any current plans to examine pedestrian kinematics using full–scale pedestrian impact tests.

Figure 5.7: POLAR III pedestrian dummy (Honda Worldwide 2008)

Chapter 6

Problem identification

6.1 Peak acceleration

Numerical tests were conducted in this work to obtain accelerations, time histories and impactor displacements in x, y and z directions. These numerical tests are discussed in detail in chapter 7. The resultant accelerations calculated from these numerical tests were used in calculating the HIC values. The HIC calculation involves an exponent of 2.5 applied to the average head acceleration measured over a window of 15ms. The result of this formulation is that small changes in the average acceleration can lead to large changes in the final HIC value.

The average acceleration of any given head acceleration curve can be increased by:

- simply increasing the magnitude of a single peak acceleration
- increasing the duration or width of a single peak
- increasing the time difference between the first and an adjacent peak
- increasing the magnitude of the acceleration of the first peak and the adjacent peaks.

The accelerations calculated from the numerical tests conducted in this work are shown in Figure 6.1 and Figure 6.2. It is evident from the curves that the HIC value increases with the magnitude of resultant acceleration and increases with the recording period for similar peak acceleration. Therefore, a low magnitude and small duration of peak acceleration is required to keep the severity of head injuries less than the limits specified by the GTR–9 and ANCAP.

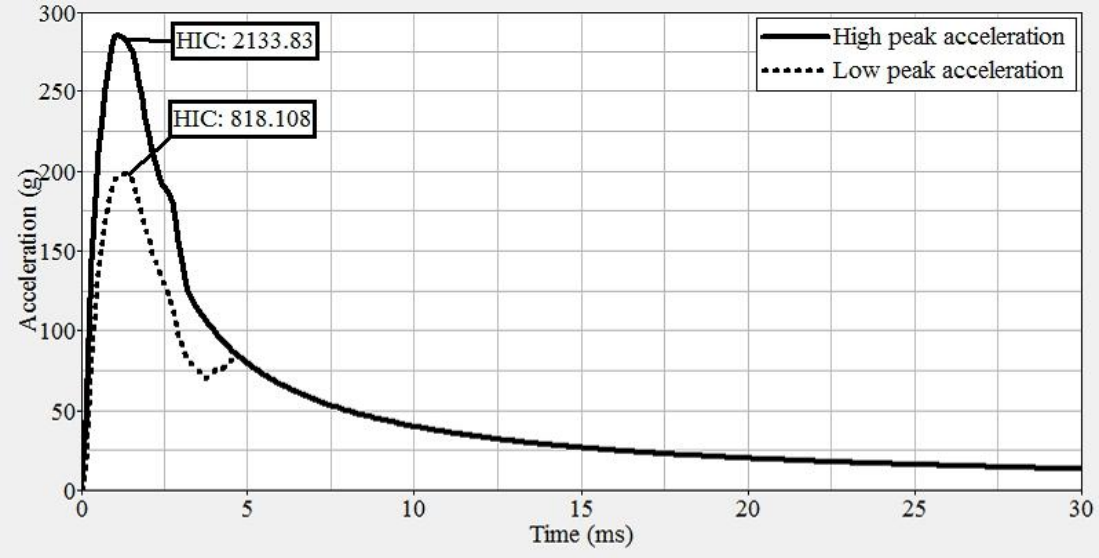

Figure 6.1: Comparison of peak acceleration magnitude

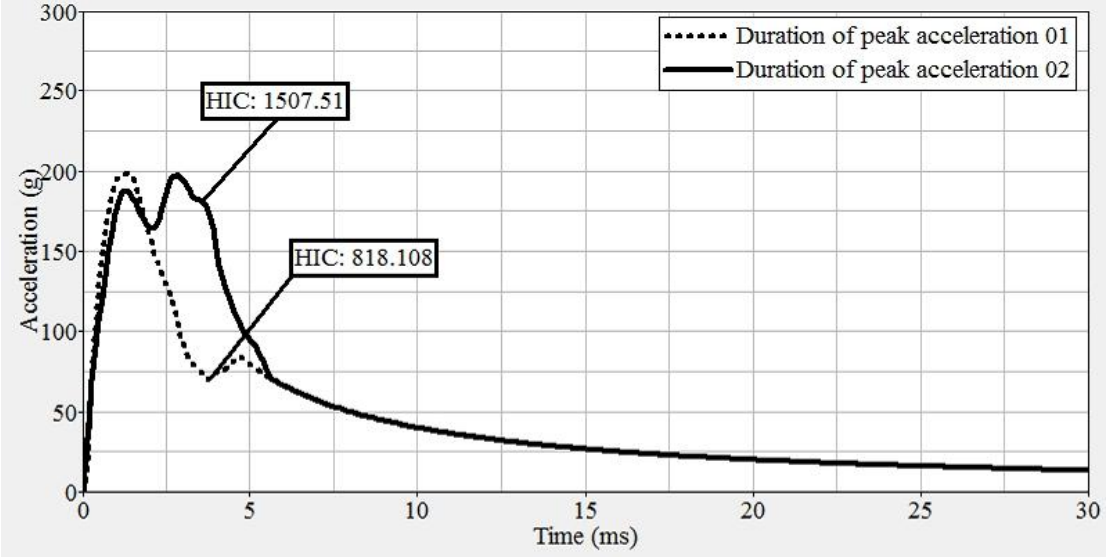

Figure 6.2: Comparison of peak acceleration duration

Decreasing the structural stiffness of the hood panels decreases the magnitude of acceleration and in turn increases the intrusion of the hood panels, otherwise known as the deformation space. It is this interplay between the measured average acceleration (and hence HIC) and the structural characteristics of the hood that requires careful development if we are to minimise our requirement for the highly valuable deformation space. Thus, optimisation of the structural stiffness of the hood panels is essential to meet the requirements for head impact regulations.

6.2 Deformation space

Pedestrian protection requires a soft, energy–absorbing hood assembly, whereas durability, noise and vibration require a hood assembly with higher structural stiffness. The properties of the direct and indirect contact surfaces of the head in a crash influence the severity of head injuries. The indirect contact surfaces are the surfaces under the hood. The three important parameters that influence the severity of pedestrian head impact injuries are the available deformation space, structural stiffness and structural inertia. In this instance, the structural inertia is the resistance given by the hood panel to changing its state to the changes in velocity and is proportional to its mass.

Among these parameters, the available deformation space between the hood assembly and the hard components within the engine bay is critical. The intensity of the contact between the hood assembly and the under hood components with high structural stiffness (secondary impact) increases the severity of pedestrian head injuries. The deformation space required to absorb the energy varies with the head impact mass, impact speed and impact angle. Intensity of the secondary impact can be reduced either by increasing the

structural stiffness and structural inertia of the inner and outer hood panels or by increasing the deformation space.

Increasing the structural stiffness decreases the displacement and in turn increases the magnitude of acceleration. The amount of deformation that the hood undergoes is reduced if hood stiffness is increased. Therefore, excessive stiffness of the hood causes severe acceleration, which in turn increases the severity of head injuries. Accordingly, increasing the structural stiffness to reduce the intensity of the secondary impact is only possible up to a point, beyond which the severity of injuries due to the contact between the hood assembly and the head impactor (primary impact) becomes excessive. The simulations from the numerical tests conducted in this work with increased structural stiffness for the inner and outer hood panels are shown in Figure 6.3. It shows that the deformation of the hood panels is reduced whereas; the structural inertia of the panels has increased.

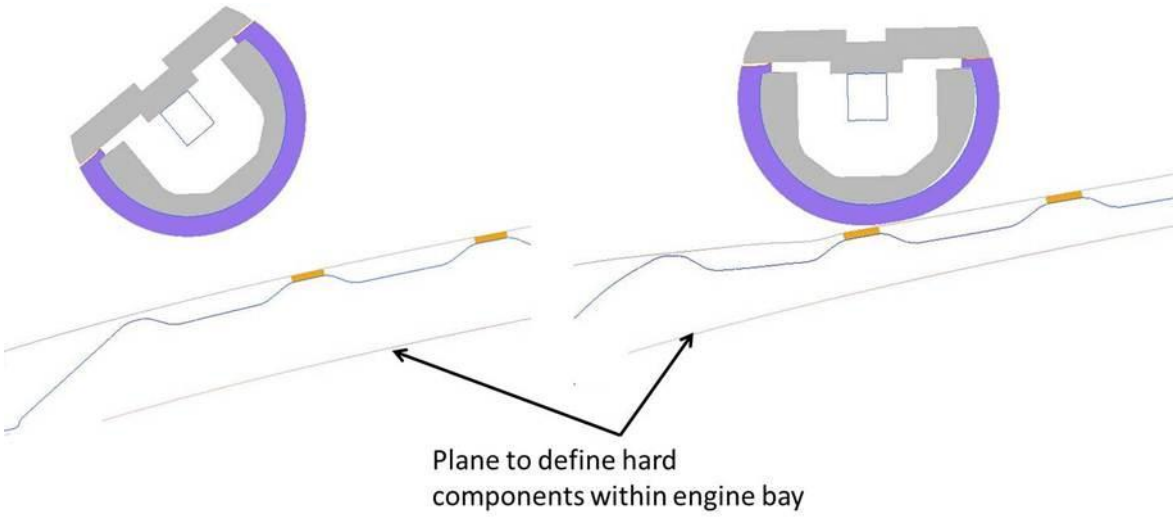

Figure 6.3: Primary impact of head with hood panels with excessive stiffness

The resultant acceleration calculated for the simulation shown in Figure 6.3 is presented in Figure 6.4, which exhibits a dominant initial peak resulting from high inertial loading due to the structural inertia of the inner and outer hood panels.

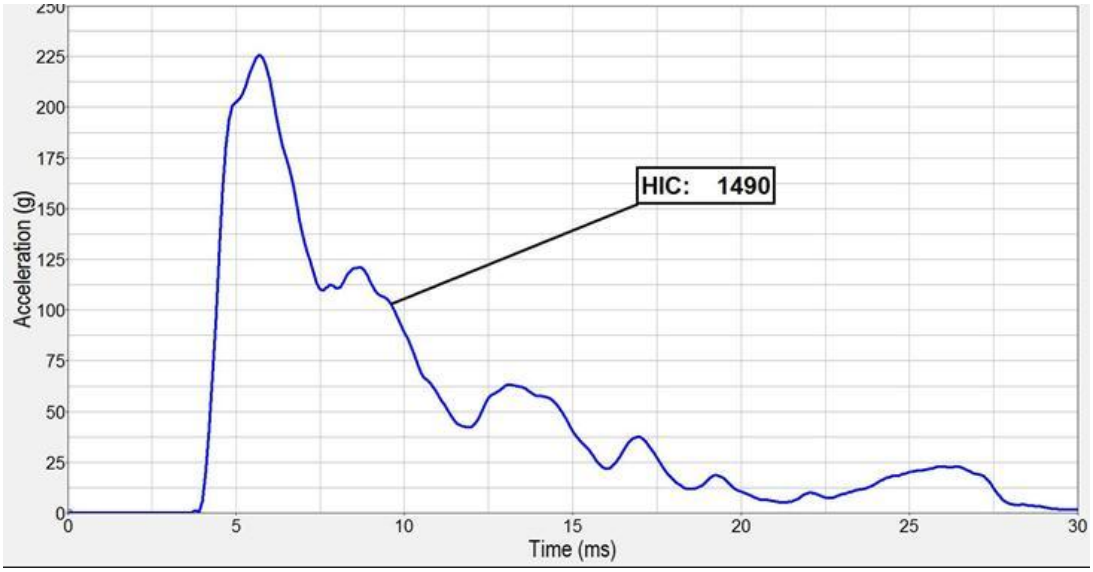

Figure 6.4: Effect of inertial loading of the head form on HIC value

Similarly, the simulation and resultant acceleration from the numerical tests conducted in this work with the lack of deformation space are presented in Figure 6.5 and Figure 6.6. These figures show that the lack of deformation space leads to direct contact of the head form with the hard components approximately 12ms from the start of the impact. This causes severe acceleration, hence increasing the risk of head injury.

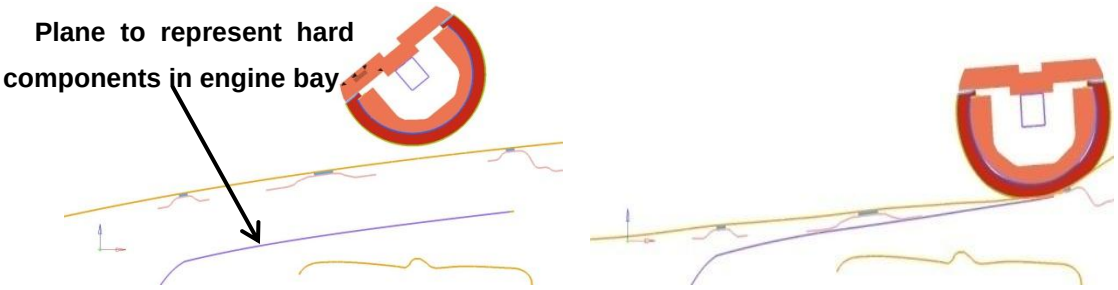

Figure 6.5: Secondary impact of head with hard components within engine bay

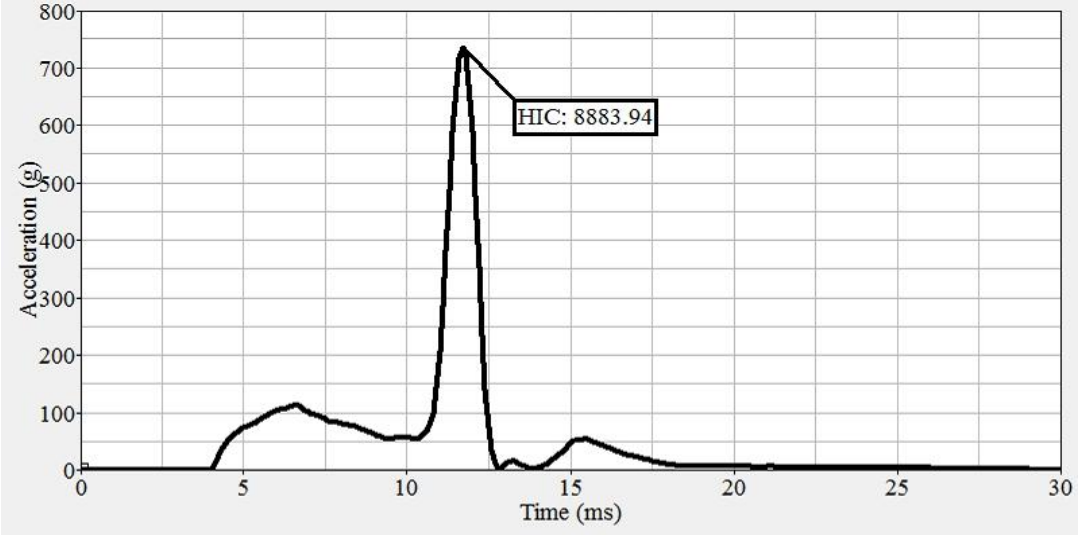

Figure 6.6: Waveform with secondary impact

While increasing the deformation space improves pedestrian protection, it may conflict with other vehicle design requirements. For example, the positioning of the hard components, such as the engine and the suspension, should meet ground clearance requirements. In addition, the relative height difference between the hood and the driver has to meet visibility requirements. Therefore, when the hood is elevated to meet the deformation space requirements for pedestrian protection, the driver also needs to be elevated to meet the visibility requirements. Thus, vehicle manufacturers need to increase the height of the car for occupant comfort, ergonomics and safety, which will compromise aerodynamics, vehicle stability and fuel economy. It might also have adverse effects on vehicle styling.

Therefore, in order to reduce the pedestrian head injury risk, it is important to optimise the hood assembly by balancing its structural stiffness for minimal deformation or risk a series of far reaching flow on effects into a whole range of areas such as engine bay packaging, occupant comfort and visibility, styling and even aerodynamics.

6.3 Influence of hood design

The structure and stiffness of the components in a hood assembly (Figure 6.7) of a car generally influence the severity of head injury in a pedestrian hood impact. To reduce the severity of head injuries closer to the edges of the hood, the hood assembly has to be weaker in this area. This will increase the deflection of the hood assembly in the middle, thus increasing the severity of head injury closer to the edges of the hood. The size of the hood also has an effect on the probability of severe head injury because, as the hood size is increased, the deflection in the middle of the hood also increases. Thus, more deformation space is required to reduce the intensity of the secondary impact.

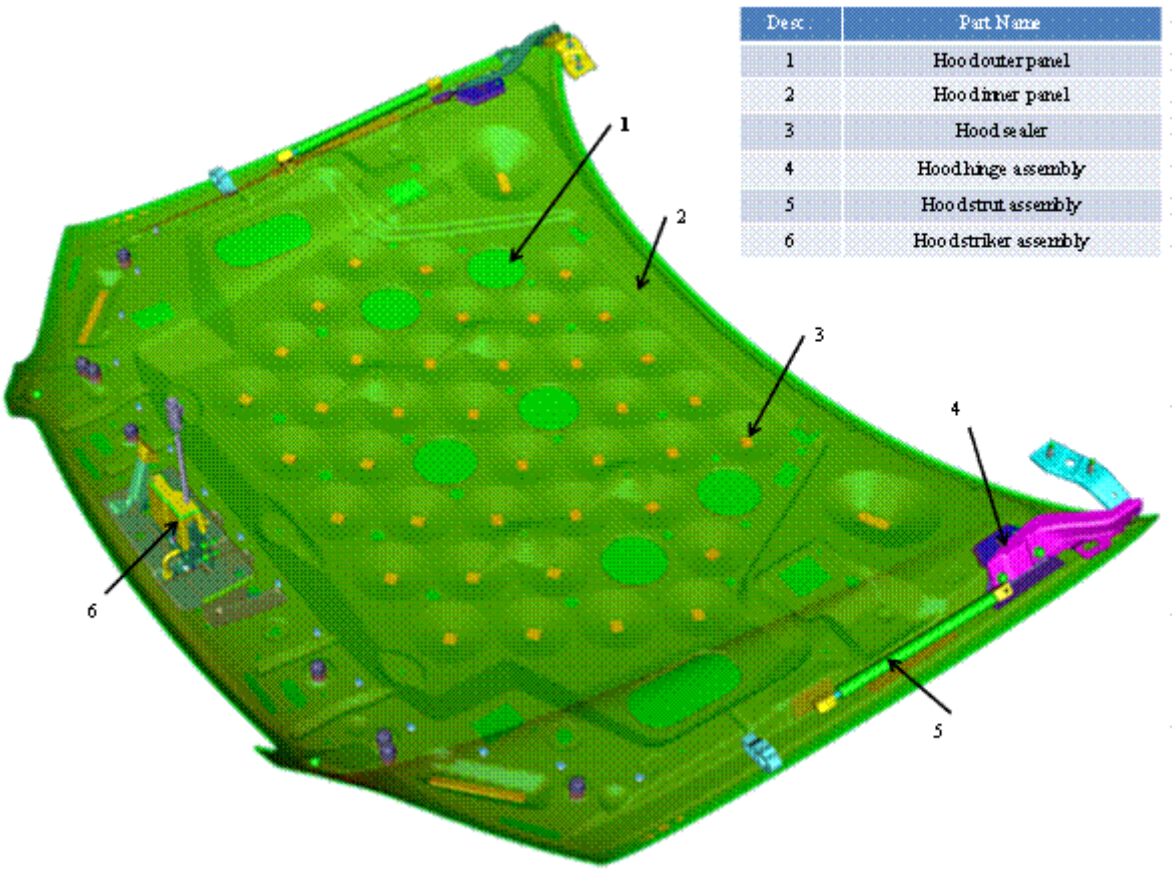

Figure 6.7: Underside view of a hood assembly

The challenge of reducing the severity of head impact near the fender can be addressed by changing the hood design from an inlaid hood (Figure 6.8) to a wraparound hood (Figure 6.9). However, the wraparound hood design raises issues related to repair costs in low–speed impacts because it is more exposed to damage.

Figure 6.8: Inlaid hood (A2Mac1 2010)

Figure 6.9: Wraparound hood (A2Mac1 2010)

The length of the hood also plays a vital role in pedestrian protection in a passenger car front–end collision with a pedestrian. In the case of a shorter hood length, the pedestrian is likely to come into contact with the A–pillar, generally an area of very high stiffness, resulting in increased risk of head injury. As the length of the hood increases, the challenge to meet the durability, noise and vibration guidelines become more difficult.

The choice of material and thickness of the outer hood panel is important in reducing the probability of severe head injuries. A combination of material and thickness with better energy absorption is favourable for pedestrian protection. The preferred material for pedestrian protection should also satisfy quality, durability, noise and vibration requirements. At present, the materials generally considered for the outer hood panel include steel, aluminium, plastic, carbon fibre and fibreglass.

The inner hood panel acts as an energy absorber and provides torsional and bending stiffness to the hood assembly. Therefore, the choice of structure, material and thickness for this component also plays a vital role in reducing the severity of head impact.

Many concepts for the structure of the inner hood panel have been considered by automakers around the world such as multi–cone, multi X pattern, frame, single skin, double skin etc.

The choice of glue that is used between the inner and outer hood panels also has an important role in reducing the severity of head injuries. The stiffness of the hood assembly also increases with the number of gluing points and glue length between the inner and outer hood panels.

Therefore, optimising the central area of a large hood poses several challenges. This work includes developing a hood configuration that provides a robust and homogeneous head

impact performance for different impact positions in the central area of the hood of a large passenger car while minimising the deformation space required.

Chapter 7

Methodology

7.1 Virtual crash simulation

The automotive industry is moving away from a vehicle development process based on extensive programs of physical testing, practical experience and observation in physical testing, because this is expensive and time consuming. It is utilising virtual assessment techniques in many areas such as assembly, fitment, appearance, durability and safety development.

The virtual assessment of crash tests requires the following:

- creating three–dimensional geometric models of all the required components to replicate the structure as accurately as possible
- converting the geometric models into FE models
- implementing the mass properties and representative material properties
- constraining the components together
- processing using high–performance computers
- post–processing to analyse the crash results.

The auto industry is devoting significant resources and time to develop three–dimensional geometric models and FE models of vehicles to use in virtual assessments in order to meet real world, regulatory and consumer metrics requirements.

It will be difficult and expensive to capture every crash situation in the physical tests, whereas virtual assessment tools enable automakers to analyse nearly every situation and develop systems to put safer cars on the roads.

Confidence in using virtual assessment for developing cars has been increasing due to the leading–edge virtual assessment technology that is evolving every day. At present, many automakers use physical tests for correlation, verification and validation purposes only. As an example, the virtual assessment for pedestrian protection using a human body model is shown in Figure 7.1.

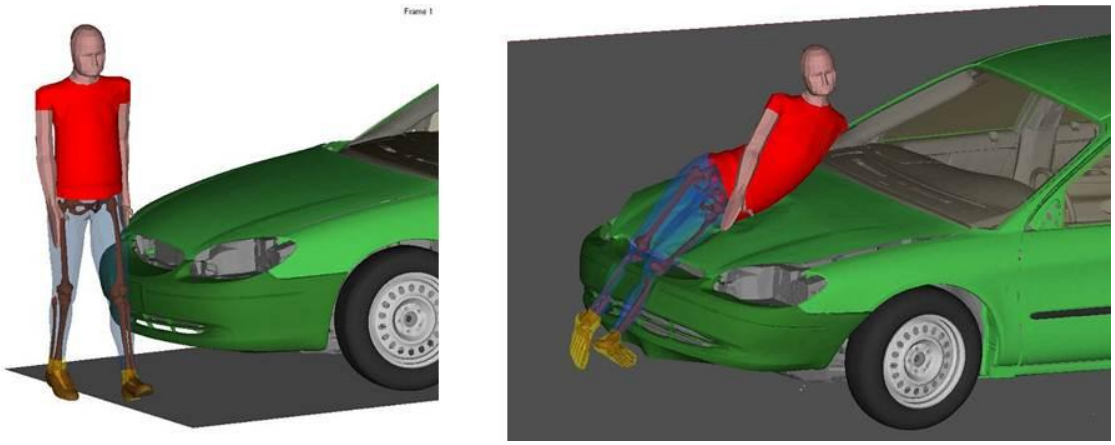

Figure 7.1: Virtual pedestrian impact test (Schoenmarkers 2011)

7.2 Parametric geometric model creation

In this research, the designs of the hood assembly were created as three–dimensional parametric geometric models using the chunky solid method in Unigraphics NX5 CAD software. The design boundaries were set up using datum planes at set coordinates. This methodology enables faster design modifications in the hood assembly.

Once a design alternative was developed, checking for fitment and clearance was carried out by virtually assembling the hood to the original donor vehicle. The mid–surface was extracted from these geometric models to enable the FE model development to assess the head impact performance.

7.3 Finite element model creation

The FE models were developed using ANSA V13 with the mid–surfaces extracted from the geometric models. PRIMER was utilised to replicate the hood interface conditions by assembling these FE models to the donor vehicle. The section, material properties, joints and constraints to the components of the hood assembly to the replicated design solution intensions were assigned using PRIMER as shown in Figure 7.2. The FE model of the head impactor was positioned at the intended impact position and angle as shown in Figure 7.3. The head impact condition of the pedestrian was simulated using LS DYNA–3D Computer Aided Engineering (CAE) software as exhibited in Figure 7.4. It shows different orientations of the head impactor at 5ms intervals for one data point. The HYPERGRAPH and HYPERVIEW programs were used to post–process the results which are shown in Figure 7.5, Figure 7.6 and Figure 7.7.

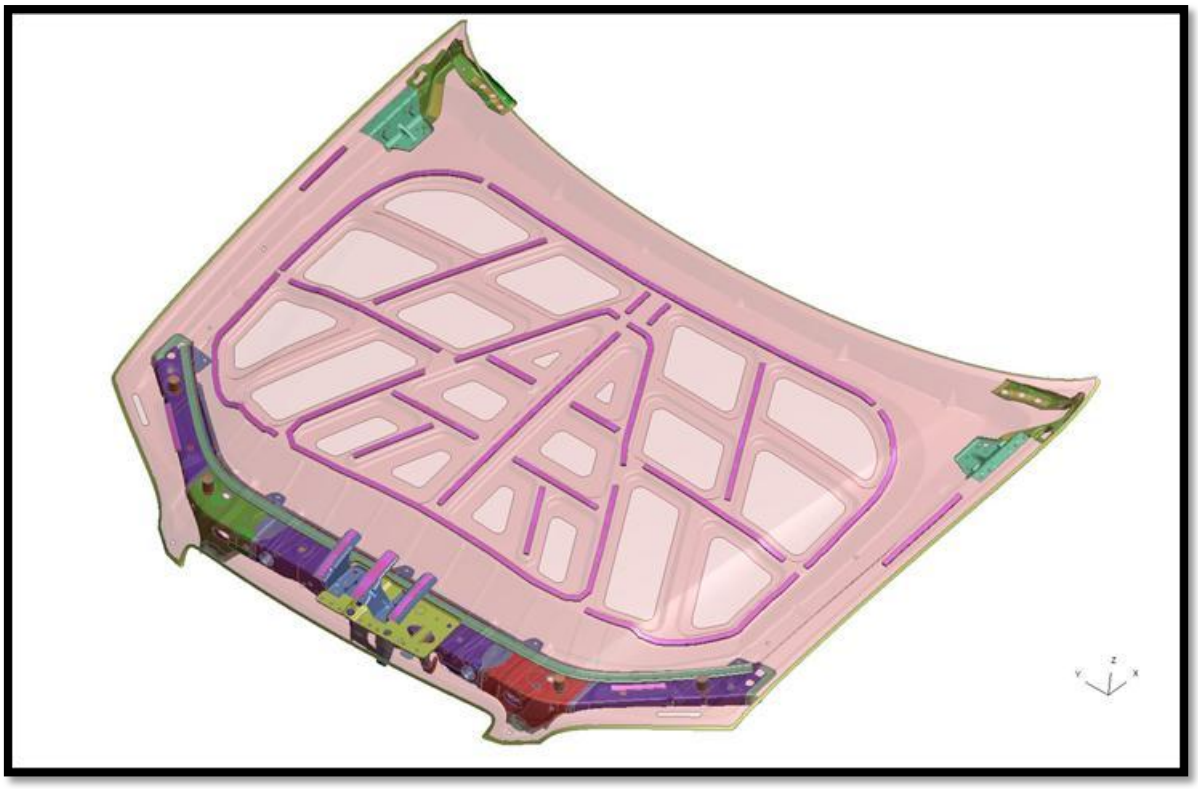

Figure 7.2: FEA model for optimisation

Figure 7.3: FEA model with head impactor for optimisation

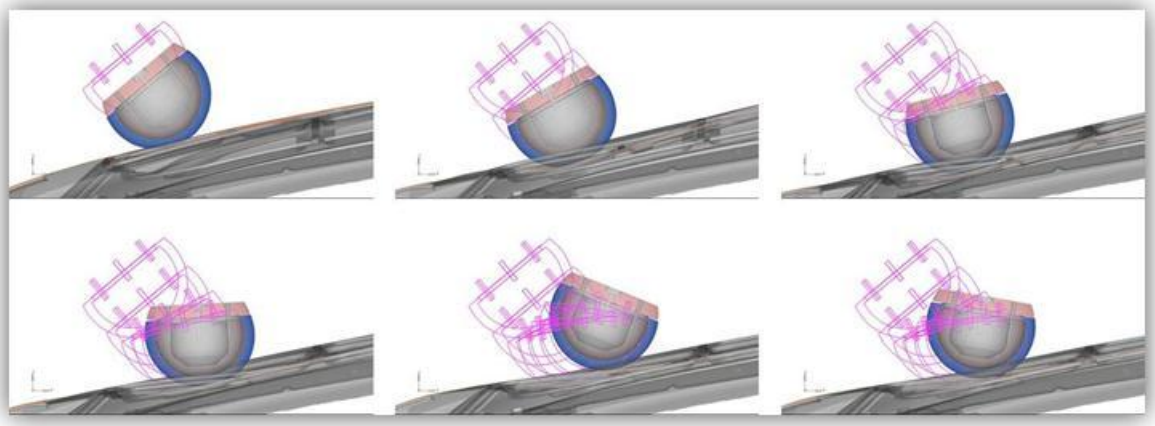

Figure 7.4: FEA model simulation using LS-DYNA for optimisation

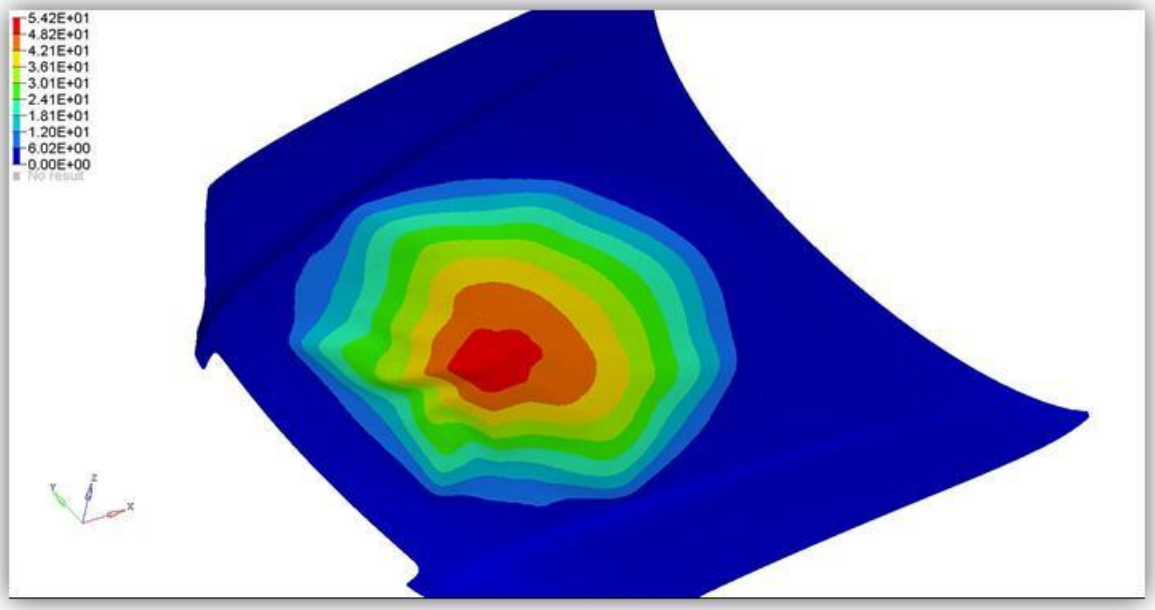

Figure 7.5: Contour plot of hood displacement using HYPERVIEW

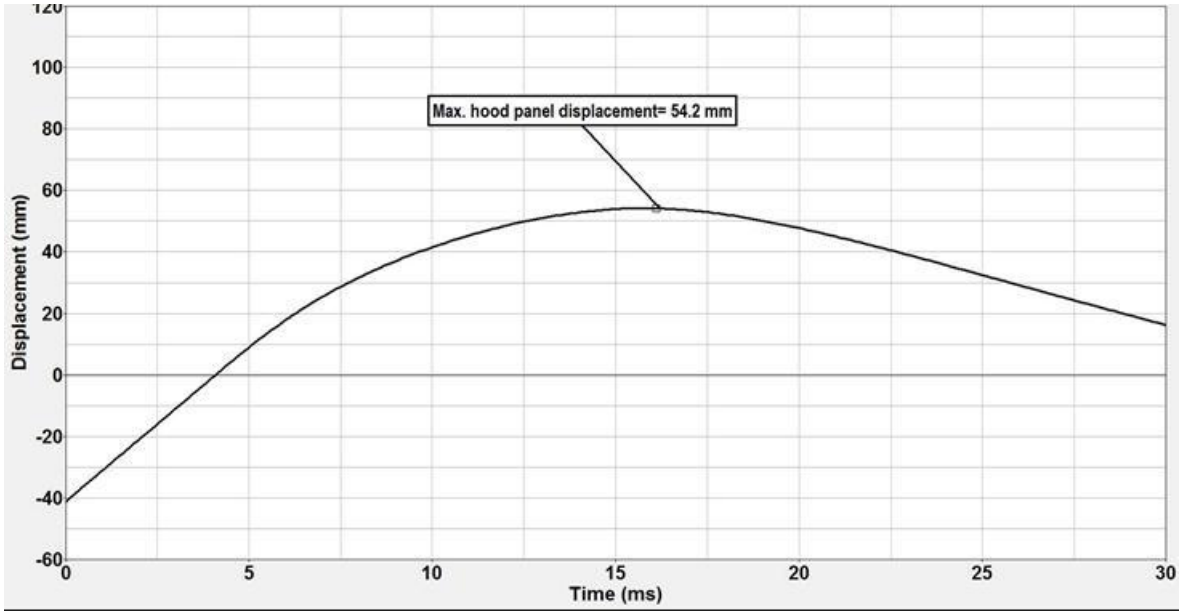

Figure 7.6: Plot of hood displacement vs. time using HYPERGRAPH

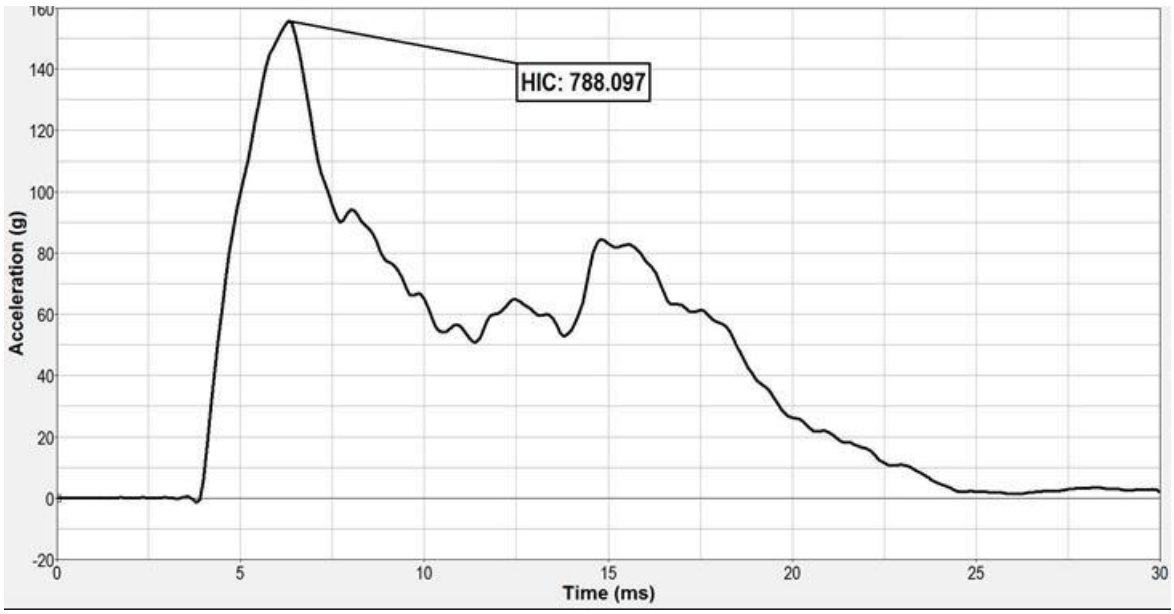

Figure 7.7: Plot of resultant acceleration vs. time using HYPERGRAPH

The energy absorption data from the finite element analysis is presented in Figure 7.8. In general, the energy absorption data is used as a quality check for the finite element model. In the finite element model constructed and utilised in this work, the energy input is from the mass and velocity of the impactor. There are no other components such as airbag is

included in the model that can influence change in total energy within the duration of the analysis. Therefore, the total energy remains constant for the duration of the head impact analysis as shown in Figure 7.8. The kinetic and internal energy plots demonstrate that the major portion of the kinetic energy is converted into internal energy. Thus, it can be stated that the finite element model does not contain errors either in contact definition or in constraints, which can influence energy fluctuations.

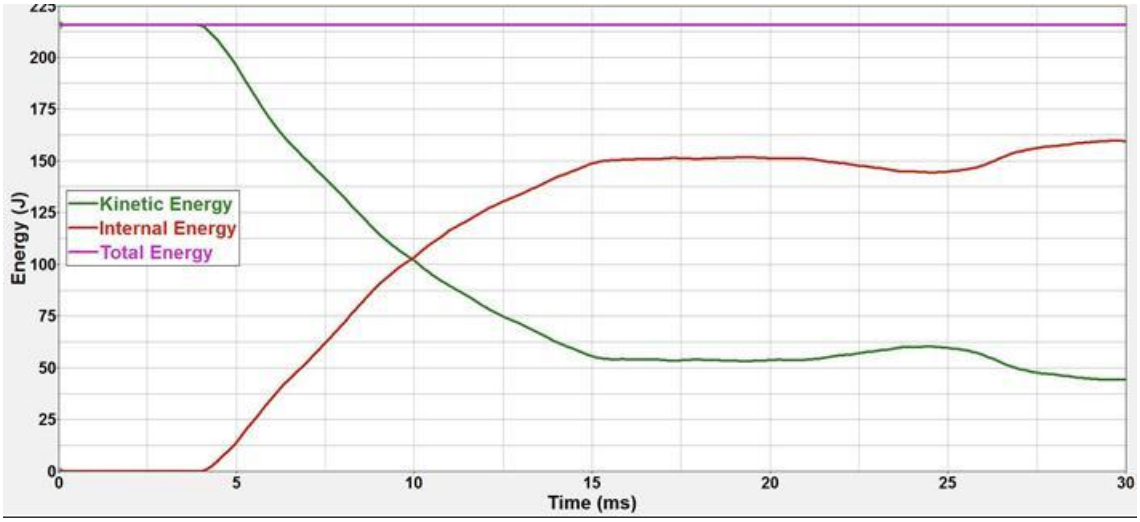

Figure 7.8: Energy plot from the finite element model

7.4 Head impact finite element model

Currently, finite element models of head impactors, complete anthropomorphic test dummies and complete human body models are being used for head impact analysis in the safety community. In this research, only the child head impactor considered as this is the impactor used in the GTR–9 and NCAP tests to assess the protection offered by a vehicle in a child head impact.

The FE model for simulating the head impact contains the hood assembly and the interfacing components to constrain the hood assembly. It contains a validated head impactor model and the prescribed requirements for the impactor such as mass, diameter, angle, position and initial velocity of the impact to match the ANCAP pedestrian protection testing protocol.

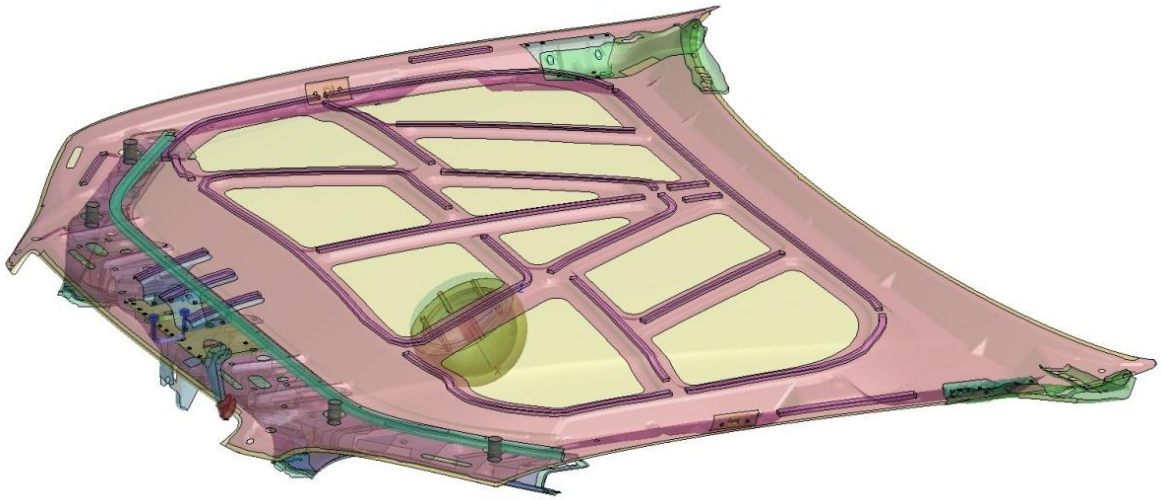

Figure 7.9: Pedestrian head impact finite element model

To minimise the CPU time for solving the FE model, the FE model was developed for only the hood assembly and the front tie bar assembly. The front tie bar assembly has been clipped, as shown in Figure 7.9. The interface between the modelled parts and the rest of the car body has been modelled by attaching it to the ground through applying appropriate boundary conditions.

The deforming components have been modelled accurately with the necessary mesh quality. This requires checking of the element length, aspect ratio, warpage and angles of the mesh in the FE model. The position and properties of the connections between the components such as the welds, joints, clinches and adhesives have been matched to the physical vehicle build. Validated material models have been used to assign the material

properties of various components used in this research. Stress–strain curves at specific strain rates have been included for the deforming components to improve the predictive accuracy of the model.

The interaction between the vehicle and impactor has been defined using the contact definitions in LS–DYNA. The coefficient of friction has been assigned to define the friction between the vehicle components and the impactor components as well as the friction between the vehicle and the impactor.

7.5 Correlating finite element simulations with experimental results

The experimental results of a large sedan already in the market and tested by ANCAP for pedestrian protection have been utilised for correlation. ANCAP tested this vehicle to assess the level of pedestrian protection offered using the Euro NCAP pedestrian subsystem testing protocol version 5.3. The pedestrian protection experimental tests were conducted at the Centre of Automotive Safety Research, Adelaide and were supervised by the author of this thesis.

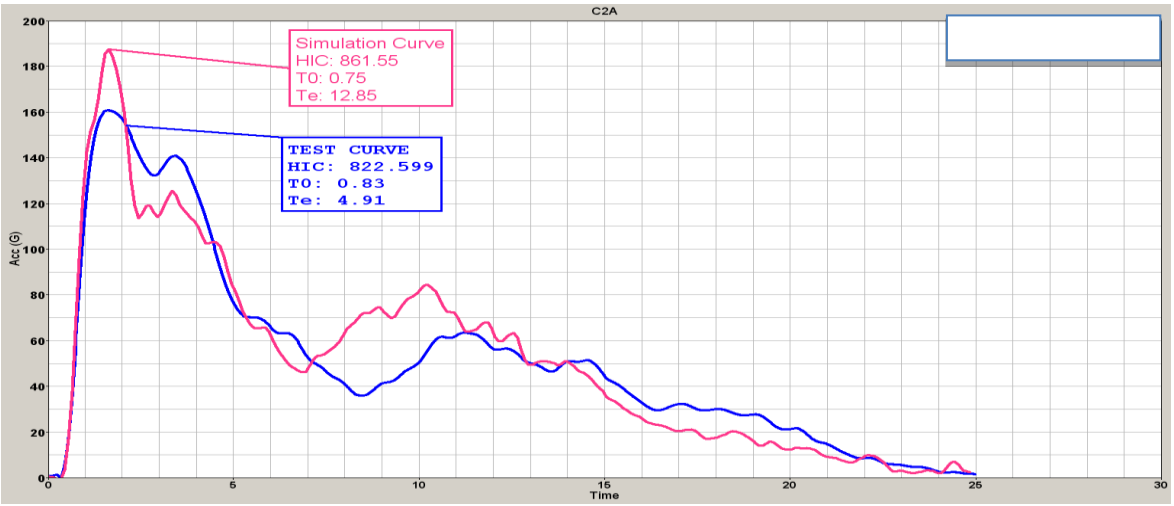

Figure 7.10: Correlation between ANCAP test and FE simulation

Figure 7.10 and Figure 7.11 show good correlation between experimental test results and CAE simulations in both measured head acceleration and the deformation pattern of the hood outer surface.

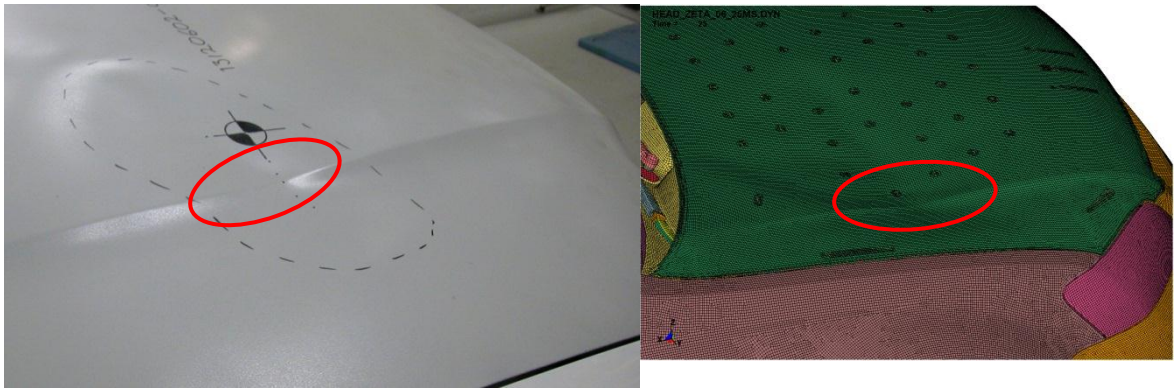

Figure 7.11: Correlation of hood deformation between ANCAP test and FE simulation

The correlation was used to calibrate the FE models to obtain good predictive accuracy in the numerical tests for the optimal hood design solution.

7.6 Computation of hood intrusion

The accelerometer, which measures the acceleration in three directions, is located at the mass centre of the impactor. In the FE model, a node has been placed at this location to represent the accelerometer and enable computation of the impactor displacement in both local and global coordinates, as shown in Figure 7.12.

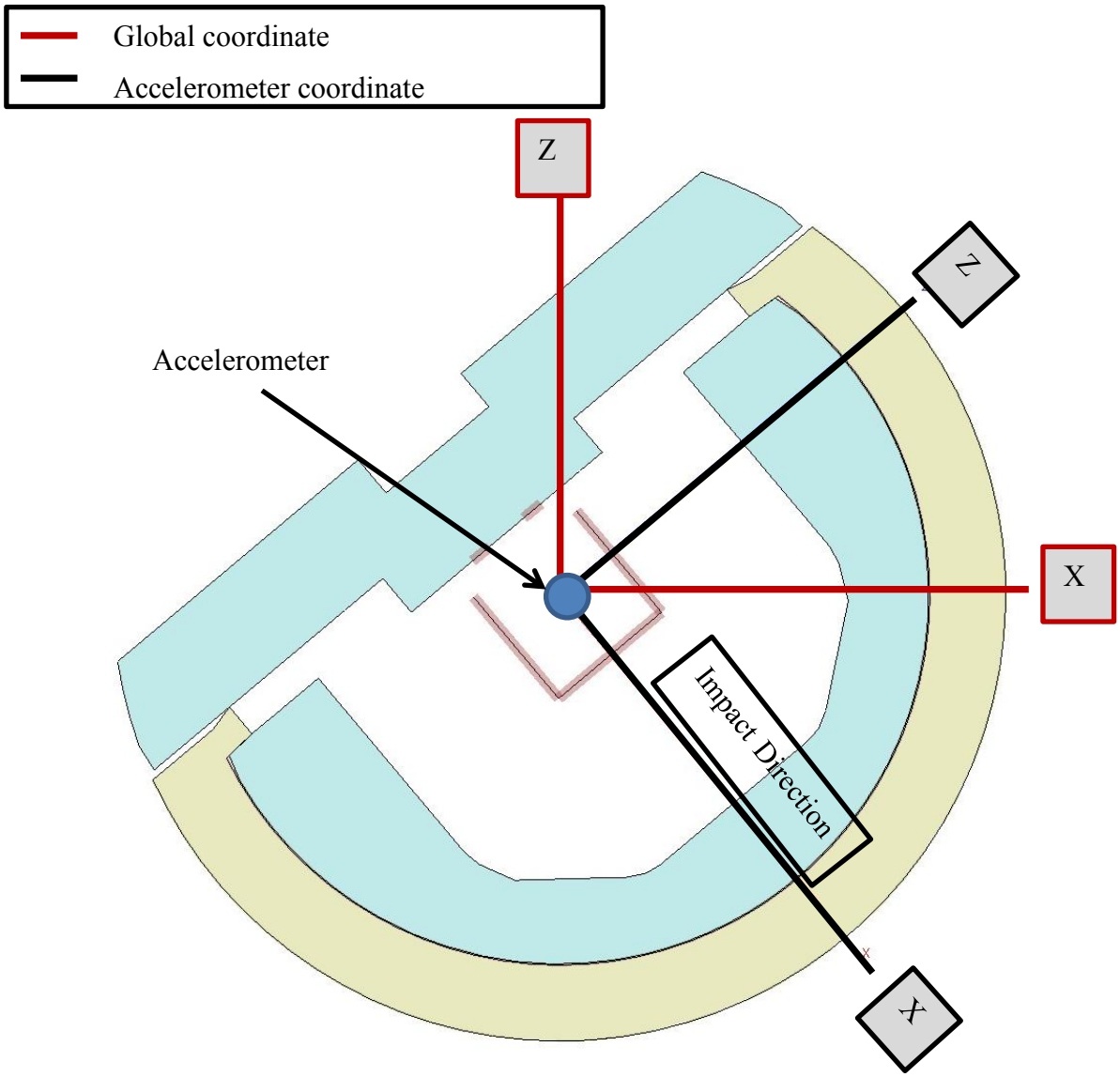

Figure 7.12: Coordinates for intrusion computation

When the displacement is determined in the impact axis using the node on the accelerometer, the displacement (Intrusion A) is more than the calculated intrusion in impact direction (Intrusion T), as shown in Figure 7.13.

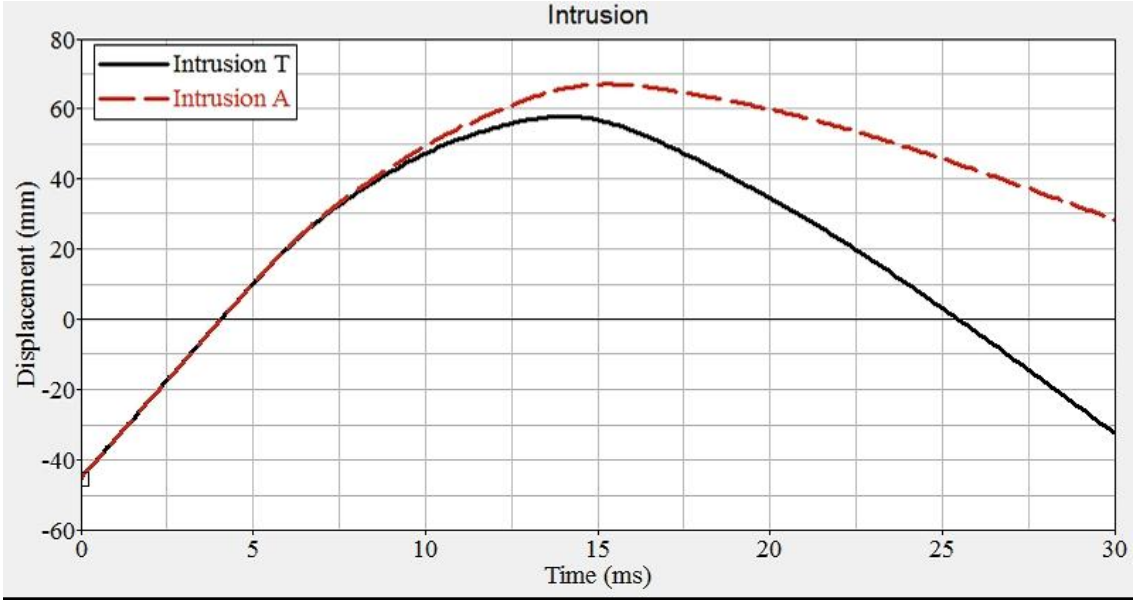

Figure 7.13: Comparison of impactor intrusion

This is due to the rotation of the accelerometer axis along with the impactor rotation in rebound as shown in Figure 7.14. Therefore, the impactor intrusion in the vertical axis, which is the Z direction, was computed in global coordinates.

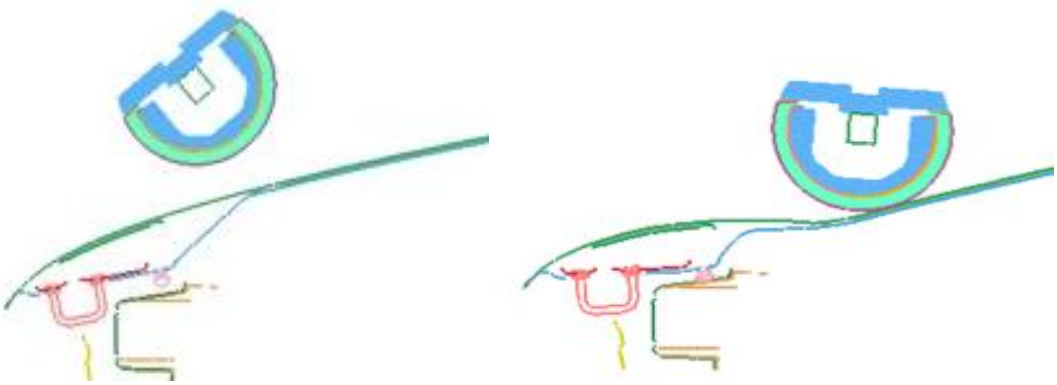

Figure 7.14: Accelerometer rotation due to impactor rebound

The intrusion computed in the Z direction was multiplied by 1/sin (θ), which was calculated using trigonometry, to derive the intrusion in the impact direction (Intrusion T) as exhibited in Figure 7.15.

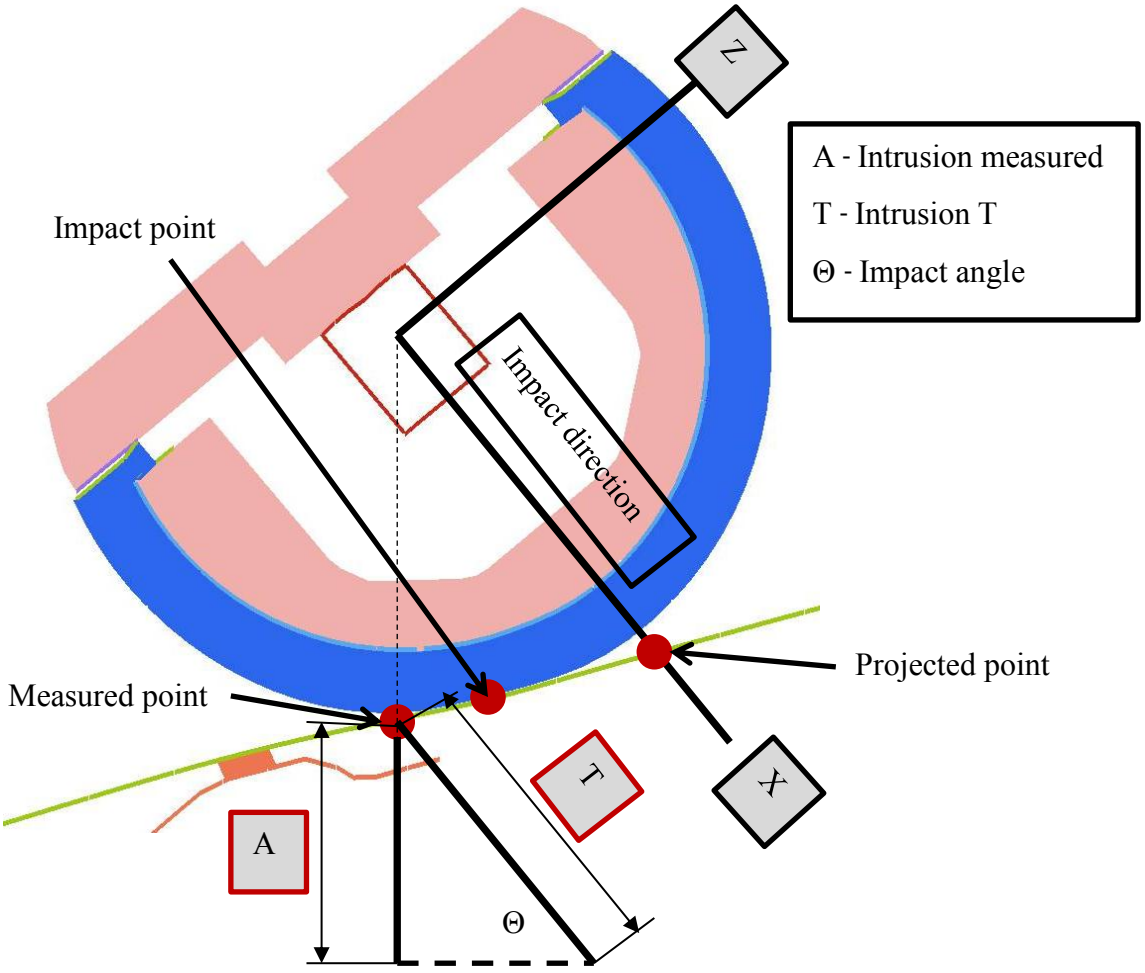

Figure 7.15: "Intrusion T" calculation method

Although "Intrusion T" was calculated from the displacement of the centre of the head impactor in the global Z direction, there could be a variation between the actual intrusion and "Intrusion T" if the first point of contact or impact point is different to the measured point. In addition, an assumption has been made that there is no compression of the head

form in the impact. In this research, the “Intrusion T” measurement has been utilised as the actual deformation space required in all the calculations and comparisons.

Chapter 8

Vehicle design for pedestrian head impact protection

8.1 Containing systems diagram

In-depth customer requirement analysis was conducted using a tool called Containing Systems Diagram. In general, it provides a visual representation of all the requirements related to a particular subsystem in a vehicle. The containing systems diagram developed in this work for the hood assembly is presented in Figure 8.1. It outlines the main functions and constraints that have to be fulfilled by the hood assembly. These functions and constraints have been taken into consideration in selecting the design parameters for improving pedestrian protection performance.

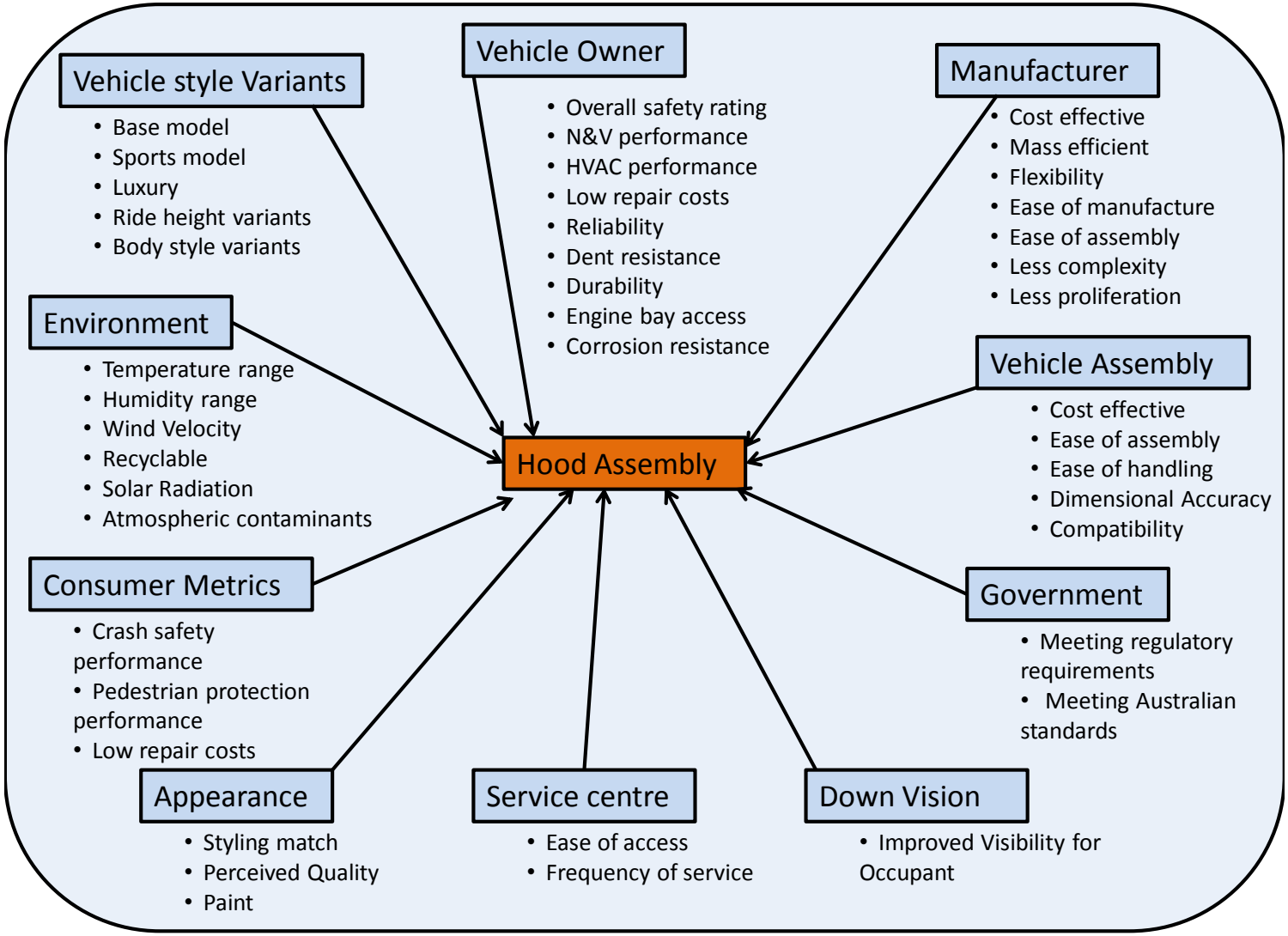

Figure 8.1: Containing systems diagram

8.2 Design space definition

The design space is the available space into which the hood assembly should fit without affecting the down vision plane, according to the regulatory requirement ECE–R125 and positioning of the components within the engine bay.

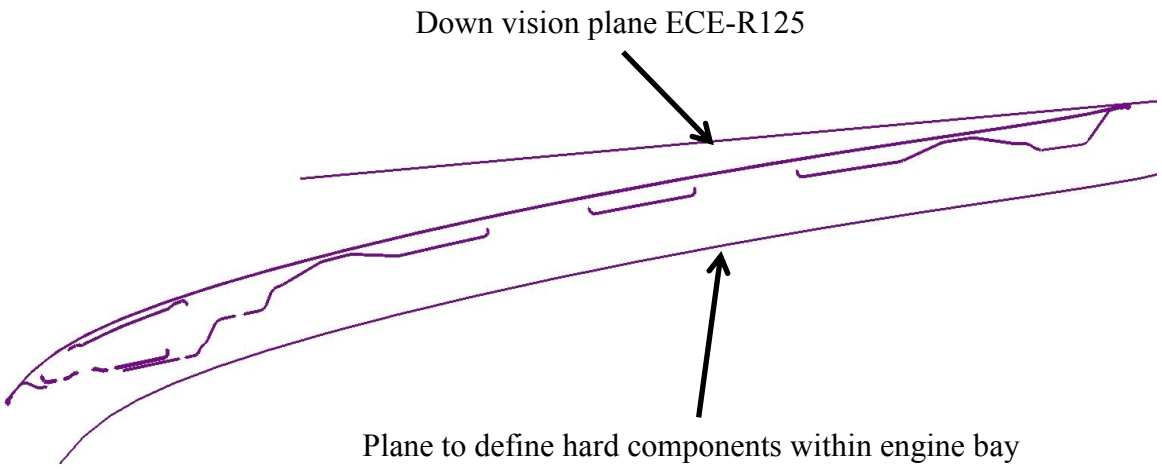

Figure 8.2: Design space for hood assembly

Figure 8.2 illustrates the available packaging space for inner and outer hood panels. The inner and outer hood panels are the two main components in the hood assembly that affect pedestrian protection performance.

Therefore, the scope of this research is to optimise the inner and outer hood panels to meet the HIC value requirements with minimal deformation, as shown in Figure 8.3. However, modifications that may be required in interfacing components to improve the pedestrian safety performance offered by the vehicle are not included in the scope of this research.

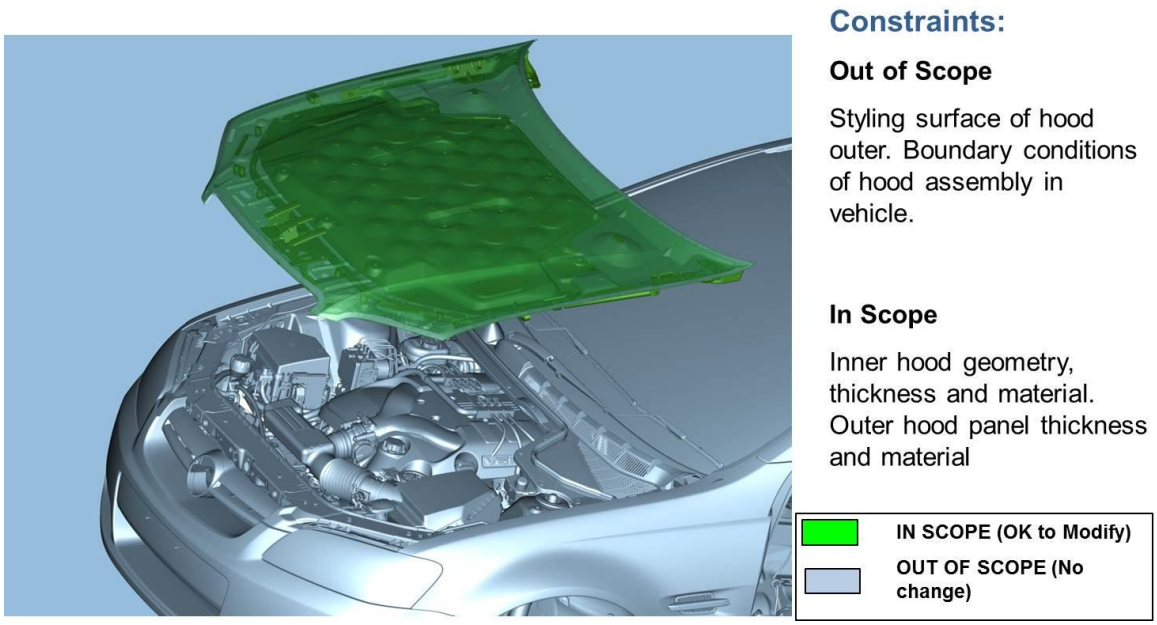

Figure 8.3: Scope of the project

8.3 Impact area definition

The head impact area on the hood was defined as per the GTR–9 test area definition. The Hood Leading Edge (HLE – Figure 8.4) or 1000 Wrap Around Distance (WAD – Figure 3.16), Hood Rear Reference Line (HRRL – Figure 8.5) and Side Reference Lines (Figure 8.6) determine the boundaries for head impact area. WAD divides the head impact area into adult and child head impact zones. WAD is the distance measured from the ground using a flexible tape held taut on the outer surface of the vehicle front structure in a vertical longitudinal plane.

In the GTR–9 protocol, the accident data and technical feasibility of regulating within the test area are the basis for WAD boundaries. The child impact area is defined from 1000 WAD or HLE to 1700 WAD and the adult head impact area are defined from 1700 WAD to HRRL or 2100 WAD. The resulting test area is as shown in Figure 8.7.

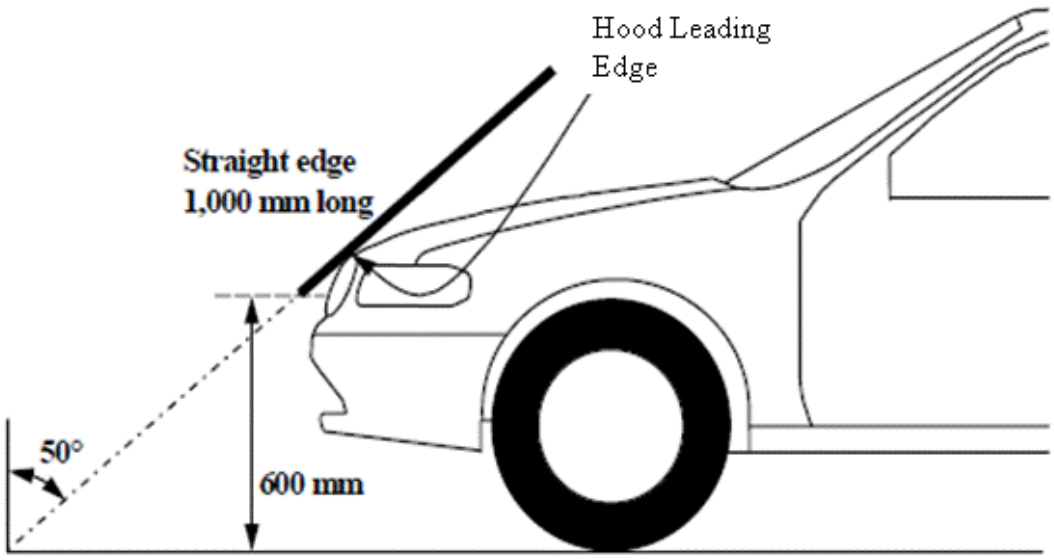

Figure 8.4: Hood leading edge (United Nations Economic Commission for Europe 1998)

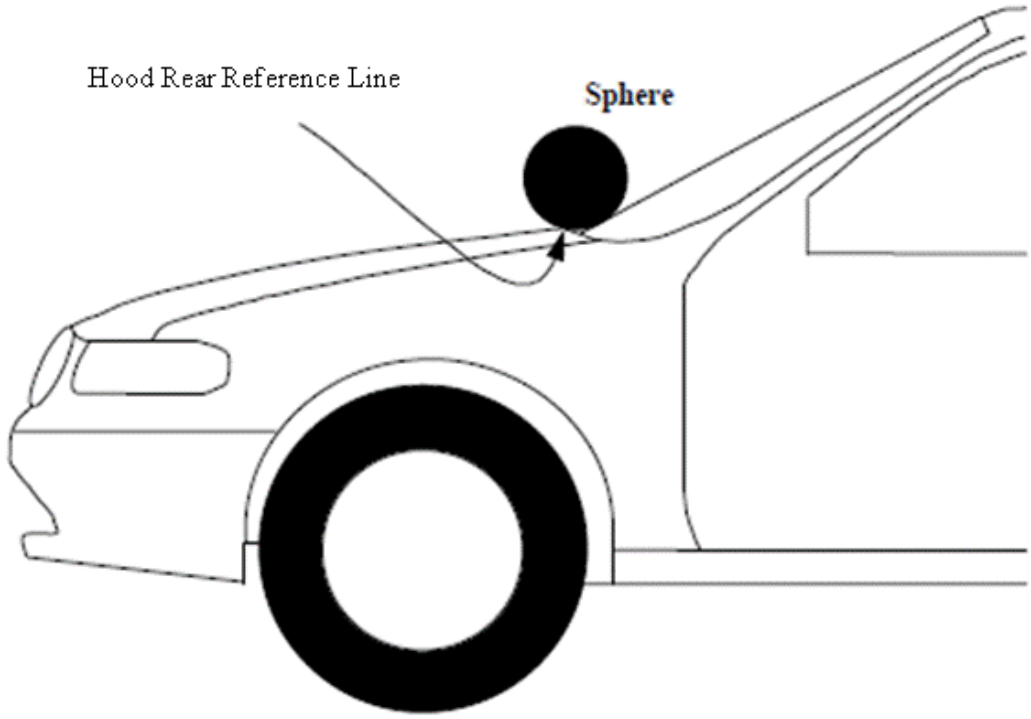

Figure 8.5: Hood rear reference line (United Nations Economic Commission for Europe 1998)

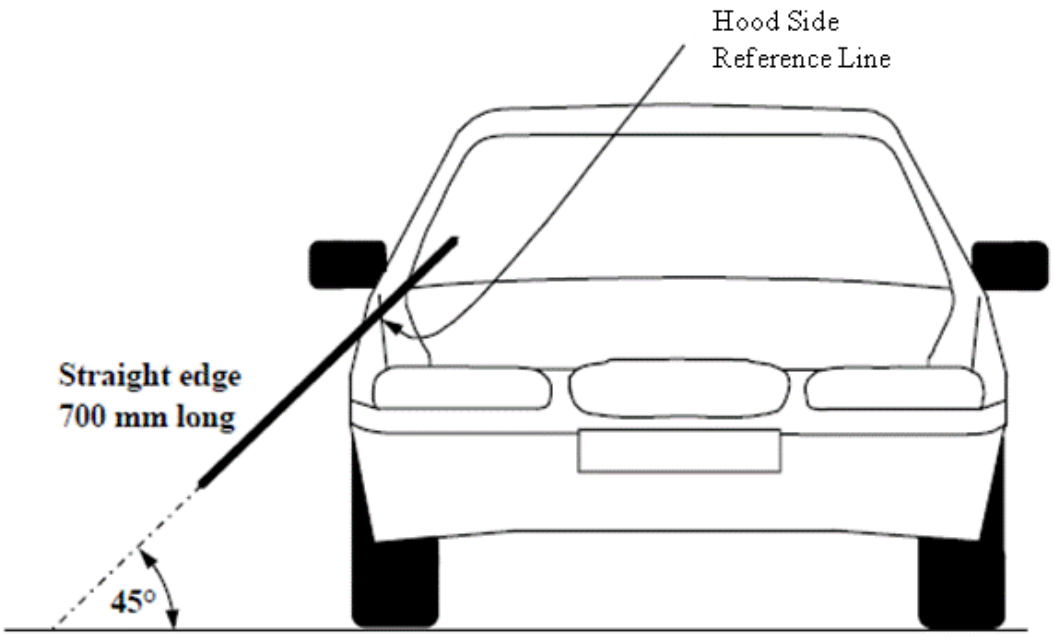

Figure 8.6: Hood side reference line (United Nations Economic Commission for Europe 1998)

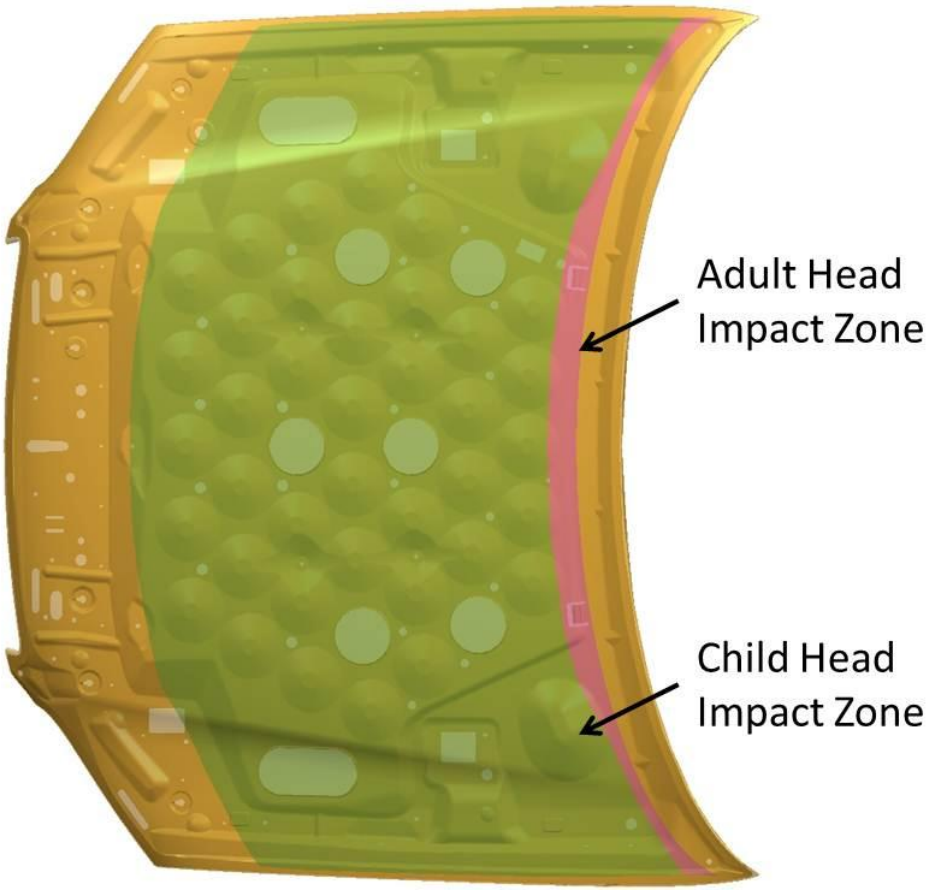

Figure 8.7: Head impact test area on hood

Figure 8.8: Impact positions considered for optimisation

A range of impact points has also been selected for the numerical simulations, varying in fore aft as well as in cross–car directions of the vehicle at regular intervals in order to analyse the central area of the hood, as shown in Figure 8.8. These impact positions are within the child head impact zone. This area has been selected because high hood intrusions occur in the central area of the hood and the interfaces around the edges prevent deformation.

The impactor speed has been set to the ANCAP requirement, 40km/h that is higher than the GTR–9 test speed, which is 35km/h, to analyse the most severe load case.

8.4 Engineering principles of good design

The engineering principles for a good hood design were applied while developing the inner hood structure concepts. The principles are as follows:

- use of maximum possible corner radii and avoidance of sharp corners
- use of smooth transitions in surface changes and avoidance of steps or discontinuities
- use of maximum possible radii at the intersection of beams
- use of effective joints to reduce the loads in surrounding beams
- use of design strategy to reduce mass and cost.

The detail designs of attachment strategy and boundary conditions are out of the scope of this research. In addition, durability, noise, vibration, dent resistance, occupant protection and other performances have not been considered in the analysis.

Chapter 9

Parameters for improving pedestrian protection

9.1 Concepts generation

Various concepts for the inner hood structure were considered. The selection of concepts was done referring to literature and the hoods available in the market that could be considered in the hood design for a large sedan as shown in Figure 9.1.

The inner hood structures considered for improving pedestrian protection performance are the beam, cut–out, skeleton, grid and multi–cone patterns.

The beam pattern has beams positioned in the fore–aft direction of the vehicle, which provides structural stiffness to the hood assembly.

The cut–out pattern is a mass–saving and cost–saving option in which the centre portion of the inner hood has a large opening.

The skeleton pattern is beams nested in an A–shape. This pattern allows improving the structural stiffness of the hood in the centre, but outboard openings reduce the mass and structural stiffness.

The multi–cone pattern is cone shaped forms nested at constant distances. This design provides homogeneous structural stiffness.

The grid pattern consists of longitudinal and lateral beams arranged at regular intervals. Thus, this pattern also should provide homogeneous structural stiffness and the cut–outs enable mass reduction.

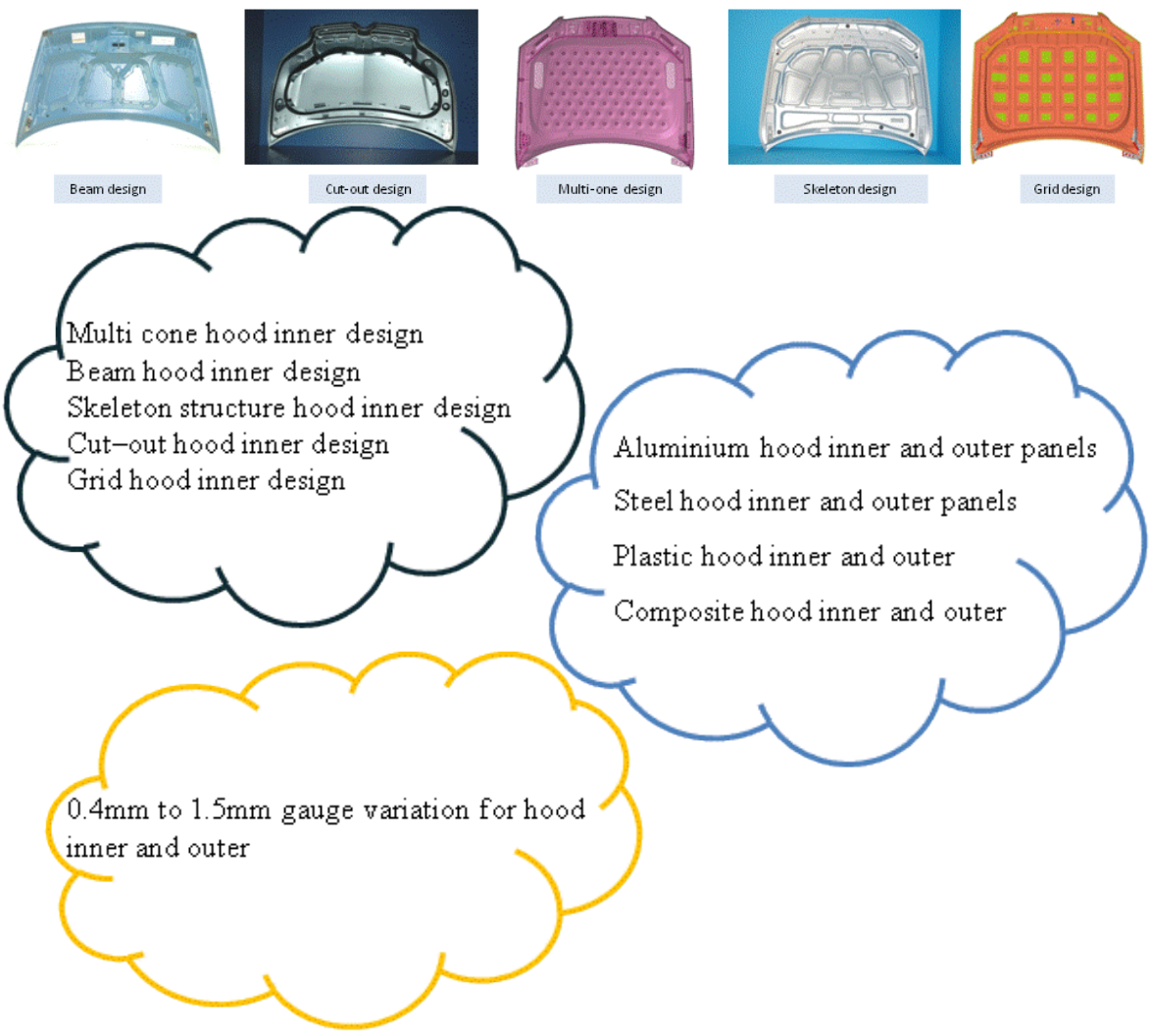

Figure 9.1: Concepts for improving pedestrian protection performance

Aluminium and steel were considered in the analysis for the inner and outer hood material because they generally meet the requirements for noise and vibration, durability and high–speed crash performances. A thickness range of 0.4mm to 1.5mm was considered for the inner and outer hood thickness, values less than 0.4mm will not meet the durability and forming requirements while those above 1.5mm will result in high structural stiffness and structural inertia as well as increased mass.

Concept / Criteria	Steel(current)	Aluminium (concept 1)	Plastic (concept 2)	Composite (concept 3)
Impact on cost		-	+	-
Impact on mass	D	+	+	+
Ease of assembly installation	A	S	+	S
Durability	T	S	-	-
Ability to withstand engine compartment heat	U	S	-	-
Hood stiffness consistency	M	S	-	-
Compatiblity with high-speed crash conditions		S	-	-
Noise and vibration		S	-	-
Long-term reliability		S	-	-
Appearance		S	-	-
Σ+ (Sum of positives)		1	3	1
Σ– (Sum of negatives)		1	7	8
ΣS (Sum of "sames")		8	0	1

Concept / Criteria	Beam design	Cut-out design (concept 1)	Multi-cone design (concept 2)	Skeleton design (concept 3)	Grid design (concept 4)
Impact on cost		+	-	-	-
Impact on mass	D	+	-	-	-
Ease of assembly installation	A	S	S	S	S
Complexity of design (manufacturability)	T	S	S	S	S
Durability	U	S	+	+	+
Hood stiffness consistency	M	-	+	+	+
Compatiblity with real-world impacts		-	+	+	+
Noise and vibration		-	+	+	+
Long-term reliability		-	+	+	+
Appearance		-	+	+	+
Σ+ (Sum of positives)		2	6	6	6
Σ– (Sum of negatives)		5	2	2	2
ΣS (Sum of "sames")		3	2	2	2

+ = Better than datum
- = Worse than datum
S = Same as datum

Figure 9.2: Pugh matrix

9.2 Concepts evaluation

The concepts mentioned in the previous section were analysed through the Pugh matrix as shown in the previous page in Figure 9.2.

Figure 9.3: Inner hood geometries chosen for developing an optimal solution

The comparison of the concepts to various performance criteria, multi–cone, skeleton and grid patterns for inner hood structure (Figure 9.3) ended up with the same merits, as well as aluminium and steel for the material. Therefore, these configurations were chosen for further evaluation. The hood attachment and boundary strategies, though may improve pedestrian protection performance, were not been taken into consideration throughout the analysis.

9.3 Control factors in scope

Design parameters such as thickness and material for the inner and outer hood panels as well as inner hood structure were considered for improving the pedestrian protection performance. Figure 9.4 shows the list of control factors that are in scope to modify the concepts selected through the Pugh matrix.

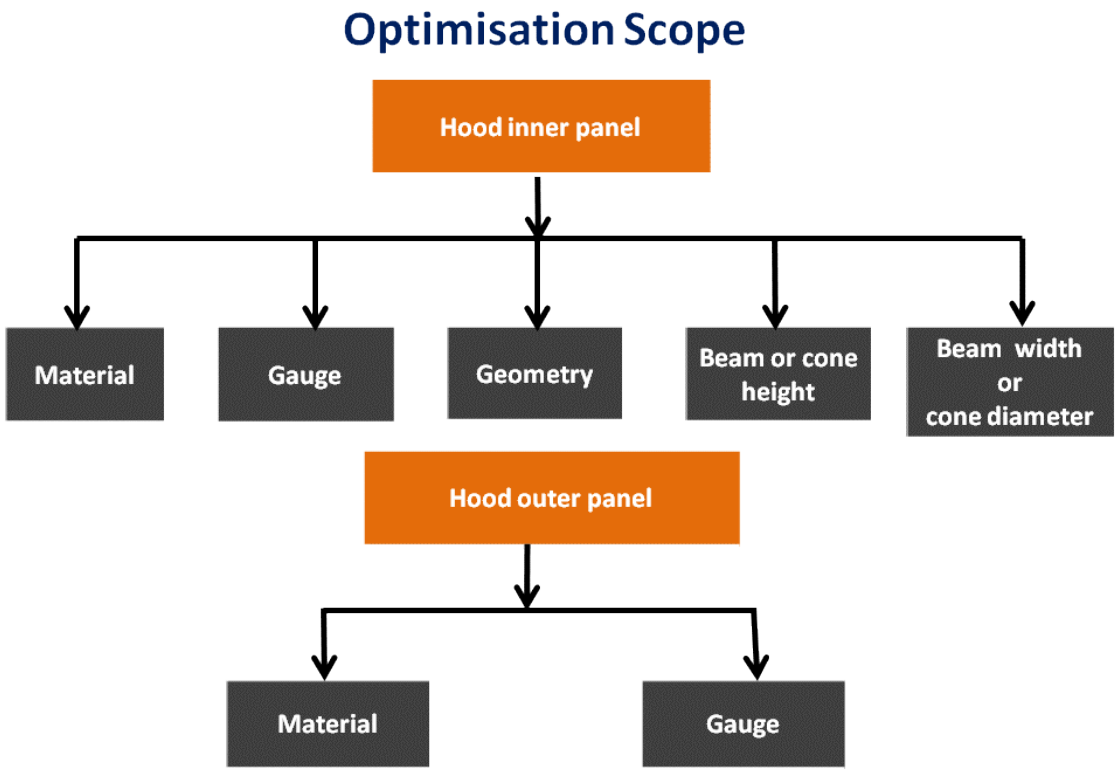

Figure 9.4: Control factors in scope for refinement

The variables considered in this study have been summarised in Table 9.1; tolerances otherwise known as noise factors that might have some influence on the resulting HIC value and the deformation of hood panels have not been considered in this research work for simplicity purposes.

Variable	Values of variable	Type of variable
Inner hood geometry	Skeleton pattern, Multi–cone pattern Grid pattern	Discrete
Inner/outer hood material	Aluminium Steel	Discrete
Inner hood gauge	0.4mm to 1.5mm	Continuous
Outer hood gauge	0.4mm to 1.5mm	Continuous
Impact position	1 to 8	Discrete

Table 9.1: Variables considered for refinement

9.4 Concepts refinement

The parameter diagram as shown below in Figure 9.5 clearly outlines the relationship between the input and output parameters.

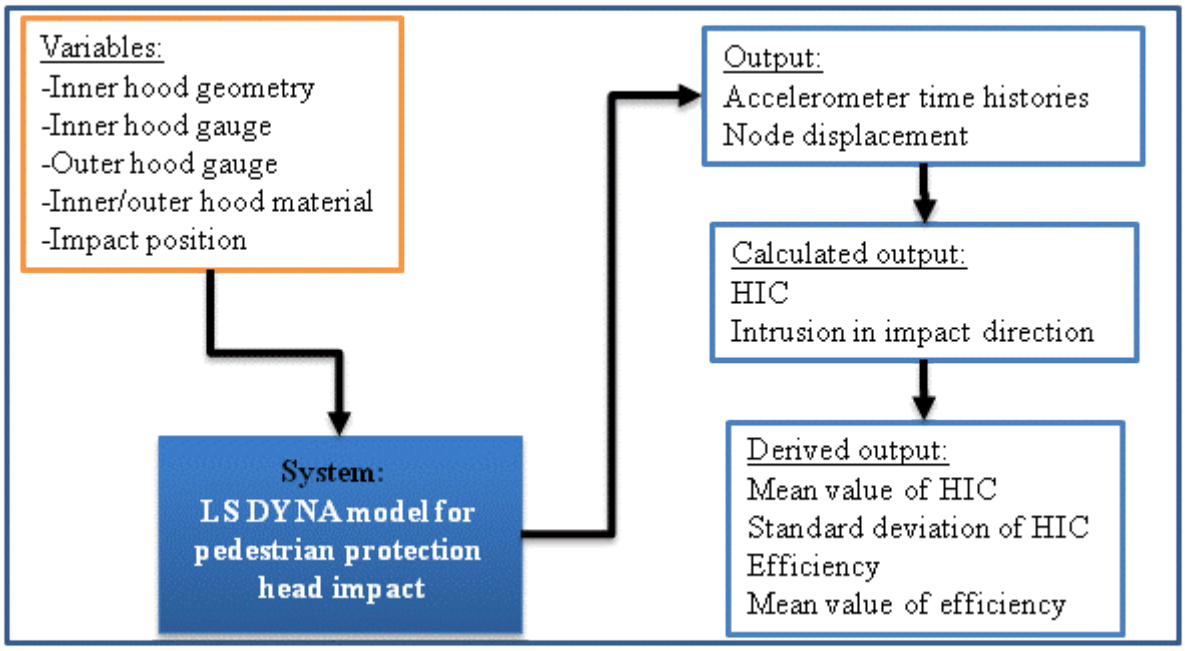

Figure 9.5: Parameter diagram

Chapter 10

Optimisation of hood panels

10.1 Methodology

Strength–two orthogonal array design of experiments was used in this work to create a matrix with the variables mentioned in Table 9.1. This matrix was utilised to create a multitude of hood designs by varying the values of these design parameters. Non–linear LS DYNA models were created to replicate pedestrian protection head impact physical testing for all the configurations as per the Design of Experiments (DOE) matrix. The accelerometer time histories were gathered as output for all numerical tests, and from that, the HIC values were calculated using Equation 3.3. The vertical intrusion of the head impactor from the node displacement was also collected to calculate the intrusion in impact direction. Accordingly, the efficiency was derived for all hood configurations. Finally, the mean value of efficiency (μ_η), the mean value of HIC (μ_{HIC}) and the standard deviation of HIC (σ_{HIC}) were derived for all the hood configurations while considering all impact positions.

The μ_η provides average efficiency between the impact positions for a given configuration of the hood assembly. Similarly, σ_{HIC} from the calculated mean value for a given

configuration of the hood assembly between the impact positions was utilised to quantify the homogeneous behaviour of the hood assembly. The μ_{HIC} provides the average HIC value between all the impact positions for a given configuration of the hood assembly. The aim was to obtain the lowest value of σ_{HIC} thus achieving better homogeneous head impact performance with the highest value of μ_{η} for HIC values less than 1000.

The Kriging response surface based approach was used as an interpolation method to predict the values for the variables considered in the improvement of pedestrian protection. The Kriging interpolation method was named after a South African mining engineer DG Krige and it has been used as a fundamental tool in the field of mining (Bohling 2005). In recent times, this method has been successfully implemented in a variety of applications. In the Kriging approach, the response surface is mapped with limited sample data in the design space followed by utilising this surface to estimate the values of variables at locations where the sample data is unavailable. In this research, response surfaces were mapped with the numerical results for μ_{η}, μ_{HIC} and σ_{HIC}.

Figure 10.1 shows the predictive accuracy of the μ_{HIC} response surface. The analysis of variance (ANOVA) technique was used to assess the relationship between the inputs and outputs as well as to identify the important variables in this study (Gelman 2004). The ANOVA charts showed that the material, thickness of the inner hood panel, thickness of the outer hood panel and the hood inner structure contribute a substantial percentage in determining the μ_{η}, μ_{HIC} and σ_{HIC} values. The ANOVA graph for the μ_{HIC} was presented in Figure 10.2.

In Figure 10.2, HOODMATL is the hood panel material, OTRGAUGE is the thickness assigned for the outer hood panel, INRGAUGE is the thickness assigned for the inner hood panel and INRGEOM is the type of structure of the inner hood.

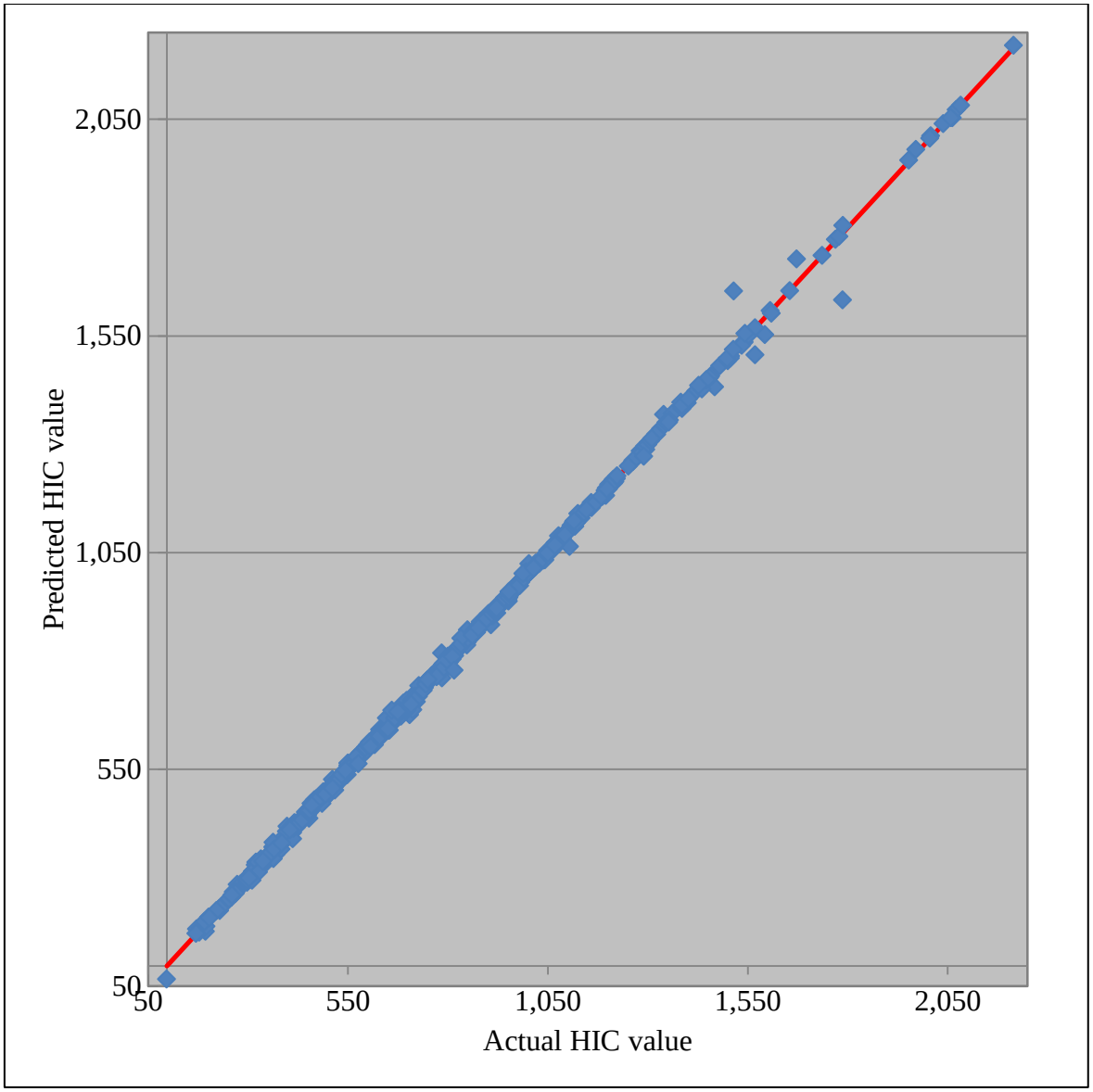

Figure 10.1: Predictability of response surface

The Monte Carlo method, which is a mathematical technique for statistical sampling was utilised to check whether any other configuration might provide a better output than the ones considered in the sample. This method generates a cloud of input variables that obey the defined properties for which the output was predicted from the existing response surfaces.

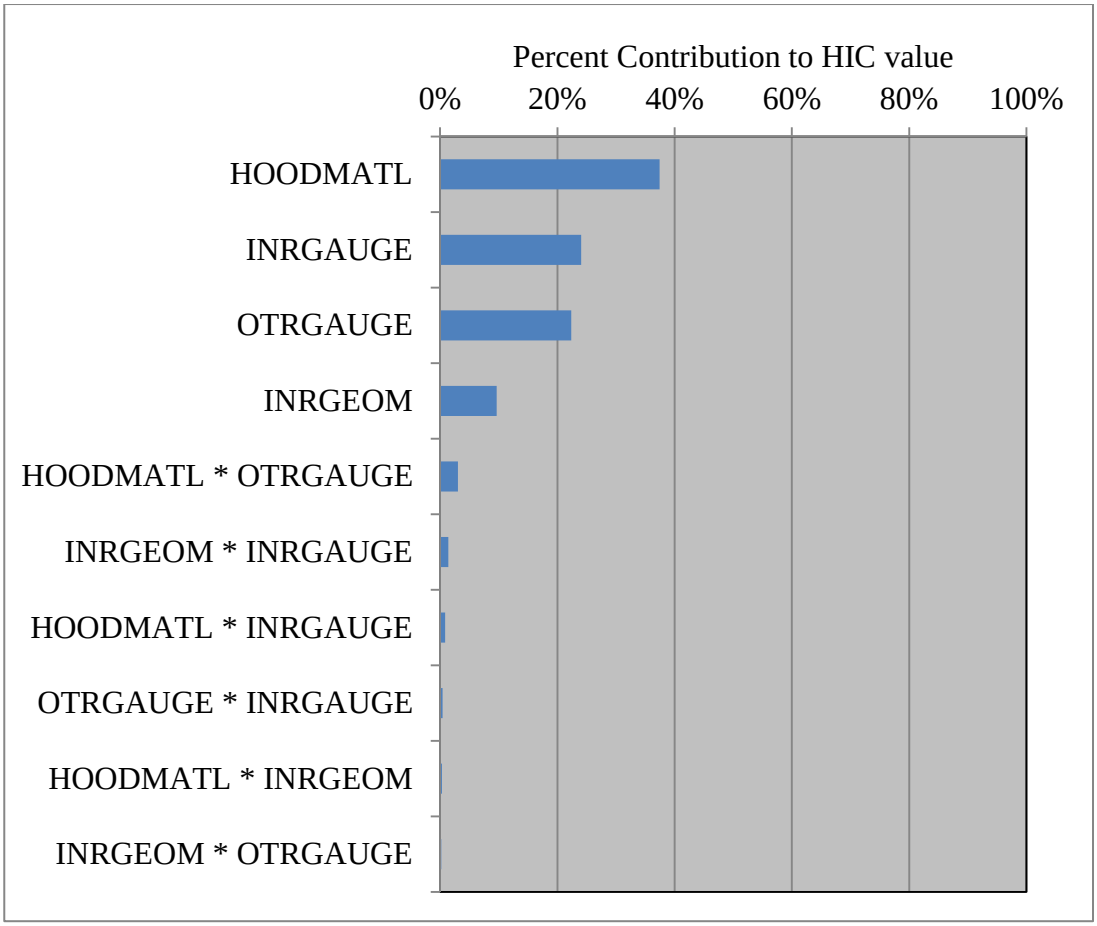

Figure 10.2: ANOVA chart for mean value of HIC

The sum of the mean value of HIC and its standard deviation ($\mu_{HIC}+\sigma_{HIC}$) provides 67% confidence to this research, assuming normal distribution (Narasimhan 1996). The aim of this study is to obtain 95% confidence by setting the HIC threshold condition to the sum of the mean value of HIC and twice its standard deviation ($\mu_{HIC}+2\sigma_{HIC}$) to be less than or equal to 1000. Aiming for 99%, robustness requires the HIC threshold condition to be the sum of the mean value of HIC and three times its standard deviation ($\mu_{HIC}+3\sigma_{HIC}$). For a production representative hood, it would be necessary to achieve all the impact positions less than the HIC value of 1000. This would be achieved through the detailed design work on a specific hood design and its interfacing conditions. Since this research focuses on a more general study looking at material, thickness and construction of hood panels, the 95% confidence limit is used.

The severity of pedestrian head injuries could be influenced either by the primary impact or by the secondary impact. These concepts were refined in two stages. The first step was the selection of the type of the inner hood structure and inner and outer hood material first by considering only primary impact followed by considering both the primary and secondary impacts. The second step was the selection of the outer hood panel thickness and the inner hood panel thickness and structure. The two–stage optimisation approach was utilised in this research to reduce the number of simulations and modelling complexity.

10.2 Selection of hood structure and material

10.2.1 Primary impact only

The components within the engine bay were not considered in this analysis model; thus, only primary impact has been taken into consideration.

In this research, the efficiency of a hood design was calculated as the ratio of the actual deformation of hood assembly ("Intrusion T") and the optimal deformation calculated from the HIC value of the corresponding analytical test. The optimal deformation is the theoretical minimum deformation needed for a given HIC value and it was calculated using Equation 10.1 (Wu & Beaudet 2007) as shown below:

$$d = 8.342 \times 10^{-3} \frac{v_0^{\frac{8}{3}}}{HIC^{\frac{2}{3}}} \qquad \textbf{Equation 10.1}$$

Where, d is the deformation and v_0 is the impact velocity.

In numerical testing, the actual deformation was computed in the Z direction and used to derive the "Intrusion T" as discussed earlier. The equation to calculate the efficiency (η) of the hood assembly is:

$$\eta = \frac{\text{Optimal deformation}}{\text{Intrusion T}} \qquad \textbf{Equation 10.2}$$

Thus, a hood configuration with maximum efficiency for an impact had minimum "Intrusion T" for a given HIC value.

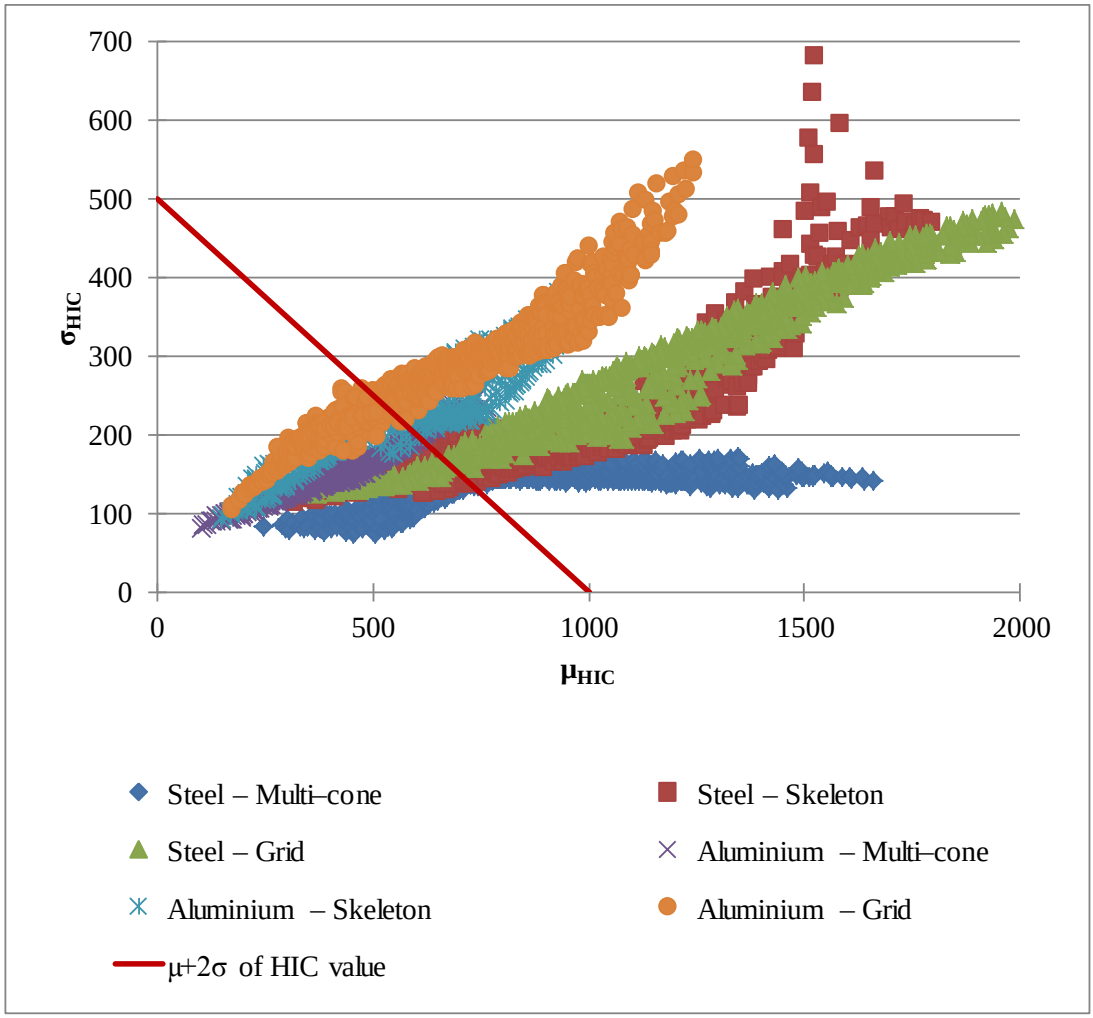

Figure 10.3: Influence of hood material and inner hood structure on HIC value

Figure 10.3 presents the predicted σ_{HIC} against corresponding μ_{HIC} plot. The data was grouped by only considering material and inner hood structure, to analyse the influence of material and inner hood structure on HIC values.

From Figure 10.3, it is evident that the HIC value less than 1000 can be obtained with all the inner hood geometries. It also shows that the HIC value less than 1000 can be obtained with both the materials, either steel or aluminium. and it is possible to achieve a mean value of HIC as low as 103, which translates to a very minor head injury. Nevertheless, this low HIC value may require very high deformation space and thin hood panels. Therefore, the sum of the mean value of HIC and twice its standard deviation ($\mu_{HIC}+2\sigma_{HIC}$) were plotted against the intrusion in impact direction ("Intrusion T"). The limit for "Intrusion T" was set to 100mm; hence, only the data less than the intrusion limit were considered for further analysis, as shown in Figure 10.4.

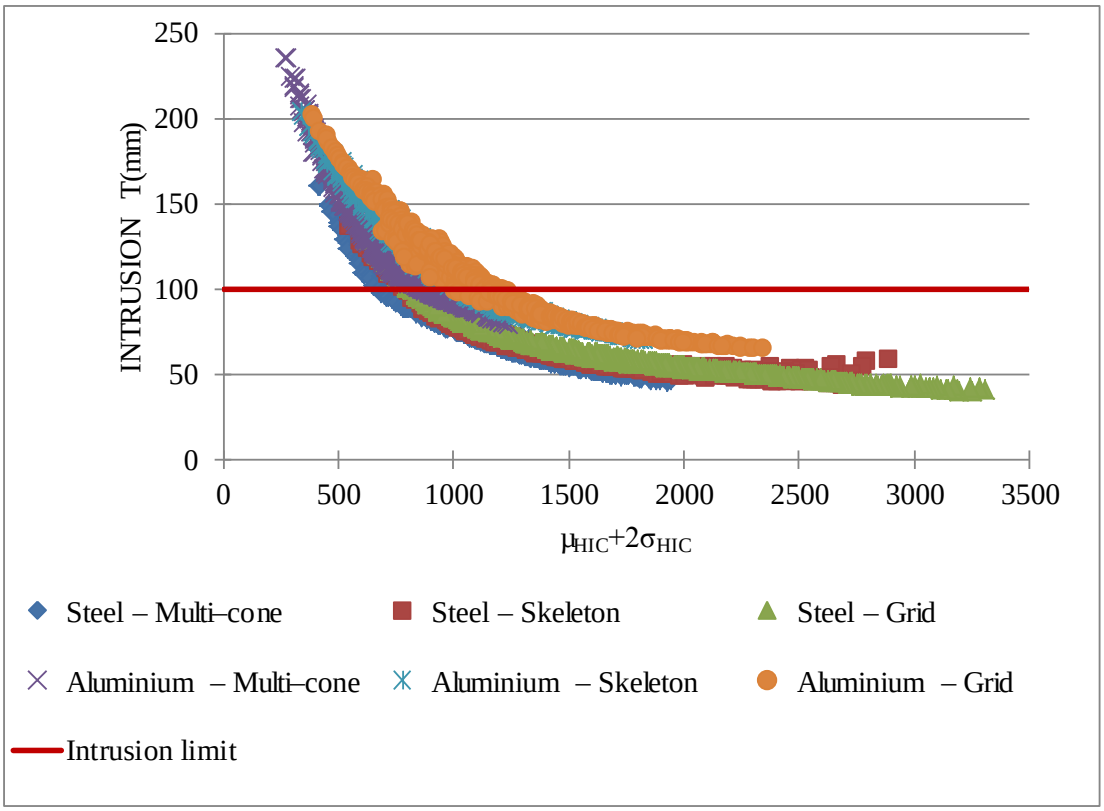

Figure 10.4: Influence of hood material and inner hood structure on intrusion

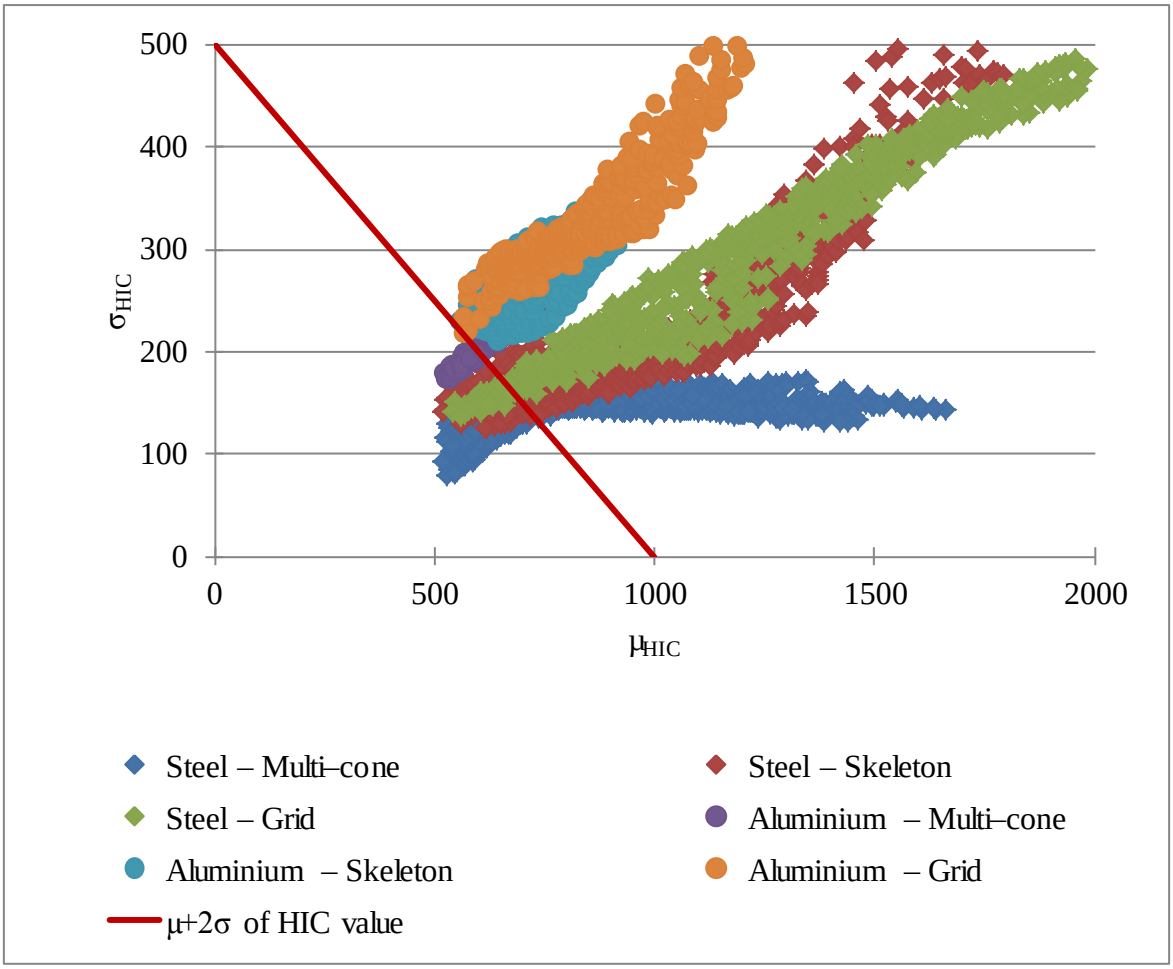

Figure 10.5: Results below HIC threshold value and intrusion limit

Figure 10.5 shows the μ_{HIC} plotted against σ_{HIC} for the data less than the intrusion limit. It also shows that robust and homogeneous behaviour below the HIC threshold value is possible with various configurations of the hood assembly. However, the multi–cone inner hood structure made of steel material provides the lowest μ_{HIC} and σ_{HIC}.

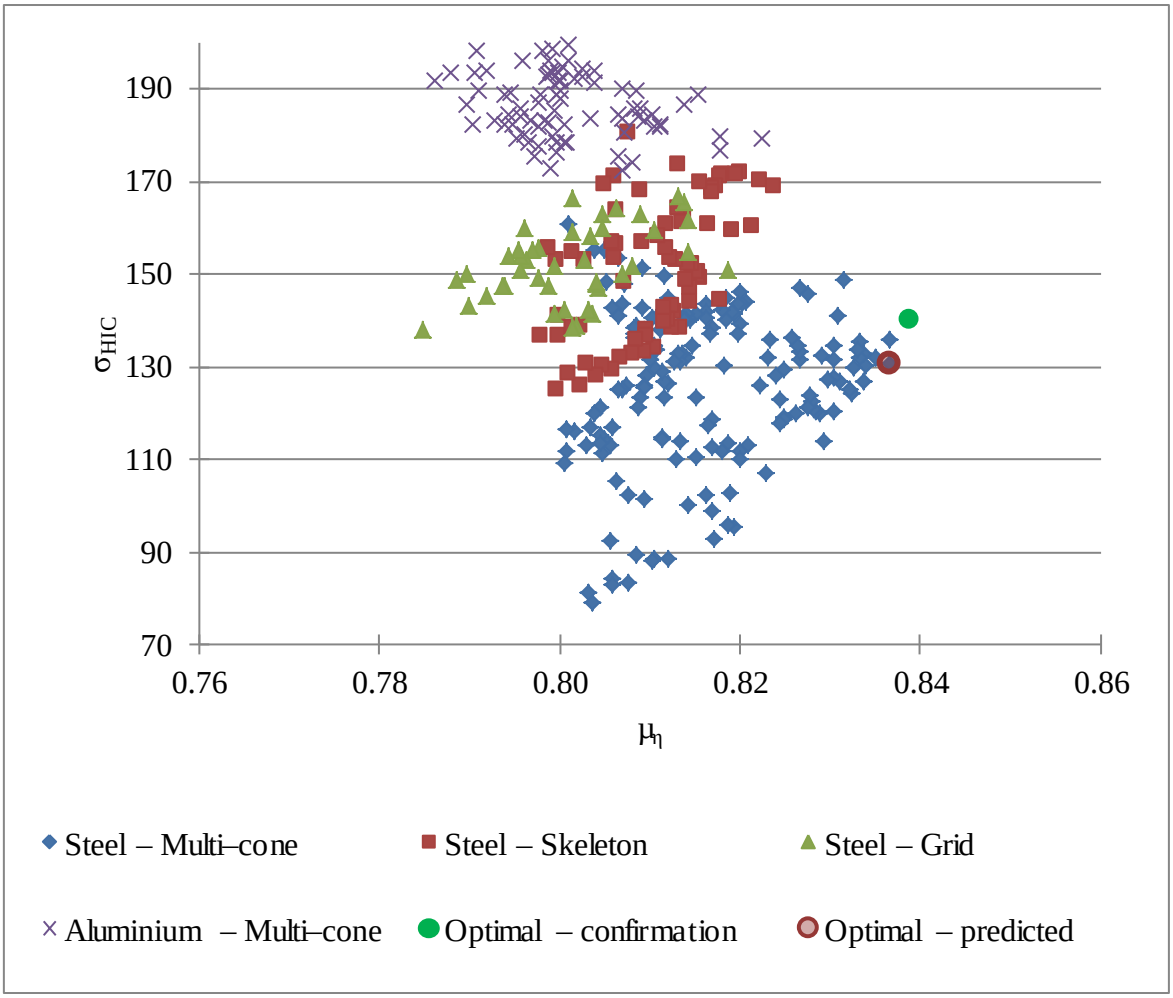

Figure 10.6: Evaluation of efficiency

Figure 10.6 shows the μ_η against respective σ_{HIC}. Among these configurations, the optimal hood configuration that provides the highest μ_η was identified as marked in Figure 10.6. The numerical tests conducted to check the predictive accuracy of this optimal solution show that the results are comparable, as shown in Figure 10.6. This showed that the deviation between the predicted and numerical values is within 0.01 and therefore it could be stated that accurate predictions can be made from the response surfaces.

The details of the results that were utilised to derive the μ_η and σ_{HIC} for the data point 'Optimal – confirmation' (Figure 10.6) are presented in the figures ranging from Figure 10.7 to Figure 10.14.

Numerical tests were conducted for eight impact locations (A-H) as shown in Figure 8.8 to derive the values for this data point and the details of the results from the numerical tests are shown in figures ranging from Figure 10.7 to Figure 10.14. The details included in these figures are,

- plot of resultant acceleration against time
- plot of the displacement of the impactor in global Z direction against time
- contour plot of the effective plastic strain
- contour plot of the magnitude of the deformation of the hood panels.

The results exhibited in figures ranging from Figure 10.7 to Figure 10.14 show that the deformation of the hood panels is not excessive, even while secondary impact is not considered, due to the optimisation of the structural stiffness of the hood panels.

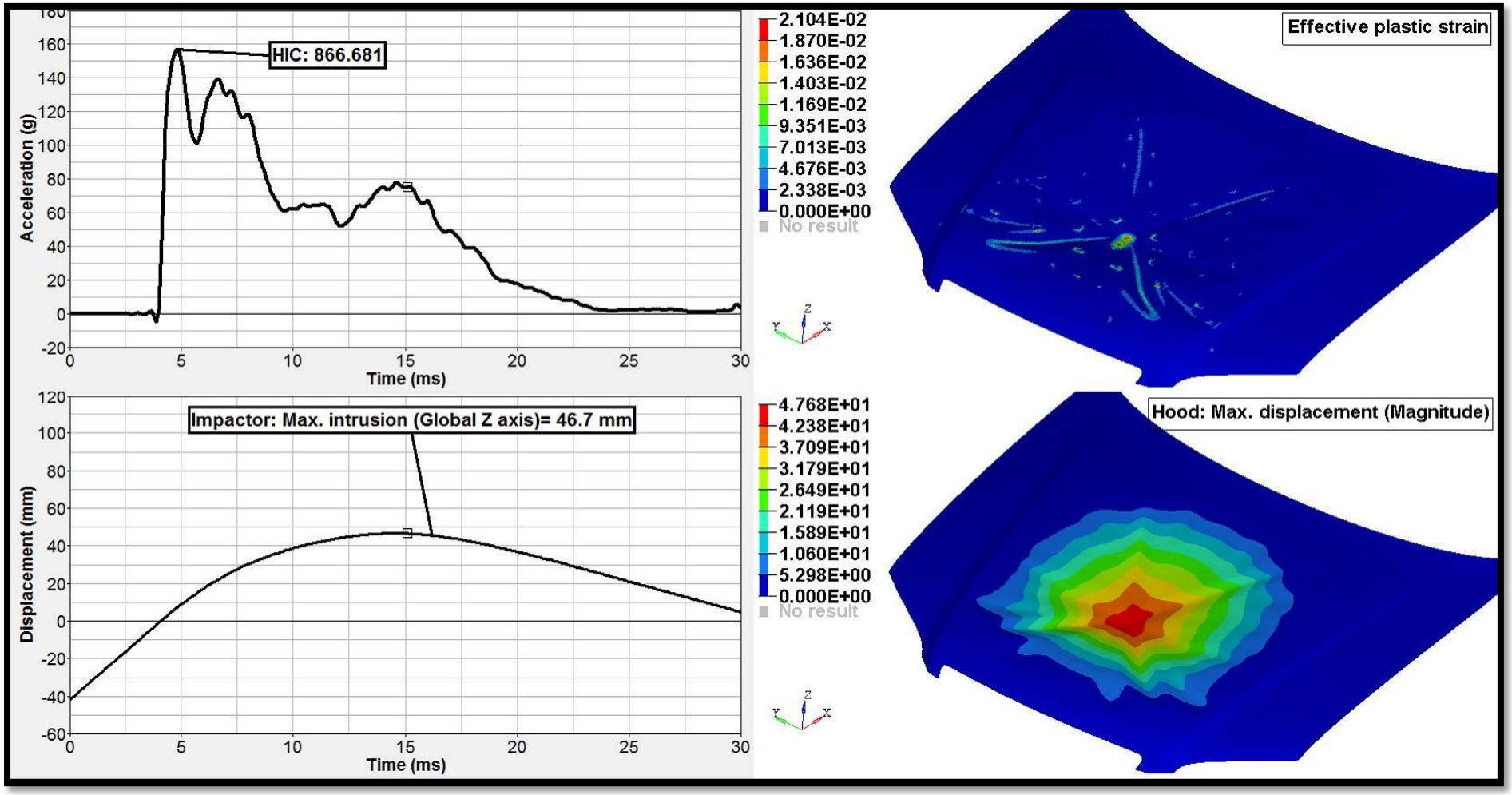

Figure 10.7: HIC value, effective plastic strain, displacement of the impactor and hood with consideration to primary impact only for point A

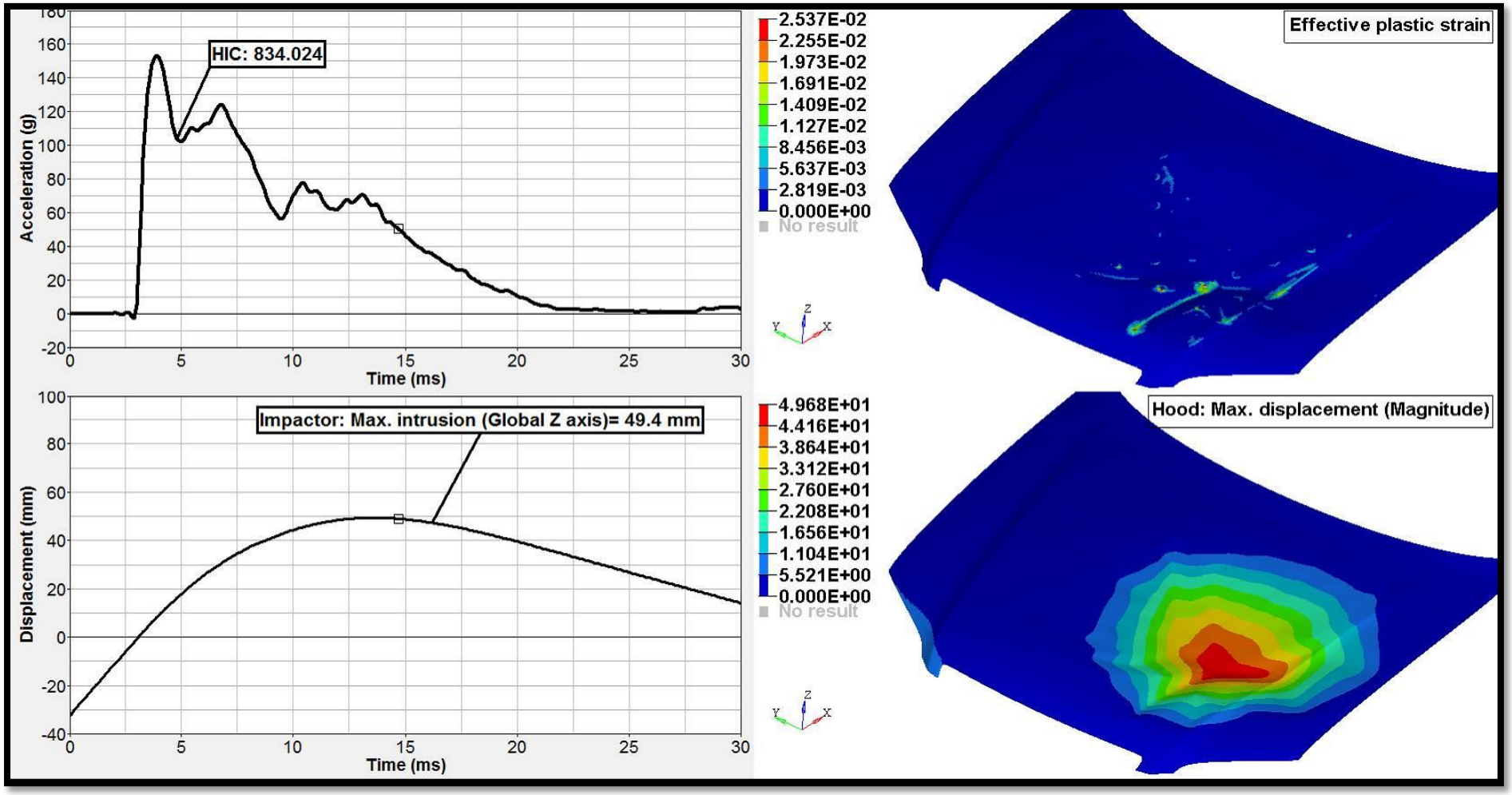

Figure 10.8: HIC value, effective plastic strain, displacement of the impactor and hood with consideration to primary impact only for point B

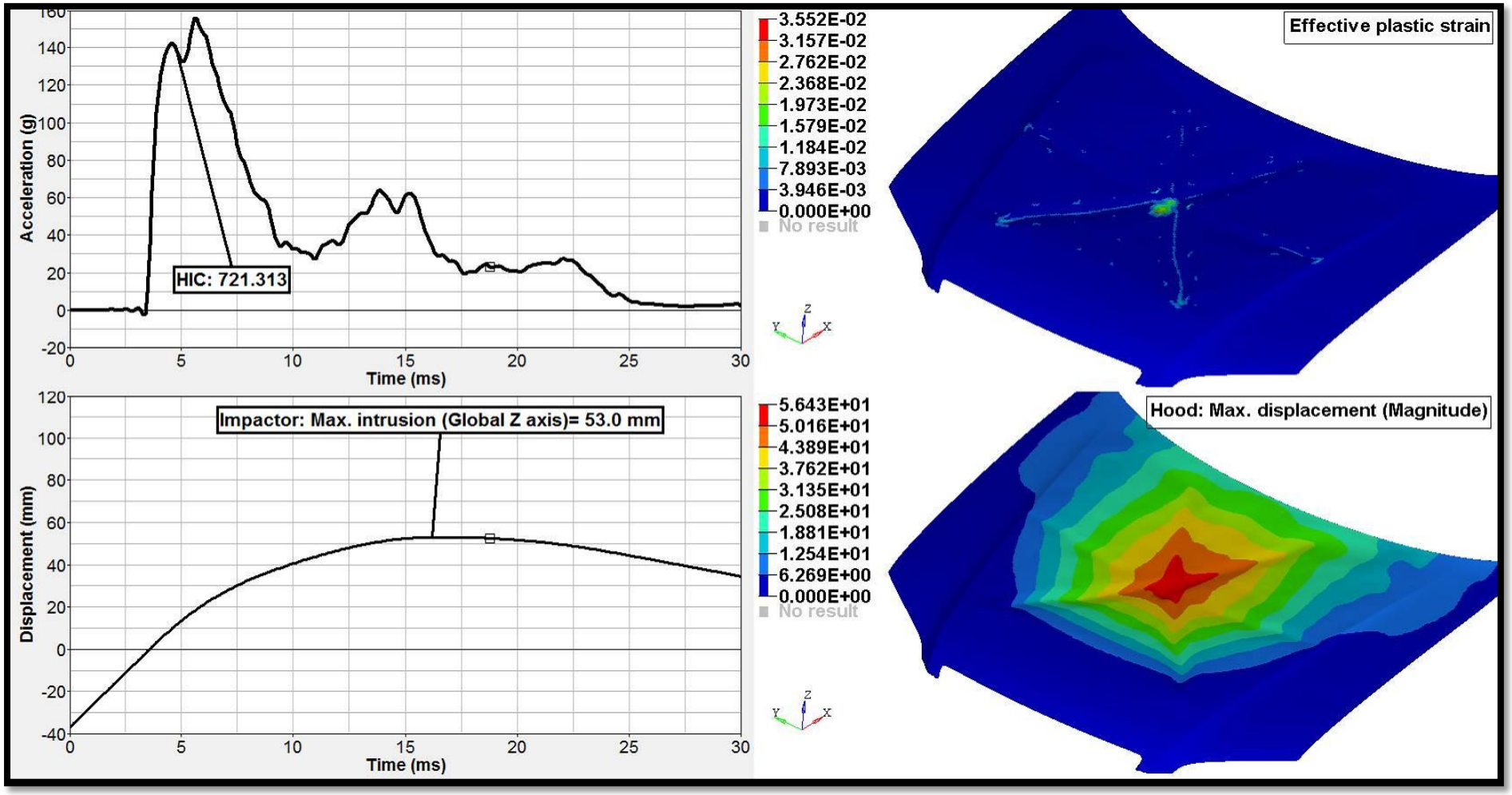

Figure 10.9: HIC value, effective plastic strain, displacement of the impactor and hood with consideration to primary impact only for point C

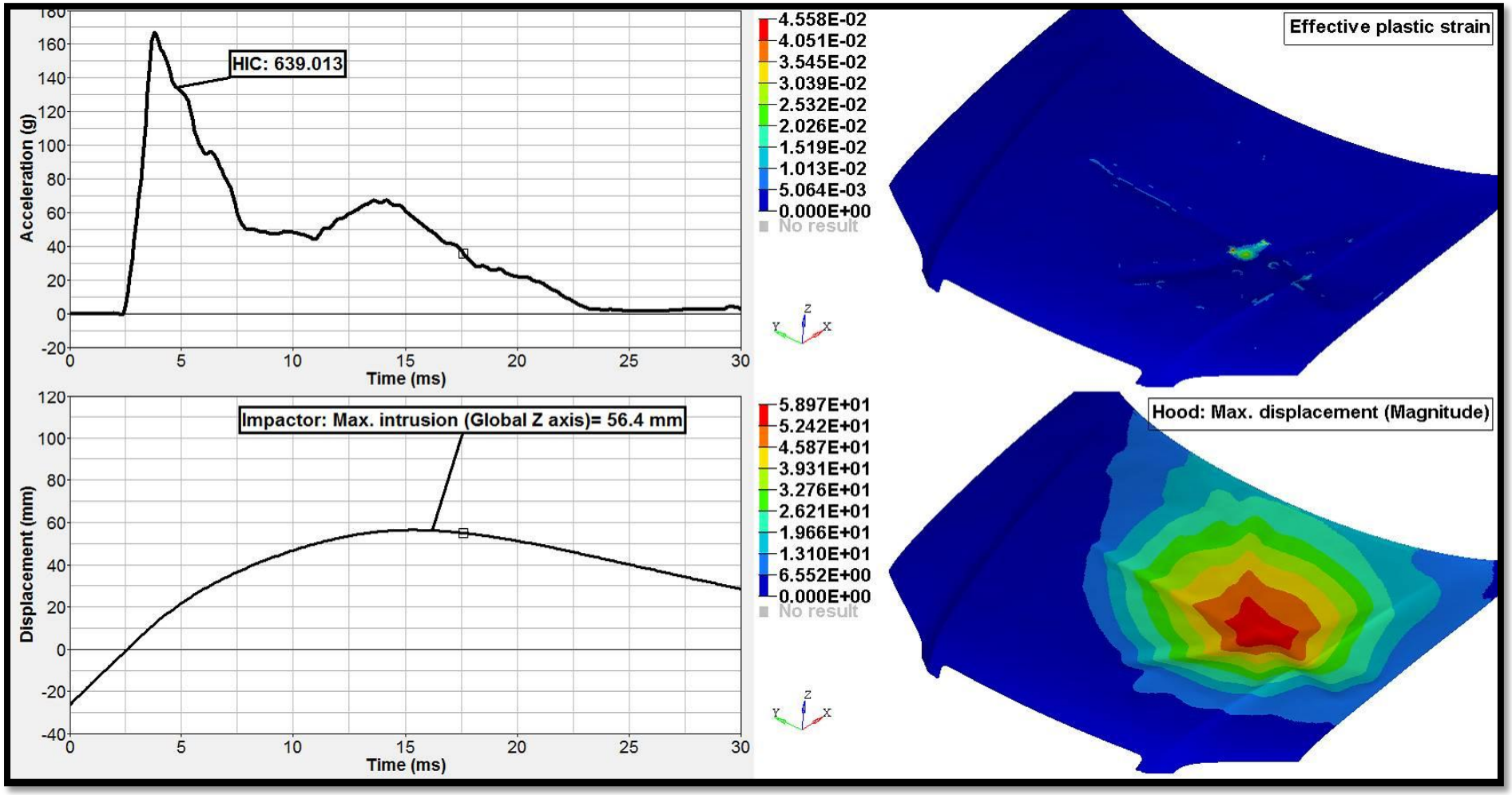

Figure 10.10: HIC value, effective plastic strain, displacement of the impactor and hood with consideration to primary impact only for point D

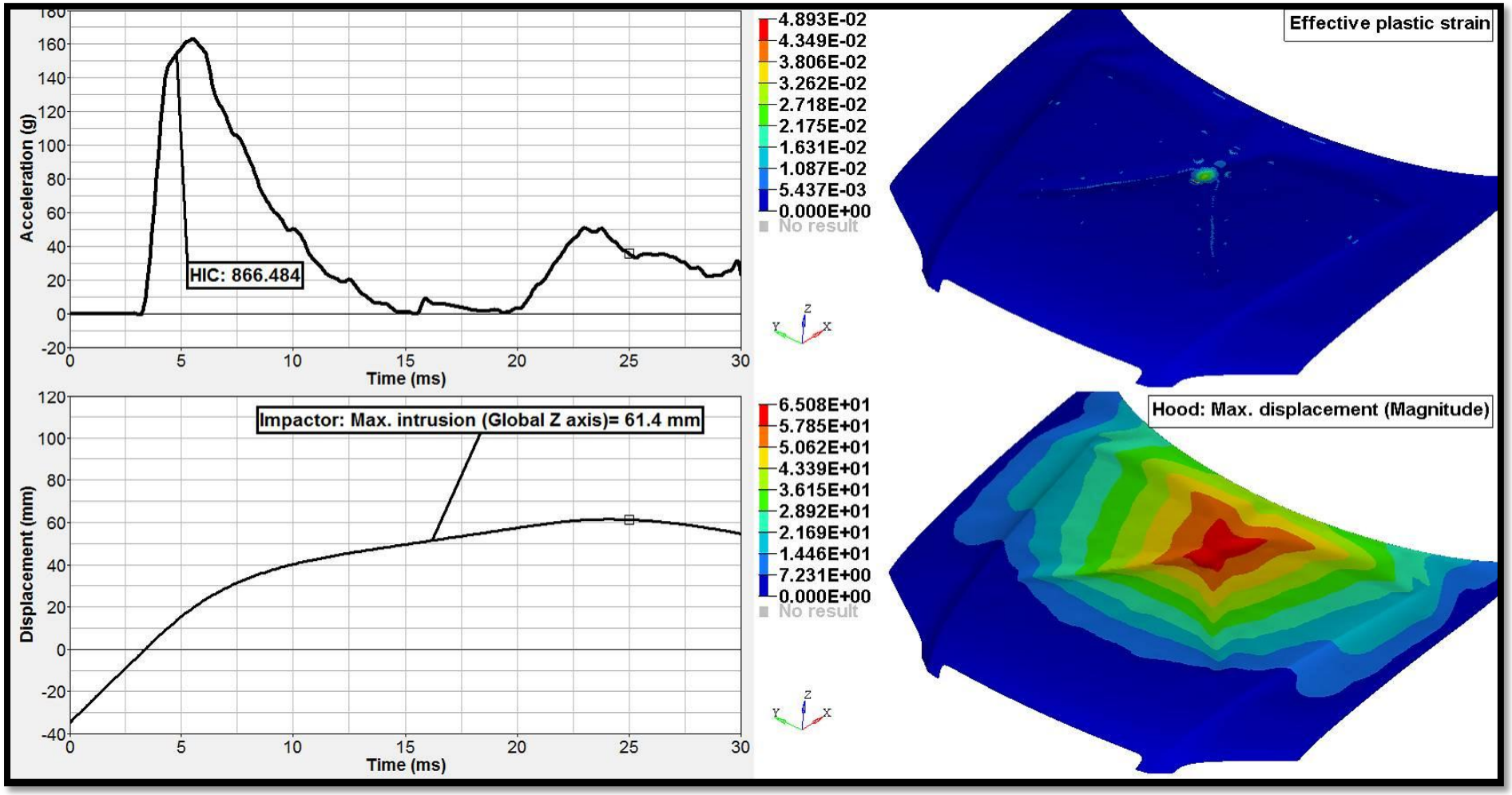

Figure 10.11: HIC value, effective plastic strain, displacement of the impactor and hood with consideration to primary impact only for point E

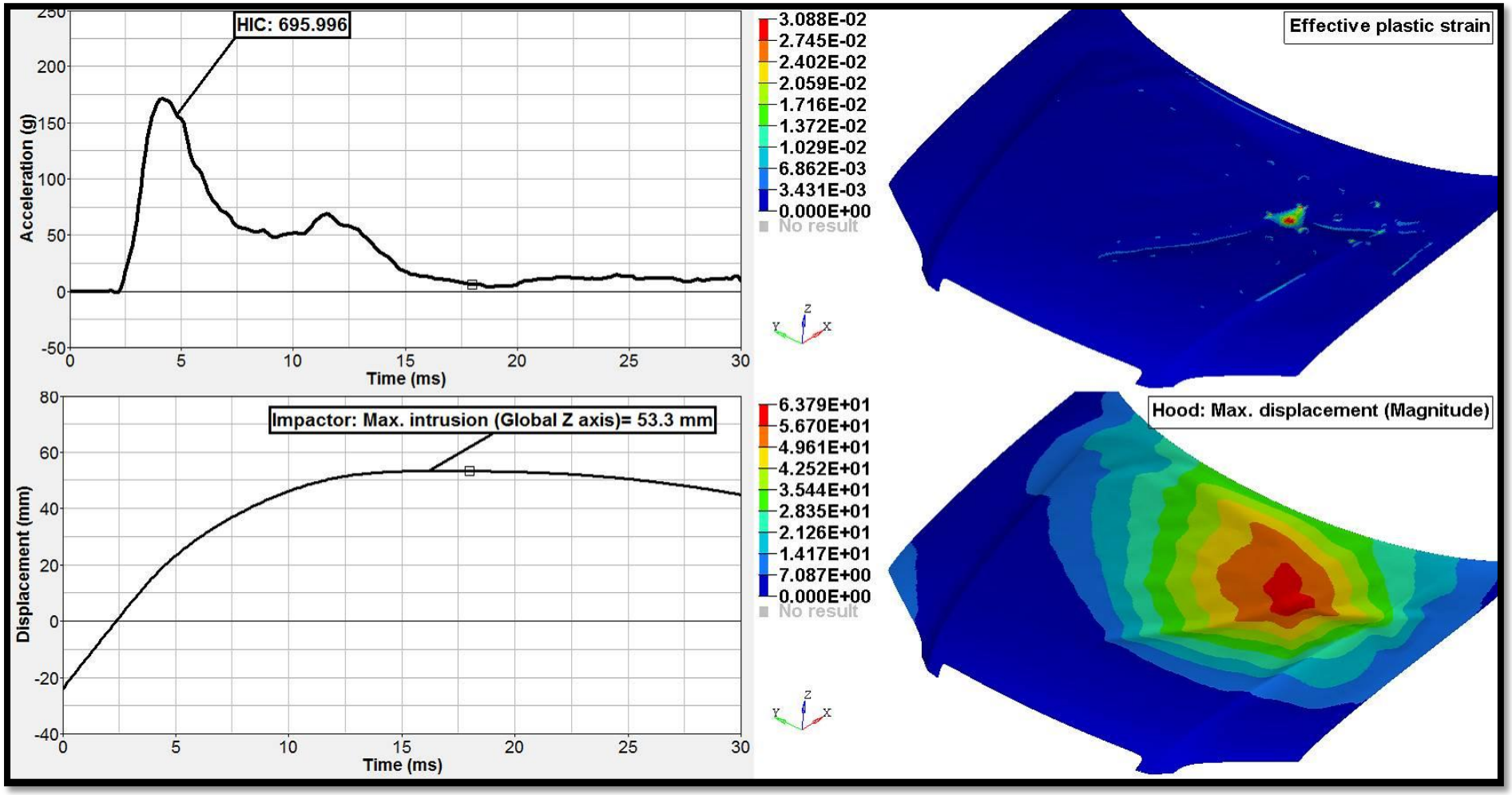

Figure 10.12: HIC value, effective plastic strain, displacement of the impactor and hood with consideration to primary impact only for point F

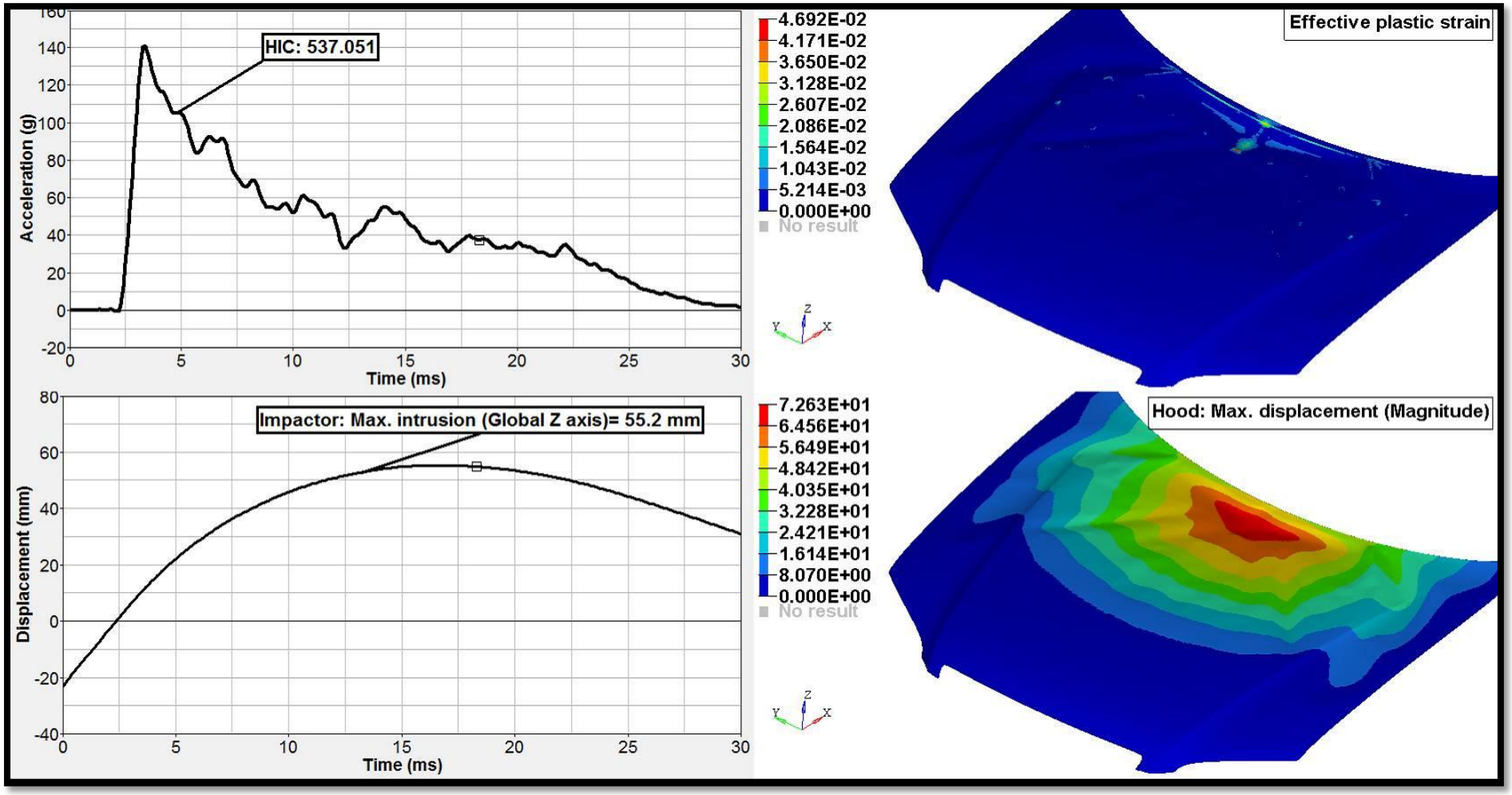

Figure 10.13: HIC value, effective plastic strain, displacement of the impactor and hood with consideration to primary impact only for point G

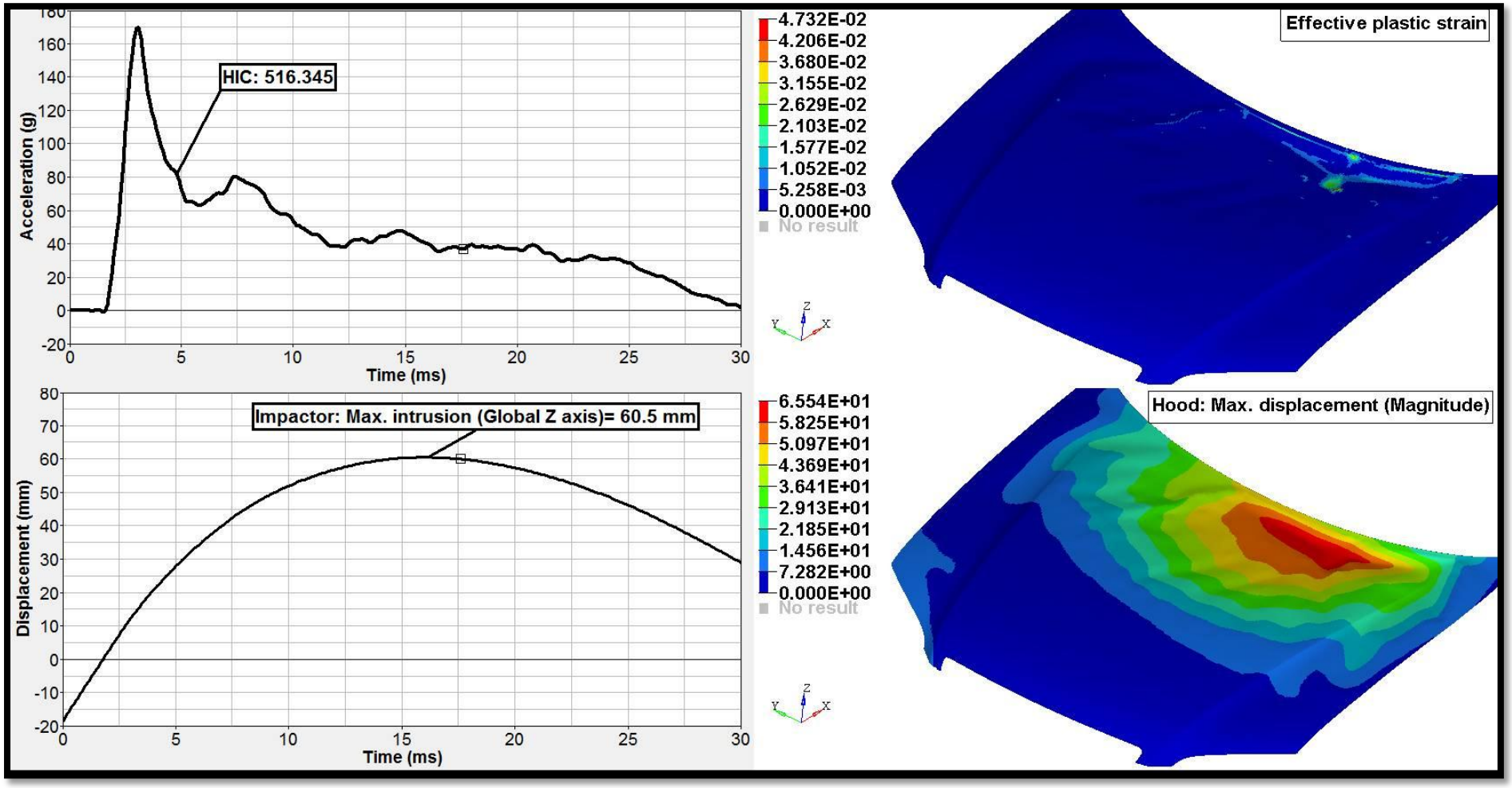

Figure 10.14: HIC value, effective plastic strain, displacement of the impactor and hood with consideration to primary impact only for point H

Thus, it could be concluded that the multi–cone inner hood structure made of steel material provides the best homogeneous performance with the highest μ_η as well as an HIC value less than 1000. Therefore, only this inner hood structure was considered for finding optimal inner and outer hood thickness.

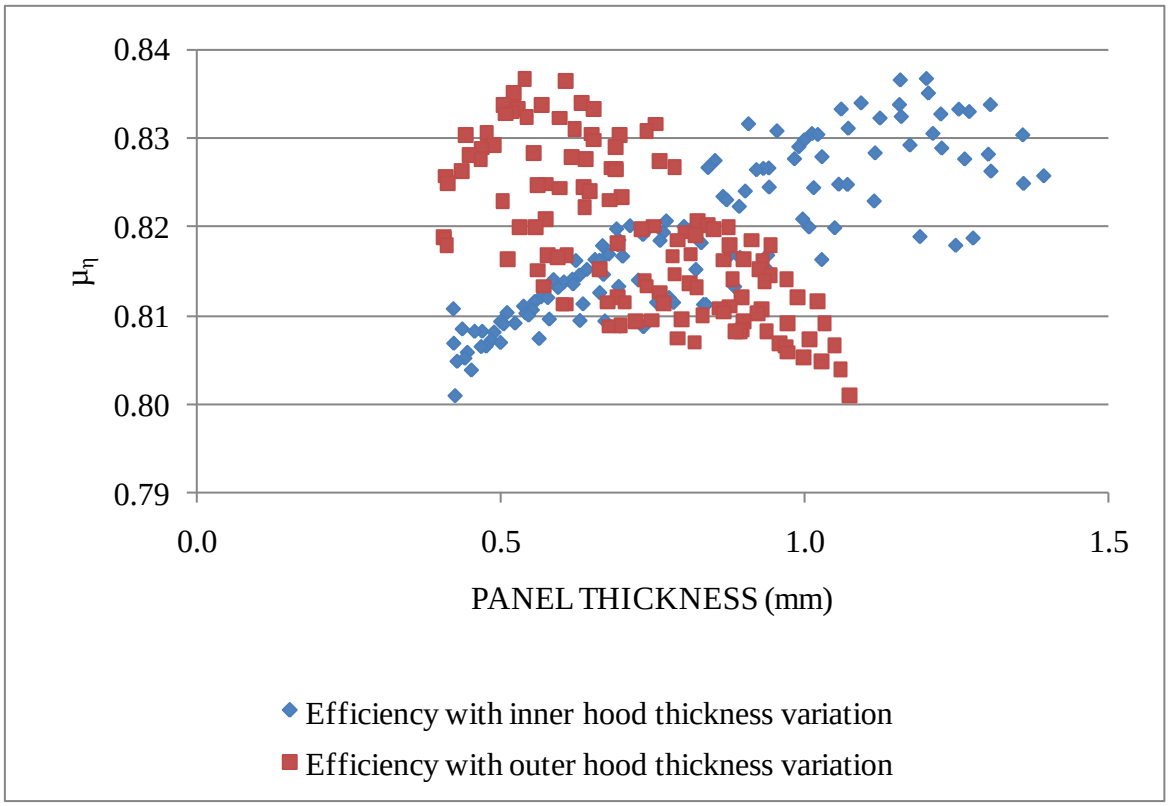

Figure 10.15: Efficiency and hood panel thickness

Figure 10.15 shows that HIC values less than the threshold value (1000) are feasible with various combinations of inner and outer hood thicknesses. The efficiency variation is only 3% for various combinations of the inner and outer hood thickness between 0.5mm and 1.4mm.

Thus, thinner inner and thicker outer hood thicknesses could be chosen within this range taking into consideration the torsional and bending stiffness, durability, noise and vibration performances.

Figure 10.16 shows the mean value of efficiency plotted against the combined inner and outer hood panel thickness. Although it could be concluded from Figure 10.15 that similar efficiency is possible with various combinations of inner and outer hood thicknesses, efficiency varies with the combined thickness of inner and outer hood, as shown in Figure 10.16. The optimal efficiency is achievable with a combined thickness of about 1.76mm. A trend line in this plot will show that the efficiency continues to increase with higher gauges but the HIC values will exceed the required limit.

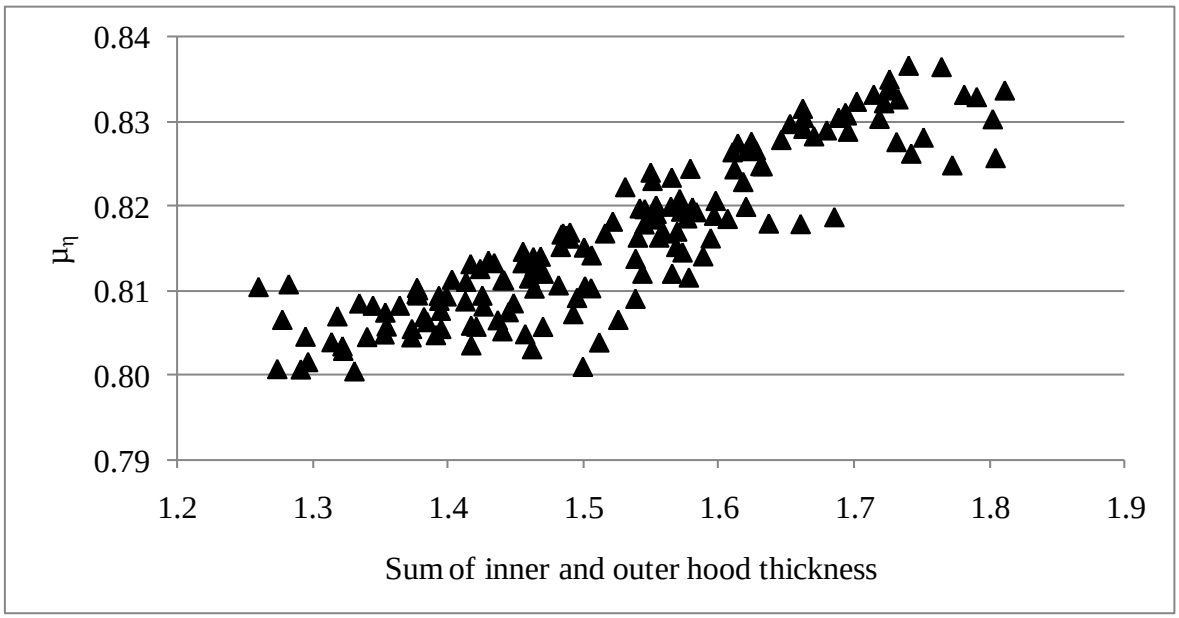

Figure 10.16: Efficiency and combined hood panel thickness relationship

The Equation 10.1 that was utilised to derive the optimal deformation was derived from the theoretical optimal waveform, which is the WSTC where the resultant acceleration is infinite at zero millisecond (Figure 3.4) and is impractical to obtain. In practice, it takes a minimum of 1 to 2 ms to reach the peak acceleration in a pedestrian head impact. Therefore, it could be concluded that in practice it is impossible to achieve 100% efficiency with any hood configuration.

From the optimal acceleration curve (Figure 3.4), the calculated optimal deformation space required for HIC value that is less than 1000 is 50.5mm. The results presented in Figure 10.16 show that 84% efficiency is possible with a steel multi–cone hood structure with a combined thickness of 1.76mm for inner and outer hood panels. The deformation space required for a hood assembly with 84% efficiency has been found to be approximately 60mm. This is in agreement with suggestions given by Wu and Beaudet , who also derived equations to calculate the optimal deformation space as shown Equation 10.1. Thus, a hood configuration with 84% efficiency could be considered as the practical limit of efficiency as well as optimal hood configuration.

10.2.2 Primary and secondary Impacts

The intensity of the secondary impact increases the severity of pedestrian head injuries. Therefore, it is essential to optimise the inner and outer hood panels to meet the HIC value requirements with pre–defined hood deformation space.

As discussed in the previous chapter, the deformation space required for the optimal configuration of the hood assembly with 84% efficiency equals approximately 60mm. To allow for a secondary impact in the simulations, a rigid plane defining the hard components within the engine bay was included in the FE model as shown in Figure 10.17. The rigid plane was defined by translating the outer hood surface in the impact direction by 60mm, which allows for a 60mm hood deformation space. Thus, primary and secondary impacts were taken into consideration in this research. The same constraints and variables used in the previous development step were considered in designing the numerical experiments.

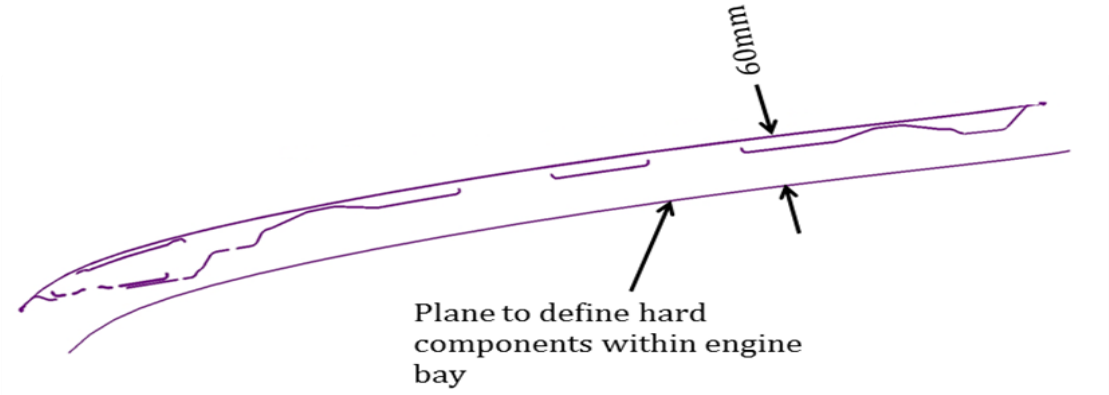

Figure 10.17: Rigid plane at 60mm to define hard components within engine bay

The mean value of HIC and its standard deviation were considered as qualifiers to ensure robust and homogeneous head impact performance while meeting the requirements for the HIC value.

The Kriging response surfaces were mapped with the mean value of HIC and its standard deviation between all impact positions for a given configuration of hood design. The data from numerical tests were utilised to create the response surface, which in turn was used to predict results for the random values for variables that obey the defined properties created with the Monte Carlo method.

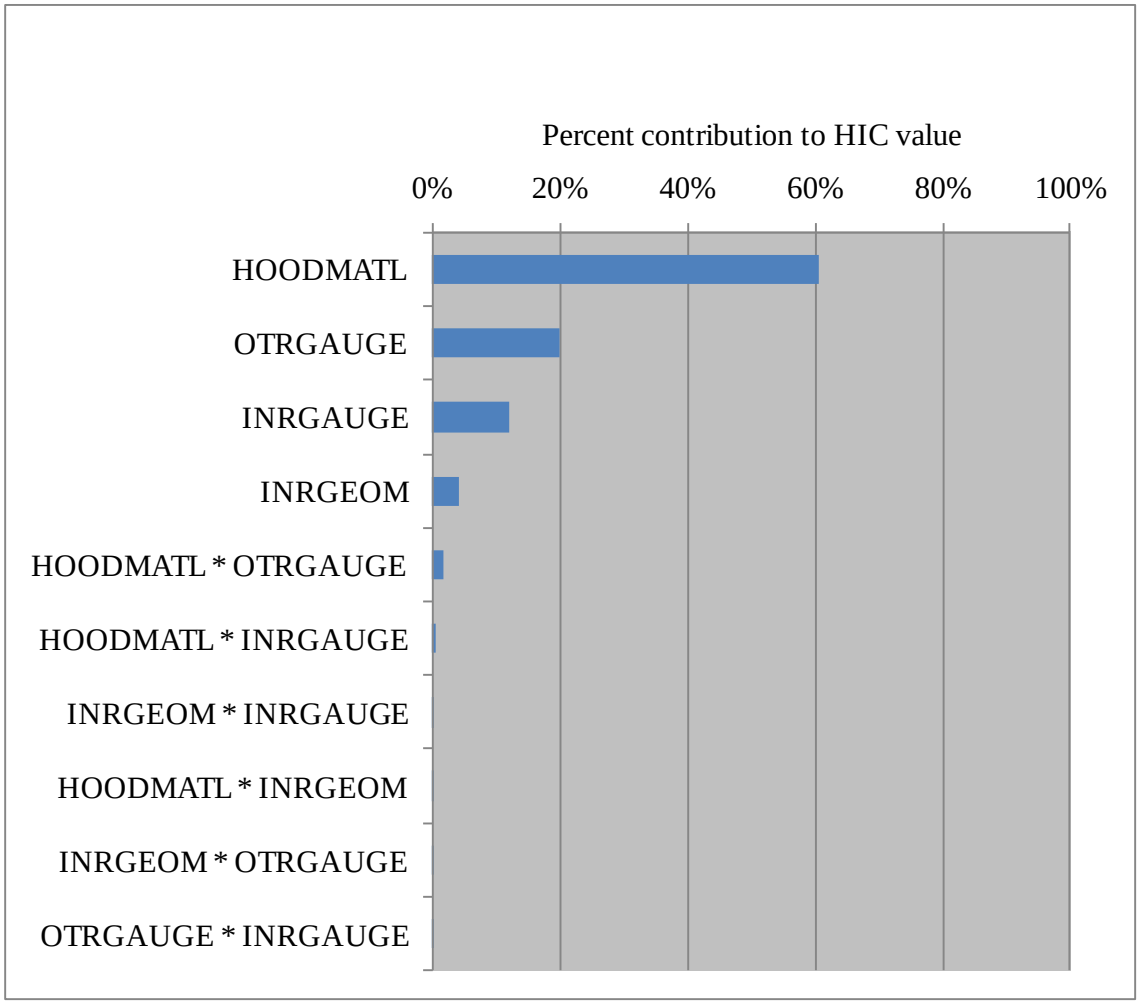

Figure 10.18: ANOVA chart for mean value of HIC

The ANOVA charts showed that as in the case when only primary impact has been considered, the material, thickness of inner hood panel, thickness of outer hood panel, and hood inner structure contribute significantly to the mean value of the HIC and its standard deviation when primary and secondary impacts were considered. Figure 10.18 shows the ANOVA graph for the mean value of HIC.

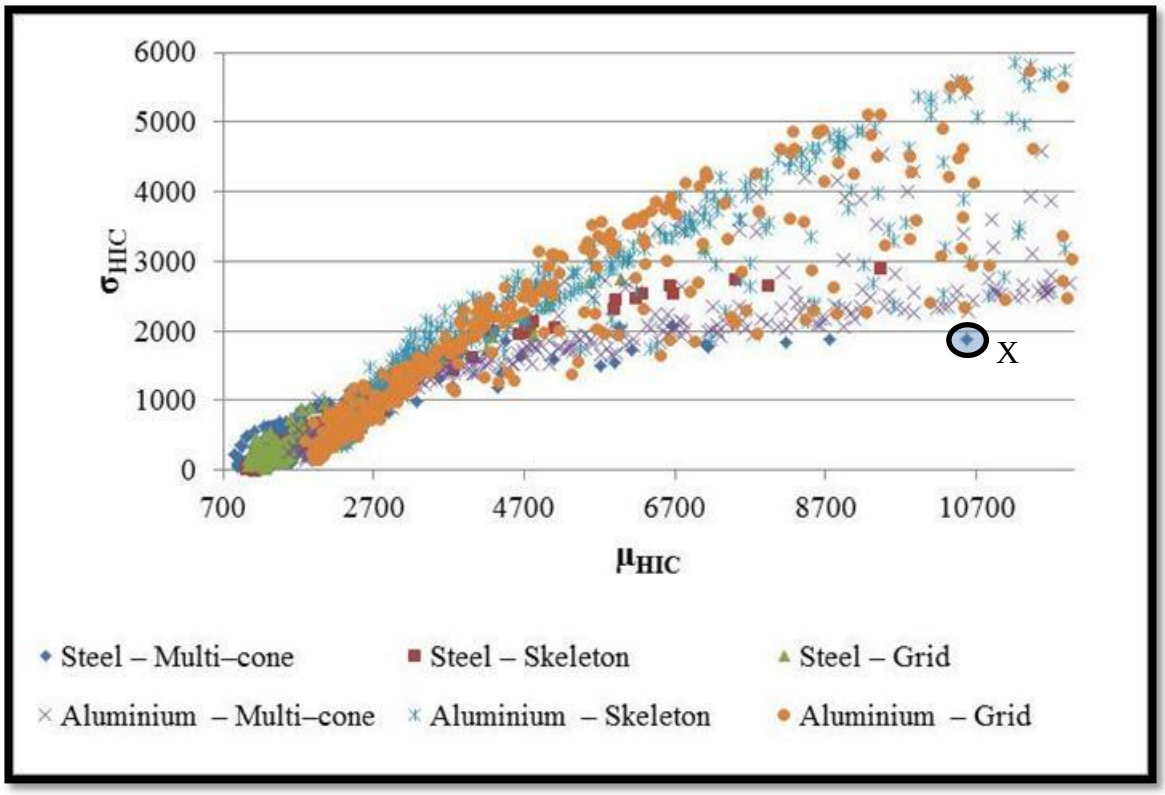

Figure 10.19: Influence of material and inner hood structure on HIC value considering secondary impact

Figure 10.19 presents the predicted value of the standard deviation of HIC against the corresponding mean value of HIC. The data were grouped by considering only material and inner hood structure, to analyse their influence on HIC values. The results indicate that, in general, steel provides a lower range of HIC value compared to aluminium for all variations in inner hood structure.

However, the mean value of HIC can be more than 10000 (Data point X in Figure 10.19); if the optimisation of the structural stiffness of the hood panels is not considered while steel material is considered for the hood panels. From the head injury curve presented in Figure 3.5, it can be stated that the mean value of HIC more than 10000 will result in fatality of the pedestrian. The details of the results from the numerical tests that were

utilised to derive the values for the data point X are shown in figures ranging from Figure 10.20 to Figure 10.27. The details are,

- plot of resultant acceleration against time
- plot of the displacement of the impactor in global Z direction against time
- contour plot of the effective plastic strain
- contour plot of the magnitude of the deformation of the hood panels.

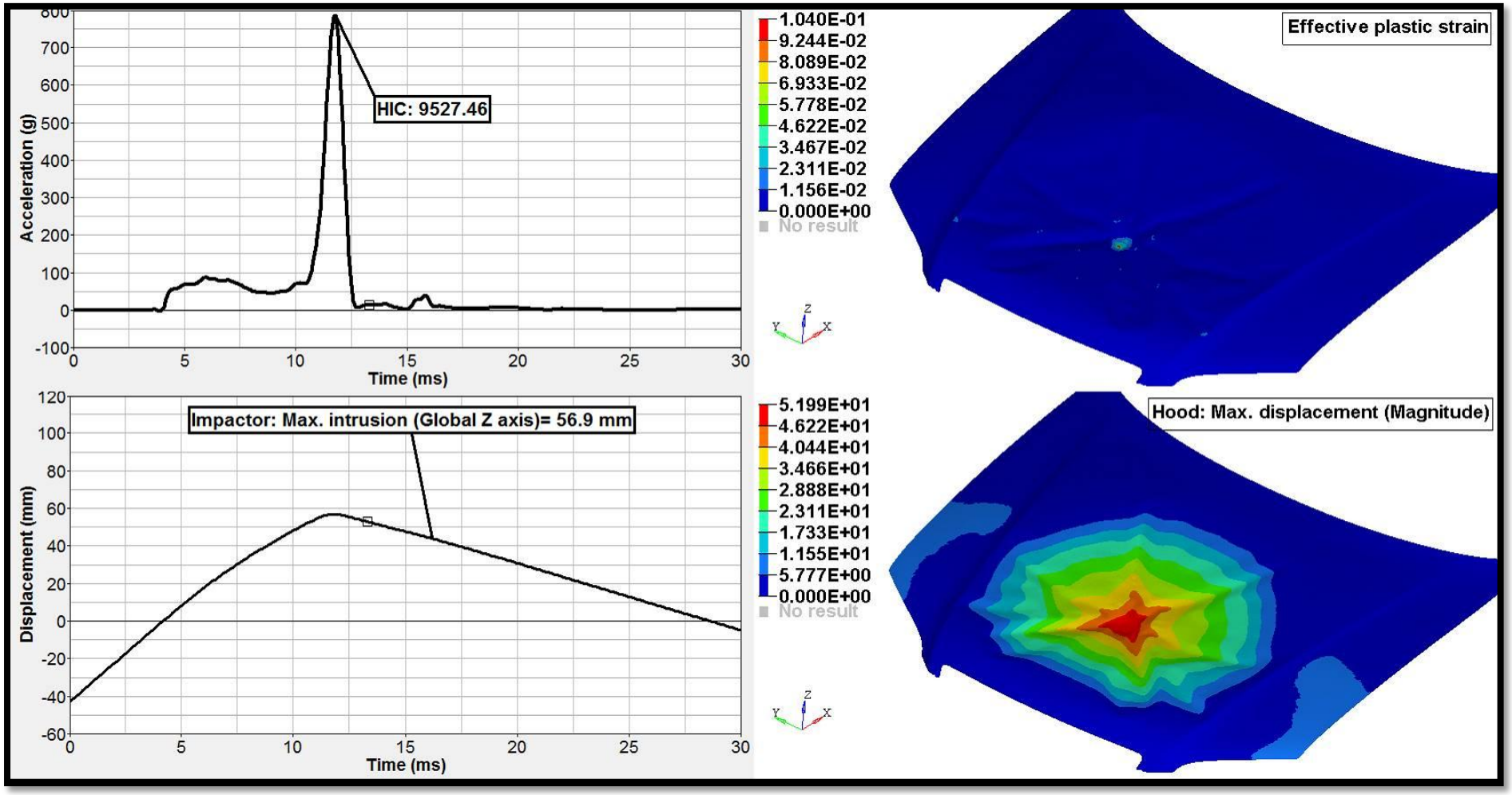

Figure 10.20: Effect of structural stiffness of the hood panels on HIC value, effective plastic strain, displacement of the impactor and hood with 60mm deformation space for point A

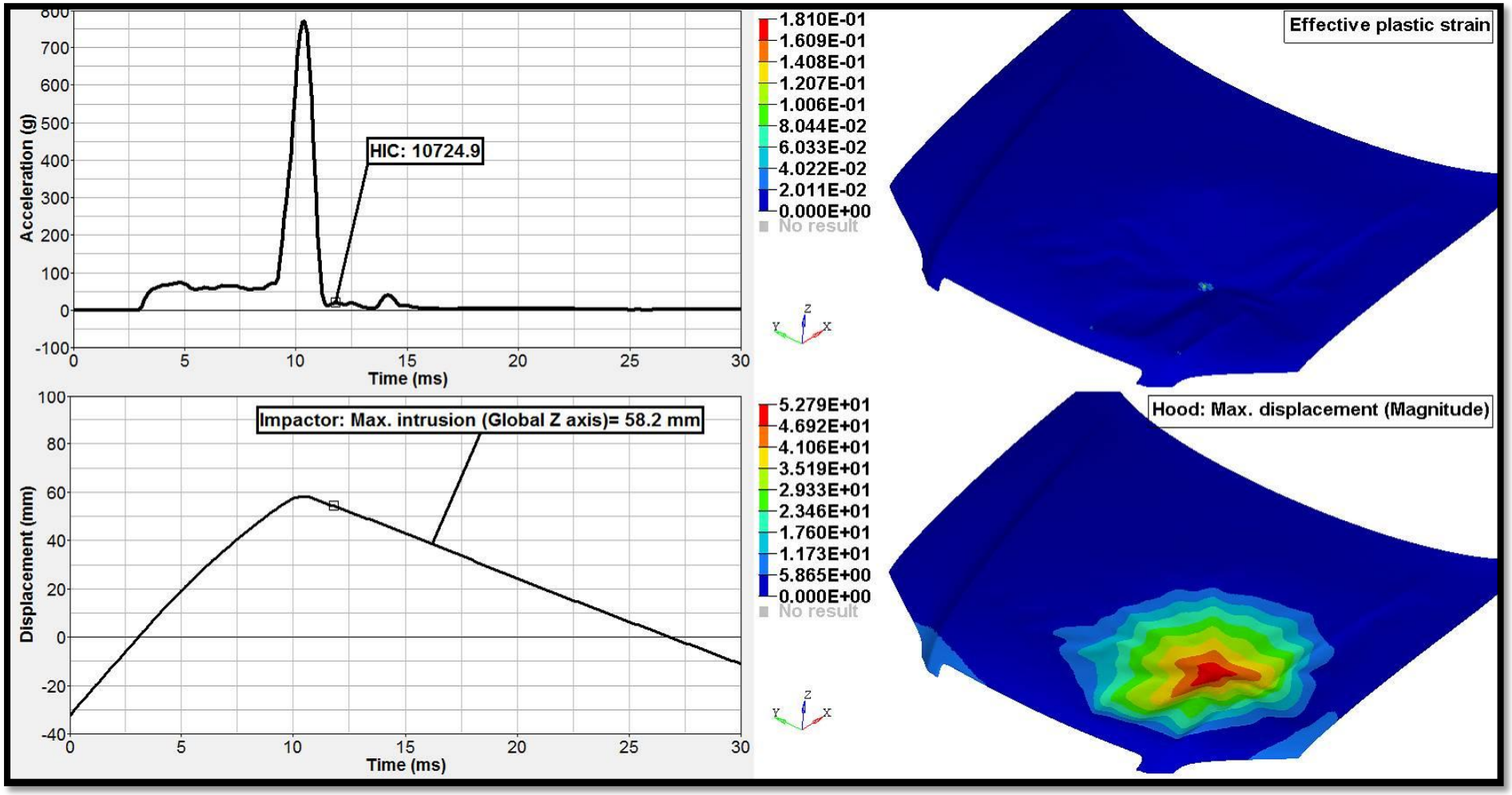

Figure 10.21: Effect of structural stiffness of the hood panels on HIC value, effective plastic strain, displacement of the impactor and hood with 60mm deformation space for point B

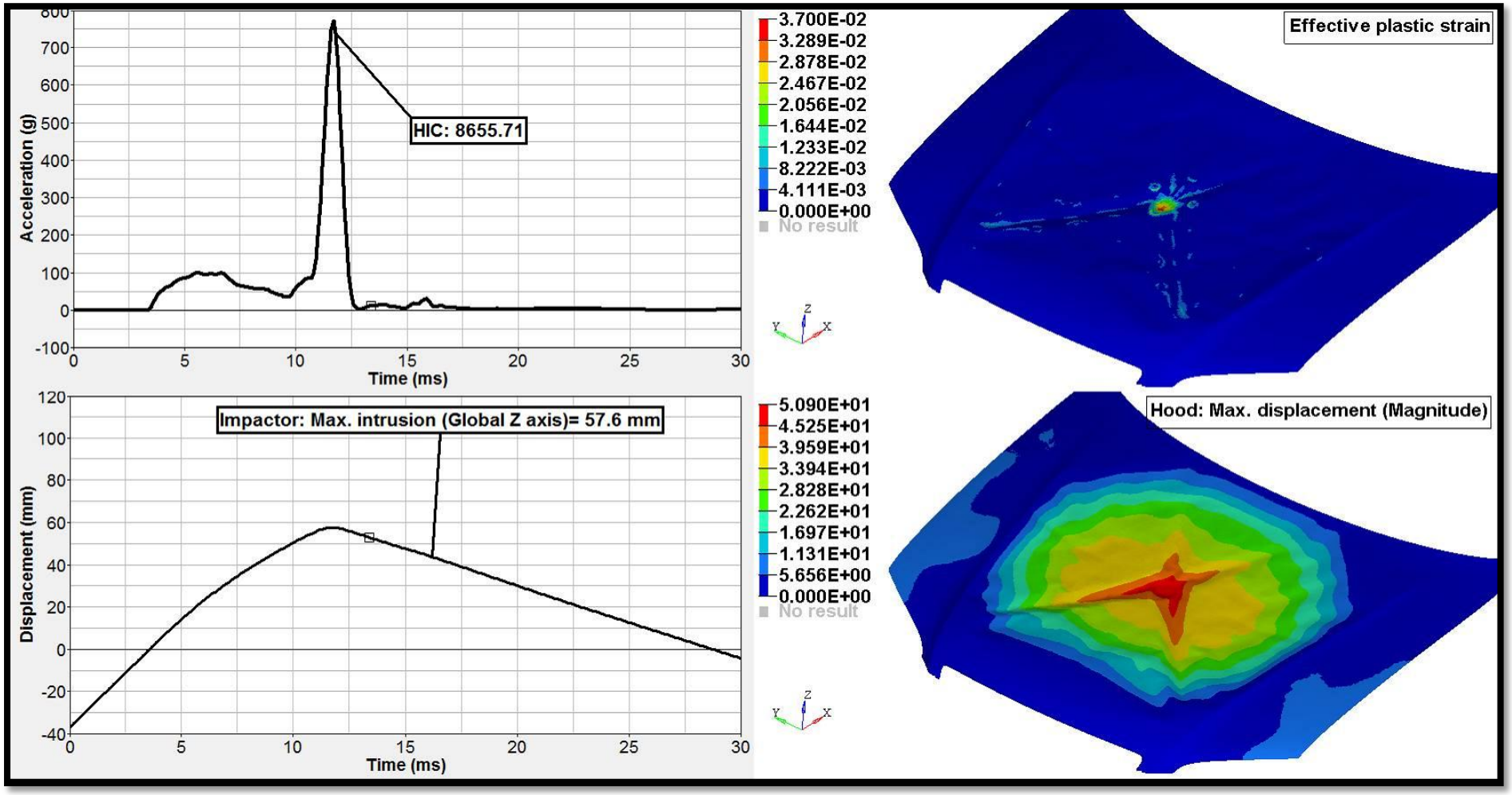

Figure 10.22: Effect of structural stiffness of the hood panels on HIC value, effective plastic strain, displacement of the impactor and hood with 60mm deformation space for point C

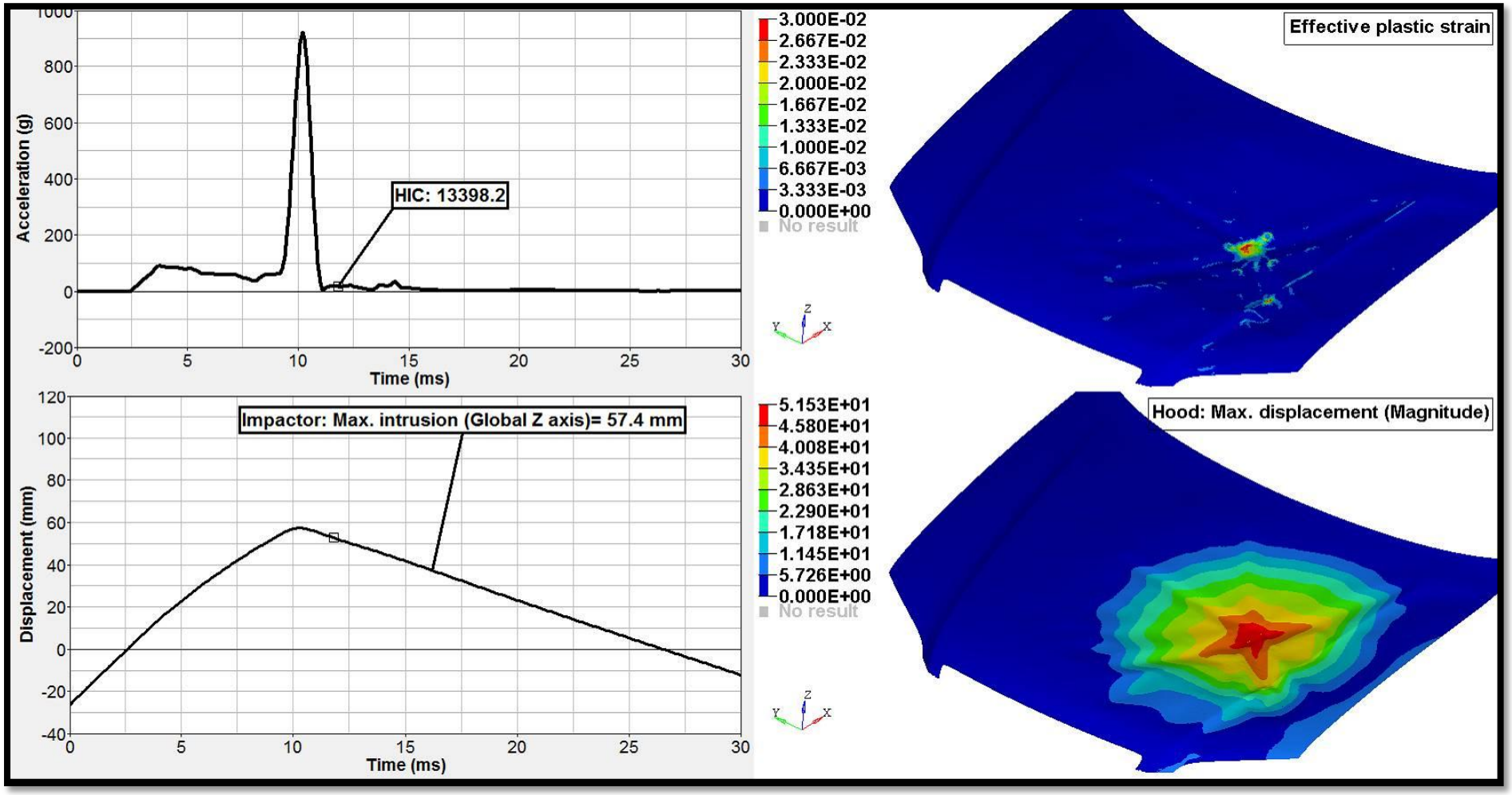

Figure 10.23: Effect of structural stiffness of the hood panels on HIC value, effective plastic strain, displacement of the impactor and hood with 60mm deformation space for point D

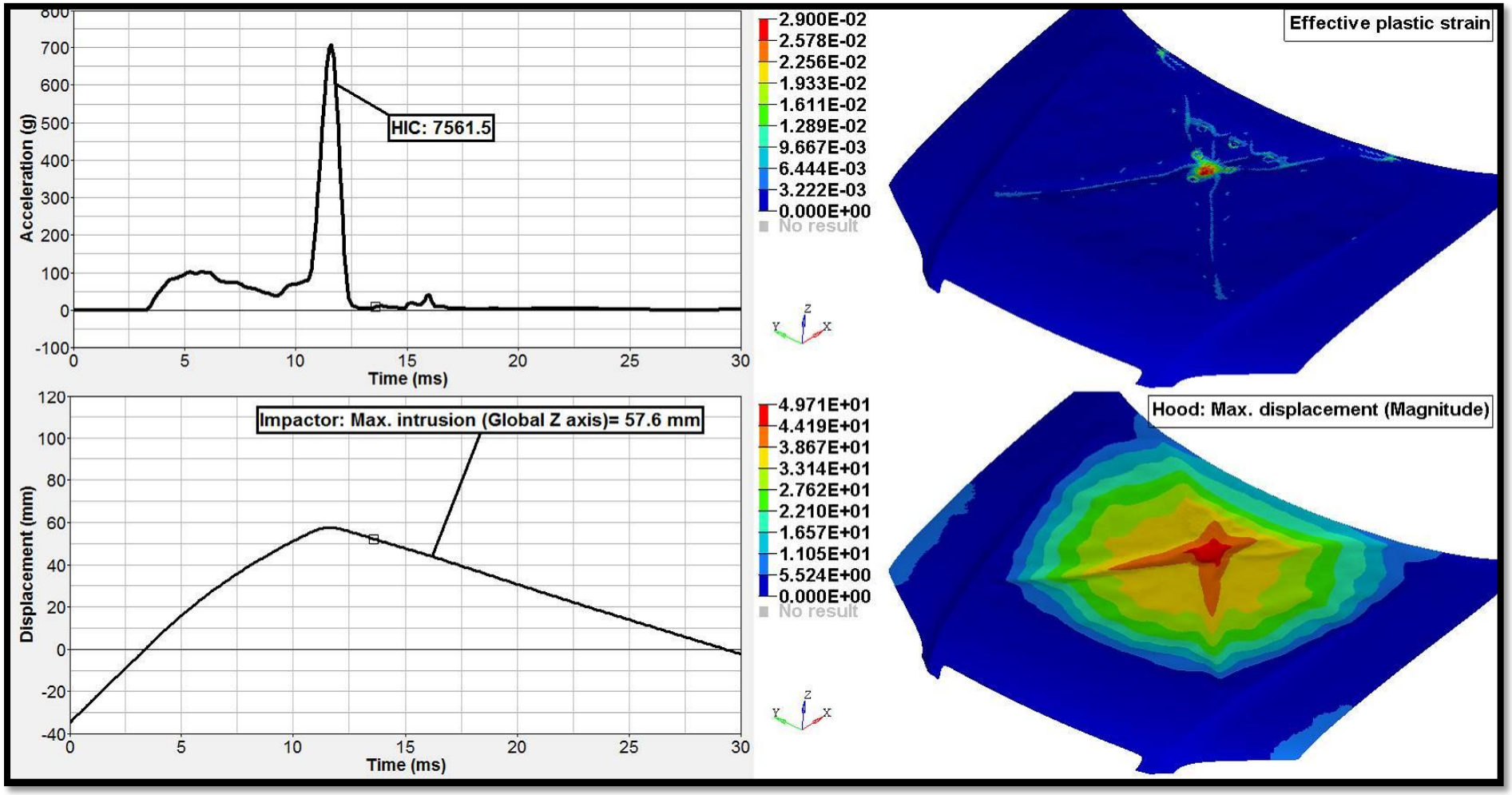

Figure 10.24: Effect of structural stiffness of the hood panels on HIC value, effective plastic strain, displacement of the impactor and hood with 60mm deformation space for point E

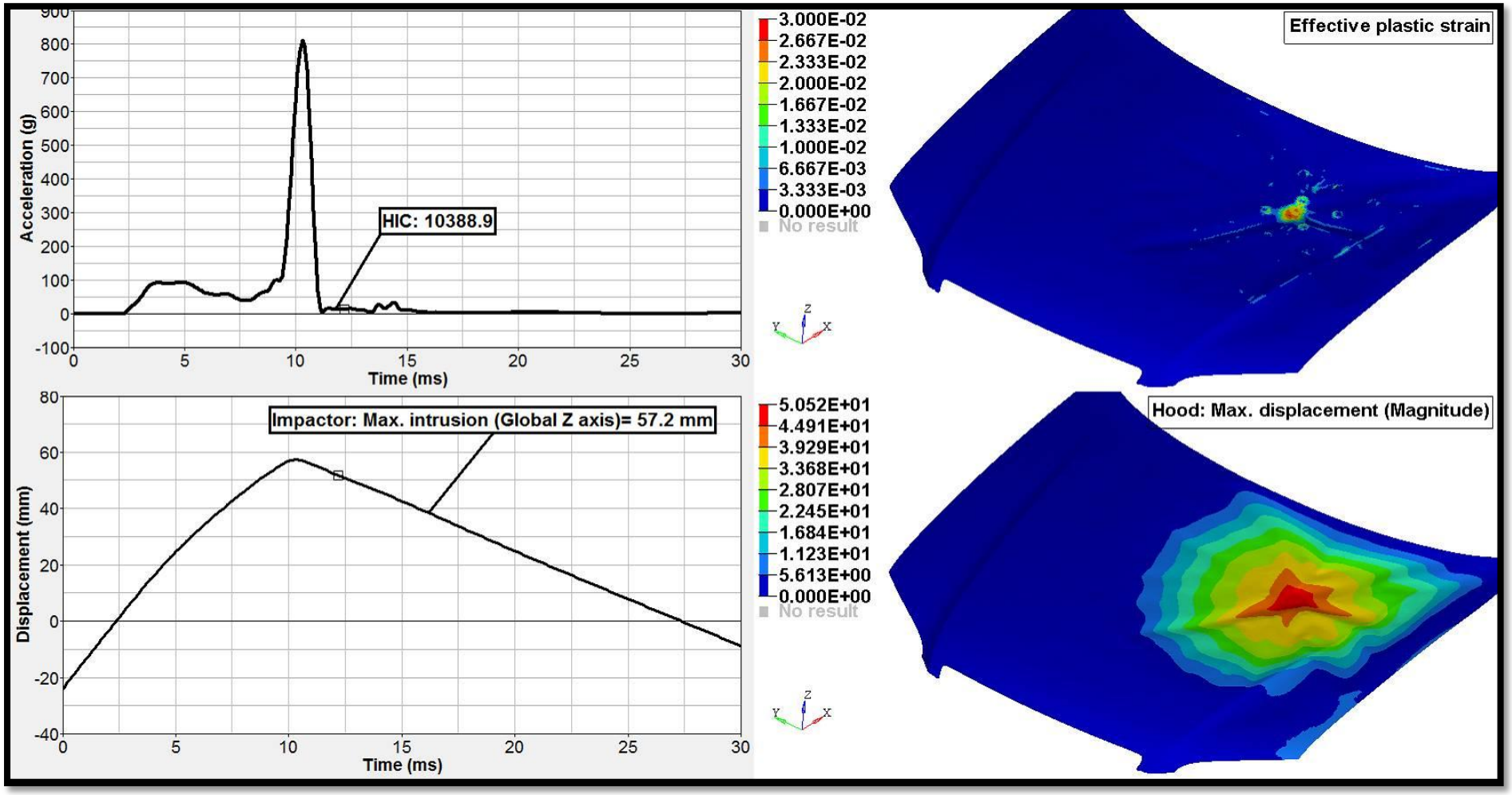

Figure 10.25: Effect of structural stiffness of the hood panels on HIC value, effective plastic strain, displacement of the impactor and hood with 60mm deformation space for point F

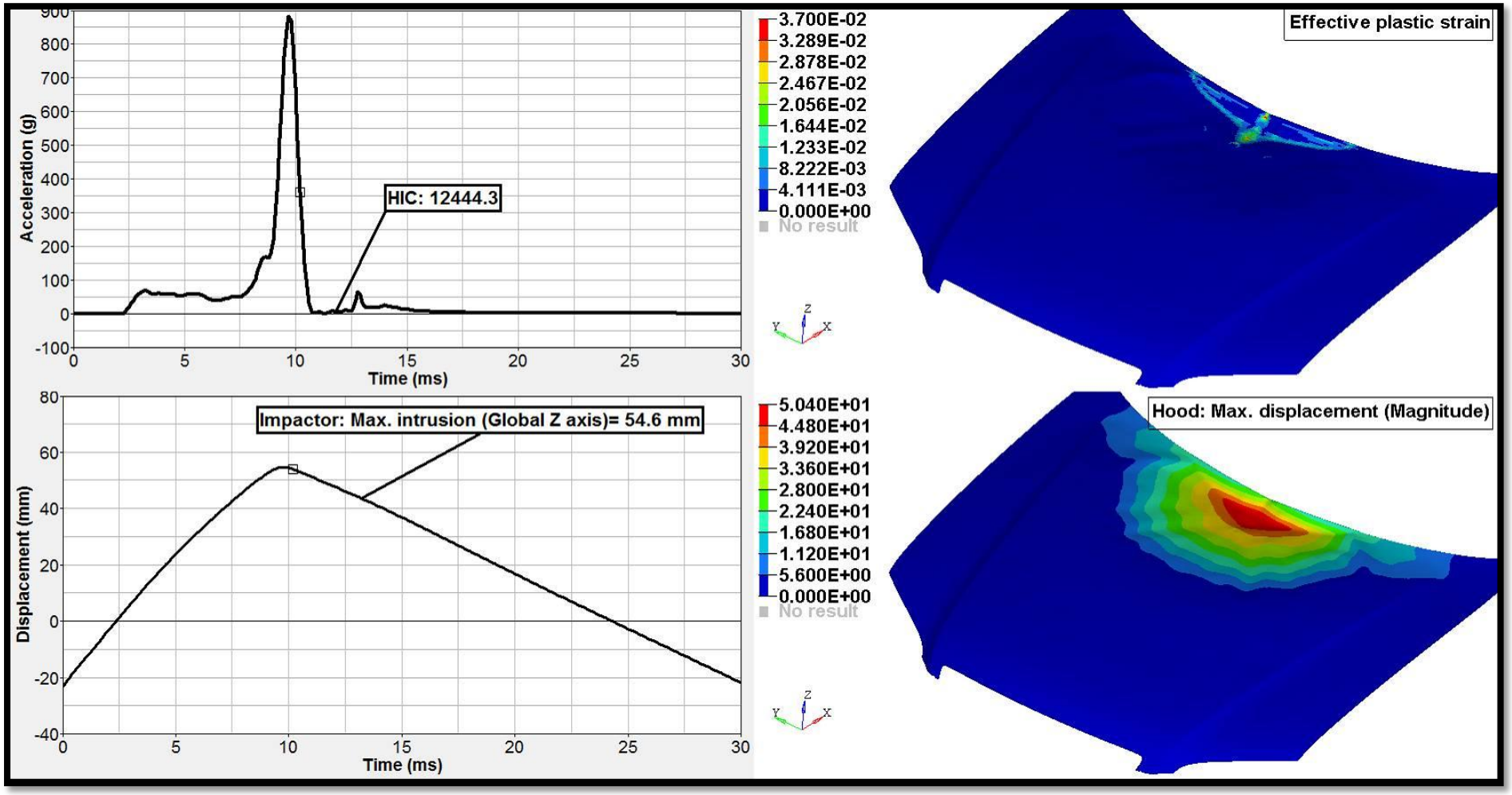

Figure 10.26: Effect of structural stiffness of the hood panels on HIC value, effective plastic strain, displacement of the impactor and hood with 60mm deformation space for point G

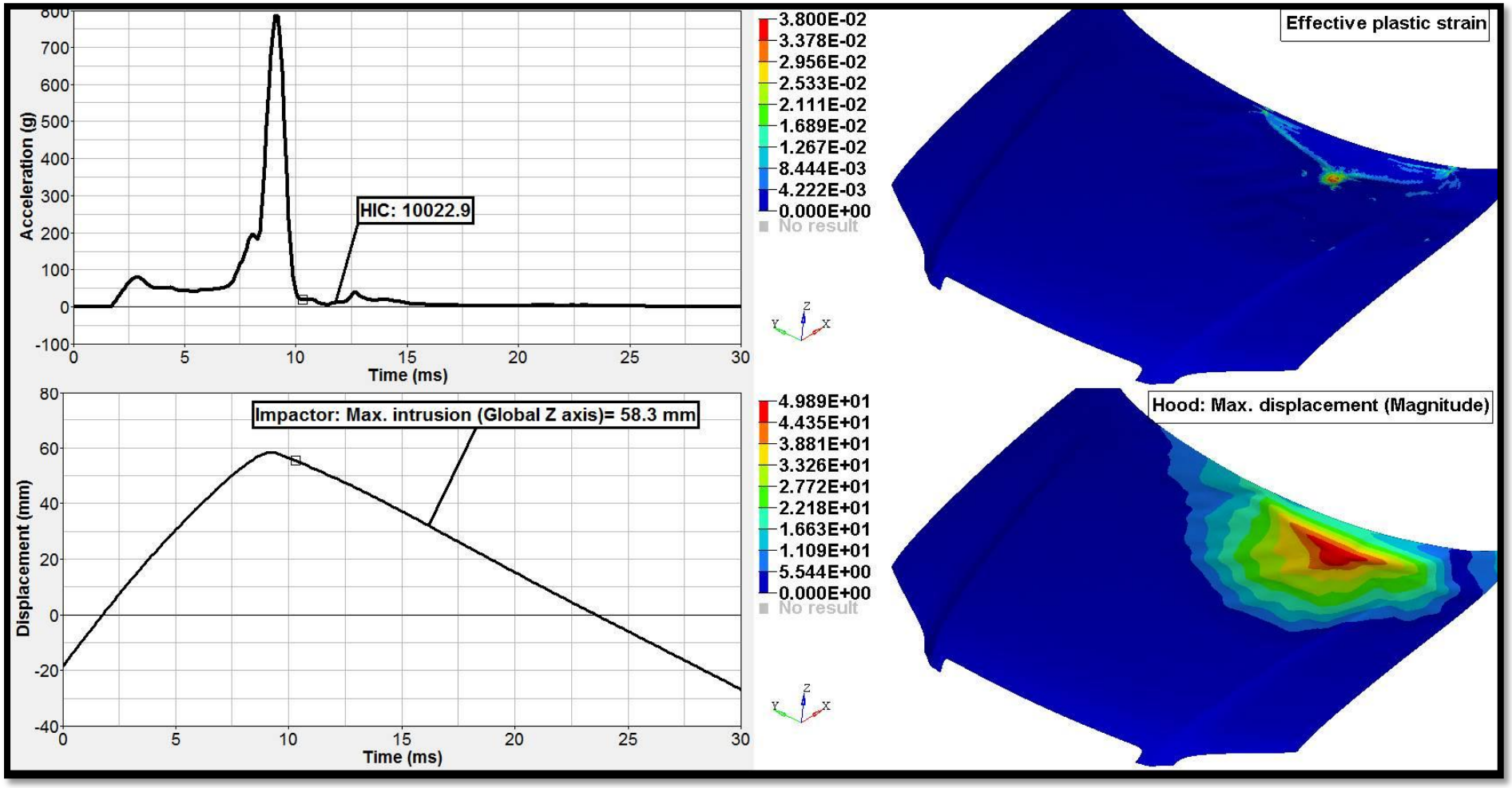

Figure 10.27: Effect of structural stiffness of the hood panels on HIC value, effective plastic strain, displacement of the impactor and hood with 60mm deformation space for point H

A close up view that focuses closer to the sum of the mean value of HIC and twice its standard deviation ($\mu_{HIC}+2\sigma_{HIC}$) equal to 1000 from Figure 10.19 is presented in Figure 10.28. It shows that a 60mm deformation space makes it possible to obtain the mean value of HIC less than 1000 but it is not enough to obtain robust and homogeneous behaviour less than the HIC threshold value. Accordingly, it could be stated that only multi–cone inner hood structure made of steel material for inner and outer hood panel shows μ_{HIC} less than 1000 with a 60mm deformation space.

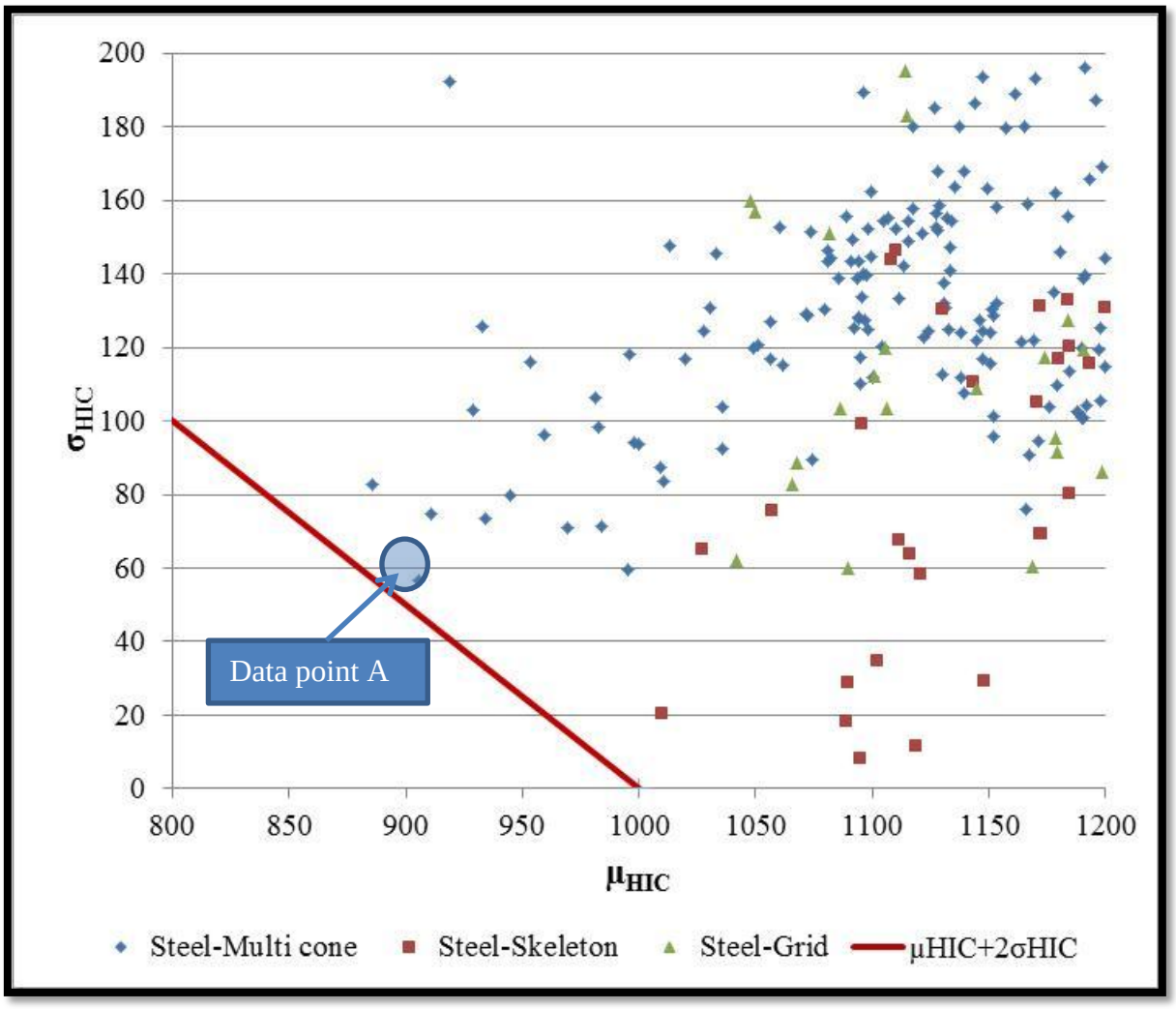

Figure 10.28: Mean value of HIC vs. twice its standard deviation for different hood configurations

Data point A is the closest point to the sum of the mean value of HIC and twice its standard deviation ($\mu_{HIC}+2\sigma_{HIC}$). The impact locations considered for this data point is shown in Figure 8.8. The details of the results from the numerical tests for the eight impact locations that were utilised to derive the values for the data point A are shown in figures ranging from Figure 10.29 to Figure 10.36. The details are,

- plot of resultant acceleration against time
- plot of the displacement of the impactor in global Z direction against time
- contour plot of the effective plastic strain
- contour plot of the magnitude of the deformation of the hood panels.

It shows that a 60mm deformation space makes it possible to obtain the HIC value less than 1000 for some impact locations but it is not enough to obtain robust and homogeneous behaviour less than the HIC threshold value. Figure 10.37 shows that the available deformation space of 60mm was utilised completely and the severity of secondary impact at approximately 14ms is high resulting in a HIC value more than 1000.

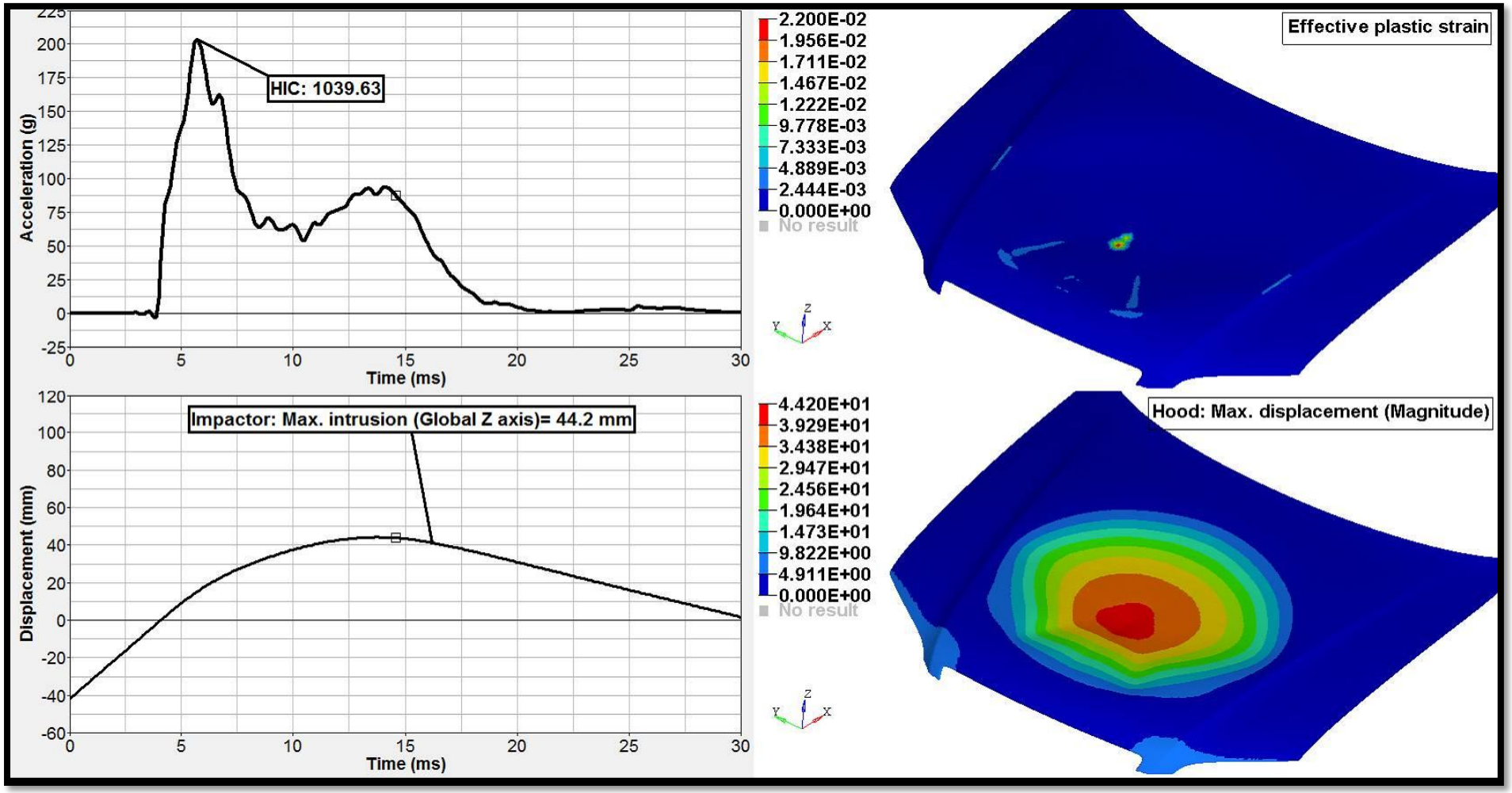

Figure 10.29: HIC value, effective plastic strain, displacement of the impactor and hood with 60mm deformation space for point A

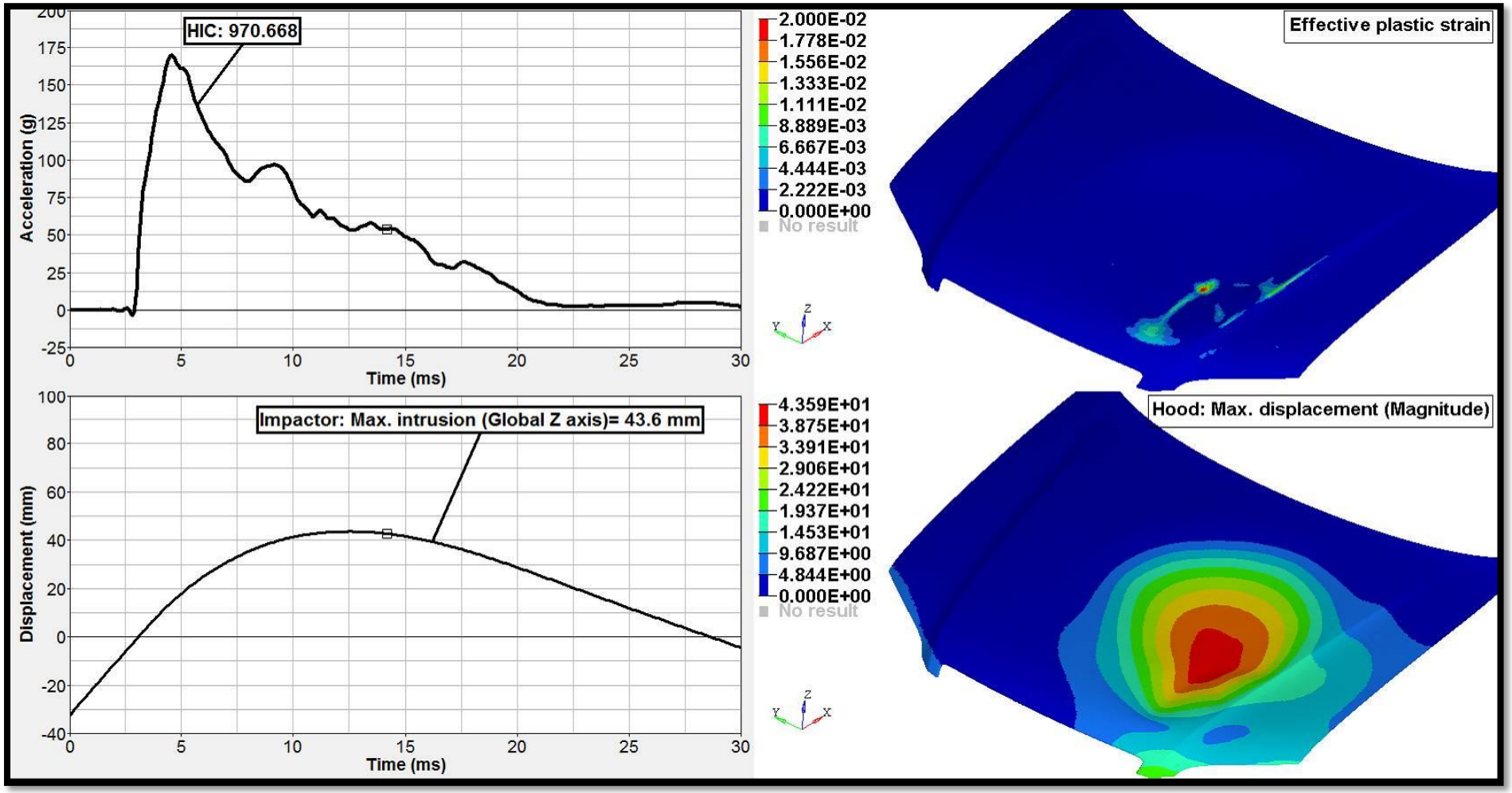

Figure 10.30: HIC value, effective plastic strain, displacement of the impactor and hood with 60mm deformation space for point B

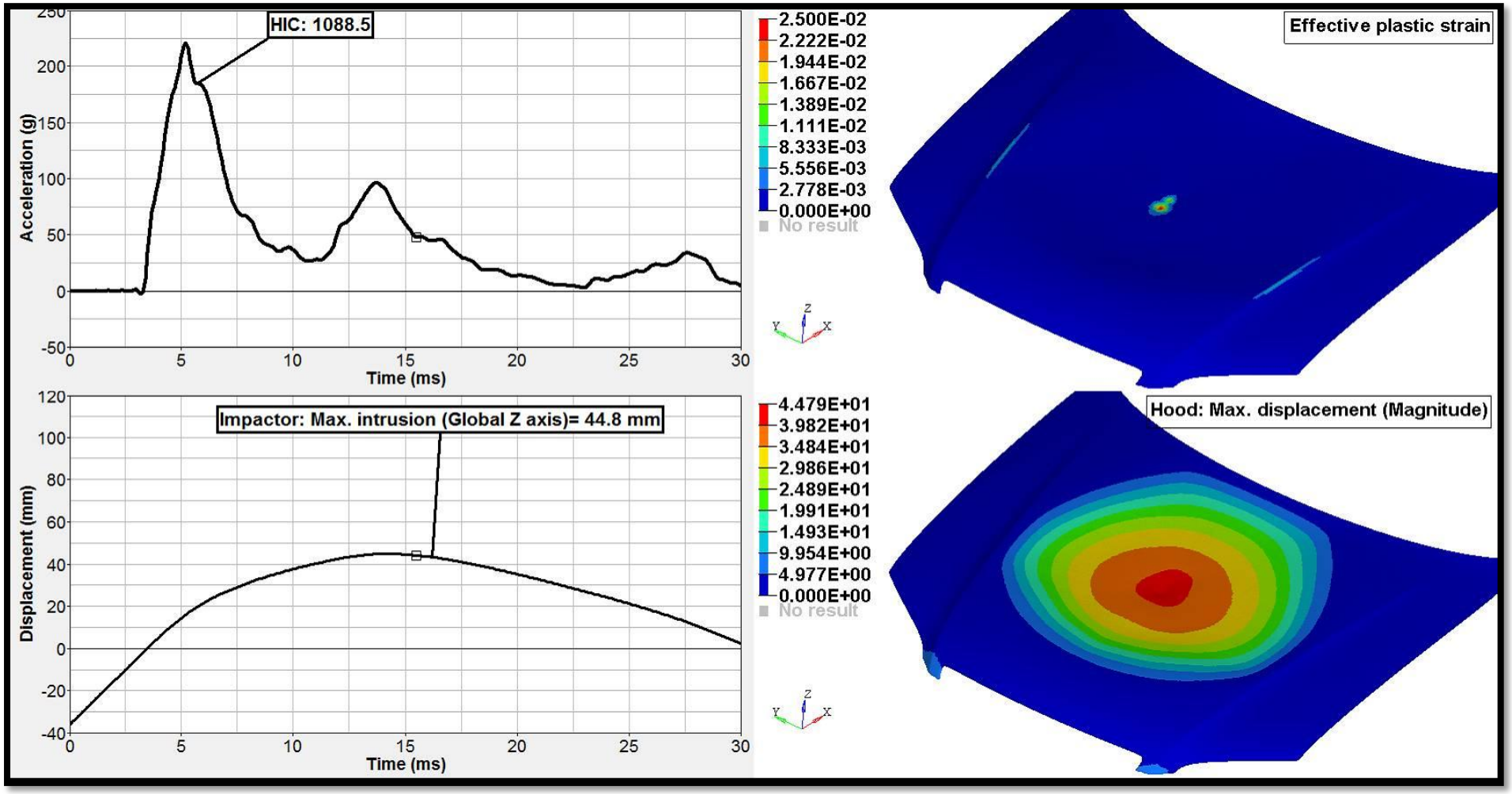

Figure 10.31: HIC value, effective plastic strain, displacement of the impactor and hood with 60mm deformation space for point C

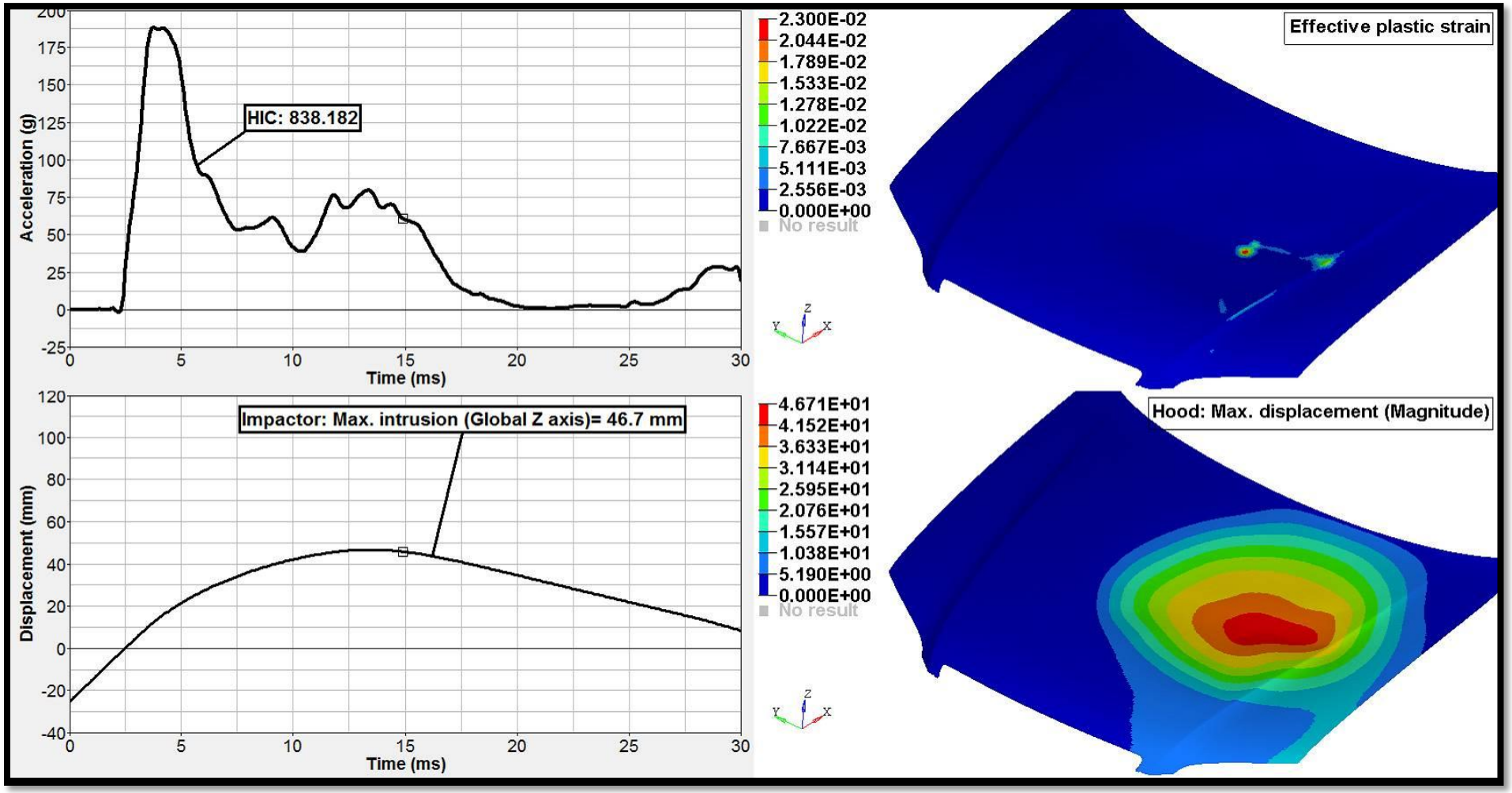

Figure 10.32: HIC value, effective plastic strain, displacement of the impactor and hood with 60mm deformation space for point D

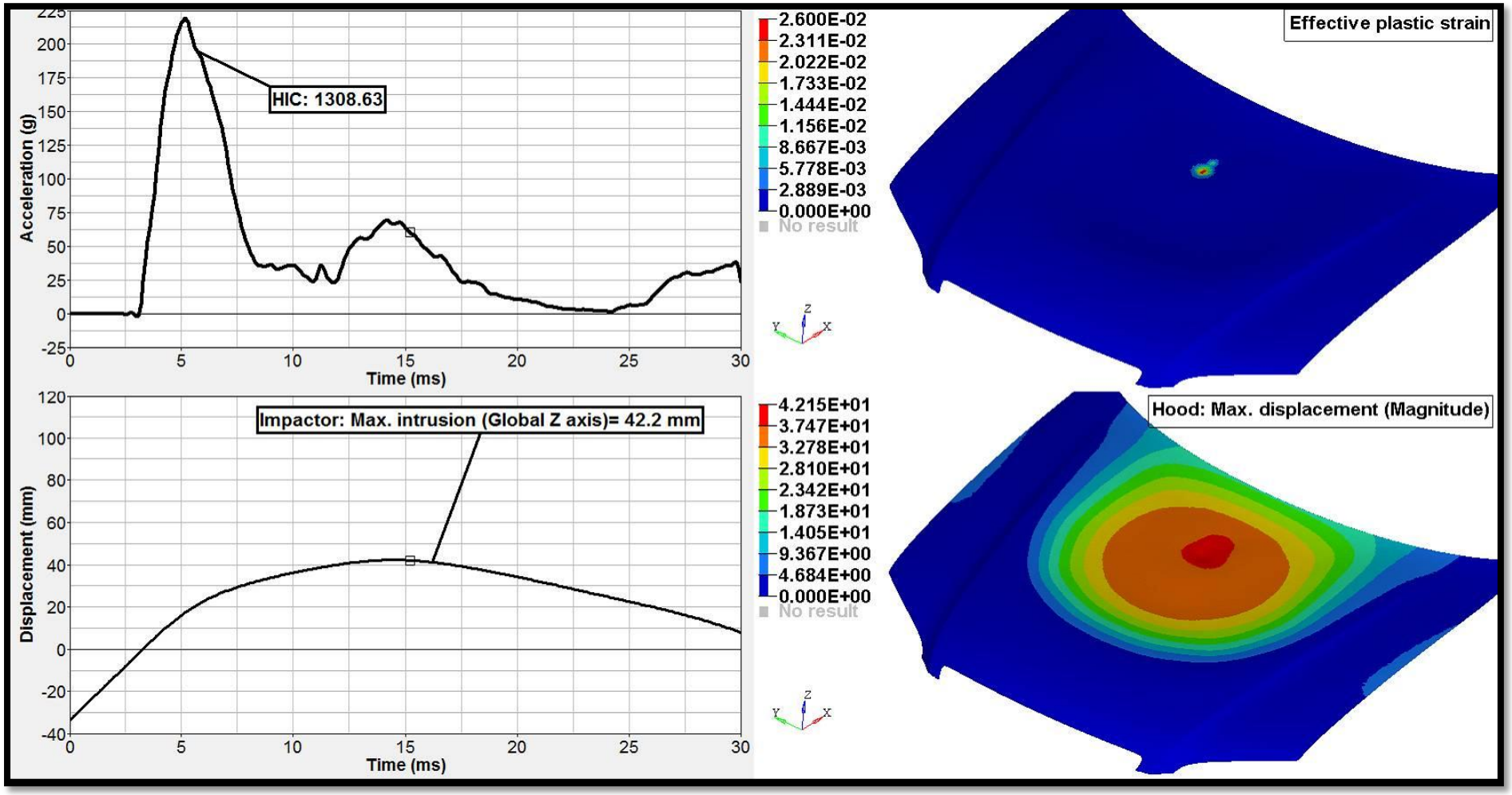

Figure 10.33: HIC value, effective plastic strain, displacement of the impactor and hood with 60mm deformation space for point E

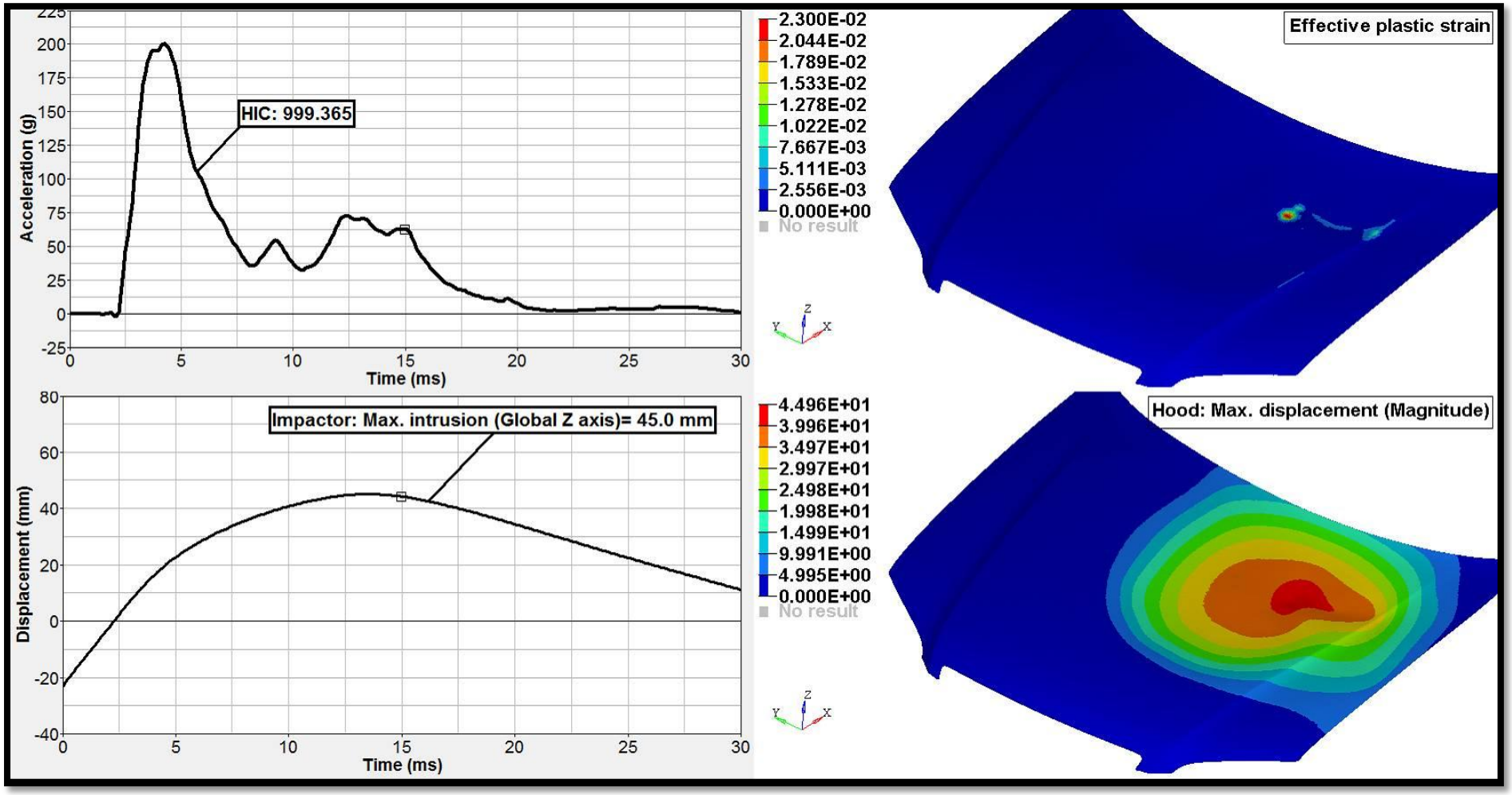

Figure 10.34: HIC value, effective plastic strain, displacement of the impactor and hood with 60mm deformation space for point F

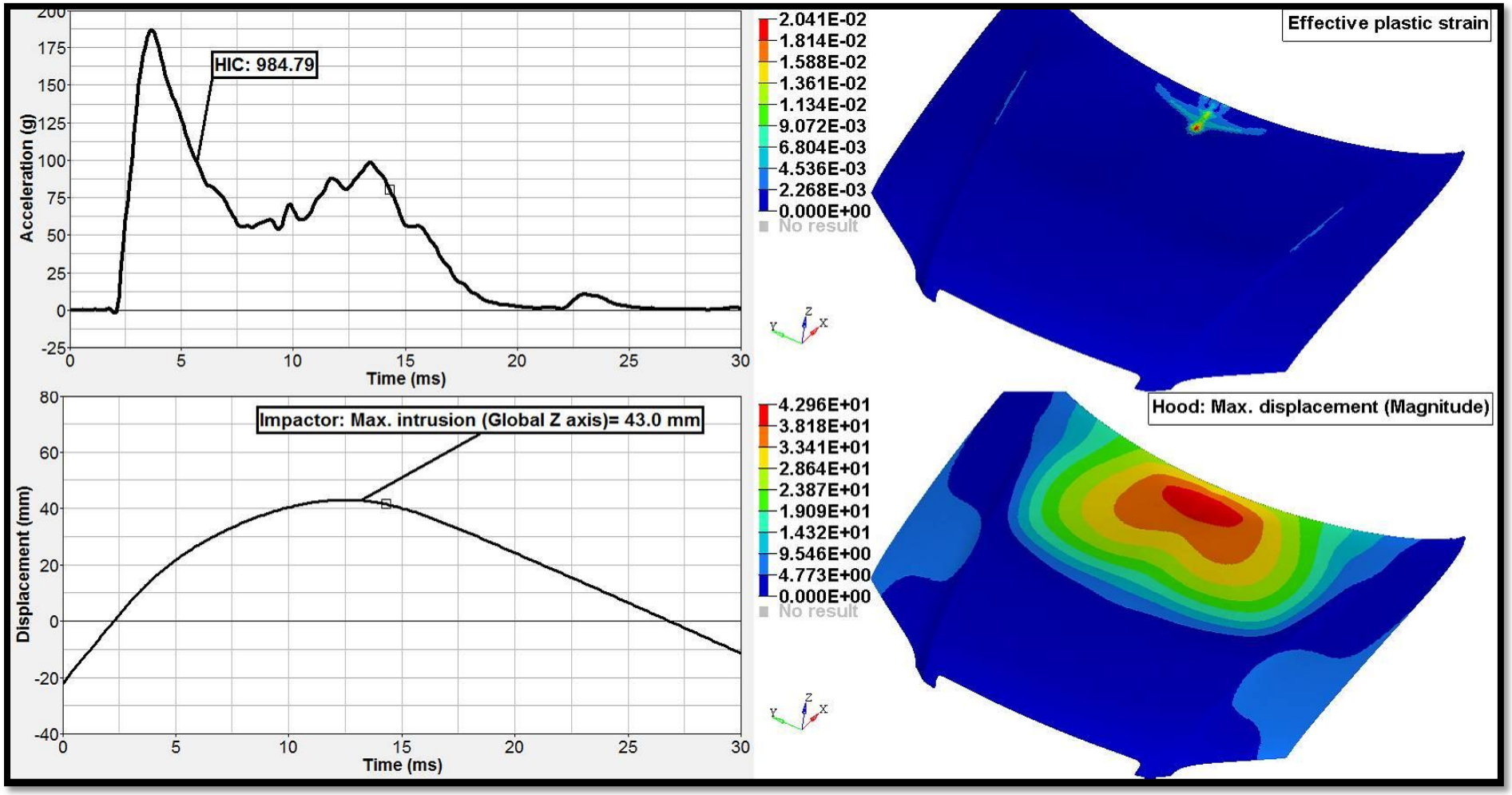

Figure 10.35: HIC value, effective plastic strain, displacement of the impactor and hood with 60mm deformation space for point G

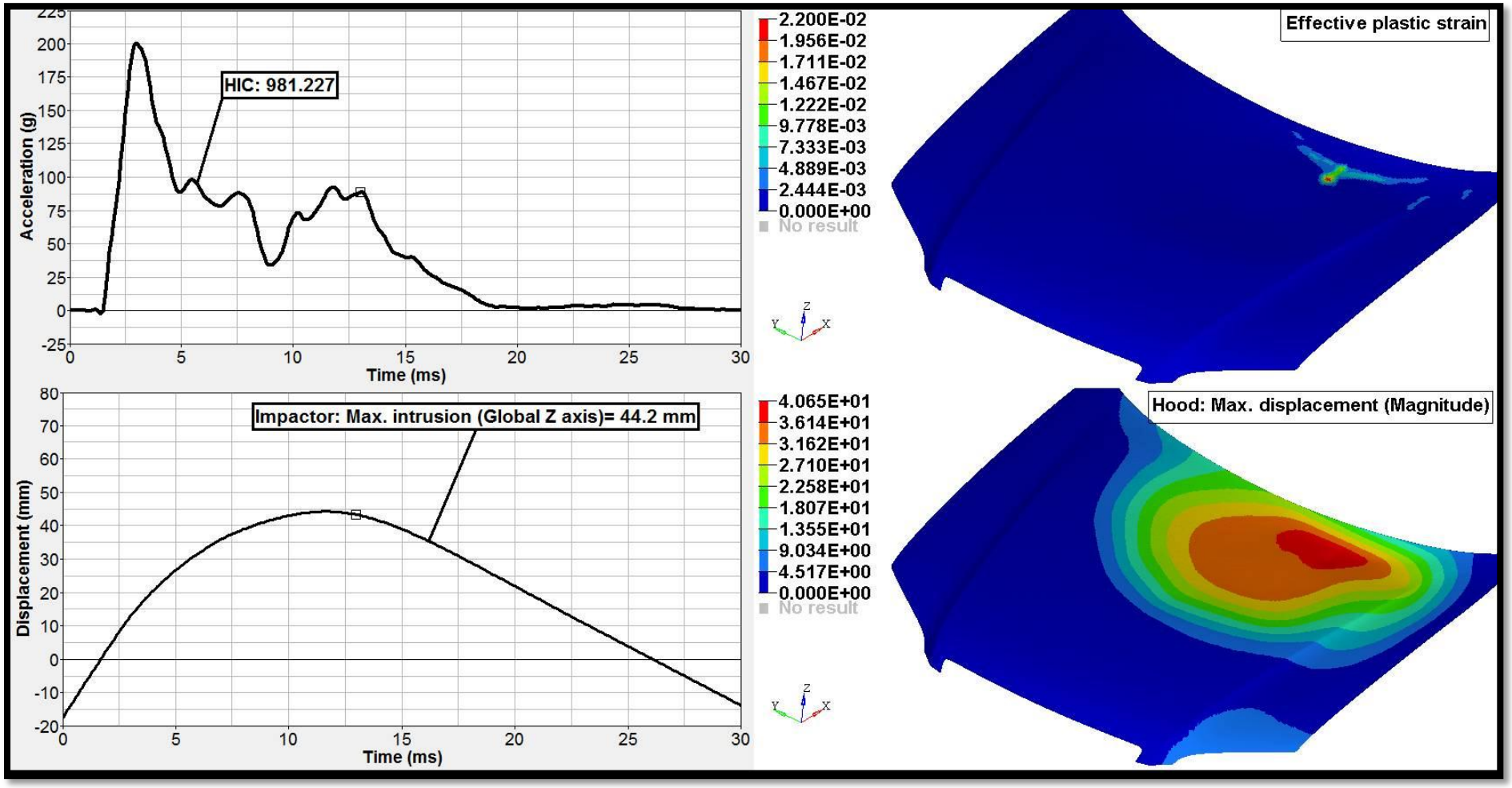

Figure 10.36: HIC value, effective plastic strain, displacement of the impactor and hood with 60mm deformation space for point H

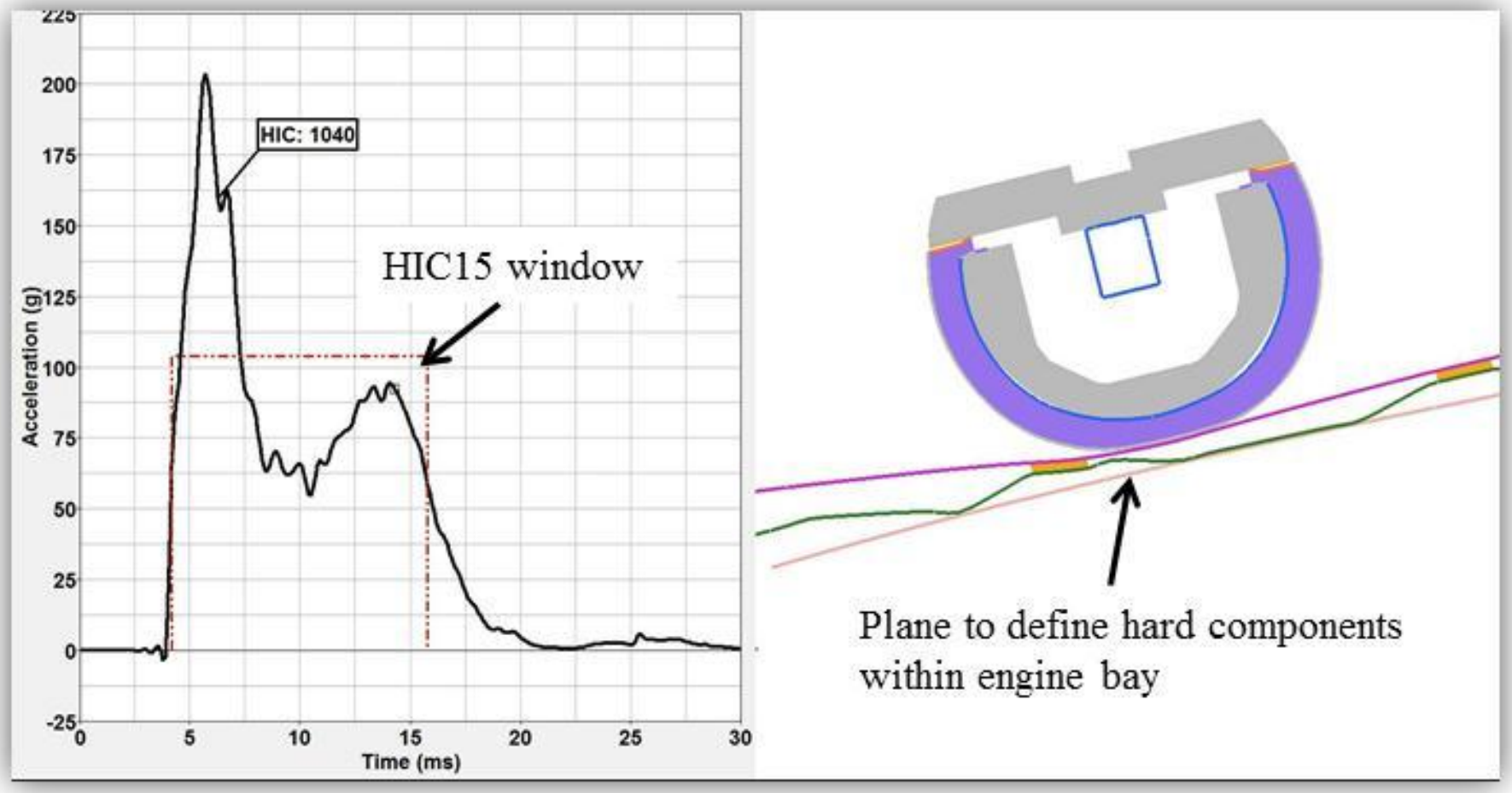

Figure 10.37: Lack of deformation space increases severity of secondary impact

Therefore, another study was carried out by increasing the deformation space to 70mm with the same variables, method and qualifiers such as the mean value of HIC and its standard deviation. These results clearly exhibit that robust and homogeneous performance with HIC value less than the threshold is achievable, in this case, with multi–cone structure for the inner hood and steel material for inner and outer hood panels. Numerical tests were conducted to confirm the predictive accuracy of the response surface and the results are shown in Figure 10.38.

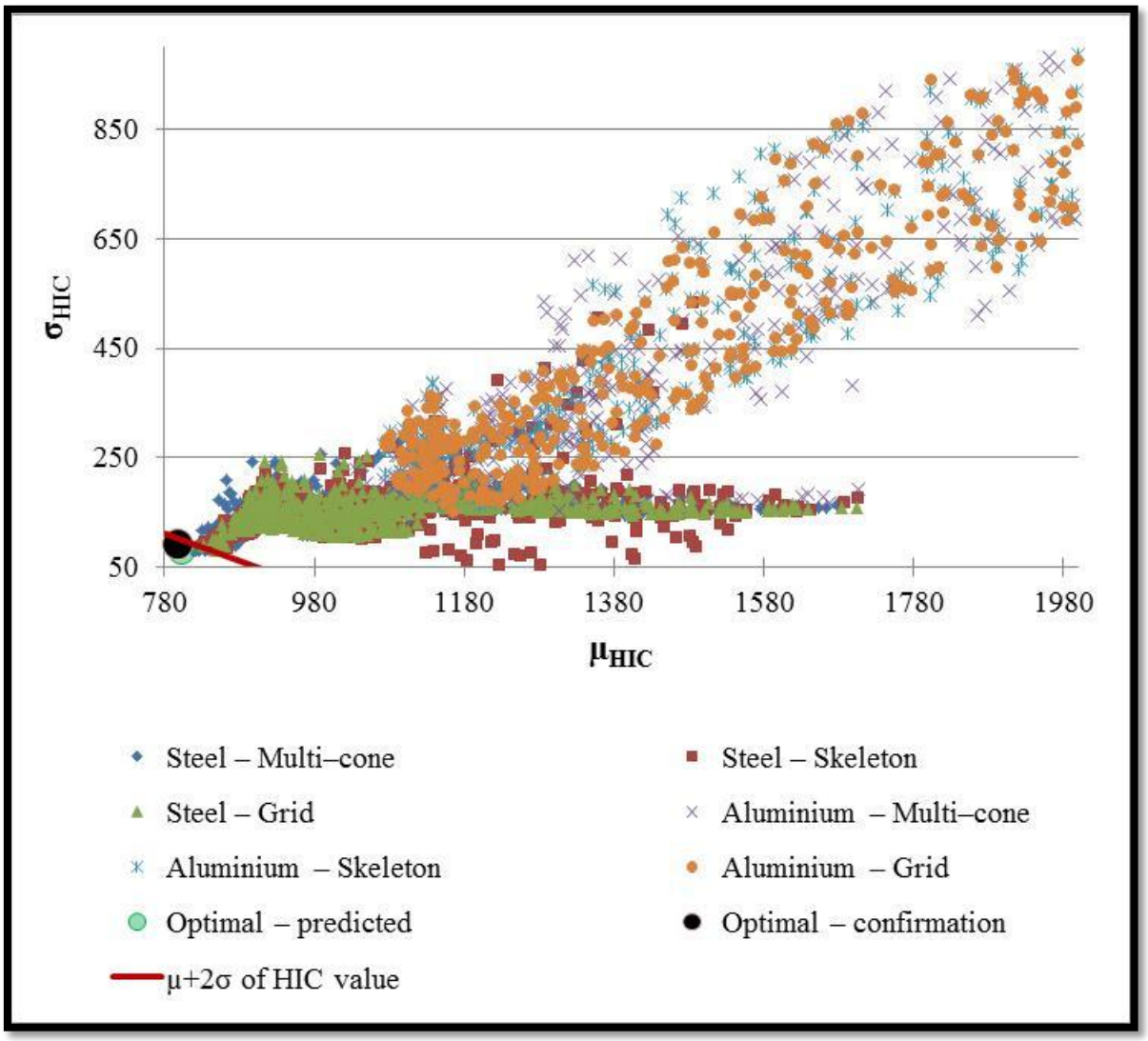

Figure 10.38: Influence of increase in deformation space on HIC values

Figure 10.39 shows the close up view of Figure 10.38, which depict close agreement between the predicted and numerical results. This ensures the accuracy of the optimal result.

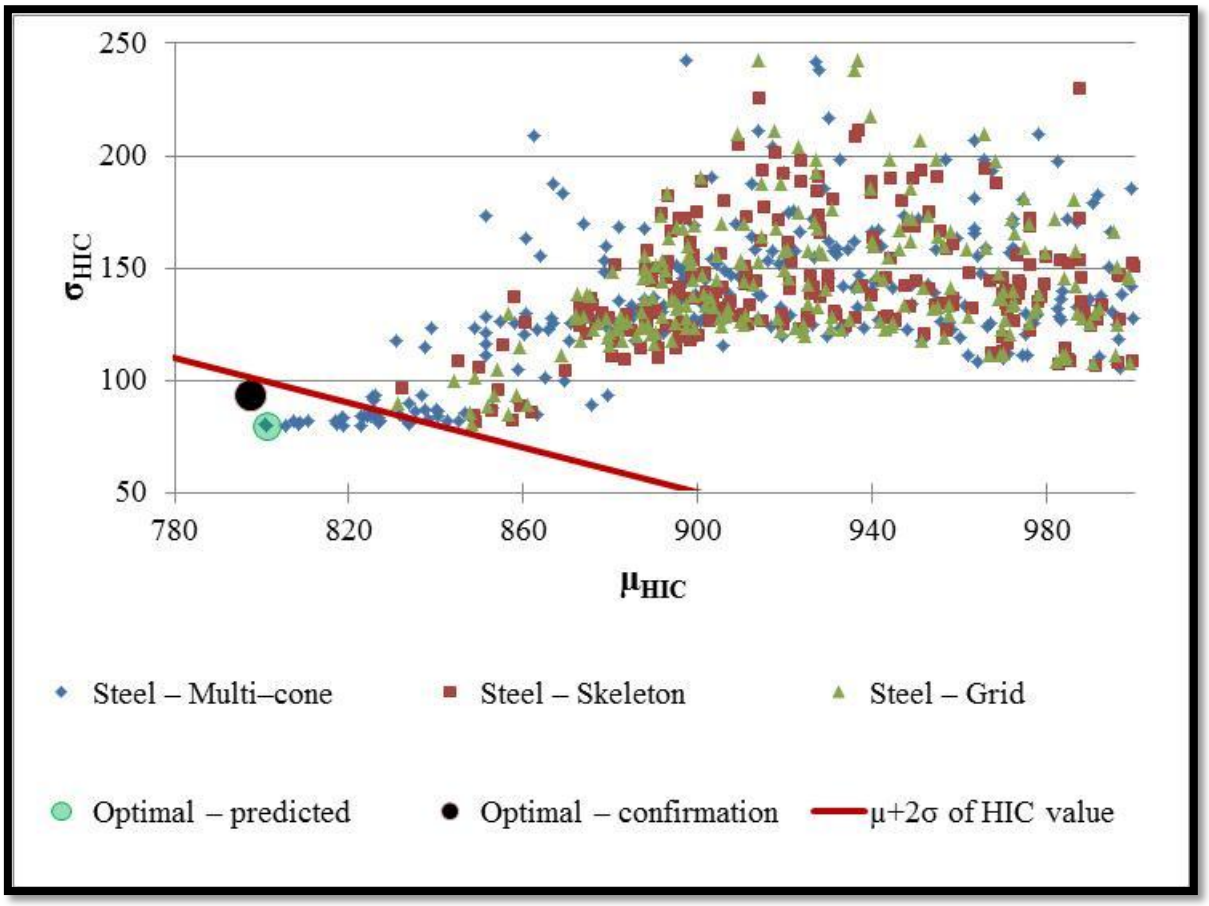

Figure 10.39: Detail view of influence of increase in deformation space on HIC values

Eight impact locations were considered to derive the values for the data point 'Optimal – confirmation' shown in Figure 10.39 . The details of the results from the numerical tests for the eight impact locations that were utilised to derive the values for this data point are shown in figures ranging from Figure 10.40 to Figure 10.47. The details are,

- plot of resultant acceleration against time
- plot of the displacement of the impactor in global Z direction against time
- contour plot of the effective plastic strain

- contour plot of the magnitude of the deformation of the hood panels.

It shows that a 70mm deformation space makes it possible to obtain the HIC value less than 1000 for seven out of eight impact locations. Nevertheless, the sum of the mean value of HIC and twice its standard deviation for this data point is less than the HIC threshold value as shown in Figure 10.39. Thus, it can be stated that it is possible to obtain the HIC value less than 1000 for all the eight impact locations if the geometry of the inner hood panel is optimised to improve the homogeneous performance of the hood panels.

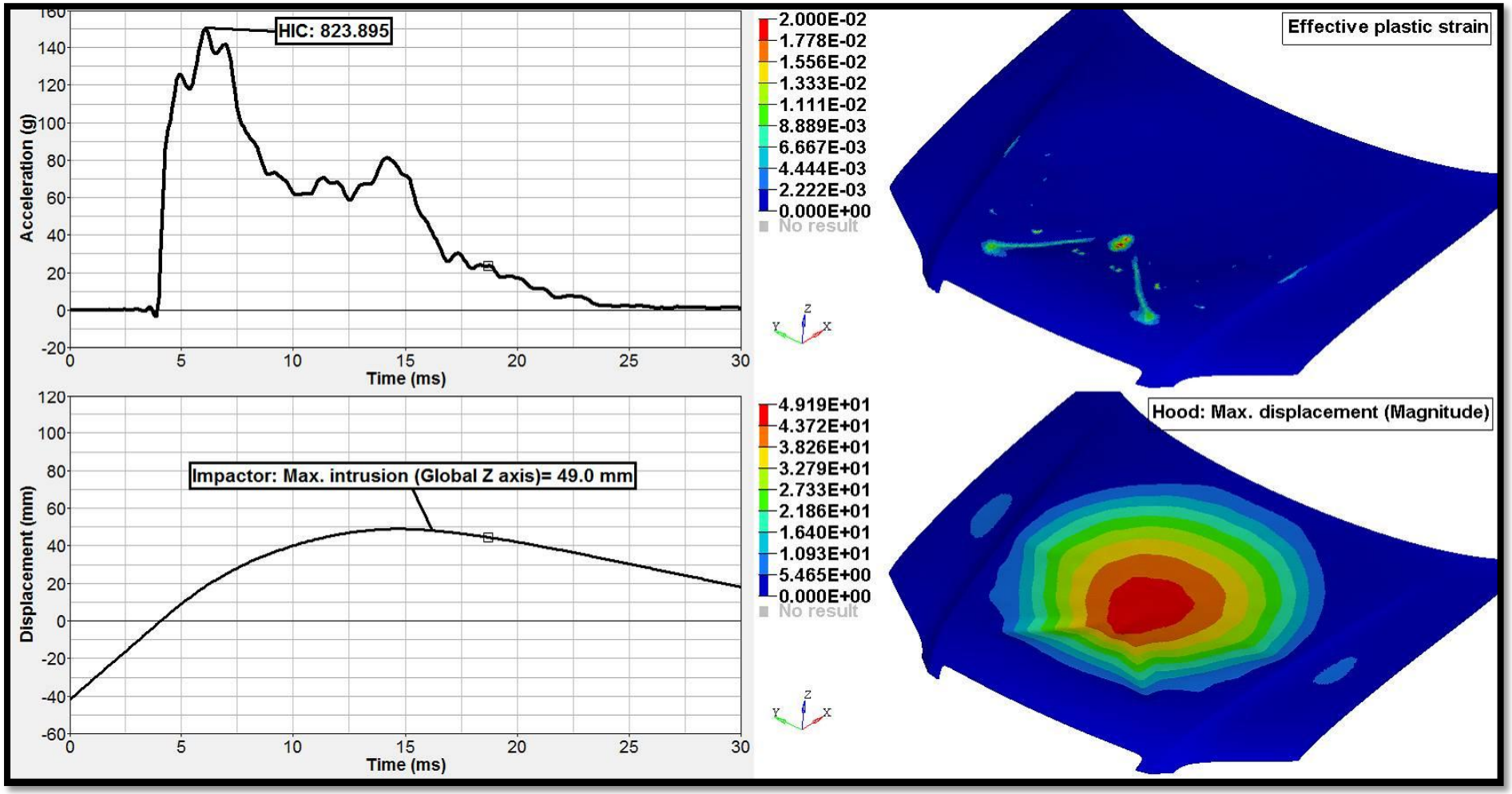

Figure 10.40: HIC value, effective plastic strain, displacement of the impactor and hood with 70mm deformation space for point A

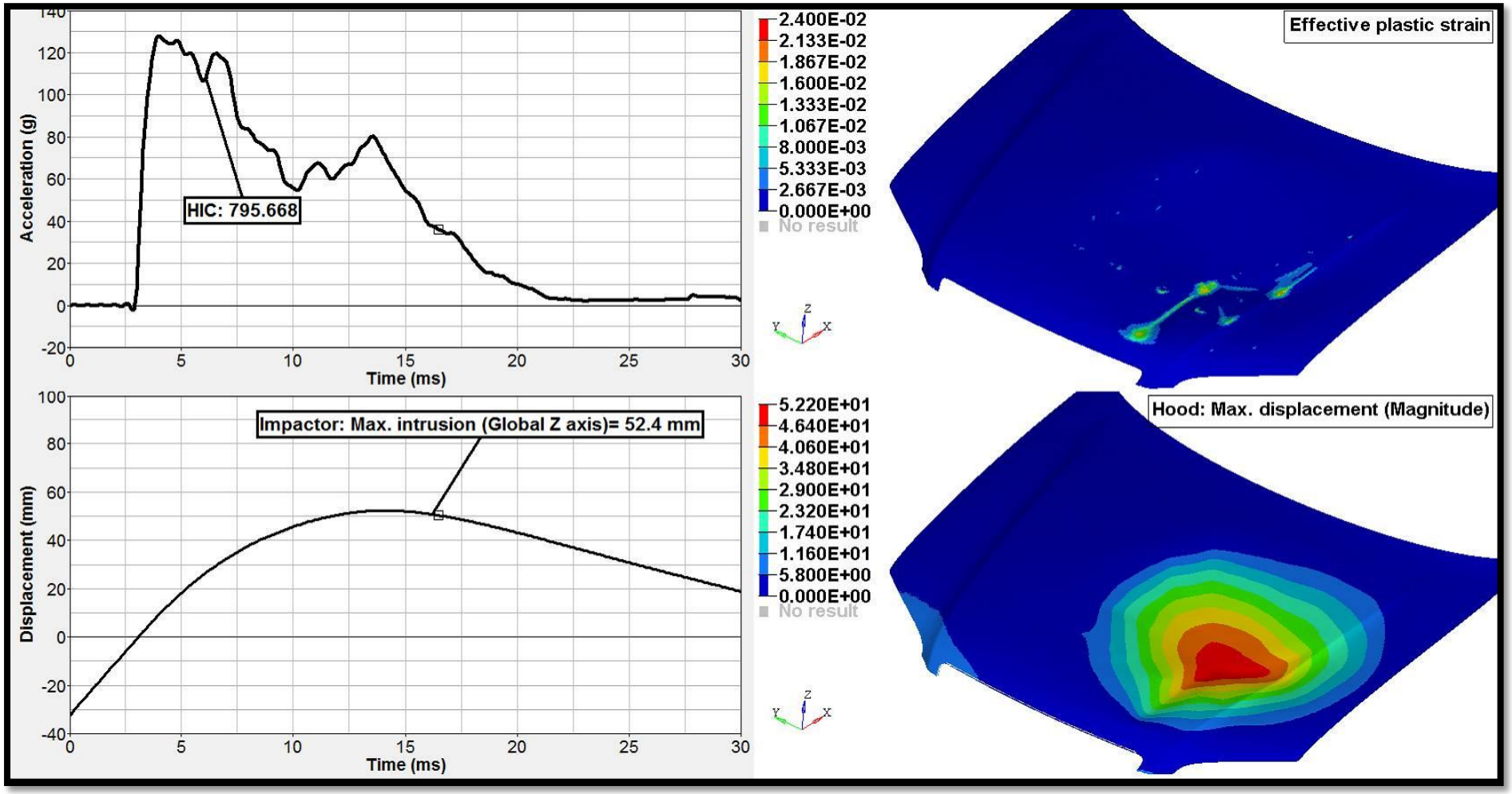

Figure 10.41: HIC value, effective plastic strain, displacement of the impactor and hood with 70mm deformation space for point B

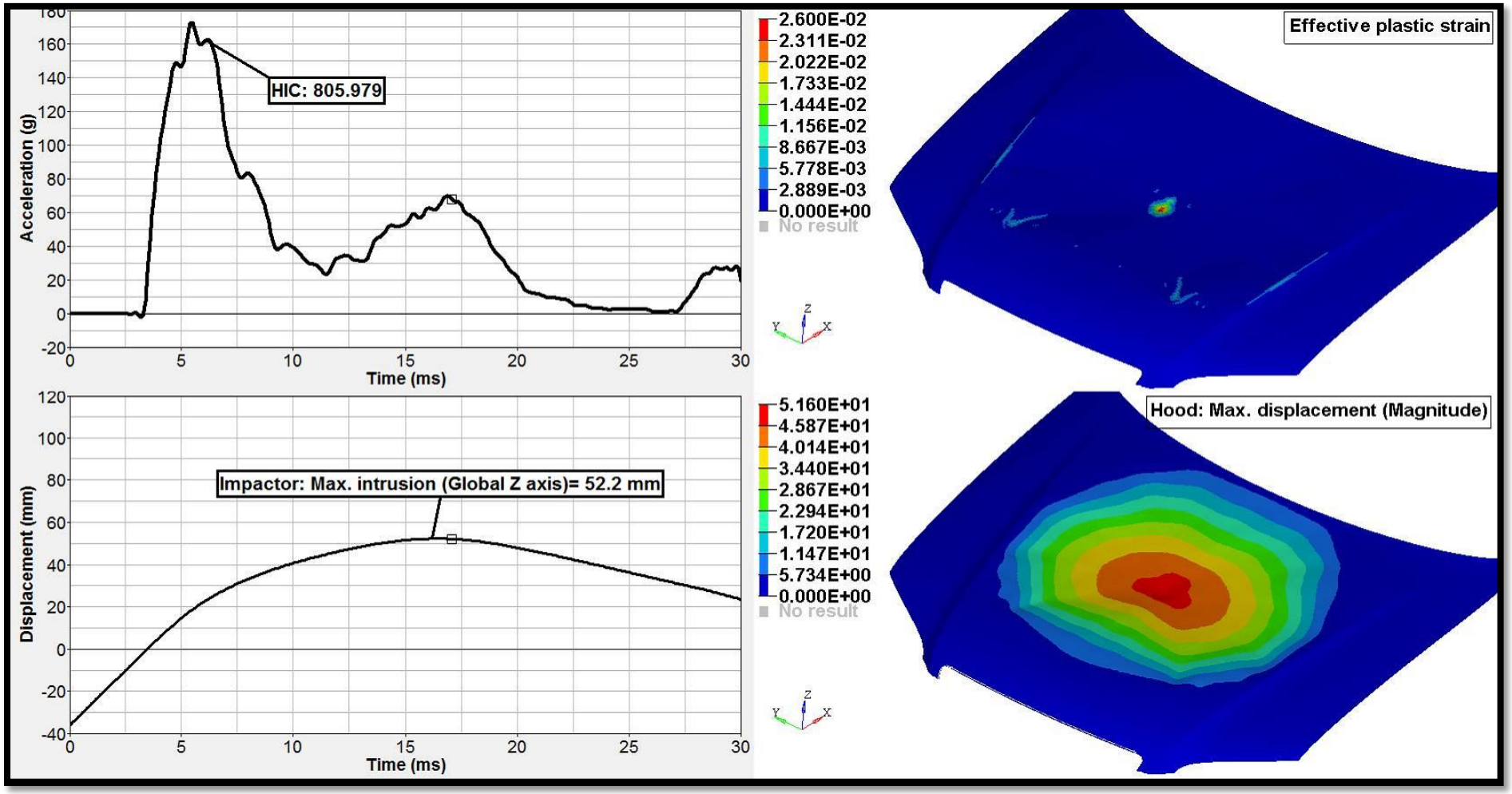

Figure 10.42: HIC value, effective plastic strain, displacement of the impactor and hood with 70mm deformation space for point C

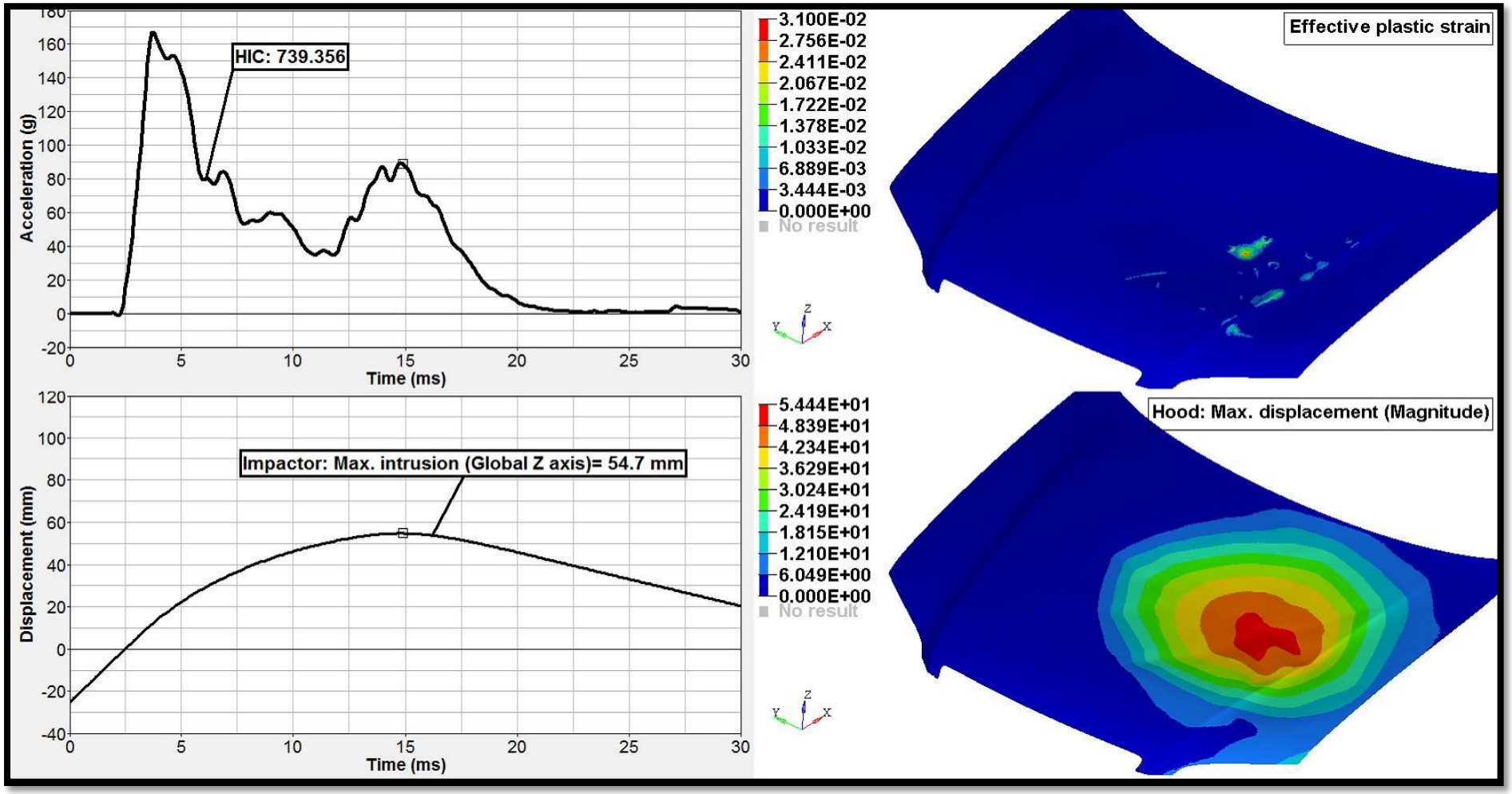

Figure 10.43: HIC value, effective plastic strain, displacement of the impactor and hood with 70mm deformation space for point D

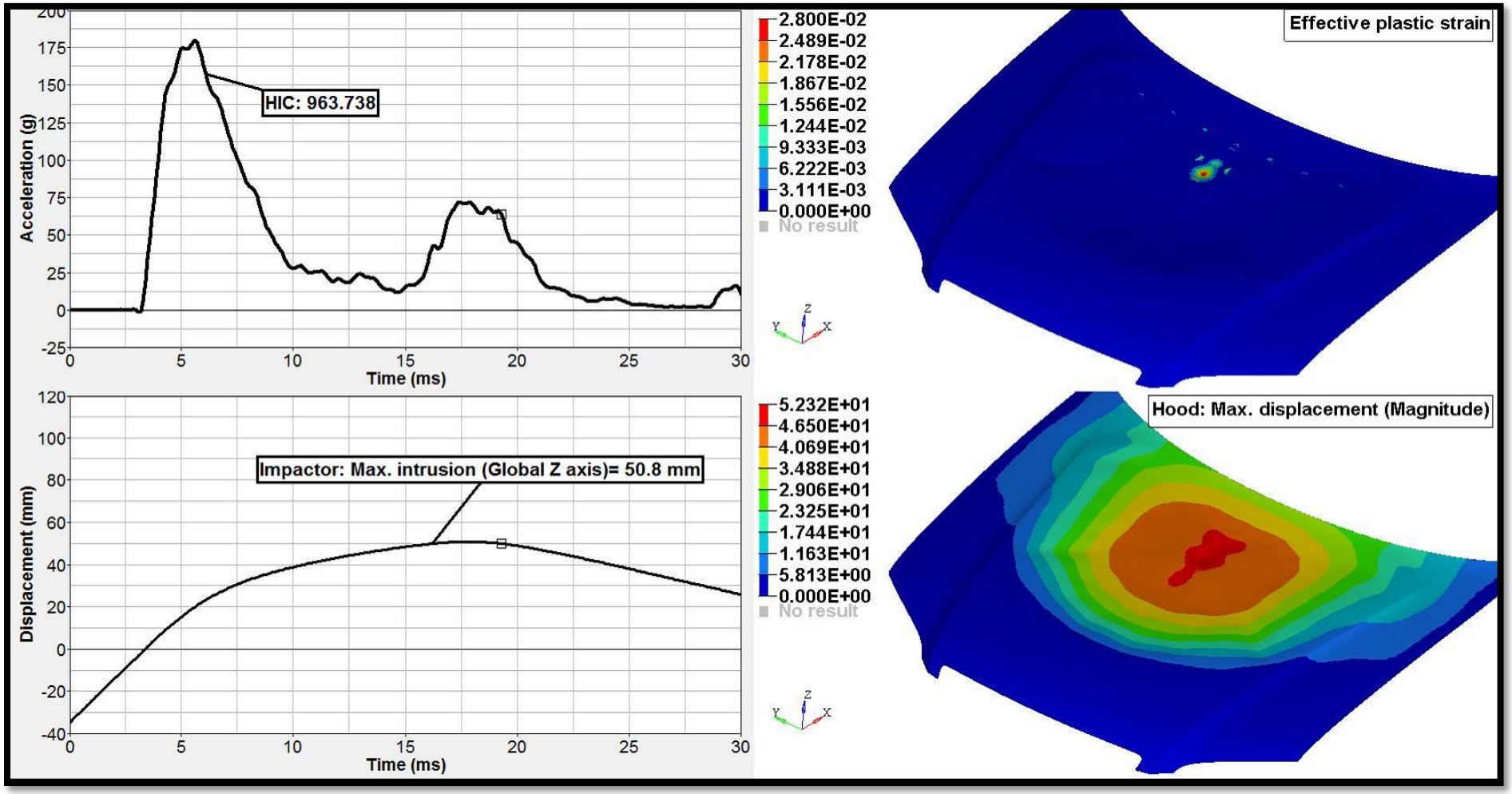

Figure 10.44: HIC value, effective plastic strain, displacement of the impactor and hood with 70mm deformation space for point E

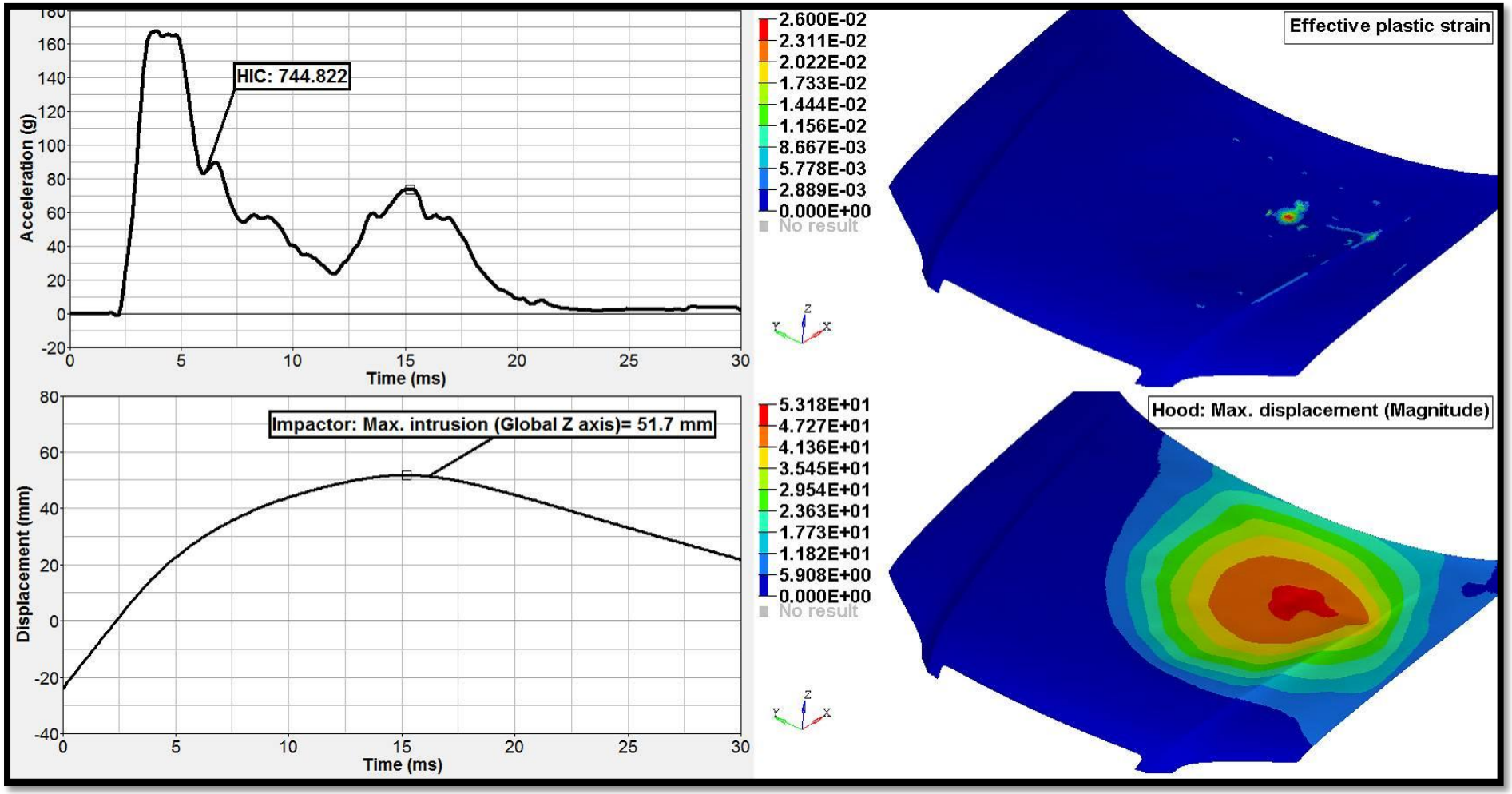

Figure 10.45: HIC value, effective plastic strain, displacement of the impactor and hood with 70mm deformation space for point F

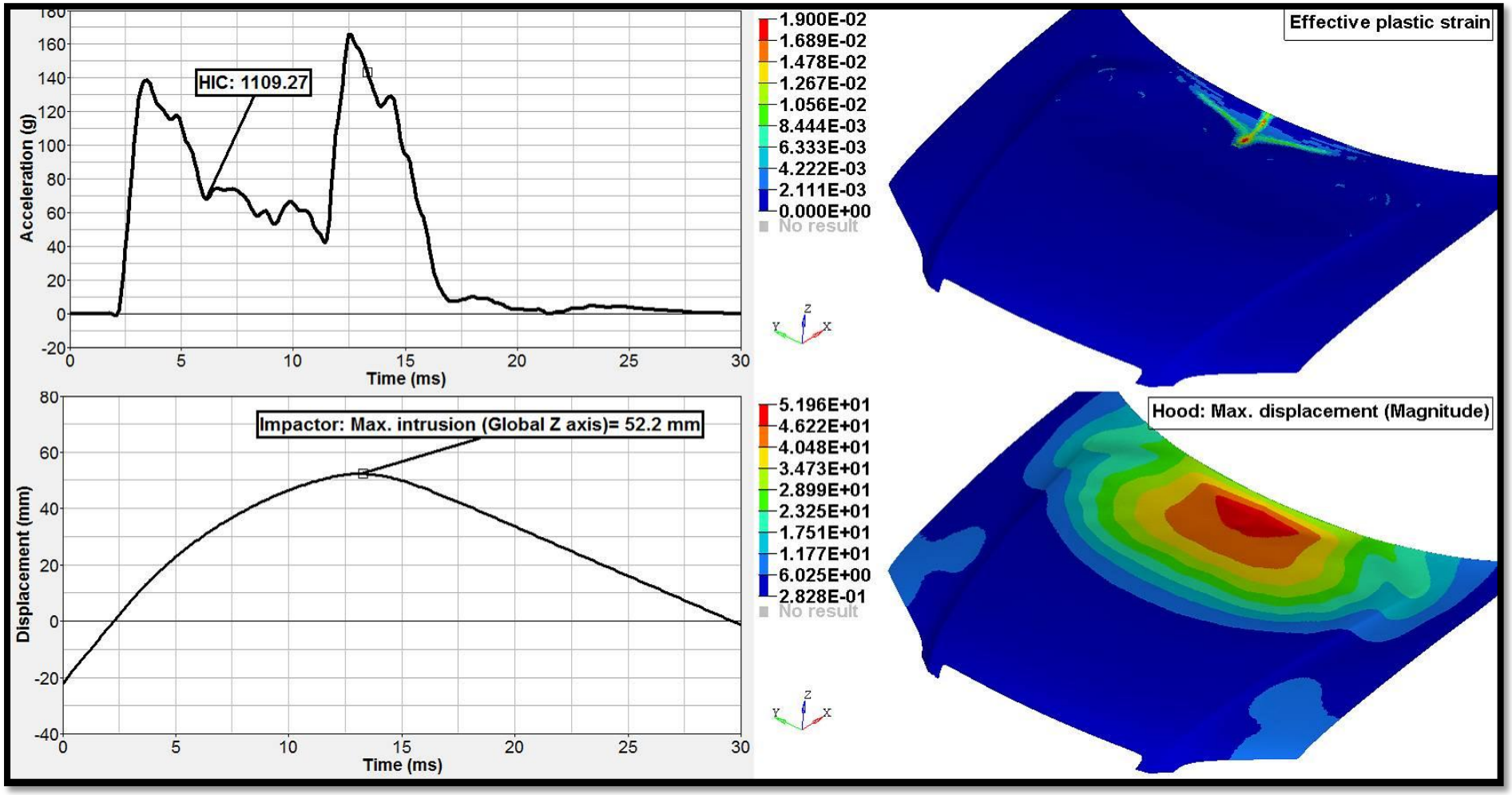

Figure 10.46: HIC value, effective plastic strain, displacement of the impactor and hood with 70mm deformation space for point G

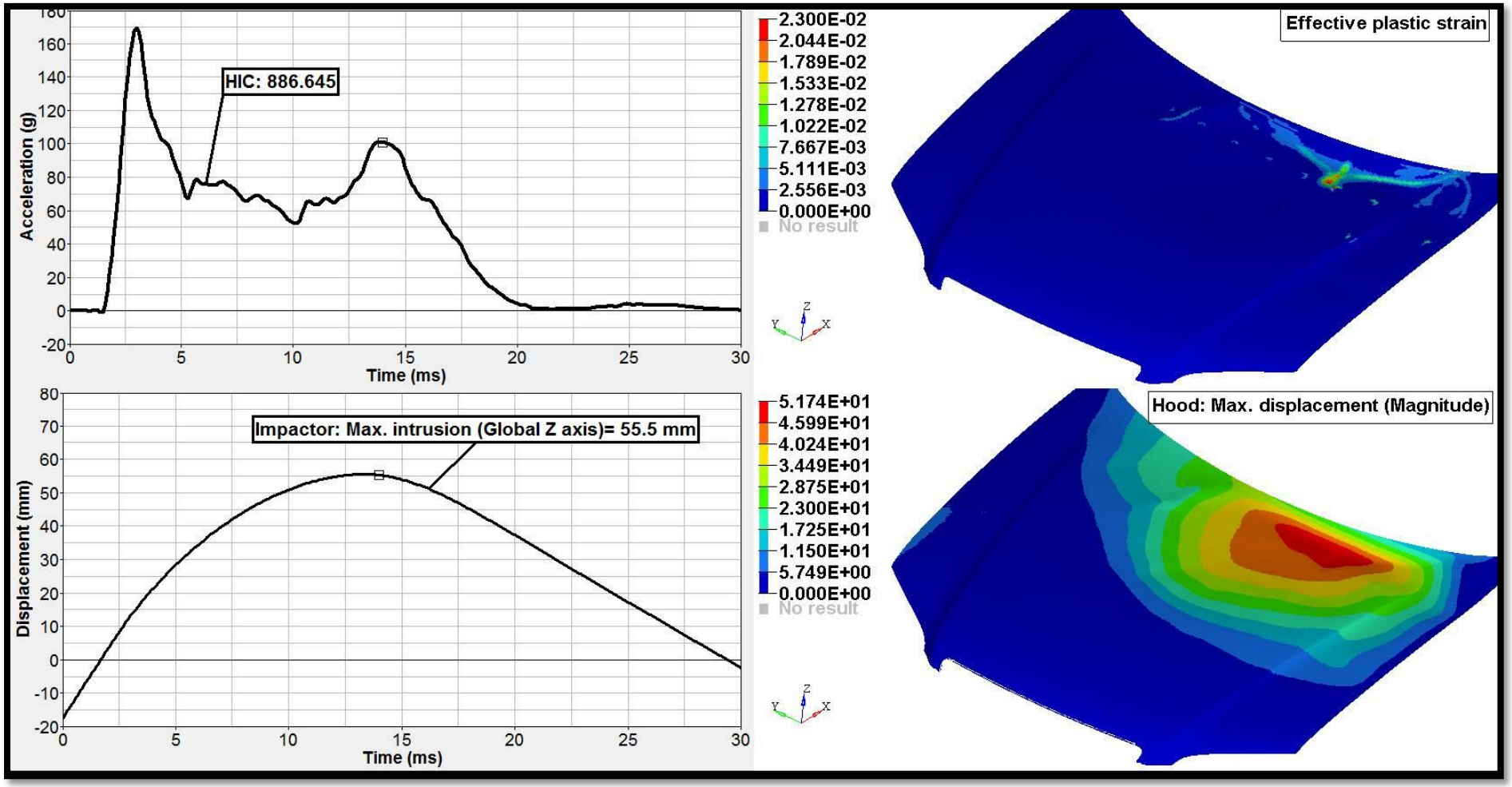

Figure 10.47: HIC value, effective plastic strain, displacement of the impactor and hood with 70mm deformation space for point H

Figure 10.48 shows the sum of the mean value of HIC and twice its standard deviation plotted against the inner and outer hood panel thicknesses. It shows that HIC value less than the threshold value is possible with various combinations of inner and outer hood thicknesses. However, it is evident that the combination of thicker outer hood and thinner inner hood enables optimal performance. Thus, the inner and outer hood thickness can be chosen within this range obviously taking into consideration the torsional and bending stiffness, durability, noise and vibration performances.

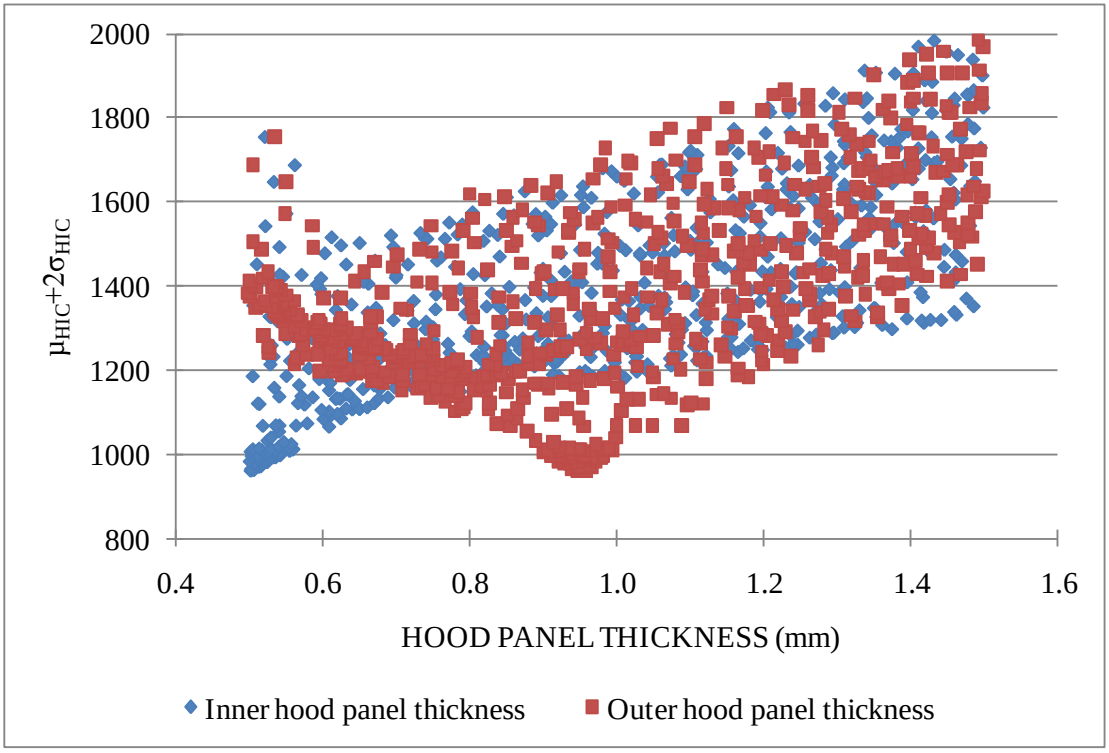

Figure 10.48: Influence of hood panel thickness on efficiency

Figure 10.49 shows the sum of the mean value of HIC and twice its standard deviation plotted against the combined inner and outer hood panel thickness. It depicts that a similar performance can be obtained with various thickness combinations while maintaining a combined thickness to ensure robust and homogeneous optimal performance. It also indicates that an increase in panel thickness is essential to lower the HIC value, in order to

reduce the intensity of the secondary impact but only to a certain limit. Beyond that limit, the HIC value increases with panel thickness due to the increase in structural stiffness and structural inertia, which leads to increasing the intensity of the primary impact.

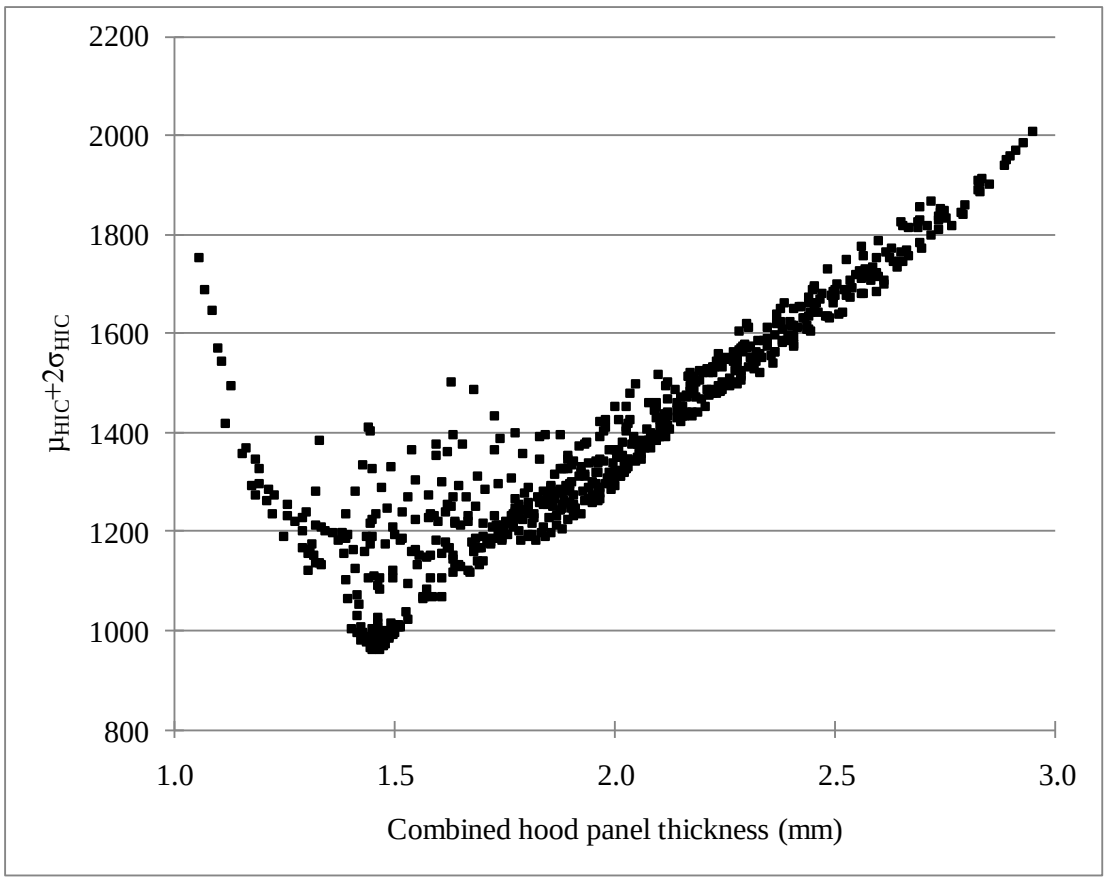

Figure 10.49: Influence of combined hood panel thickness on efficiency

10.3 Optimisation of panel thickness and cone design

The next step of the research is to optimise the inner hood by varying cone depth and cone angle in the multi–cone inner hood structure made of steel material while maintaining constant minor diameter and constant gap between the cones as shown in Figure 10.50.

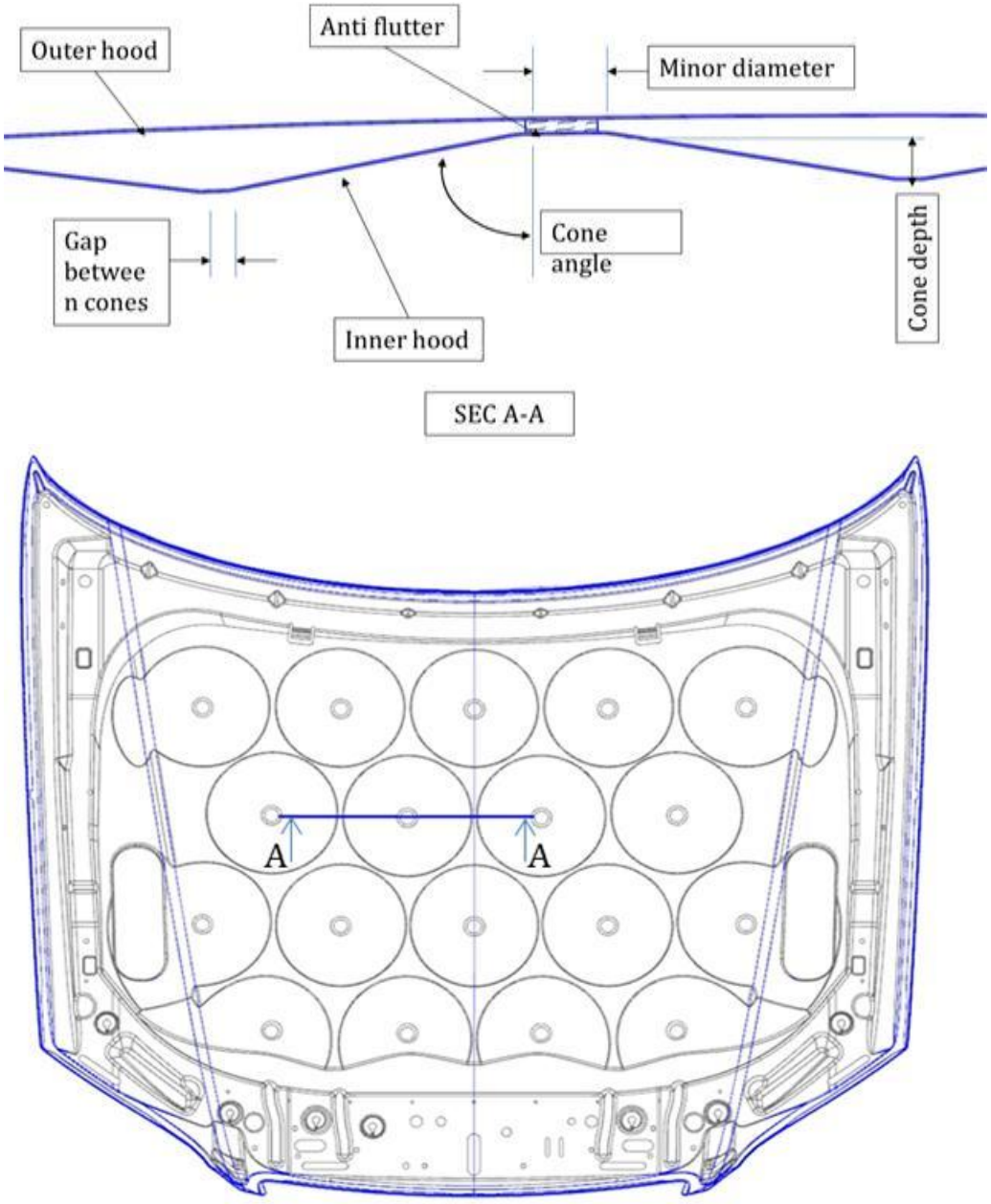

Figure 10.50: Cross-section of hood assembly

Variable	Values of Variable	Type of Variable
Cone angle	120°, 140°, 160°	Discrete
Cone depth	5mm, 10mm, 15mm	Discrete
Inner hood gauge	0.4mm to 1.2mm at 0.1mm increments	Discrete
Outer hood gauge	0.4mm to 1.2mm at 0.1mm increments	Discrete
Impact Position	1 to 8	Discrete

Table 10.1: Variables considered in improving pedestrian protection performance

Table 10.1 shows the values for the variables. A minimum of 120degrees included angle has been chosen for the cone angles because this enables good energy absorption and is formable with less strain to the panel. The maximum limit was chosen as 160degrees for included angle because cones with larger angles are closer to flat with larger major diameter, which would result in a lower number of cones. Similarly, cone depth less than 5mm will result in smaller corner radii and more than 15mm increases the complexity to forming and increases mass.

From Figure 10.48, it could be concluded that optimum performance is possible with inner and outer hood panel thickness varying from 0.5mm and 1.0mm. Therefore, the panel range of 0.4mm to 1.2mm was considered for inner and outer hood panel thickness at 0.1mm intervals to ensure that all relevant conditions have been considered. The same impact positions as in previous studies were utilised for this optimisation step as well.

Three–dimensional geometric models and FE models have been created with consideration to the full factorial of cone depth and cone angle (3*3=9) as shown in Figure 10.51 while maintaining a constant minor diameter of the cone and constant gap between the cones.

These hood models were assembled to the existing FE model with rigid plane at 70mm from the hood outer surface to represent the hard components within the engine bay. The FE models were created as per the DOE matrix in order to conduct numerical tests. The accelerometer time histories were gathered from each test and the HIC value were calculated to derive the mean value of HIC and its standard deviation. Then the response surfaces were created with this data to predict the optimal configuration for hood panels.

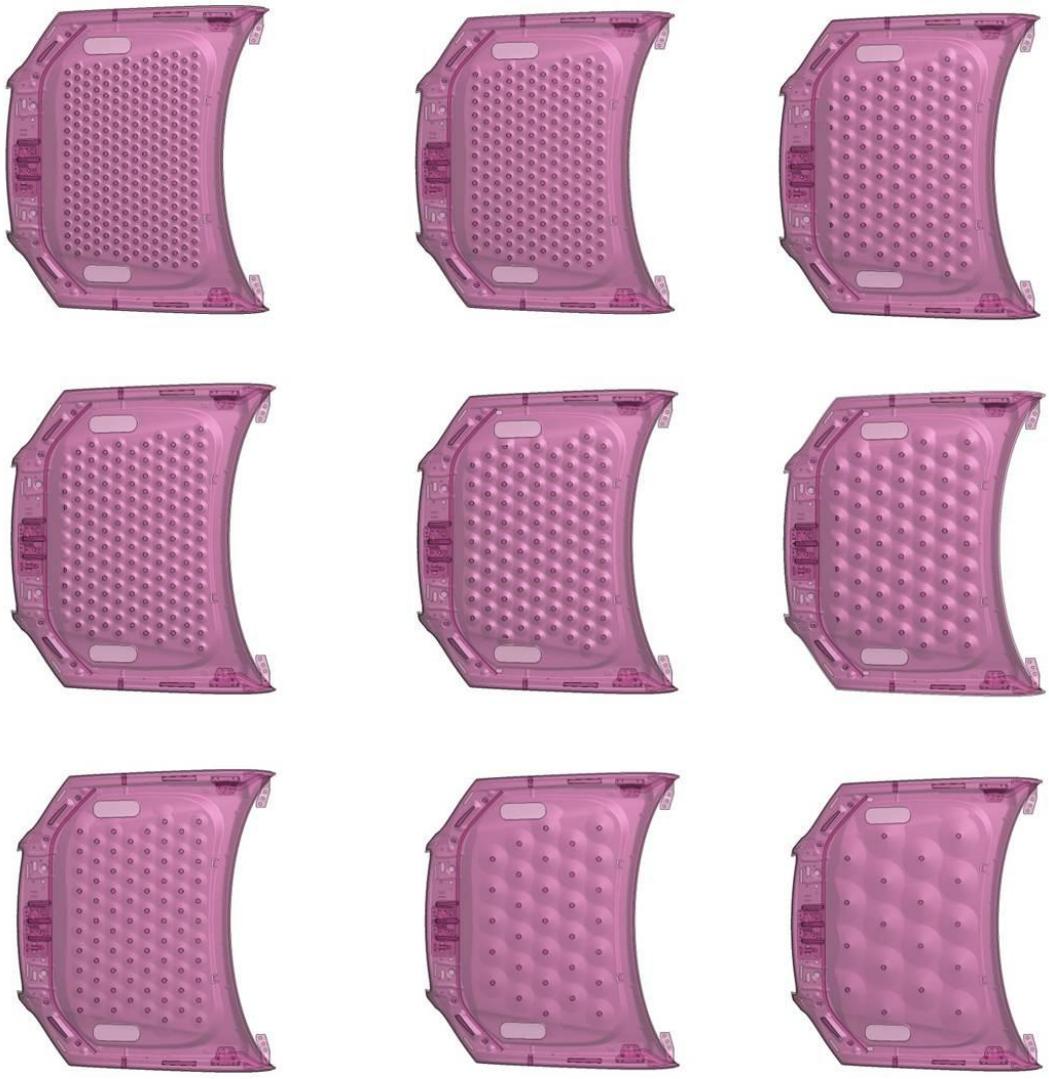

Figure 10.51: Inner hood geometric models

Figure 10.52 shows the mean value of HIC against its standard deviation for various panel gauges grouped by cone structure. It shows that it is possible to obtain robust

homogeneous performance less than the HIC threshold value with various combinations of cone angle and depth. However, the minimum mean value less than the HIC threshold value is feasible with 160degrees cone angle with 15mm cone depth.

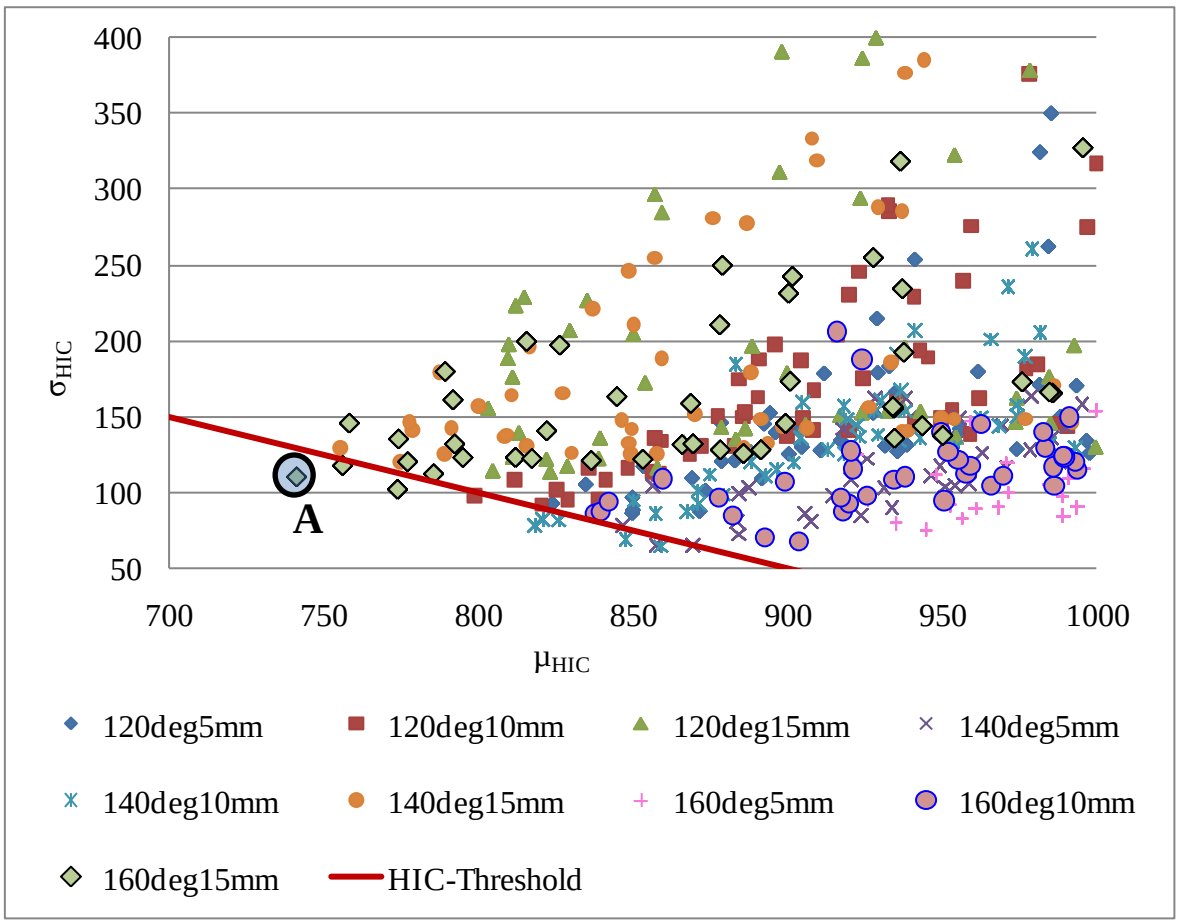

Figure 10.52: Influence of cone structure on HIC values

Eight impact locations were considered to the values for the data point A shown in Figure 10.52. The details of the results from the numerical tests for the eight impact locations that were utilised to derive the values for this data point are shown in figures ranging from Figure 10.53 to Figure 10.60. The details are,

- plot of resultant acceleration against time
- plot of the displacement of the impactor in global Z direction against time
- contour plot of the effective plastic strain

- contour plot of the magnitude of the deformation of the hood panels.

The plots in the figures ranging from Figure 10.53 to Figure 10.60 show that it is possible to obtain the HIC value less than 1000 for all the eight impact locations while the optimisation of inner hood geometry is considered.

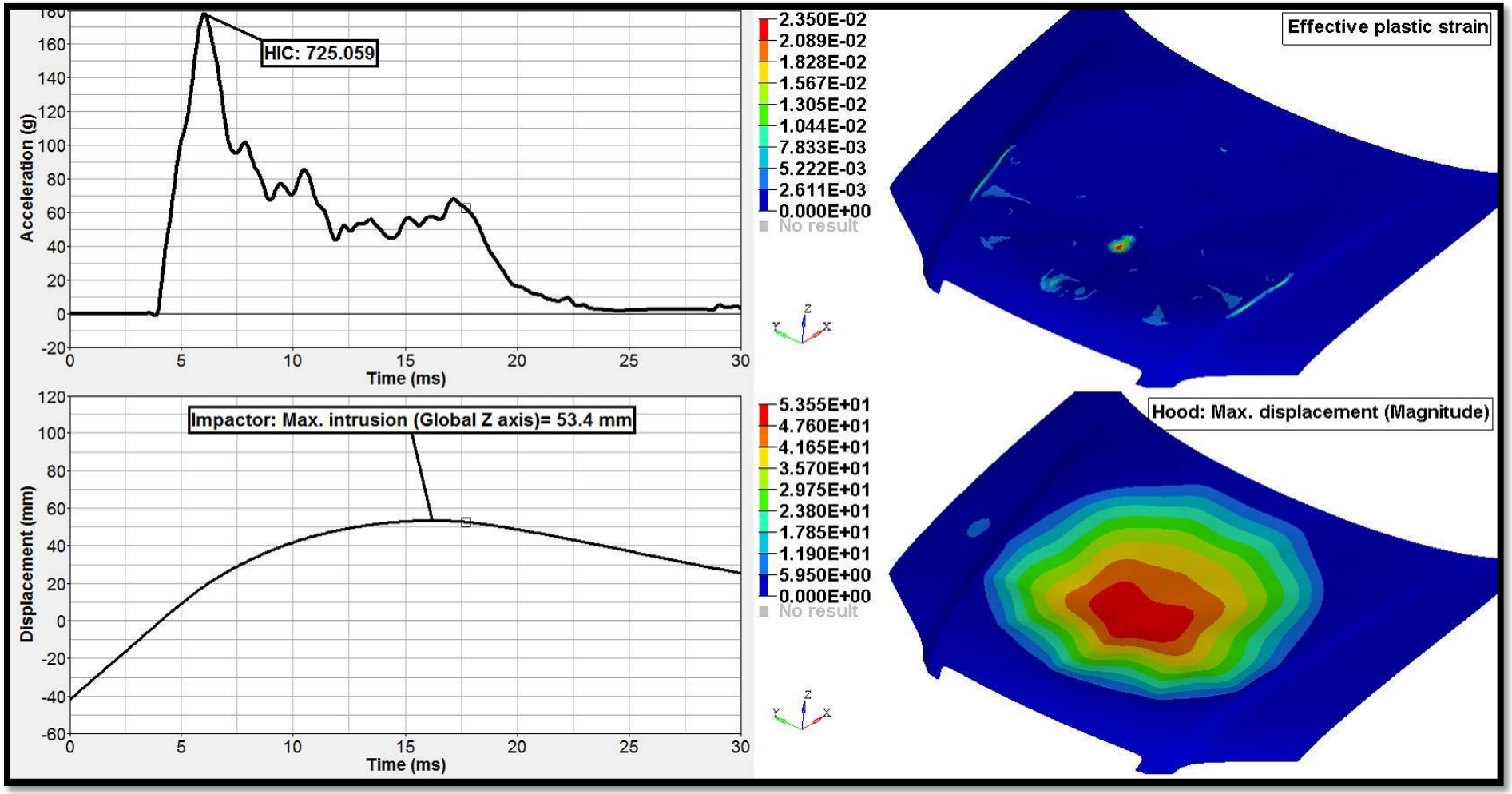

Figure 10.53: Effect of inner hood geometry optimisation on HIC value, effective plastic strain, displacement of the impactor and hood with 70mm deformation space for point A

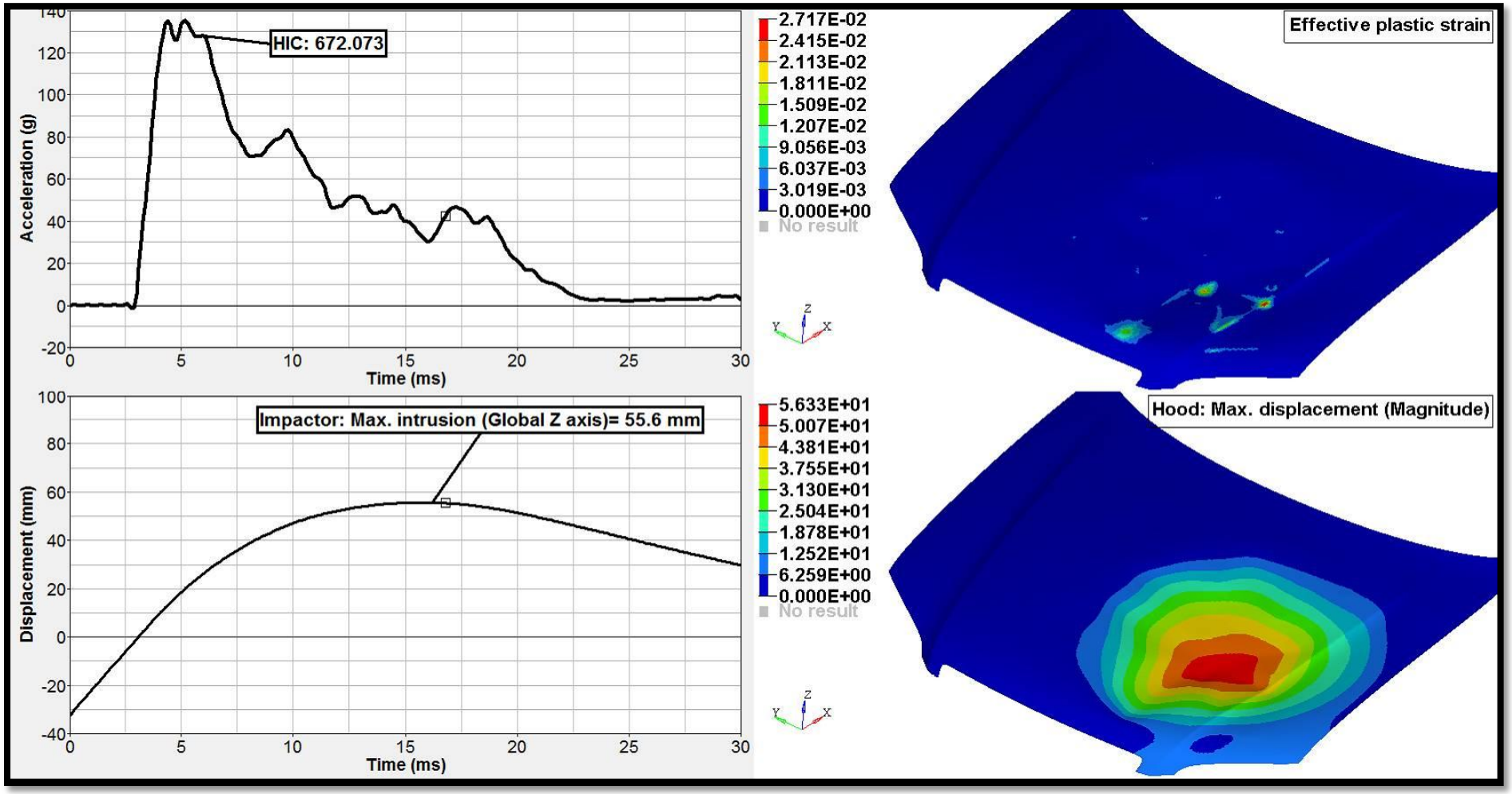

Figure 10.54: Effect of inner hood geometry optimisation on HIC value, effective plastic strain, displacement of the impactor and hood with 70mm deformation space for point B

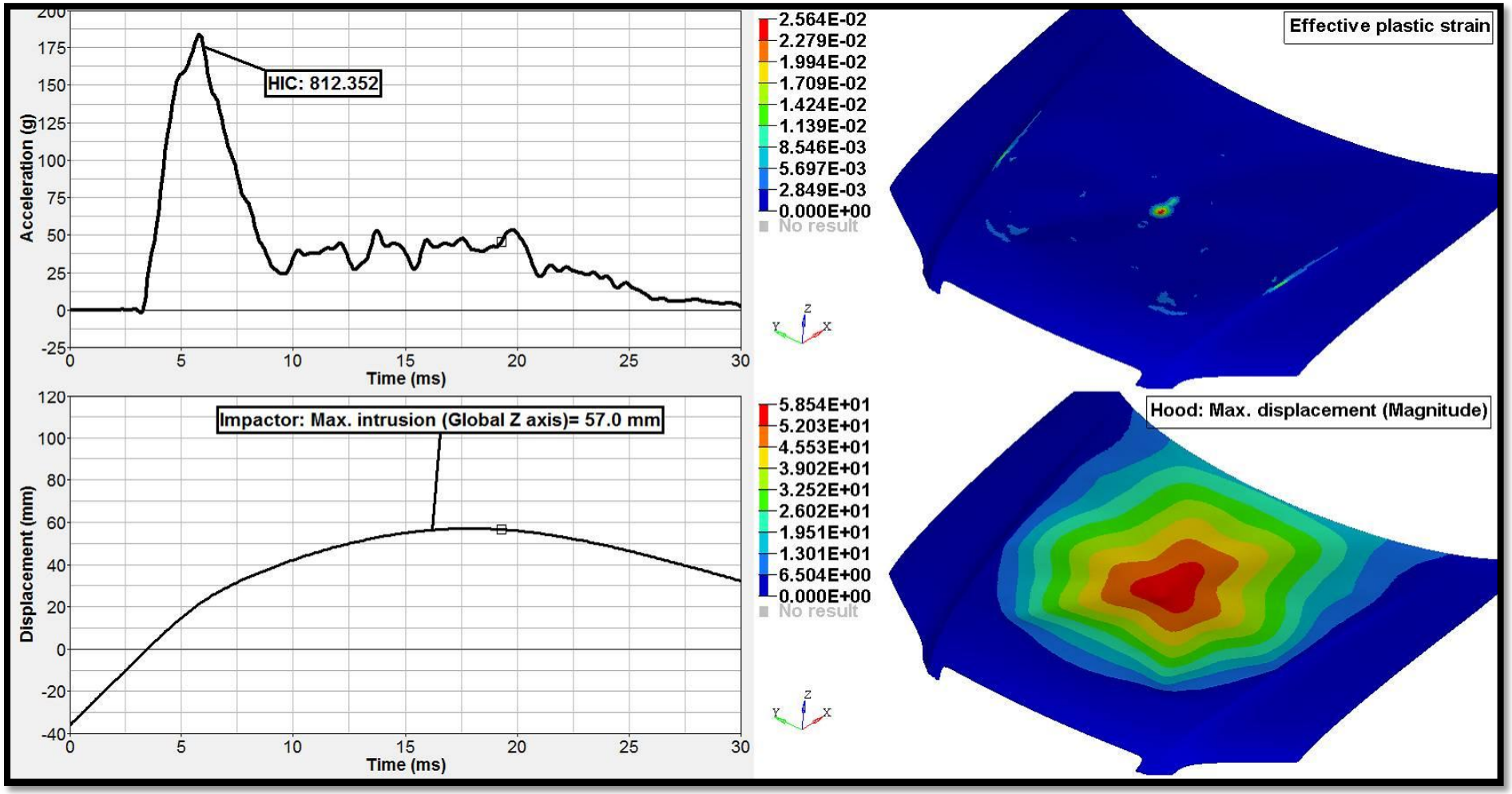

Figure 10.55: Effect of inner hood geometry optimisation on HIC value, effective plastic strain, displacement of the impactor and hood with 70mm deformation space for point C

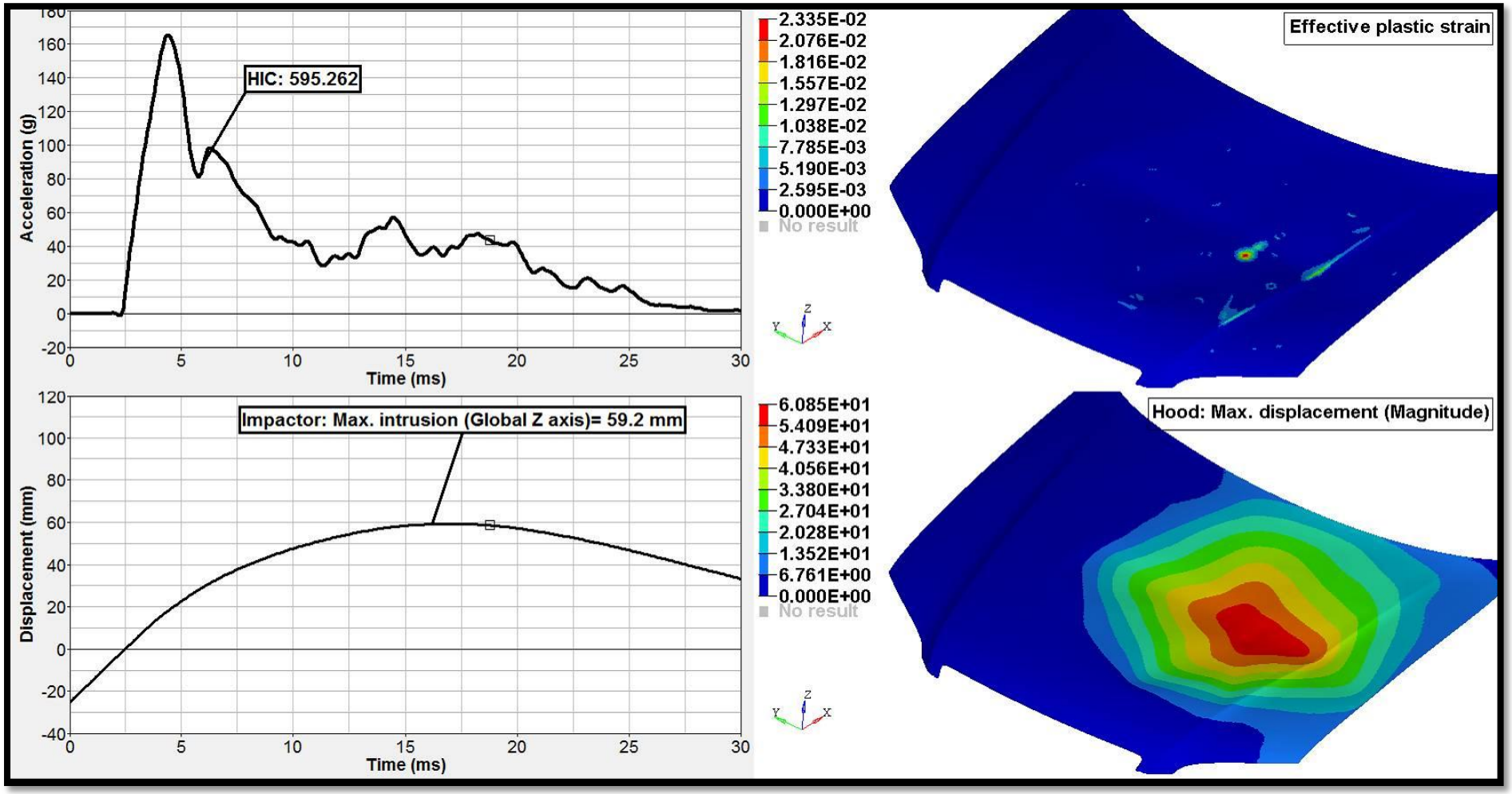

Figure 10.56: Effect of inner hood geometry optimisation on HIC value, effective plastic strain, displacement of the impactor and hood with 70mm deformation space for point D

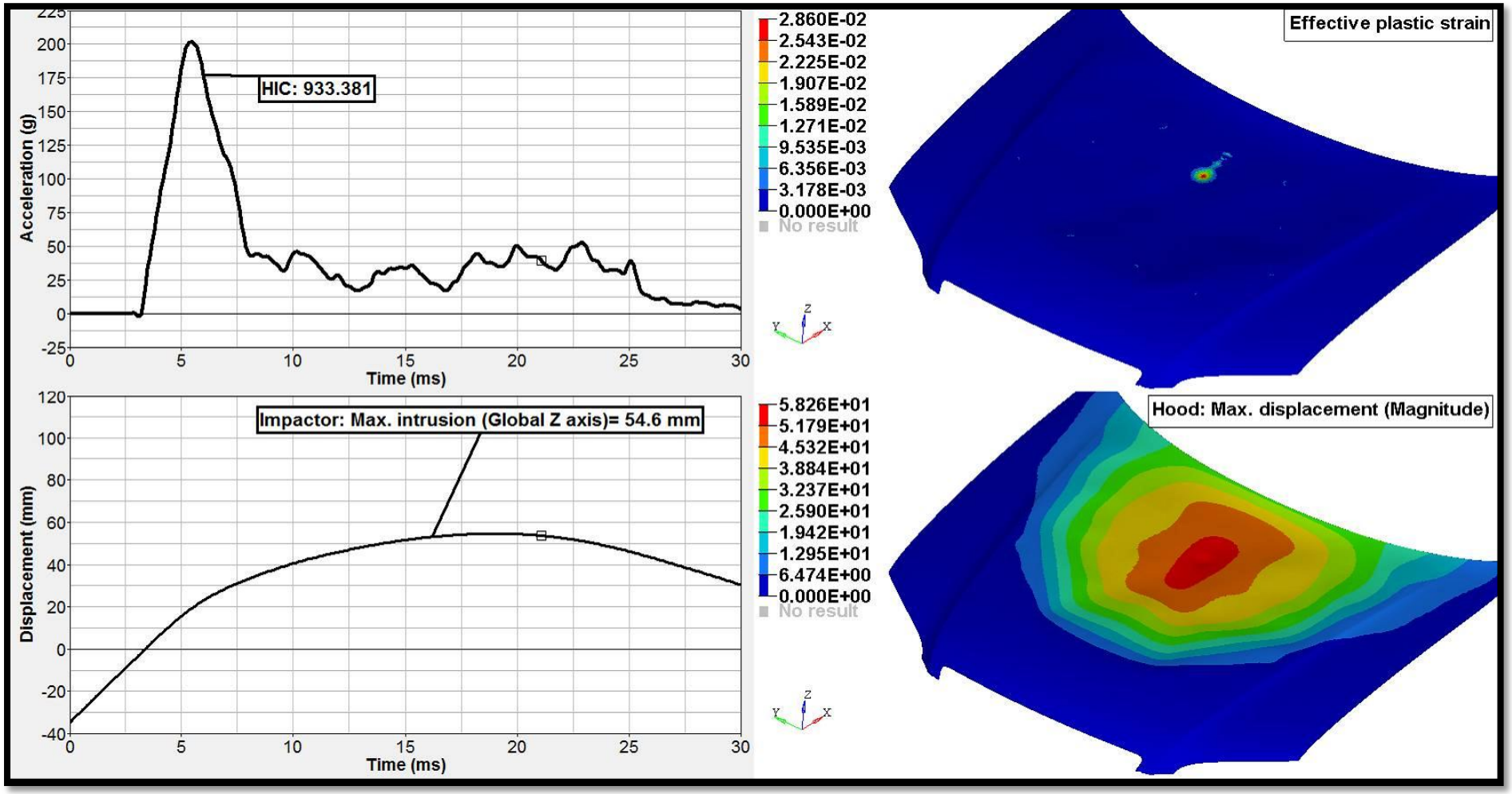

Figure 10.57: Effect of inner hood geometry optimisation on HIC value, effective plastic strain, displacement of the impactor and hood with 70mm deformation space for point E

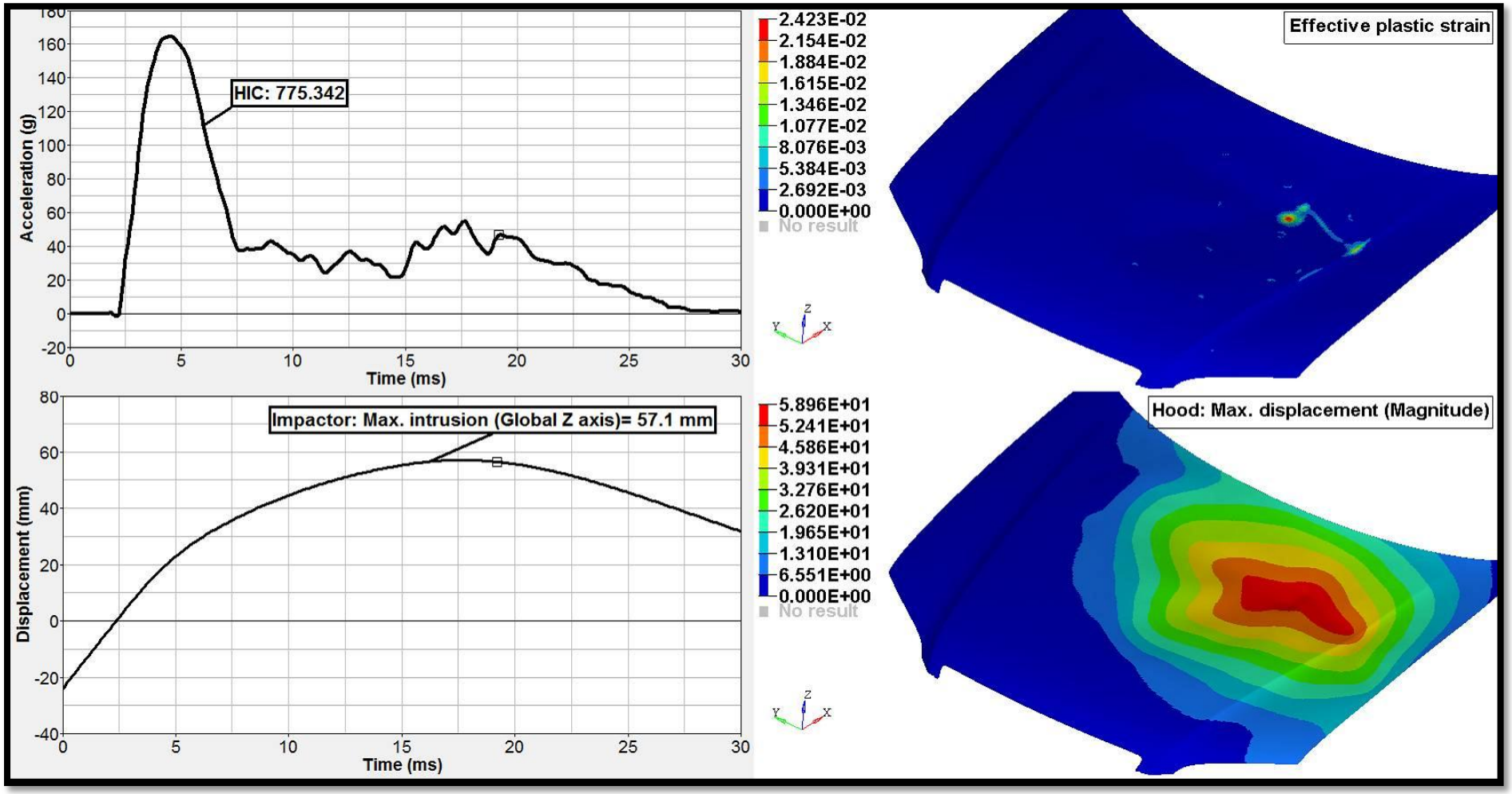

Figure 10.58: Effect of inner hood geometry optimisation on HIC value, effective plastic strain, displacement of the impactor and hood with 70mm deformation space for point F

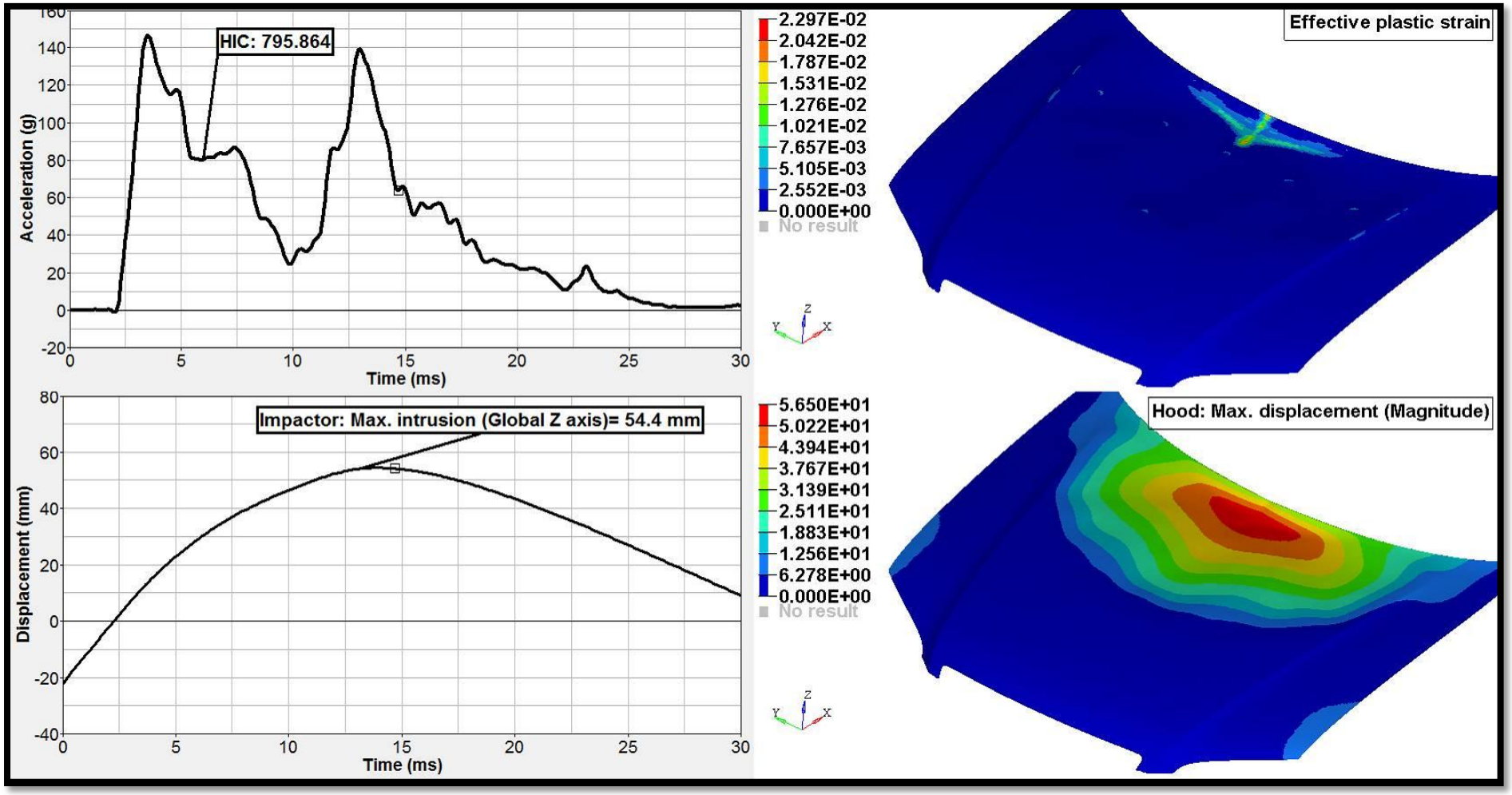

Figure 10.59: Effect of inner hood geometry optimisation on HIC value, effective plastic strain, displacement of the impactor and hood with 70mm deformation space for point G

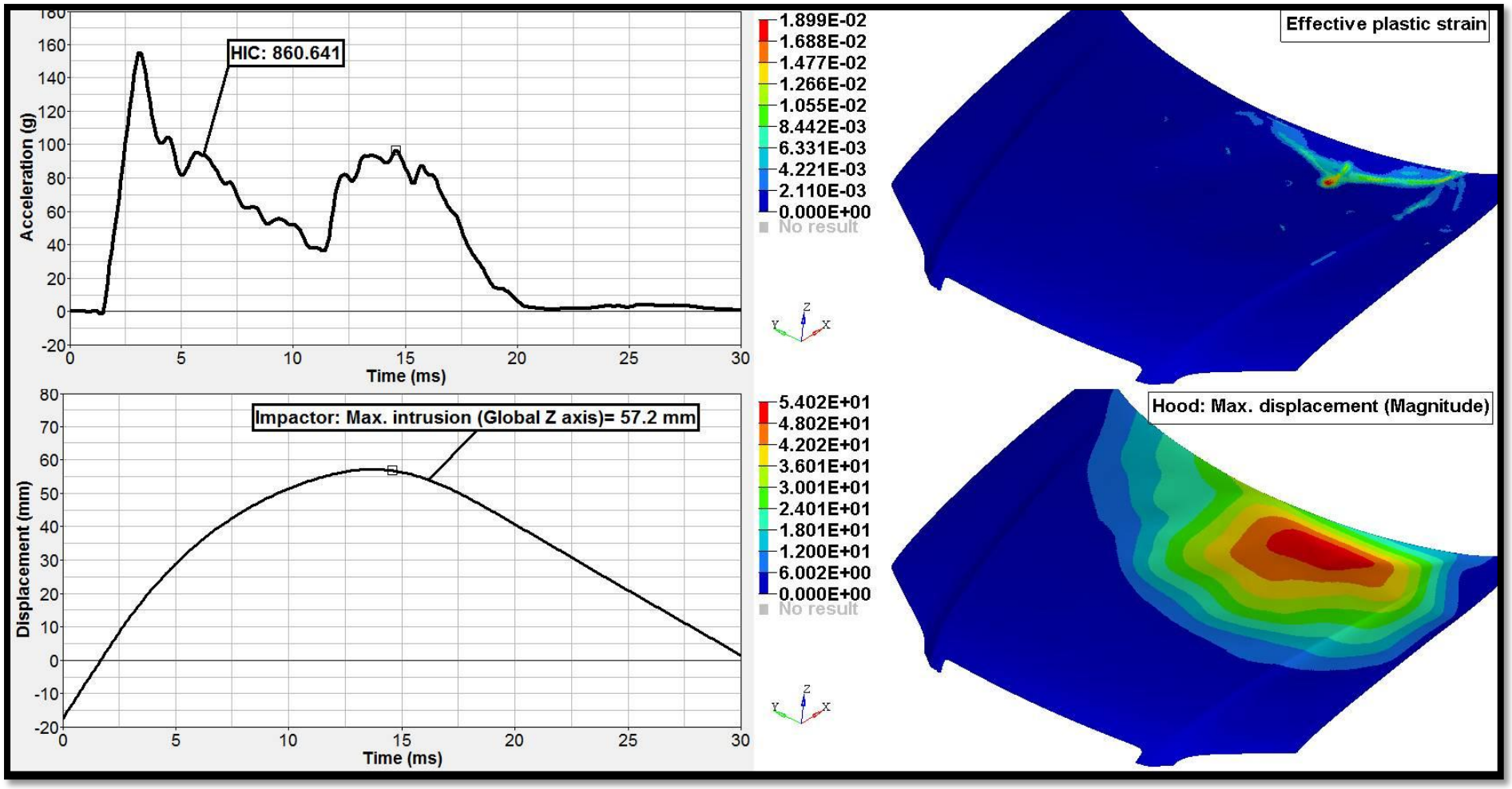

Figure 10.60: Effect of inner hood geometry optimisation on HIC value, effective plastic strain, displacement of the impactor and hood with 70mm deformation space for point H

Figure 10.61 shows the sum of the mean value of HIC and twice its standard deviation plotted against the inner and outer hood panel thickness. From that, it could be concluded that similar performance is attainable with various combinations of thicker outer hood and thinner inner hood panel thickness.

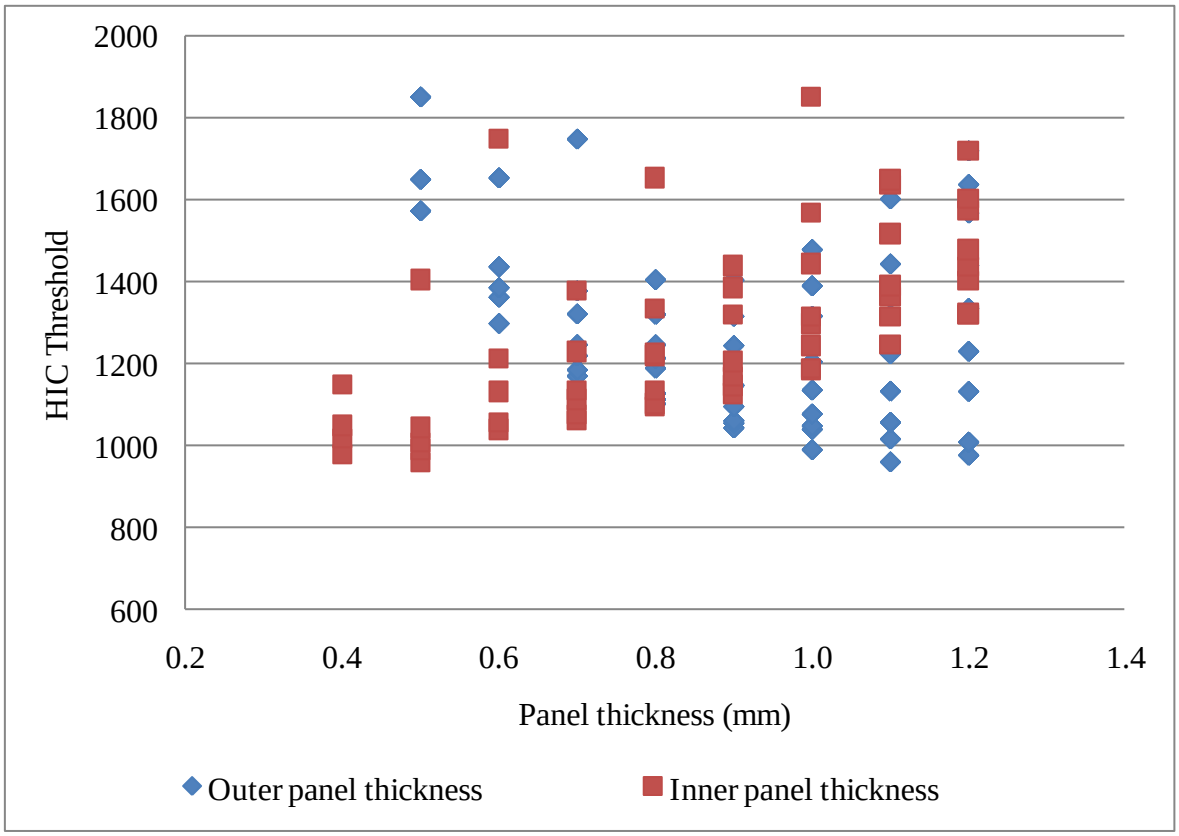

Figure 10.61: Influence of hood panel thickness on HIC value

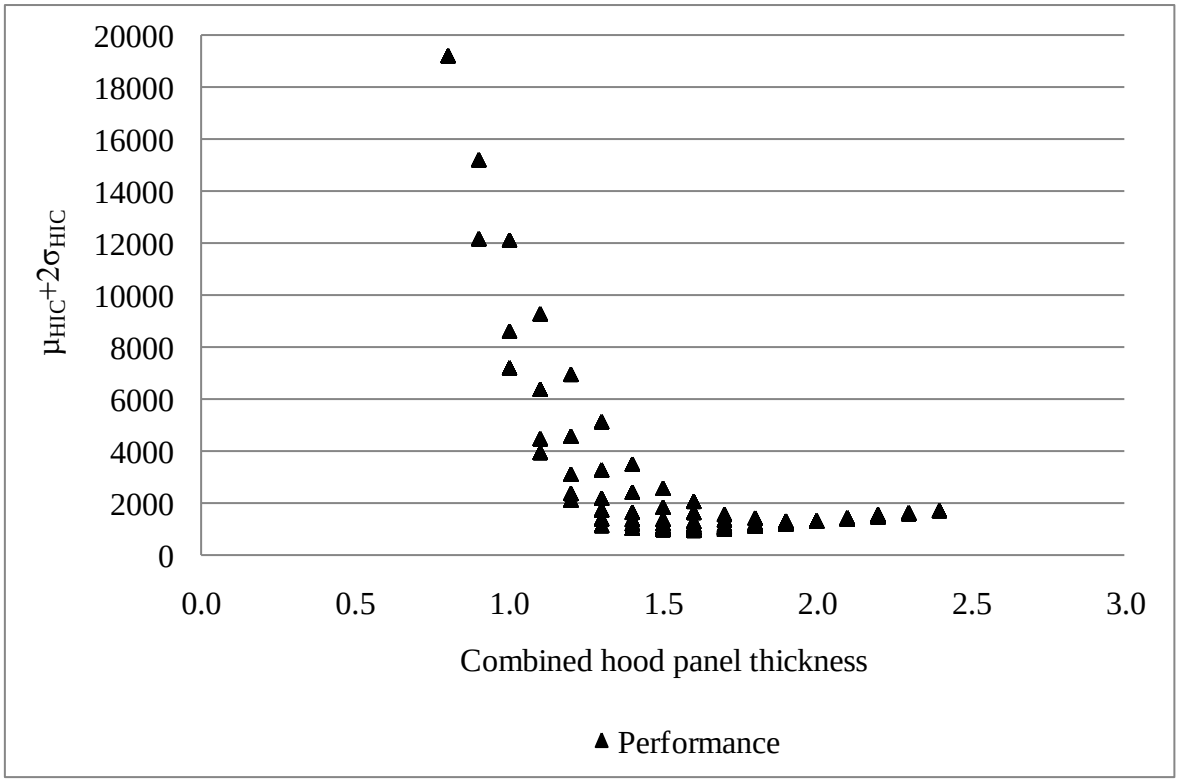

Figure 10.62: Influence of combined hood panel thickness on HIC value

Figure 10.62 shows that the HIC value increases rapidly when the combined thickness of hood panels is below the optimal panel thickness, due to the intensity of the secondary impact. The HIC value slowly ramps up when the combined thickness is higher than the optimal thickness. From this graph, it could be stated that a combined hood panel thickness of about 1.6mm made of steel material shows optimal head impact performance.

Figure 10.63 presents values for the combined inner and outer hood panel thicknesses used in various vehicle models. Vehicle manufacturers balance the deformation space, mass, noise, vibration, durability and pedestrian protection requirements when selecting the panel thickness.

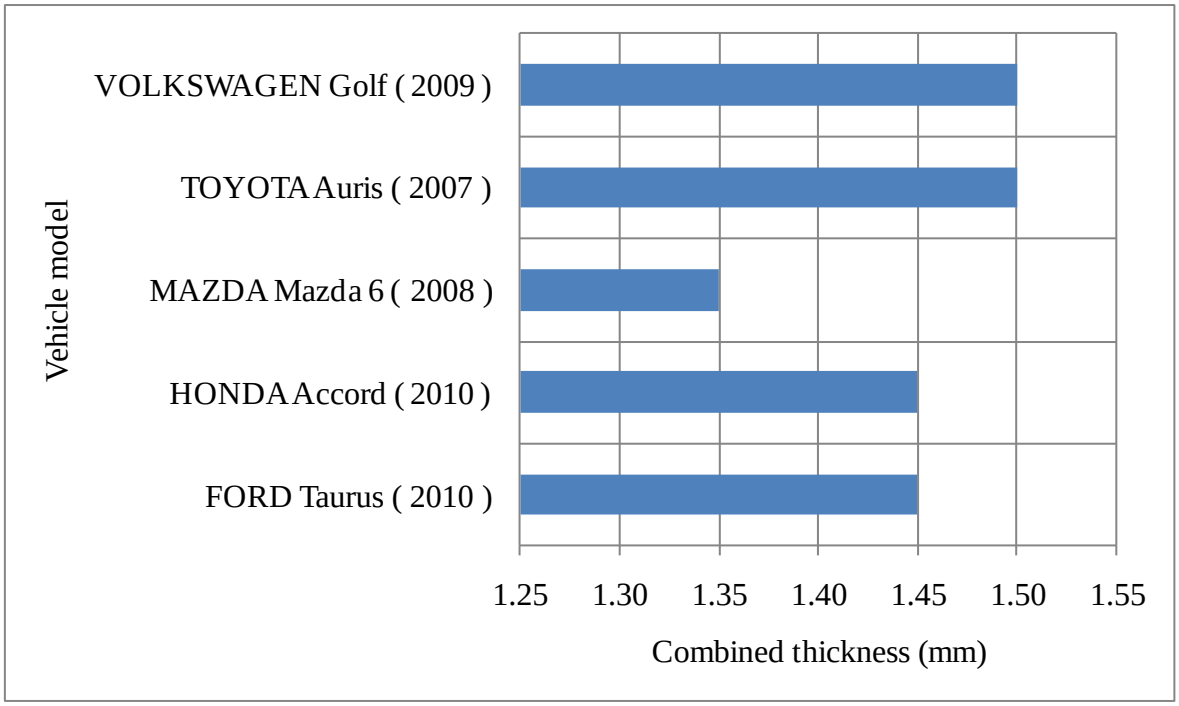

Figure 10.63: Combined thickness of steel outer and inner hood panels in various vehicles

To check the effect of allowing 70mm deformation space, impact has been simulated with different values of deformation space within the range from 60mm to 74mm. Same variables and qualifiers such as the mean value of HIC and its standard deviation have been used in the analysis. Comparison of $\mu_{HIC}+2\sigma_{HIC}$ for various deformation space as shown in Figure 10.64 indicates that a minimum of about 69mm deformation space is required to obtain robust and homogeneous head impact performance when considering both primary and secondary impacts.

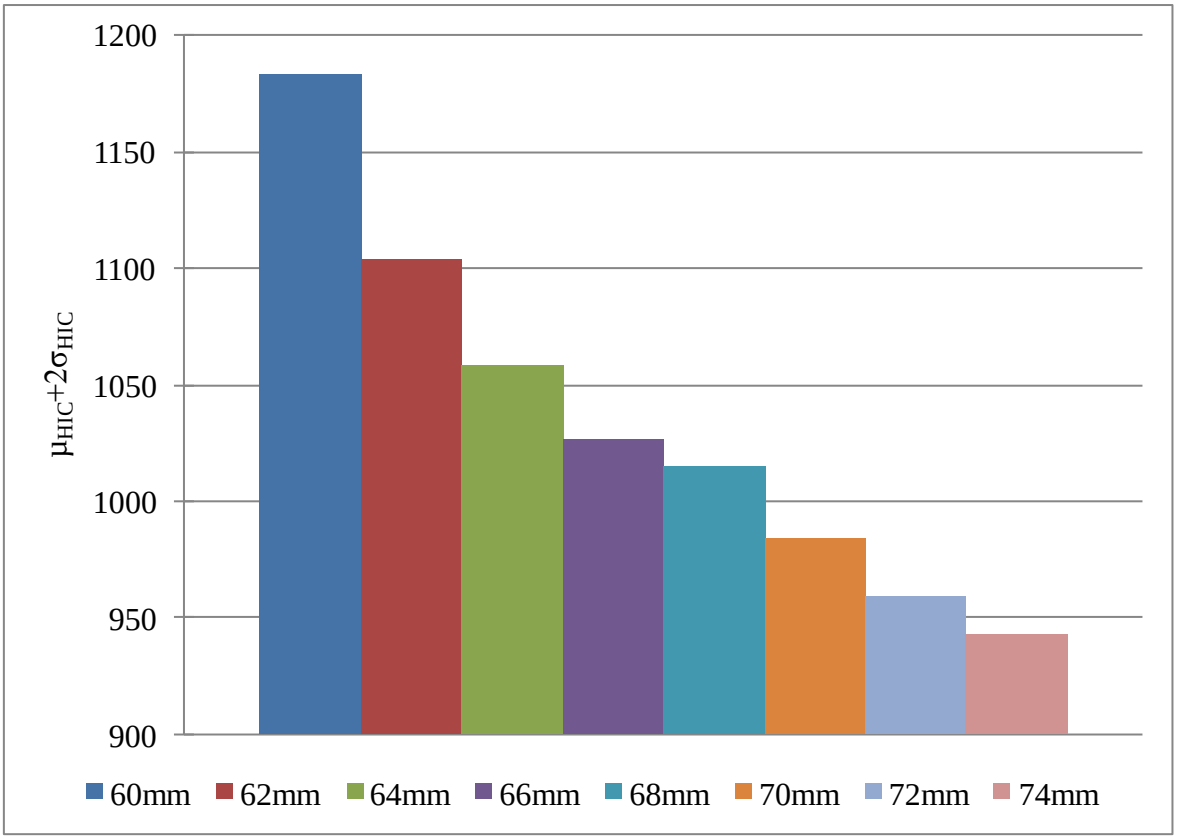

Figure 10.64: Influence of deformation space on HIC value (steel)

Therefore, it can be stated that a multi–cone hood inner structure made of steel with approximately 1.6mm of combined thickness of thinner inner and thicker outer hood panels requires a deformation space of about 69mm to obtain robust and homogeneous head impact performance.

10.4 Optimisation of panel thickness for aluminium material

From the previous optimisation steps, it was identified that multi–cone structure for inner hood gave optimal head impact performance for steel and aluminium hood panels. However, it was also noticed that a 70mm deformation space was not enough to obtain the HIC value less than 1000 when hood panels are made of aluminium. Thus, another study was conducted with deformation space of 80mm for aluminium hood panels with multi–cone inner hood structure.

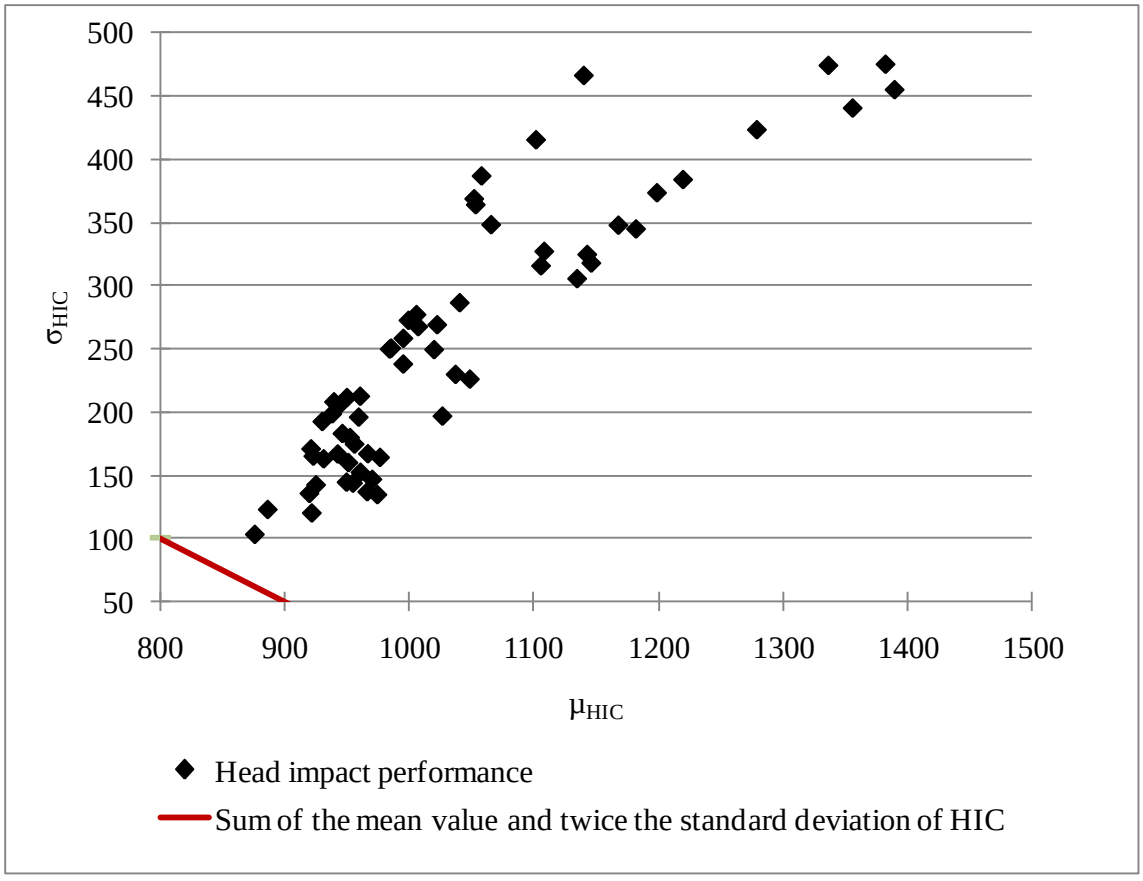

Figure 10.65: Head impact performance with 80mm deformation space

Figure 10.65 shows the mean value of HIC plotted against its standard deviation. The head impact performance results from this study shows that 80mm is enough to obtain the mean value of HIC less than 1000, although it is not enough to provide robust head impact performance.

Therefore, analysis was carried out by increasing the deformation space to 85mm from 80mm. The plot of inner and outer hood panel thickness against the $\mu_{HIC}+2\sigma_{HIC}$ in Figure 10.66 shows that it is possible to obtain robust head impact performance with HIC value less than the compliance threshold with a 85mm deformation space. Inner hood thickness of 0.58mm and outer hood thickness of 1.5mm show optimal head impact performance with aluminium hood panels.

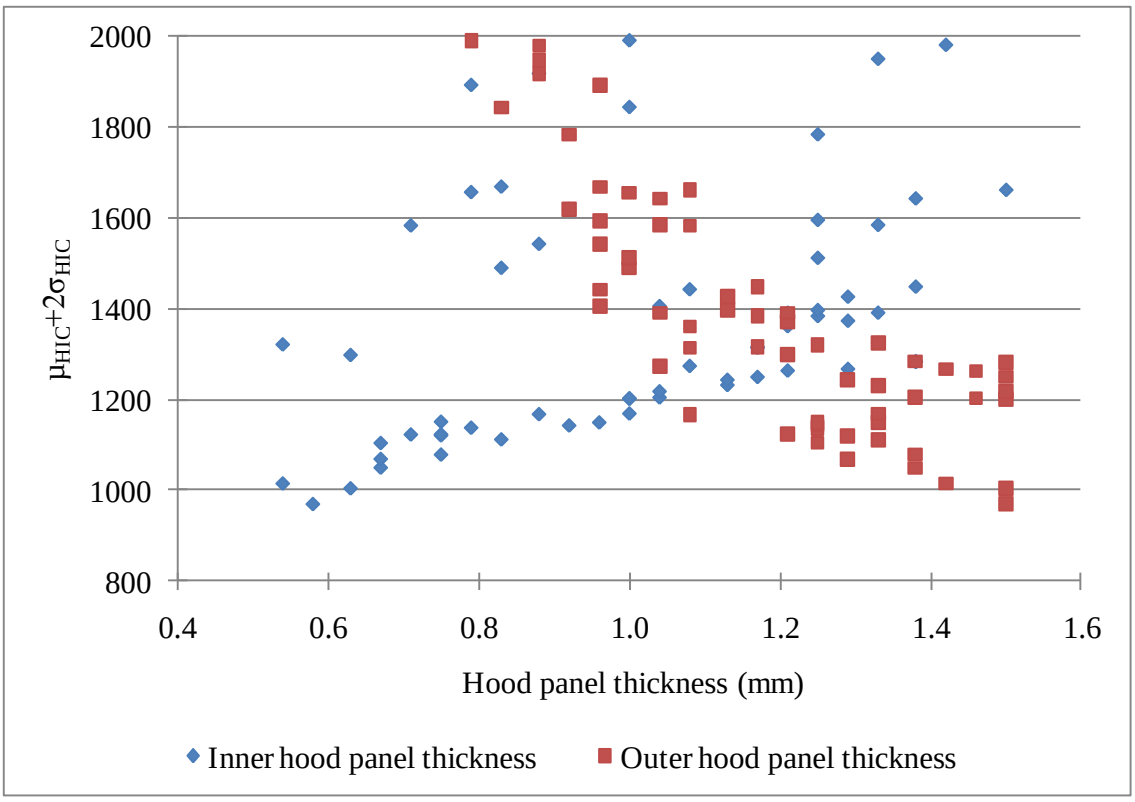

Figure 10.66: Influence of hood panel thickness on HIC value (aluminium)

Figure 10.67 shows that the HIC value increases rapidly when the combined thickness of hood panels is below the optimal panel thickness, due to the intensity of the secondary impact. The HIC value slowly ramps up when the combined thickness is higher than the optimal thickness.

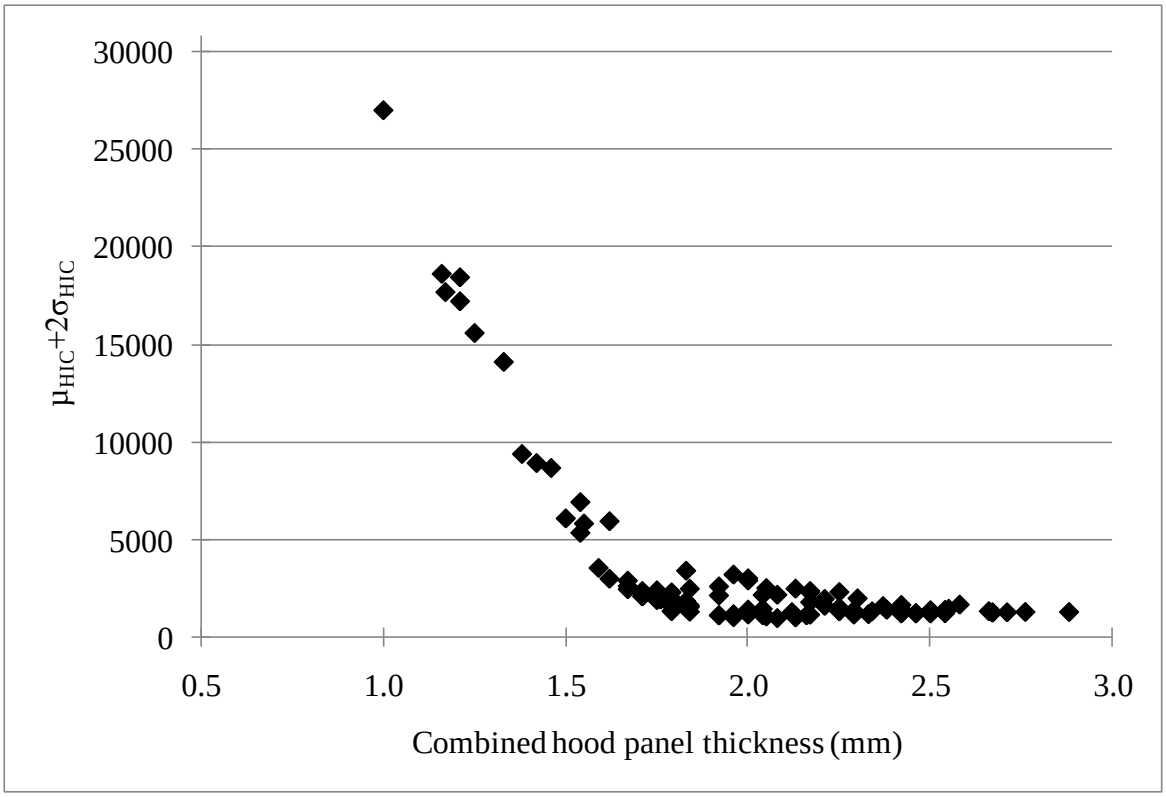

Figure 10.67: Influence of combined hood panel thickness on HIC value (aluminium)

Figure 10.68 presents a close–up view of the optimal performance from Figure 10.67. From this graph, it could be stated that combined hood panel thickness of 2.1mm with aluminium material shows optimal head impact performance.

Figure 10.69 presents the combined inner and outer hood panel thickness used in various vehicle models. As mentioned earlier, vehicle manufacturers balance the deformation space, mass, noise, vibration, durability and pedestrian protection requirements when selecting the inner and outer hood panel thicknesses.

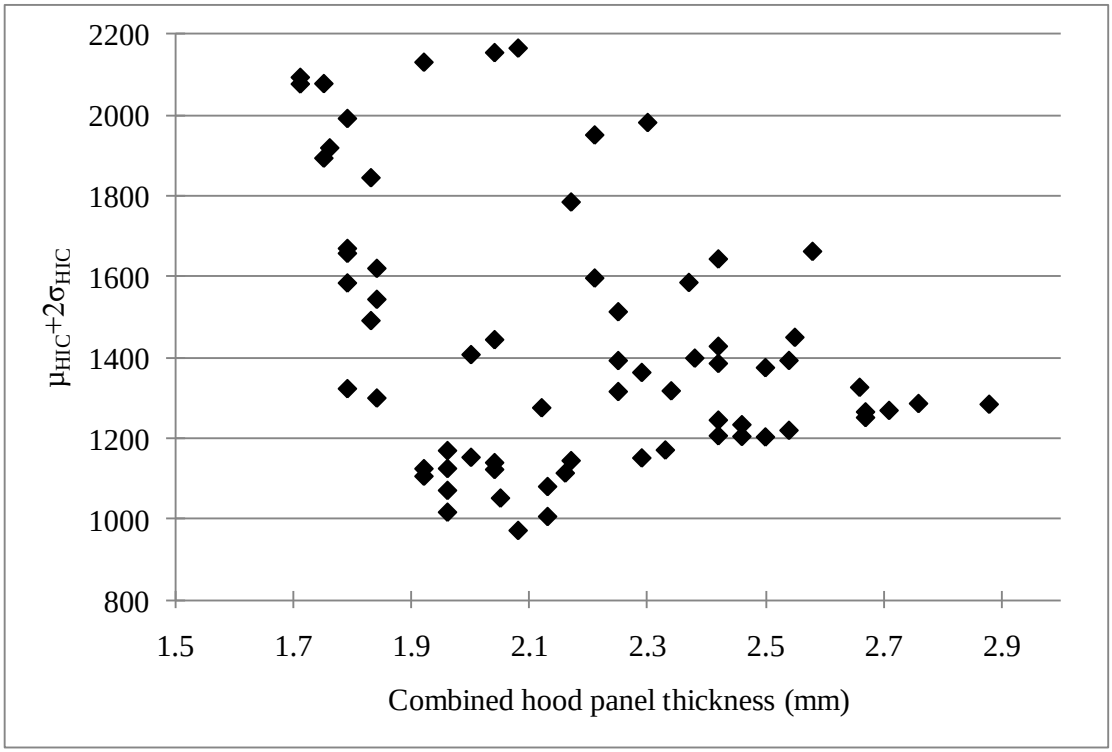

Figure 10.68: Combined hood panel thickness vs. the sum of the mean value of HIC and twice its standard deviation (aluminium)

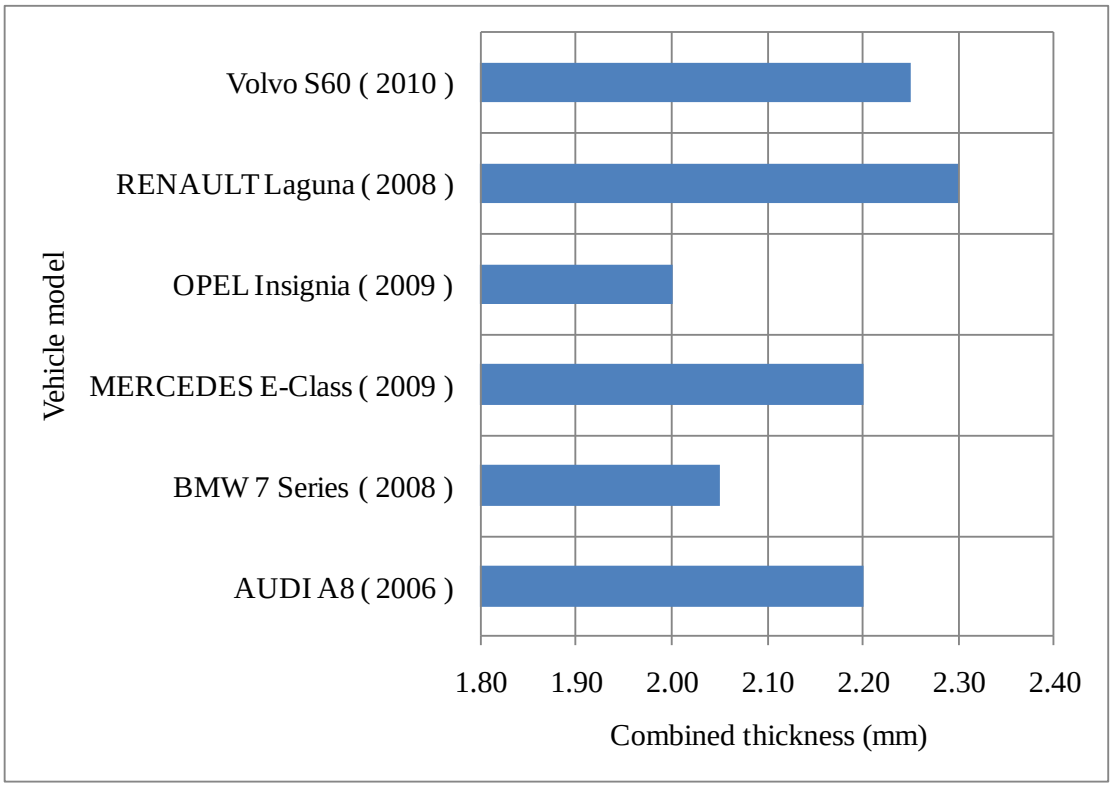

Figure 10.69: Combined thickness of aluminium outer and inner hood panels in various vehicles

To check the effect of allowing 85mm deformation space, impact has been simulated with different values of deformation space within the range from 80mm to 85mm. Same variables and qualifiers such as the mean value of HIC and its standard deviation have been used in the analysis. Comparison of $\mu_{HIC}+2\sigma_{HIC}$ for various deformation space as shown in Figure 10.70 indicates that a minimum of about 84mm deformation space is required to obtain robust and homogeneous head impact performance when considering both primary and secondary impacts.

Therefore, it can be stated that multi–cone inner hood structure made of aluminium with approximately 2.1mm of combined thickness of thinner inner and thicker outer hood panels require a deformation space of about 84mm to obtain robust and homogeneous head impact performance.

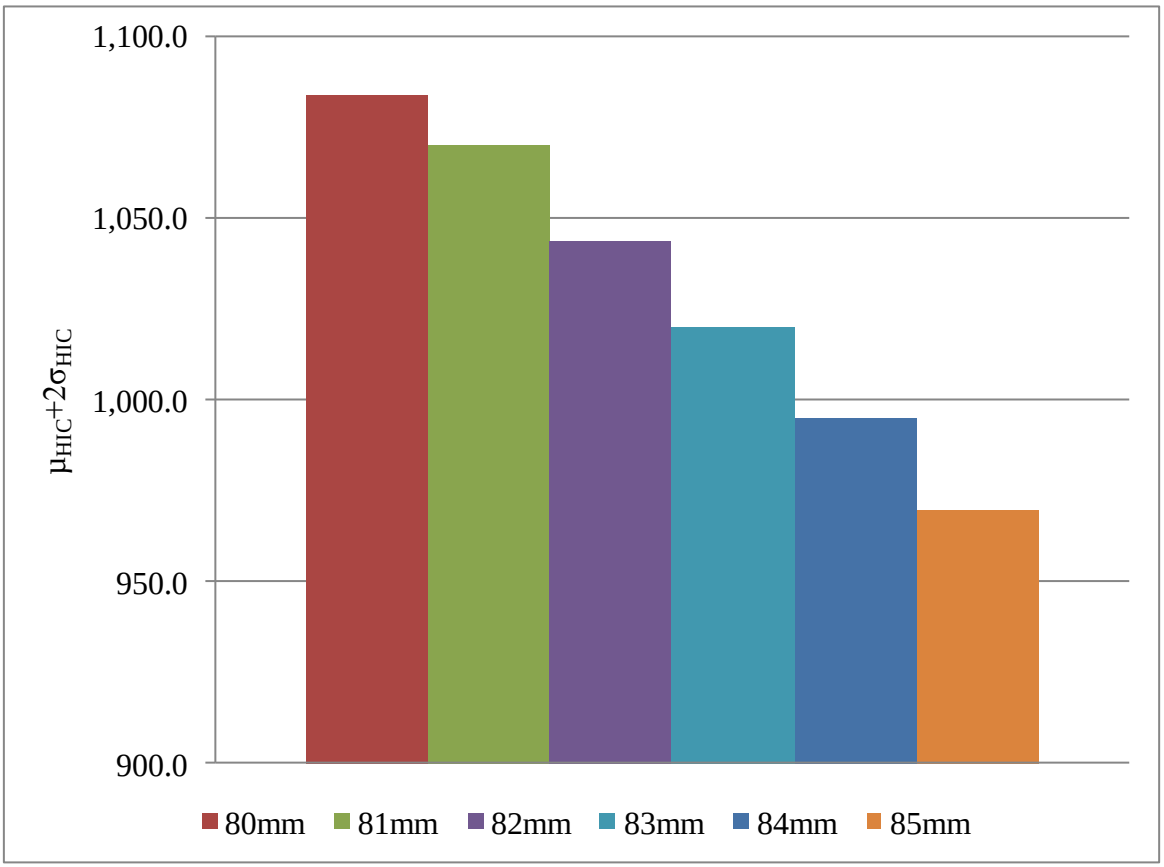

Figure 10.70: Influence of deformation space on HIC value (aluminium)

Chapter 11

Final design concept

The plots of the resultant acceleration against time curve, known as waveform, for steel and aluminium hood assemblies were compared to the theoretical and realistic optimal waveforms.

As mentioned in previous chapters, the realistic optimal waveform is the combination of peak acceleration ramping up within one or two milliseconds from the start of head impact followed by acceleration ramping down to a lower value that minimises the head injury. This waveform requires minimum deformation space for a given HIC value, in this instance 1000. The basis of the realistic optimal waveform is the theoretical optimal waveform in which the resultant acceleration reaches infinity at the beginning of the impact, but is impractical to obtain.

Figure 11.1 presents the head impact performance of a steel hood configuration with multi–cone inner hood structure with 0.5mm for inner hood panel thickness and 1.1mm for outer hood panel thickness. The aluminium hood assembly was analysed with a combined thickness of inner and outer panels of 2.7mm. It shows that similar magnitudes of peak acceleration are possible with steel and aluminium by varying the panel thickness.

Aluminium material however, provides a higher HIC value compared to steel due to an increase in acceleration in the later part of the impact duration.

The peak acceleration of approximately 175g within 2ms is feasible due to the structural stiffness of the thicker outer hood panel, and the acceleration ramps down as the head contacts the thinner inner hood panel in the optimal hood configuration.

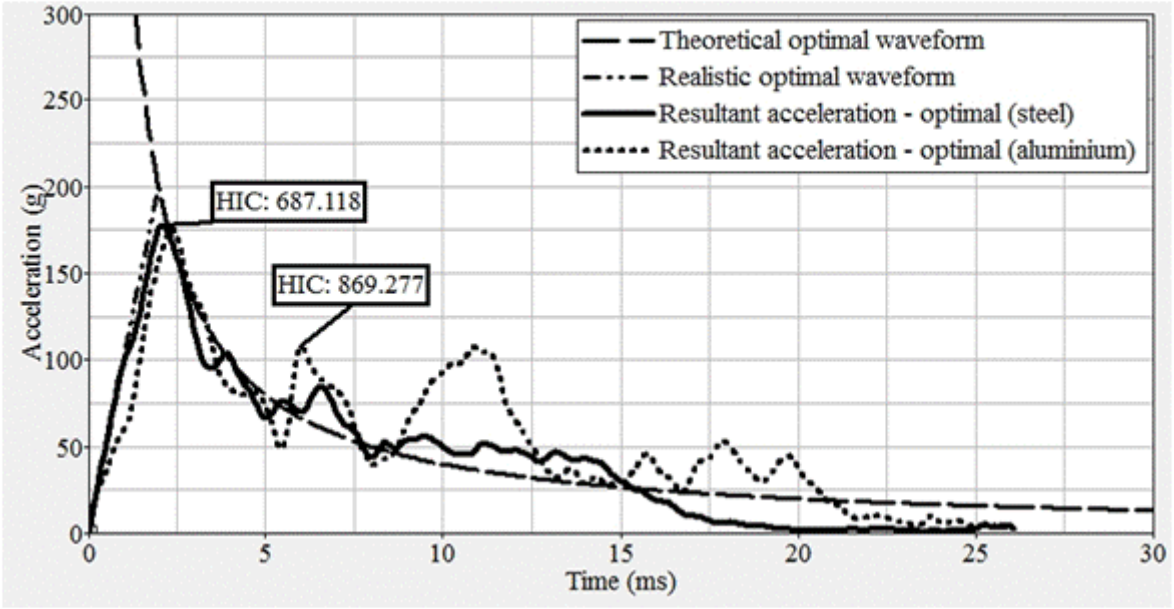

Figure 11.1: Waveform comparison-70mm deformation space

The plots in Figure 11.2 show that the optimal hood configuration with aluminium material does not match the realistic optimal waveform, because it is not optimal for deformation space.

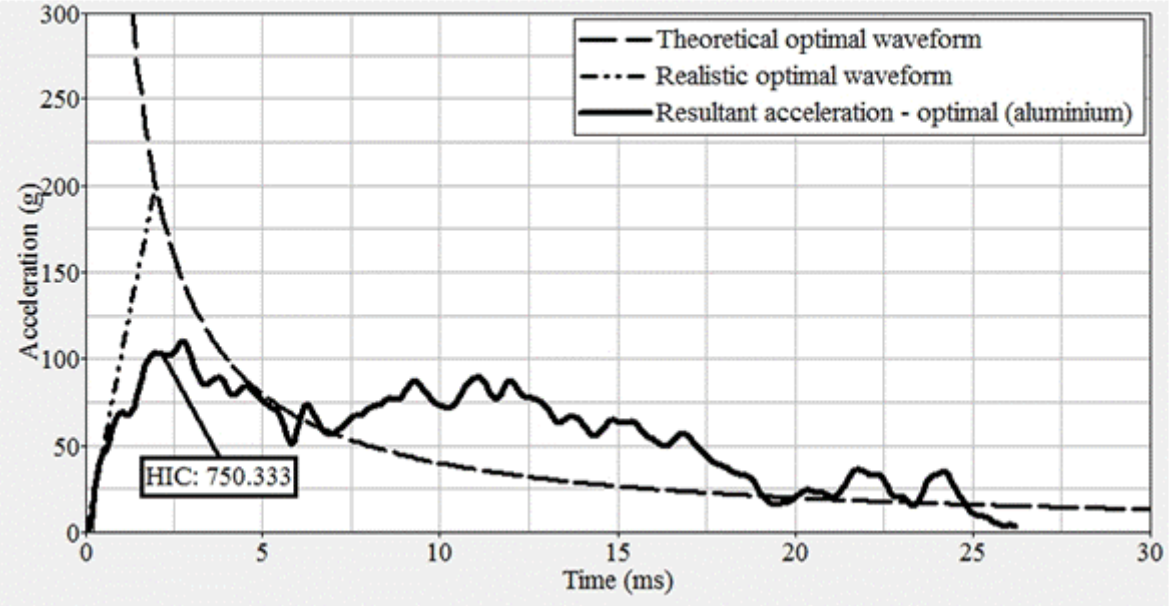

Figure 11.2: Waveform comparison-aluminium with 85mm deformation space

Chapter 12

Discussion

Since the magnitude of peak acceleration and rebound velocity have substantial influence on the HIC value of pedestrian when colliding with the front of a passenger car, as shown in chapter 11, the factors affecting the magnitude of peak acceleration were investigated by creating an ANOVA chart for peak acceleration.

In Figure 12.1, HOODMATL is the hood panel material, OTRGAUGE is the thickness assigned for the outer hood panel, INRGAUGE is the thickness assigned for the inner hood panel and INRGEOM is the type of structure of the inner hood.

The ANOVA chart showed that hood material had the highest effect on the magnitude of peak acceleration. Outer hood panel thickness was the next contributing factor, followed by inner hood panel thickness and inner hood structure respectively, as shown in Figure 12.1. These findings support the results seen in chapter 11, where increase in panel thickness was required for aluminium hood panels to match the peak acceleration of steel panels.

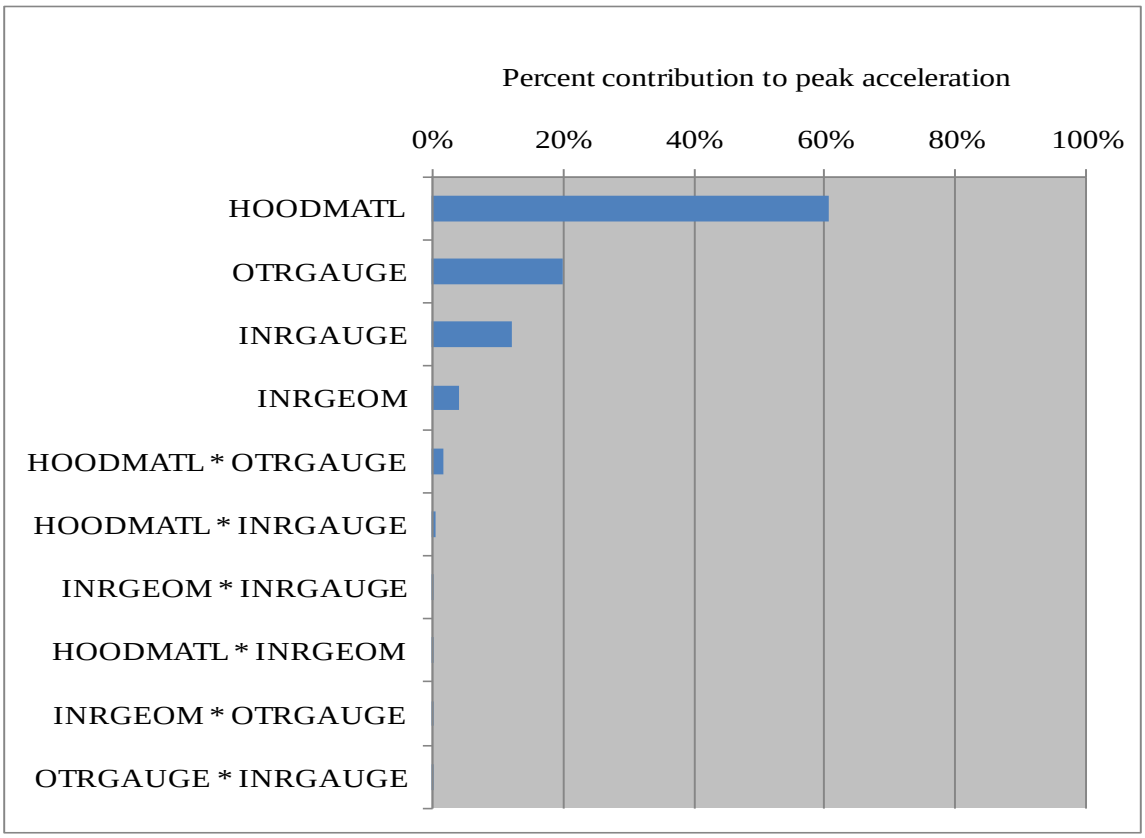

Figure 12.1: ANOVA chart for peak acceleration

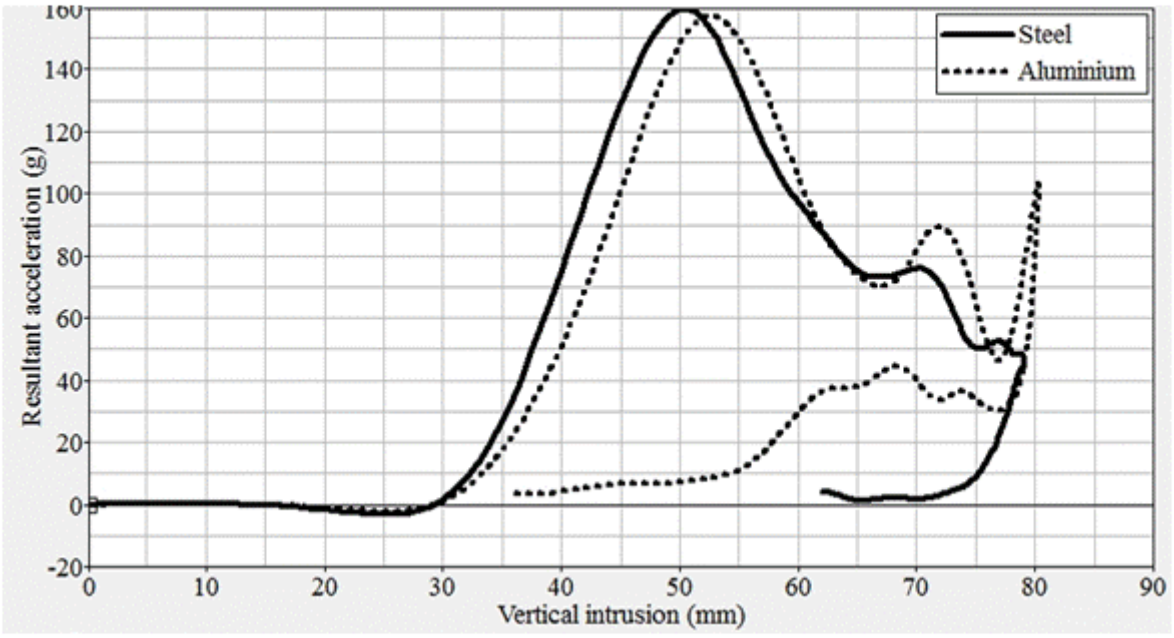

Figure 12.2: Resultant acceleration against vertical intrusion

To understand the reason for the increase in HIC value of pedestrian when colliding with hood panels made of aluminium (shown in Figure 11.1); the resultant acceleration was plotted against vertical intrusion, as shown in Figure 12.2. Although both steel and aluminium result in similar values for peak acceleration and total vertical intrusion, the value of HIC varied between them.

This prompted a comparison between the average values of the rebound velocity of the hood for various impact positions for both materials as presented in Figure 12.3. This shows that in general, the rebound velocity for aluminium is approximately 2.2 times higher than that for steel.

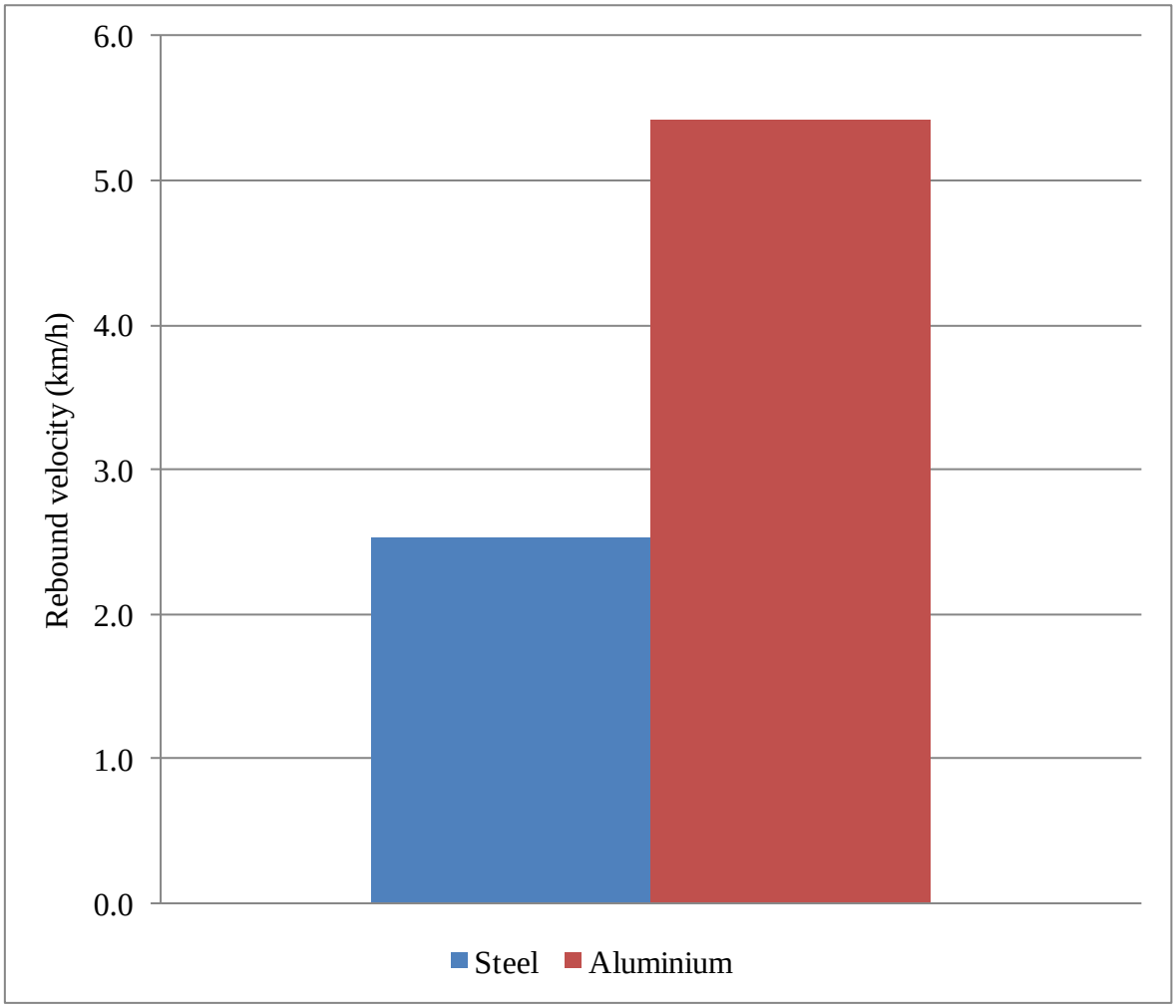

Figure 12.3: Comparison of rebound velocities

Equation 3.3 shows that the integration of the resultant acceleration, which is velocity, is used in the calculation of HIC value. Thus, an increase in the rebound velocity increases the HIC value. Therefore, further exploration has been carried out to understand the exact reason for this increase in rebound velocity in aluminium hood panels.

To understand the basic concepts behind the difference in rebound velocities, a simple example has been studied theoretically. The strain energy for steel and aluminium was calculated for a simplified beam with a rectangular cross section to demonstrate the difference in stored elastic energy. To simplify the calculation, the beam is assumed to be loaded to its elastic bending moment.

$$U_e = \int_O^L \frac{M^2}{2EI} dx \qquad \textbf{Equation 12.1}$$

Where, U_e is the strain energy in the beam due to the load, M is the bending moment, E is the Young's modulus and I is the sectional modulus.

Equation 12.2 below shows the distribution of stress in a beam:

$$\sigma_y = \frac{My}{I} \qquad \textbf{Equation 12.2}$$

Where, y is equal to half of the thickness of the beam, that is, t/2, assuming t is the thickness of the beam. Therefore, it can be written as follows:

$$M = \frac{\sigma_y b t^2}{6} \qquad \textbf{Equation 12.3}$$

Where, σ_y is the stress at yield point and b is the width of the beam.

Substitution of Equation 12.3 in Equation 12.1 provides the following:

$$U_e = \frac{{\sigma_y}^2 btl}{6E} \qquad \textbf{Equation 12.4}$$

In which, l is the length of the beam.

If we assume same length and width of the beam for aluminium and steel, the calculation of the ratio of elastic strain energy between aluminium and steel is as follows:

$$\frac{U_e\ of\ aluminium}{U_e\ of\ steel} = \frac{{\sigma_{y(al)}}^2 t_{al}}{E_{al}} \times \frac{E_{st}}{{\sigma_{y(st)}}^2 t_{st}} \qquad \textbf{Equation 12.5}$$

Where, t_{al} is the thickness value assigned for aluminium, in this case, 2.7mm; t_{st} is the thickness value assigned for steel, in this case 1.6mm, E_{al} is the Young's modulus value for aluminium that is 70,000MPa, and E_{st} is the young's modulus value for steel that is 200,000MPa.

The yield strength of the aluminium material used in this example is assumed to have $\sigma_y(al)$ while the yield strength of the steel material is assumed to be $\sigma_y(st)$. It was assumed in this work that $\sigma_y(al) = \sigma_y(st)$ as the aluminium material selected for hood panels has yield strength close to that of steel grade usually used to manufacture hood panels.

When these values were substituted in Equation 12.5, the ratio of the elastic strain energy of steel to aluminium was 1:4.8.

Therefore, it could be stated that when loaded to same level of stress, hood panels made with aluminium store 4.8 more times the elastic strain energy stored by steel. This causes an increase in rebound velocity by using the equation shown below:

$$U_e = \frac{mv^2}{2}$$ **Equation 12.6**

Where, m is the mass and v is the velocity of the head.

So, 4.8 times increase in elastic strain energy leads to 2.2 times increase in rebound velocity. This coincides with the average value of rebound velocities comparison, shown in Figure 12.3.

In Equation 12.4, the stored elastic strain energy is proportional to the thickness. Thus, the value of rebound velocity could be reduced by reducing the thickness. However, this change will increase the deformation space due to the reduction in structural stiffness. Since the structural stiffness of aluminium is lower than steel, reduction in panel thickness to reduce the rebound velocity will increase the deformation of hood made of aluminium. Therefore, it could be stated that aluminium requires more deformation space in comparison to steel to meet pedestrian head injury requirements.

Steel hood panels exhibit lower rebound velocity, which matches the realistic optimal waveform. Therefore, the preferred choice of material for hood panels is steel if the main objective is to reduce the deformation space. The benefits of minimising the deformation space are significant. They include the freedom of styling, improved aerodynamics, and hence improvements in vehicle stability and fuel economy. If the main objective is to reduce mass, then the preferred choice for hood panels is aluminium; however, this will require more deformation space.

The area for aluminium and steel hood panels were the same in this study. Thus, when 2.7mm for aluminium and 1.6mm for steel was substituted for panel thickness value along

with their respective density values, the result showed 42% less mass for aluminium hood assembly compared to steel hood assembly.

Chapter 13

Conclusion

The main objective of this work was to develop a methodology for optimising the hood assembly for minimal deformation with robust and homogeneous impact behaviour while meeting pedestrian head injury requirements. In practice, the design of the outer and inner hood panels must meet all general design requirements in addition to pedestrian head impact performance. Achievement of design criteria for homogeneous impact performance for the pedestrian head could aid in meeting the general design requirements.

In this research, the important design parameters were identified and a design of experiments matrix was created. Then, three–dimensional geometric models and FE models were created to the design parameters defined in the design of experiments matrix. The results from the numerical experiments were utilised to create the response surfaces for the mean value of efficiency (μ_η), the mean value of HIC (μ_{HIC}) and the standard deviation of HIC (σ_{HIC}). The Analysis of Variance (ANOVA) technique was used to quantify the contribution of design parameters in determining HIC value and efficiency. Then these data were filtered with the condition that the sum of the mean value of HIC and twice its standard deviation ($\mu_{HIC}+2\sigma_{HIC}$) should be less than or equal to 1000. This was

done to match the head injury value specified by the GTR–9 and ANCAP and to produce 95% confidence in the results of this optimisation, assuming normal distribution.

The filtered data was compared using σ_{HIC} as a qualifier for homogeneous performance and μ_{η} as a qualifier for minimal deformation of outer and inner hood panels. This resulted in the identification of the multi–cone pattern for hood inner structure as the best structure for both steel and aluminium compared to other structures. Further refinement indicated that steel was the preferred choice of material for the hood assembly to obtain robust and homogeneous head impact performance with minimal deformation compared to other materials.

Findings from this study showed that it is possible to obtain HIC values less than the threshold value, while achieving similar efficiencies for various combinations of thinner inner and thicker outer hood panels. However, efficiency variation was noticed when changing the value of the combined thickness of inner and outer hood panels.

The results showed that it is possible to obtain μ_{HIC} less than 1000 with 60mm deformation space with a multi–cone structure made of steel of about 1.8mm of combined inner and outer hood thickness, but this is not enough to obtain robust and homogeneous behaviour less than the HIC threshold value when secondary impact is considered.

Therefore, impact has been simulated with different values of deformation space within the range from 60mm to 74mm. Same variables and qualifiers such as the mean value of HIC and its standard deviation have been utilised in the analysis. The results indicated that a minimum of about 69mm deformation space was required to obtain robust and homogeneous head impact performance when considering both primary and secondary impact.

In conclusion, multi–cone inner hood structure made of steel for inner and outer hood panels is the preferred choice for hood assembly when minimal deformation is the main requirement for the vehicle design team.

Following the selection of hood structure and material, the multi–cone structure was optimised by varying the angle and depth of cones while maintaining a constant gap between the cones. With this result, it was concluded that a robust and optimal result is possible from the following design parameters: multi–cone structure for inner hood; steel for inner and outer hood material; 1.6mm thickness for inner and outer hood combination; 160 degrees including angle for cones; and 15mm cone depth.

Another study was conducted to quantify the minimum deformation space required for the aluminium hood system. The multi–cone structure for the inner hood required the least amount of deformation space in comparison to other geometries. Impact simulation with 80mm of deformation space showed that it is possible to obtain μ_{HIC} less than 1000, but this is not enough to obtain robust and homogeneous behaviour below the HIC threshold value when secondary impact is considered. Thus, impact has been simulated with different values of deformation space within the range from 80mm to 85mm. The same variables and qualifiers such as the mean value of HIC and its standard deviation have been utilised in this analysis. The results indicated that a minimum of about 84mm deformation space was required to obtain robust and homogeneous head impact performance when considering both primary and secondary impact.

In conclusion, a robust and homogeneous pedestrian head impact performance is possible from the following design parameters for aluminium hood panels: multi–cone structure for inner hood, and approximately 2.1mm combined thickness with thinner inner and thicker outer hood combination.

Chapter 14

Recommendations for further work

Vehicle design for pedestrian protection requires improvements in many components in the vehicle front–end such as the lower bumper system, upper bumper system, interfaces of hood assembly to the vehicle and hood assembly. To optimise the vehicle front–ends to improve pedestrian protection performance while meeting all the other requirements of vehicle design is a very large scope of work. In this research, the development of optimisation methodology of large–size hoods for robust and homogeneous performance with minimal deformation was completed while meeting pedestrian performance requirements for head impact.

The analysis in this research was carried out with a 3.5kg child head impactor fired at 50degrees impact angle from the horizontal plane, as shown in Figure 4.8. In summary, the hood configuration was optimised for that given mass and angle of impact, and if an area required both a child head impactor (3.5kg) and an adult head impactor (4.5kg), compromises would need to be made to accommodate various masses and angles of impact. Further studies, however may be required to optimise medium and smaller size hoods. Similarly, work may be required to optimise components such as hood hinges, A–pillar,

base of windscreen, wiper assembly, fender brackets, under hood components, glue between inner and outer hood panels and hood latch.

Although many key parameters were identified and optimised, further work would be required to maximise the head impact performance in pedestrian protection offered by vehicles without compromising all other requirements such as occupant safety, quality, fuel economy, durability and low repair costs. However, a foundation had been laid for continued research in improving the pedestrian protection offered by vehicle front–ends in a pedestrian collision with a passenger car.

References

A2Mac1 2010, *Automotive benchmarking*, viewed 22 March 2010, <http://a2mac1.com/home>.

Advani, SH & Owings, RP 1974, *Evaluation of head injury criteria*, SAE Technical Paper 740083, Automotive Engineering Congress and Exposition, Detroit, Michigan, SAE International, Warrendale, Pennsylvania, USA.

Ashton, SJ 1980, *A preliminary assessment of the potential for pedestrian injury reduction through vehicle design*, SAE Technical Paper 801315, 24th Stapp Car Crash Conference, Troy, Michigan, SAE International, Warrendale, Pennsylvania, USA.

Australasian New Car Assessment Program 2010, viewed 09 November 2010, <http://ancap.com.au/home>.

Australasian New Car Assessment Program 2011, *ANCAP rating road map 2011-2015*, ANCAP, viewed 12 July 2011, <http://www.ancap.com.au/admin/uploadfiles/ANCAP%20Road%20Map%20Published%20Version%20Master.pdf>.

Australasian New Car Assessment Program 2011, *ANCAP notes on the assessment protocol, Version 4.9*, ANCAP, viewed 28 July 2011,

<http://ancap.com.au/admin/uploadfiles/ANCAP_assessment_notes_apr11.pdf>.

Autoliv 2009, *Driven for life*, viewed 09 January 2010, <http://www.autoliv.com/wps/wcm/connect/autoliv/Home/What+We+Do/Recent%20Innovations/Pedestrian%20Protection>.

Baleki, DdM & Ferreira, AS 2008, *Development of hood geometries for pedestrian head impact*, SAE Technical Paper 2008-36-0003, SAE Brasil 2008 Congress and Exhibit, Sao Paulo, Brazil, SAE International, Warrendale, Pennsylvania, USA.

Bernd, M, Christoph, W, Ulrike, G, Anton, D & Frank, M 2004, 'Active pedestrian protection-system development'.

Bohling, G 2005, *Kriging*, University of Kansas, viewed 28 July 2011, <http://people.ku.edu/~gbohling/cpe940/Kriging.pdf>.

Bovenkerk, J, Christian Sahr, Oliver Zander & KALLISKE., J 2009, *New Modular Assessm ent M ethods For Pedestrian Protection In The Event O f Head Impacts In The Windscreen Area*, Paper Number 09-0159, PROCEEDINGS OF THE 21ST (ESV) INTERNATIONAL TECHNICAL CONFERENCE ON THE ENHANCED SAFETY OF VEHICLES, STUTTGART, GERMANY. 2009.

CARE (EU road accidents database) 2011, *Fatalities by transport mode in EU countries included in CARE*, viewed 10 October 2011,

<http://ec.europa.eu/transport/road_safety/pdf/statistics/2009_transport_mode_graph.pdf>.

Cavallero, C, Cesari, D, Ramet, M, Billault, P, Farisse, J, Seriat-Gautier, B & Bonnoit, J 1983, *Improvement of pedestrian safety: influence of shape of passenger car-front structures upon pedestrian kinematics and injuries: evaluation based on 50 cadaver tests*, SAE Technical Paper 830624, SAE International Congress and Exposition, Detroit, Michigan, SAE International, Warrendale, Pennsylvania, USA.

Cavallero, C & ONSER, LdCedB, Bron, France 1983, *Improvement of pedestrian safety: influence of shape of passenger car-front structures upon pedestrian kinematics and injuries: evaluation based on 50 cadaver tests*, Society of Automotive Engineers, Inc., Warrendale, Pennsylvania, USA.

Centre of automotive safety research 2007, *Head impact test machine*, The University of Adelaide, viewed 17 December 2009, <http://casr.adelaide.edu.au/impact.html>.

Cornell Aeronautical Laboratory Inc., TRD 1971, *Research in impact protection for pedestrians and cyclists*, SASI-711635.

Elert, G 2001, *Number of cars*, Glenn Elert, viewed 16 June 2010, <http://hypertextbook.com/facts/2001/MarinaStasenko.shtml>.

European Commission 2010, *Road safety*, viewed 13 February 2010, <http://ec.europa.eu/transport/road_safety/specialist/statistics/trends>.

European New Car Assessment Programme 2011, *Assessment protocol-adult occupant protection, Version 5.3*, Euro NCAP, viewed 12 July 2011, <http://www.euroncap.com/files/Euro-NCAP-Assessment-Protocol---AOP---v5-3---0-f8eeb014-2b0d-483e-8129-09bda409ccff.pdf>.

Fowler, JE, Harris, J 1982, *Practical vehicle design for pedestrian protection*, SAE Technical Paper 826030, Ninth International Technical Conference on Experimental Safety Vehicles (1982), Kyoto, Japan, National Highway Traffic Safety Administration, Washington, D.C., USA.

Funk, JR, Duma, SM, Manoogian, SJ & Rowson, S 2007, 'Biomechanical risk estimates for mild traumatic brain injury', paper presented to 51st Annual Proceedings Association for the Advancement of Automotive Medicine, October 15, 2007 - October 17, 2007, Melbourne, VIC, Australia.

Gadd, CW 1966, *Use of a weighted-impulse criterion for estimating injury hazard*, SAE Technical Paper 660793, Society of automotive engineers, Warrendale, Pennsylvania, USA.

Gelman, A 2004, *Analysis of variance-why it is more important than ever*, Columbia University, viewed 28 July 2011, <http://www.stat.columbia.edu/~gelman/research/published/banova7.pdf>.

Hardy, BJ, Lawrence, GJL, M, KI, P, SIC, A, CJ, G, C & S, BR 2007, *A study of possible future developments of methods to protect pedestrians and other vulnerable road users*, UPR/VE/061/07, TRL Limited.

Harzheim, L & Warnecke, U 2011, 'Anti-Roll Bar Link Toggling: Investigation and Optimization of a Robustness Problem'.

Hodgson, VR, Thomas, LM & Brinn, J 1973, *Concussion levels determined by HPR windshield impacts*, SAE Technical Paper 730970, 17th Stapp Car Crash Conference Oklahoma City, Oklahoma, USA, Society of Automotive Engineers, Warrendale, Pennsylvania, USA.

Honda Worldwide 2008, *Honda to begin using third generation pedestrian dummy in crash tests to enable evaluation of injuries to the lower back and upper leg*, viewed 17 December 2009, <http://world.honda.com/news/2008/4080918POLAR-III/>.

Hutchinson, J, Kaiser, MJ & Lankarani, HM 1998, 'The Head Injury Criterion (HIC) functional', *Applied Mathematics and Computation*, vol. 96, no. 1, pp. 1-16.

Ikeda, K, Ishitobi, H, Corp., TM & Ltd., KATP 2003, 'Development of aluminum hood structure for pedestrian protection'.

Kam, CY, Kerrigan, J, Meissner, M, Drinkwater, C, Murphy, D, Bolton, J, Arregui, C, Kendall, R, Ivarsson, J, Crandall, J, Deng, B, Wang, JT, Kerkeling, C & Hahn, W 2005, *Design of a full-scale impact system for analysis of vehicle pedestrian collisions*, SAE Technical Paper 2005-01-1875, SAE World Congress, Detroit, Michigan, SAE International, Warrendale, Pennsylvania, USA :.

Kerkeling, C, Schafer, J & Thompson, GM 2005, 'Structural hood and hinge concepts for pedestrian protection', paper presented to Experimental Safety Vehicles Conference, Washington D.C., <http://www-nrd.nhtsa.dot.gov/pdf/esv/esv19/05-0304-W.pdf)>.

Krenn, M, Mlekusch, B, Wilfling, C, Dobida, F, Deutscher, E & GmbH, CT 2003, 'Development and evaluation of a kinematic hood for pedestrian protection'.

Lawrence, GJL *The next steps for pedestrian protection test methods*.

Lim, GG, Chou, CC, Patel, RN, Shahab, SA & Patel, PJ 1995, *Estimating the minimum space to meet federal interior head impact requirement*, SAE Technical Paper 950333, SAE International Congress and Exposition, Detroit, Michigan, SAE International, Warrendale, Pennsylvania, USA.

Mizuno, Y 2003, *SUMMARY OF IHRA PEDESTRIAN SAFETY WG ACTIVITIES (2003) – PROPOSED TEST METHODS TO EVALUATE PEDESTRIAN PROTECTION OFFERED BY PASSENGER CARS*.

Narasimhan, B 1996, *The normal distribution*, Stanford University, viewed 28 July 2011, <http://www-stat.stanford.edu/~naras/jsm/NormalDensity/NormalDensity.html>.

National highway traffic safety administration 2009, viewed 10 October 2011, <http://www-fars.nhtsa.dot.gov/People/PeoplePedestrians.aspx>.

Nice, K 2001, *How crash testing works*, How stuff works, viewed 22 May 2010, <http://auto.howstuffworks.com/car-driving-safety/accidents-hazardous-conditions/crash-test2.htm>.

Nissan *Pop up engine hood for pedestrian protection*, viewed 21 September 2010, <http://www.nissan-global.com/EN/TECHNOLOGY/INTRODUCTION/DETAILS/PUEHFPP>.

Oh, C, Kang, YS, Youn, Y & Konosu, A 2008, 'Development of probabilistic pedestrian fatality model for characterizing pedestrian-vehicle collisions', *International Journal of Automotive Technology*, vol. 9, no. 2, p. 6.

Prasad, P & Mertz, HJ 1985, *The position of the United States delegation to the ISO Working Group 6 on the use of HIC in the automotive environment*, SAE Technical Paper 851246, SAE Government Industry Meeting and Exposition, Washington, DC, USA, SAE International, Warrendale, Pennsylvania, USA.

Ryan, GA & McLean, AJ 1965, 'Pedestrian survival'.

Safe car guide 2009, *Australian New Car Assessment Program*, viewed 25 November 2009, <http://www.safecarguide.com/exp/ancap/ancap.htm>.

Schmitt, K-U, Niederer, P, Muser, M & Walz, F 2007, 'Head Injuries,Trauma Biomechanics', in Springer Berlin Heidelberg, pp. 55-81.

Schoenmarkers, F 2011, *MADYMO human models for EuroNCAP pedestrian safety assessment*, TASS, Einsteinlann 6, 2289 CC Rijswijk, Netherlands, viewed 22 October 2012,

<http://www.altairhtc.com/europe/EHTC2011-Abstracts/EHTC-Presentations-2011/Session_10/EuroNCAP_Humanmodels_forHTCEurope_TASS_format.pdf>.

Synaptic analysis consulting group inc viewed 23 February 2011, <http://www.synapacg.com/casestudies_pedestrian.html >.

The European Parliament and of the council 2003, *Directive 2003/102/EC of the European Parliament and of the Council of 17 December 2003*, 06/12/2003, <http://eur-lex.europa.eu/LexUriServ/LexUriServ.do?uri=OJ:L:2003:321:0015:0015:EN:PDF>.

The World Bank 2001, *Road Safety*, The World Bank, viewed 15 July 2011, <http://www.worldbank.org/transport/roads/safety.htm>.

The World Bank 2006, *Making roads safe around the world*, The World Bank, viewed 15 July 2011, <http://web.worldbank.org/WBSITE/EXTERNAL/NEWS/0,,contentMDK:21102761~pagePK:34370~piPK:34424~theSitePK:4607,00.html>.

Transport Accident Commision 2012, *Daily road toll update*, , viewed 22 October 2012, <http://www.tac.vic.gov.au/jsp/statistics/roadtollcurrent.do?areaID=23&tierID=1&navID=2>.

Transport Research Laboratory 2012, *Pedestrian Safety*, Transport Research Laboratory, viewed 15 October 2012, <http://www.trl.co.uk/research_development/improving_safety/user_safety/pedestrian_safety.htm>.

Trauma.org *Trauma scoring*, viewed 10 October 2011, <http://www.trauma.org/archive/scores/ais.html>.

United Nations Economic Commission for Europe 1998, *Global technical regulation No. 9 (Pedestrian safety)*, United Nations viewed 12 July 2011, <http://live.unece.org/trans/main/wp29/wp29wgs/wp29gen/wp29registry/gtr9.html>.

Versace, J 1971, *A review of the severity index*, SAE Technical Paper 710881, 15th Stapp Car Crash Conference, San Diego, California, USA, SAE International, Warrendale, Pennsylvania, USA.

Wanke, T, Thompson, GM & Christoph, K 2005, 'Pedestrian measures for the Opel ZAFIRA II', paper presented to Experimental Safety Vehicles Conference, Washington D.C., <http://www-nrd.nhtsa.dot.gov/pdf/esv/esv19/05-0237-O.pdf>.

World Health Organization 2010, *Global status report on road safety: time for action*, World Health Organization, viewed 12 August 2010, <http://www.who.int/violence_injury_prevention/road_safety_status/2009>.

World Health Organization 2011, *Violence and injury prevention and disability*, World Health Organization, viewed 10 October 2011,

<http://www.who.int/violence_injury_prevention/road_safety_status/multimedia/pictures/en/index.html>.

Worldometers 2010, *World statistics updated in real time*, Worldometers, viewed 15 July 2011, <http://www.worldometers.info/cars/>.

Wu, J & Beaudet, B 2007, 'Optimization of head impact waveform to minimize HIC', *2007 World Congress*.

Zhou, Q 1997, 'An analytical study of system variables for meeting FMVSS 201 head impact requirements', paper presented to Proceedings of the 1998 ASME International Mechanical Engineering Congress and Exposition.